FAULT LOCATION ON EHV LINES USING WIDEBAND SPREAD SPECTRUM TECHNIQUES

A Thesis submitted for the Doctorate of Philosophy Degree
by Victor Taylor
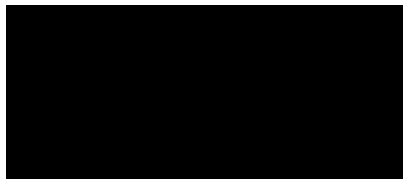
Department of Electrical and Electronic Engineering,

Victoria University of Technology,

Footscray Campus,

Victoria,

Australia

November 1999

Declaration of Originality

This thesis contains no material which has been accepted for the award of any other degree or diploma at any university. To the best of my knowledge and belief, it contains no material previously published or written by another person, except where due reference is made in the text of the thesis.

Victor Taylor

TABLE OF CONTENTS

LIST OF PRINCIPAL SYMBOLS

The following symbols are common to the whole thesis. Further line symbols, used only in Chapter 5, are listed at the start of that chapter.

Frequency

f = frequency

$\omega = 2\pi f$ = angular frequency

f_0 = carrier frequency

f_s = sample frequency

f_k = discrete frequencies

Δf = frequency shift

$\Delta\phi$ = phase shift

Line

v = average speed of propagation of signal down line

c = speed of light

D = line length

R_F = fault resistance (usually single phase-ground)

x = distance to fault from sending end

δx = error in range estimate

$\alpha = \alpha(f)$ = average line attenuation per unit length (dB/km)

$\alpha_i = \alpha_i(f)$ = line attenuation per unit length (km^{-1}) of mode i

$\beta_i = \beta_i(f)$ = line phase shift per unit length (radian/km) of mode i

$\gamma_i = \alpha_i + j\beta_i$ = propagation constant for mode i

Time

t = time

τ = time delay between the received signal and the transmitted signal

t_i, τ_i = discrete time samples

N_P = number of sample points in digitised waveforms

Signal

s(t) = transmitted signal

r(t) = received signal

R(f) = the Fourier Transform of r(t)

T = pulse width of rectangular pulse

B = RF bandwidth of line probing signal (single-sided)

R_c = code bit (chip) rate

L = code length

$T_P = L/R_c$ = period of spread spectrum signal

u(t) = bandlimited code

u_k = sample points of bandlimited code (k = 0,1,..,N_P-1)

Power and Energy

P_{TX} = power transmitted from communications room

E_{TX} = energy transmitted from communications room

V_P = peak voltage from transmitter leakage entering receiver

V_{P_F} = peak voltage of primary reflection from fault entering receiver

$S = P_{RX\_F}$ = power in primary reflection off fault entering receiver

E = energy contained in primary reflection off fault entering receiver

V_N = noise floor entering receiver

N = noise power entering receiver

N_0 = noise power per Hz (single-sided)

$N_i(f)$ = noise frequency spectra

Signal Processing

$y_m(\tau)$ = matched filter output

$y(\tau)$ = correlator output with quadrature components

$|y(\tau)|$ = correlation coefficient

$\rho(\tau)$ = auto-correlation function

$\Im$ = Discrete Fourier Transform (DFT)

$\Im_{f_0}$ = Discrete Fourier Transform (DFT) at carrier frequency f_0

$\Im^{-1}$ = inverse DFT

N_A = number of times waveform is averaged in receiver

T_{circ}, k_{ct}, k_m = micro-processor computation times

LIST OF PRINCIPAL ACRONYMS

EHV = extra-high voltage

PLC = power line carrier

SFG = separation filter group

CVT = capacitive voltage transformer

SECV = State Electricity Commission of Victoria

DOC = Department of Communications

RF = radio-frequency

SSB = single sideband

BPSK = biphase shift keying

MLS = maximal length sequence

PN = pseudo-noise

BW = bandwidth

BWL = bandwidth limited

LPF = low-pass filter

BPF = band-pass filter

SNR = Signal-to-Noise ratio

DFT = Discrete Fourier Transform

FFT = Fast Fourier Transform

DSP = Digital Signal Processing

LSB = least significant bit

MFLOPS = millions of floating point operations per second

ABSTRACT

Electrical authorities require fast and accurate fault locators to protect the quality of supply and reduce outage times. Spread spectrum techniques perform well in high noise environments such as power lines and their use in radar ranging is well known. Existing power line carrier (PLC) equipment may be used to transmit a direct sequence signal down a faulted EHV line. The fault position may then be calculated from correlation analysis of the reflected waveforms.

This fault location process has been simulated on a digital computer taking into account the frequency variation of the PLC interface and line parameters over the spread spectrum bandwidth. The effect of waveform characteristics, fault location and resistance are examined for a 100 km double transposed line with a single phase to ground fault. Results indicate that the receiver will locate permanent faults to within 0.5 km (0.5% of line length).

Prototype data acquisition hardware has been constructed and on-line results are presented for a 225 km 330 kV line. Line reflections were identified within an accuracy of 1.6 km (0.71% of line length) even though the channel bandwidth was limited to 50 kHz by external constraints. It is shown that accuracy is dependent on channel bandwidth, signal to noise ratio and waveform energy. It is suggested that a further increase in accuracy is possible by referencing the received signal to known impedance discontinuities such as the transpositions. Fault location accuracy down to one span should be possible using this technique which will work on both energised and de-energised lines.

Short code lengths are necessary for high speed operation and for the location of transient faults. Short MLS codes have poor sensitivity because of high residual correlation. Optimal signal processing and code selection for shorter codes with maximum sensitivity are reviewed. On-line results show that the sensitivity can be improved by at least an order of magnitude when using orthonormal codes or DC offset removal. The technique therefore appears to be suitable for high speed operation.

1. INTRODUCTION

1.1   FAULTS ON EHV LINES

Electric utilities use extra-high voltage (EHV) transmission lines hundreds of kilometres long to carry power from centres of generation to areas of consumption. The power lines often travel over inhospitable terrain which makes the location and repair of faults difficult. Obviously any break in supply is undesirable and if it does occur then the customer expects it to be restored as soon as possible. There is a need therefore for quick and accurate fault location. This thesis describes a new method of fault location which has the potential to meet both these requirements. In addition the scheme is low cost and uses the existing power line carrier (PLC) infrastructure.

1.1.1   Types of Faults

A *series* fault is the opening of two conductors which are normally joined together for proper operation. There is no involvement of the earth or any interconnection between phases. A *shunt* fault is the joining together, either as a short circuit or through some impedance, of any combinations of the cables and earth. For example, phase-phase faults involve the coming together of two conductors and phase-ground faults occur when a conductor is shorted to the earth. In Victoria, Australia, the frequency of occurrence of shunt faults is as follows:

single line to ground	90%
line to line	5%
line to line to ground	3%
line to line to line	2%

Faults may be of a transient nature and may be removed by de-energising the equipment for a short period of time, or the fault may be of such severity that the line is inoperational until repairs are made. Most faults are of the transient type.

1.1.2   Effects of Faults

1. Reduction of line voltage interrupting the power supply to the consumer and causing maloperation of pressure coil relays.

2. Damage may be caused to the power system and other apparatus due to overheating and abnormal mechanical forces.

3. Power system instability.

In normal operation the power system protection network will rapidly (within one or two mains cycles) detect the fault, determine the area of malfunction and isolate the impaired line through the opening of relays.

1.2 NEED FOR FAST, ACCURATE FAULT LOCATORS

Transient faults can impair the line equipment, degrading the quality of supply, and faults which do not permit circuit breaker reclosure diminish the reliability of supply. Fast and accurate fault locators are clearly of benefit to society.

Cable patrols to monitor in situ conditions are very expensive so that remote sensing of line parameters represents a more economical means of protecting this capital intensive infrastructure. More than 50 years of research into fault location have produced two approaches to remote sensing of the fault position.

1. Measurements of waveforms existing immediately after the fault

2. Measurements of waveforms injected down the line.

Any remote sensing method must be compatible with the operational environment of the power system and not disturb existing services. The *detection* of noise imbedded signals reflecting off power grid topologies and the *estimation* of fault locations from these waveforms are the twin problems to be solved for successful EHV line diagnostics.

As far as the author is aware, no single fault locator exists which accurately locates all the different types of faults and which meets the stringent demands of the hostile power line environment. Fault location is still a major area of research worldwide.

1.3 ORGANISATION OF THESIS

PLC communication networks have been used on EHV lines for many years. They are used for telephony, protection signalling and data transmission. The bandwidth available for PLC transmission usually falls within the range of 40 kHz to 500 kHz. Not all of this bandwidth is available for continuous transmission because of

compatibility problems with other radio services. In Australia the band between 200 kHz and 400 kHz falls into this category. Spread spectrum modulation, traditionally used in military applications, is a method of sending information down a channel over a wide bandwidth with low power spectral density. These broadband signals cannot be detected by users of the same spectrum and so are ideal for non-invasive probing of power grids. The work on this thesis concentrates on a fault location technique which uses the PLC network to transmit and receive spread spectrum waveshapes.

Chapter 2 discusses the different types of faults on EHV lines and outlines the requirements of a fault locator. The major part of the chapter is a review of the different fault location methods engineered by researchers this century.

Chapter 3 overviews the power system telecommunication system and discusses in some detail the operation of the PLC network, particularly in the Australian context. The characteristics of EHV lines at PLC frequencies are then given and the requirements of a fault locator using the PLC network are listed. Finally system design equations for such a fault locator are detailed.

Chapter 4 looks at waveform design and optimal signal processing techniques applied to traditional and pulse compression waveforms. Waveform design objectives for EHV line fault location are listed, and a strategy for the construction of optimal remote sensing waveforms is outlined. Spread spectrum waveforms and their advantages in the PLC environment are introduced, and their application to ranging is quantified. The chapter concludes with system design equations and performance predictions for an EHV line fault locator transmitting and receiving spread spectrum waveshapes using the PLC channel.

To test these predictions and to investigate the effects of modal propagation on EHV lines at PLC frequencies a simulation program was written that models the frequency dependent PLC line interface and distortion produced as signals at PLC frequencies propagate along EHV lines. These simulation results are presented in Chapter 5.

Chapter 6 presents hardware design for a data acquisition system to transmit and receive a spread spectrum waveform down an EHV line using the PLC channel. On-line results are given for a 225 km 330 kV line.

Chapter 7 looks at ways of increasing the dynamic range for high-speed operation

using short codes, and Chapter 8 concludes the thesis and suggests areas for further improvement. The work has led to a number of publications and these are referenced in the final chapter.

2. FAULT LOCATION ON EHV LINES

2.1 INTRODUCTION

Electricity supply authorities world wide require quicker and more accurate fault location methods in order to improve the quality of supply and decrease outage times. This chapter briefly overviews the different types of faults (section 2.2), the requirements of an ideal fault locator (section 2.3) and techniques used by other researchers for fault location (section 2.4). Some faults, such as those due to high voltage breakdown, require the presence of the mains voltage in order to be observable, while others, called sustained faults (eg. a conductor shorted to ground), can usually be measured on de-energised lines [1].

2.2 TYPES OF FAULTS

The following classification is taken from [1]

2.2.1 Latent Faults

Insulation deterioration impairs the over voltage performance of the line. There is arcing at high voltages caused by surges and transient overvoltage conditions, although operation at normal voltages is unimpaired.

2.2.2 Momentary Faults

Momentary arcing due to transient conditions not causing permanent damage (eg minor lightning flashover). Also called nonpermanent or transient faults.

2.2.3 High-breakdown Faults

Faults which are apparent when there is mains voltage on the line but which do not show up at low voltages. Reclosure of the breakers is impossible.

2.2.4 Sustained Faults

Faults which are apparent when there is mains voltage or low voltage on the line. High-breakdown and sustained faults prevent successful reclosure, and are consequently sometimes classified together as sustained or permanent faults.

2.3 REQUIREMENTS OF A FAULT LOCATOR

A fault locator for use on EHV lines should have the following attributes:

1) **Accuracy**

   a) It must have high accuracy, preferably to within one span.

   b) It should be capable of operating over the entire length of the line with high accuracy.

2) **Discrimination**

   a) It should have high sensitivity to variations in line parameters.

   b) It should have fast response to (possibly transient) deviations in line conditions.

   c) Must be able to discriminate between faults and line impedance changes due to non-fault conditions.

3) **Robustness**

   a) It must operate in the high noise environment of power lines and not be affected by or affect the mains supply.

   b) It should be capable of operating on both electrified and dormant lines - hence the clearance of faults may be verified without reclosing the circuit breakers.

   c) It should work on a variety of lines, single and double circuit lines, lines with and without transpositions, lines with high shunt capacitance etc.

   d) It must not be affected by external conditions, such as faults on nearby lines, weather conditions and impedance variation (loading changes) at the line ends.

4) **Utility**

   a) Results should be easily interpreted by operators or computer.

   b) Equipment must be designed for substation installation and should be simple, rugged, safe, cheap and require low maintenance.

   c) To improve consumer service the results should be quickly available, as fault location information is used to route supply around the disrupted area.

d)   The system must work whatever the fault inception phase.

2.4   METHODS OF FAULT LOCATION

2.4.1   Current Techniques

The most commonly used method of fault location on EHV lines is the reactance ratio measuring technique [2]. An unfaulted line of total impedance jX_N will, when faulted, have an impedance up to the fault position of jX_F. As X_N is known, measuring the ratio X_F/X_N from line end voltage and current measurements, will give the distance to the fault. Visual inspections of lines are also used as a fault locating technique.

2.4.2   Classification of Fault Location Methods

Figure 2.1 illustrates the most important methods for locating faults on EHV lines developed in over 50 years of research [3] [4]. Definitions of terms used are now given, which introduces the detailed literature review of these techniques.

Passive vs Active Active sensing fault location methods rely on the generation and transmission of a known signal across the power network. Passive techniques are based upon the measurement of waveforms existing immediately after fault inception - no other signal is required.

Quantity Measured - Power Frequency vs High Frequency Waveforms existing immediately after fault inception typically consist of a steady state power frequency sinusoid together with transient high frequency components and an exponentially decaying DC value [5].

Fault location algorithms using power frequency measurements are passive techniques that use estimates of the power frequency sinusoids. Typically these methods are based on power frequency lumped parameter transmission line models and require filtering to extract the steady state fault signals.

The high frequency methods use measurements at frequencies higher than the power frequency and its harmonics. Techniques which use the high frequency fault generated transients (with frequencies ranging from approximately 150 to 1000 Hz [6]) may be either active or passive, and techniques which depend upon the generation

Fault Location Methods

```
                    Fault Location Methods
                    ╱                    ╲
              Visual methods    Methods using measurements made at terminals
                                        ╱              ╲
                    Power frequency measurements    High frequency measurements
                    (electrical quantity).  Passive methods    (travelling waves)
                                                    ╱          ╲
        Measurements of fault generated surges   Transmitted waveform measurements
                        ╱         ╲                       Active methods
              Methods based on   Other methods              ╱         ╲
              propagation delay                    Methods based on   Resonance
              measurements                         propagation delay   frequency
                                                   measurements         method
```

Figure 2.1 *Classification of fault location methods.*

and transmission of high frequency waveforms are, by definition, active. Distributed parameter line models or telegraph equations are used.

Single-ended vs Double-ended Single-ended methods have the fault location equipment located at one end of the line, while double-ended methods have equipment located at both ends of the line.

The different categories of Fig. 2.1 and the contribution of different researchers are now considered in detail.

2.4.3   Visual Inspection

Patrols by foot, car helicopter or aeroplane can be used to locate all kinds of faults with varying success. Obviously long lines present a problem and there may be minimal visual impairment with momentary and latent faults. Some researchers have

applied a signal to the line which is patrolled with a receiving device - the received signal changes near the point of the fault [1].

2.4.4   Electrical Quantity Measurements

The basic principle of the reactance ratio measurement technique is described above in section 2.4.1. These are the most widespread fault location methods in use by power utilities. Sant and Paintankar [2] reported accuracies of 2% for single-end feed lines. For double-end feed lines the fault is fed by currents from both ends of the line and if these are out of phase the fault resistance R_F will appear complex. This produces errors in the estimated fault position. Compensation for the fault locator inputs for this case are given, and accuracies of 5% were described, provided the fault impedance is less than 36 Ω. The fault locator operates in less than two cycles from when the relay delivers a trip output and so is suitable for both transient and permanent short circuit faults.

Several researchers have attempted to overcome the degrading effect the apparent fault reactance has on fault location accuracy. Wiszniewski [7] gives corrective equations so that the line reactances measured from one of the line do in fact become proportional to the distance to the fault. The modifications are based on estimates of the phase shift between the current at the line end and the current flowing through the fault resistance. This is a non-iterative technique and no simulation or test accuracies are given.

Limitations of the impedance or reactance measuring techniques are outlined in [8] as follows:

♦ unsuitable for use on series compensated and DC lines

♦ gives ambiguous results on teed circuits

♦ subject to errors if

• the fault resistance is high and the line is fed from both ends

• the fault arc is unstable

• there are circuits running in parallel with the faulted line over part(s) of its length

The work of subsequent researchers attempts to overcome these limitations.

Eriksson *et al* [9] use a more complete power network model, where the infeed from the grid beyond the remote end is taken into account. Source impedances and pre-fault load current values are also used for compensating the apparent reactance of the fault. In field tests on phase-phase and phase-ground faults, fault positions were calculated to within 3%.

Tagaki *et al* [10] derive an algorithm that takes into account the load flow and the fault resistance. There is also compensation for cross-coupling between phases or from adjacent circuits. It took 50-70 msec from the fault occurrence for the fault location to be estimated. Field tests were conducted on a 71.2 km long line consisting of two transmission lines in parallel. Single phase-ground and two phase-ground faults were located to within 1 km.

Westlin and Bubenko [5] apply the Newton-Raphson method to estimate the power frequency voltages and currents using a least squares method. The faulted transmission line equations which are solved are nonlinear, so the iterative technique is required - the equations are solved for R_F and x. Simulations were done of a 47.3 km long line, first with a single phase to ground fault and then with a double phase to ground fault, both with $R_F = 5\ \Omega$ and x = 38.3 km. The results of the fault location algorithm were $R_F = 16.5\ \Omega$, x = 38.3 km and $R_F = 4.6\ \Omega$, x = 39.3 km respectively.

Tagaki *et al* [11] also use the Newton-Raphson method to solve non-linear equations derived using steady state superposition on a loss-less faulted line. The algorithm is based on the Fourier analysis of a faulted network. Simulations with x = 11 km and $R_F = 0$, $R_F = 10\ \Omega$, both converged to x = 11.02 km. The effects of fault resistance, line loss, load characteristic and waveform distortion on fault location accuracy were investigated.

Richards and Tan [12] derive a lumped parameter model of the line using least squares analysis on voltage and current measurements. The fault location algorithm also estimates R_F and does not require filtering of the high frequency transients. For a single phase-ground fault at the mid-point of a 100 mile transmission line, simulation results gave 1% fault location accuracy for $R_F < 30\ \Omega$, and 6% accuracy for $R_F = 100\ \Omega$. It was noted that for $R_F = 300\ \Omega$ the fault may not be recognised as a fault because of the small fault current.

Lawrence and Waser [13] transformed the s-domain lumped parameter circuit representation of a transmission line into the z-domain for sampled data analysis. A phase network model was used which incorporates cross-coupling effects in self and mutual impedance terms. Field tests on a 167.5 mile long line with a fault at x = 112 miles estimated the fault location at x = 110.9 miles.

Sachdev and Agarwal [14] give a non-iterative technique which uses positive sequence voltages and currents as calculated by digital impedance relays. Simulation results gave accuracies less than 5% of the line length. The accuracies were degraded near the middle of the line where fault currents had equal contributions from the terminal at each end of the line.

Cook in [15] gives three algorithms for calculating the position of a fault. The first two methods require measurements at both ends of the line as in [14] - one algorithm requires two impedances for the solution of a quadratic equation and the second algorithm needs two impedances and two relay currents (again as in [14]) for the solution of a linear equation. The third method requires only voltage and current measurements at one end of the line. Simulation results on a 10 mile long 132 kV line gave fault location accuracies for all three methods of the order of 0.5% for phase-phase and phase-ground faults.

Johns and Jamali [16] consider various sources of error not taken into account in some previous fault location algorithms. These are the effect of untransposed lines, shunt capacitance, fault resistance, remote source impedance setting and the distorting effects that capacitive voltage transformers (CVTs) have on high frequency fault transients. The algorithm uses post-fault voltage and current measurements from both line ends and derives the fault position from the modal theory of signal propagation along multiphase transmission lines. Simulation results for single and double phase-ground faults with $R_F = 100 \ \Omega$, for lines of lengths 100 km and 250 km and for various line geometries, gave fault location accuracies within 1%.

Aggarwal *et al* in [17] extend this method to teed feeders. Measurements are made simultaneously at each of the three terminals. Simulation results were done for fault resistances up to 400 Ω and for different fault positions and circuit geometries. Fault locations were all estimated to within 1%.

Johns *et al* [18] present a method for locating resistive single phase-ground faults using voltage and current measurements at one end of the transmission line. Applying the modal theory of multi-phase signal propagation to a faulted 3-phase system an equation is derived for the admittance matrix (as a function of x) at the fault position. The magnitude and phase of the elements of the matrix give the faulted phase and fault position respectively. A feature of the algorithm is insensitivity to values of the remote source impedance. Simulation using the electromagnetic transients program (EMTP) showed the algorithm to be accurate to within 4% with known remote source impedance for $R_F \leq 50 \, \Omega$.

2.4.5   Fault Generated Surge Measurements

2.4.5.1   Propagation Delay Measurements

Firstly we look at the fault locators that directly measure the time of travel of the fault generated surges.

In an early paper Stevens and Stringfield [19] describe a Type A and a Type B fault locator used by the Bonneville Power Administration. The principle of the single-ended passive Type A fault locator is illustrated in Fig. 2.2, and the principle of the double-ended active type B fault locator is illustrated in Fig. 2.3.

When a fault occurs, travelling wave transients propagate away from the fault at a speed close to the speed of light. The Type A fault locator, placed at one end of the overhead line, starts a timer when the arrival of a fault generated surge is detected. The travelling wave reflects off the line end, travels back to the fault, is reflected again, and this double reflection travels back to the line end where the Type A fault locator is situated. The time duration between the arrivals of the successive waves is recorded and provides a measure of the fault location.

With the type B fault locator there are surge detectors at each end of the line, and a radio, microwave or power line carrier transmitter at the remote end, with a receiver at the local end. When a fault generated transient is detected at the remote end a signal is transmitted from this end to the local end of the line, at a known time delay after the surge detection. The difference in detection times of the surges at each end gives the fault location.

Figure 2.2 *Type A fault locator.*

Figure 2.3 *Type B fault locator.*

During field tests with the Type A fault locator on a 72 mile long, 220 kV line, single phase-ground faults at x = 58 and 64 miles were located to within 1 mile. Spurious reflections due to transpositions and river crossings were negligible. No results were reported for the type B fault locator. Both types complete their measurements before the fault arc is extinguished. The precision of the measurements depends primarily on the steepness of the wave front.

Gale *et al* [8] describe a Type A and a Type D fault locator. The Type D fault locator is similar to the Type B except that there is synchronised timing at the local and

remote ends (using, for example GPS receivers), eliminating the need for the transmitter and receiver. The arrival of fault generated transients is recorded at each end of the line - the difference in the time of arrival at each end allows the fault position to be calculated. The Type D is therefore a passive double-ended technique. Multiple reflections made interpretation of the Type A data difficult. In field tests using the Type A fault locator on a 67 km long line, the length of the line was measured from transit times of the surges as 67.0 km. The Type D method allows for easier interpretation of the results at the expense of remote synchronisation. Test results on a 10.4 km long line with x = 0 gave fault position estimates varying from - 0.2 to 0.1 km. Test results with x = 4.3 km gave fault position estimates of 4.3 and 4.15 km.

The next three papers which are reviewed are primarily concerned with distance protection. They are mentioned here because the algorithms produce fault location estimates and because they use correlation techniques which are well suited to the noisy power line environment. However the goal of the protection schemes is to determine if the fault is internal or external to certain protected areas, not to produce an accurate fault position estimate.

Vitins in [6] assumes that the distributed inductance and capacitance of the line are independent of frequency and that line losses are concentrated at the ends. Under these conditions the telegraph equations reduce to the wave equation, which has as solution the linear superposition of two waves travelling in opposite directions along the line. These two waves are easily related to the voltages and currents on the line. Correlation integrals between weighting functions and the travelling waves are evaluated from line voltage and current measurements. One of the integrals has a time delay which is varied - when the time delay corresponds to the time of travel from the fault the correlation vectors coincide. The effects of high frequency transients and the exponentially decaying DC transient are investigated. Simulation and experimental results presented emphasise the success of the technique for directional discrimination of the fault location, rather than success at finding the absolute fault position.

Crossley and McLaren in [20] describe a measuring relay point which is not at the end of the line. The fault generated surge travels out from the fault past the relay point and reflects off the line end. This second reflection travels back past the relay point

and is recorded (W1), reflects off the fault, and travels back past the relay point (W2). Correlation analysis of the waveforms W1 and W2 gives the time delay between them and hence the distance from the relay point to the fault. Using modal analysis [21] the waveshapes are decomposed into their modal components, and it is the modal velocities which are used to convert time delays to distances. In simulations for a single phase-ground fault with R_F = 75 Ω located 240 km from the relay, the fault position was calculated to be 195 km from the relay. A 3-phase fault, not involving the earth, 160 km from the relay was located accurately. The accuracy of the technique as a fault locator depends upon the fault location, the fault type, and the point on the wave at which the fault occurs.

Christopoulos *et al* in [22] describe a cross-correlation technique similar in principle to that of [20]. Again the fault location accuracies were poor.

Finally in this section we look at two simulation papers which are also primarily concerned with protection rather than fault location. They are reviewed because they use PLC equipment to measure high frequency fault induced transients. In [23] Agrawal uses the method of Johns and Aggarwal [24] to simulate a single-phase to ground fault on a 100 km long 400 kV 3-phase line. The PLC line coupling equipment consists of a coupling capacitor in series with an inductor, a resistor and a parallel RLC circuit going to ground. The voltage was measured across the parallel RLC circuit. This stack tuner circuitry constitutes a bandpass filter of bandwidth 5 kHz with a centre frequency that can be set to 100, 200 or 300 kHz. Simulation results showed decaying high frequency transient oscillations of around 30 μsec duration entering both ends of the line. The peak voltages varied from 70 V to 30 kV and were shown to depend on the centre frequency of the bandpass filter and the fault inception angle.

In [25] Agrawal extends the simulations to arcing faults, caused by transient overvoltage line conditions, using a piece-wise linear arc V-I characteristic incorporating re-ignition. Correlation analysis of the stack tuner output was used for protection purposes. Simulation results showed arcing fault responses repeating every half mains cycle for both 90° and 0° fault inception angle. Travelling wave based protection schemes had previously failed for 0° fault inception angle.

2.4.5.2   Other methods

Here we look at the fault location algorithms which are not based on direct measurement of the time of travel of the fault generated surges.

In [26] Tagaki *et al* generalise their steady state Fourier method of [11] to a Laplace Transform based method. The superposition principle is applied to the transient state analysis of a faulted network. In simulation results using EMTP (Electromagnetic Transients Programme [27]) the fault location algorithm estimated fault positions to within 1.5%. The effects of transmission line loss, fault resistance, DC offset current and load impedance on fault location accuracy were studied.

Ibe and Cory [28] start with the telegraph equations and use voltage and current samples 5 msec after fault inception to generate voltage and current profiles along the line using the method of characteristics. Three different criteria functions to give the fault location were calculated from these profiles. These were second derivatives of limited integrals along the line of, respectively, the square of the voltage, the square of the current, and the product of these two. Each criterion function has a maximum at the fault position. Simulation results on two and three terminal networks gave accuracies of between 0.07 and 3.2%. Faults with resistances up to 300 Ω were located by the algorithm. The accuracy was dependent on the window length of the fault data and the sampling interval. A window length of four times the wave transit time was necessary for good results.

Ranjbar *et al* in [29] criticise the use of a criterion function which is proportional to the integral of the square of the voltage over a limited interval. They point out that if the fault inception angle (the phase angle of the sending end voltage at fault inception) is near zero, then there is no minimum of the criterion function at the fault point. As an alternative to the noise enhancing differentiations done in [28], they suggest the use of a criterion function which is proportional to the absolute value of the voltage at each point along the line during a limited time interval. Also a lower sampling rate is required by this criterion function. Simulation results are presented, and the accuracy is half the distance between the calculated points of the criterion function.

2.4.6 Active Travelling Wave Measurements

2.4.6.1 Propagation Delay Measurements

These are the classic radar like techniques where a signal is sent down a faulted line and the return time taken for the reflection from the fault to travel back to the receiver provides an estimate of the fault position. Type C uses a single pulse and Type F uses repetitive pulses. The former requires a narrow pulse width for good resolution and minimum range performance, and high peak powers for good accuracy and maximum range performance. The latter can use lower powers and averaging to reduce noise; this reduces the response time.

Leslie and Kidd in [30] describe echo-ranging equipment which was tested on EHV lines. At first they were connecting to dead lines and using a 24 μsec DC pulse of amplitude up to 1000 V. It was found that a 100 V pulse usually sufficed. For connecting to live lines a coupling capacitor is mandatory and it was found that the transmission of the DC pulse through the capacitor produced an on-line signal consisting of two sharp pulses of opposite polarity separated by 24 μsec and each about 1 μsec in duration. This expanded the frequency spectrum of the signal out to 1 MHz. To avoid interference to power line carrier equipment they used a 24 μsec long 250 kHz RF burst which was passed relatively undistorted by the coupling capacitor. The length of the pulse limits the minimum range to around 3.6 km. It was found that the practical limit in sensitivity was that fault resistance that produced the same magnitude echo as that from the transpositions. For a phase-phase fault this was found to be a resistance of 10000 Ω, and for a single phase-ground fault the maximum resistance was $R_F = 10\ \Omega$.

Spaulding and Diemond [31] describe an EHV line echo-ranger that uses a 1 μsec DC pulse from a 10 kV source. When a line fault was detected a phase selecting relay system connected the fault locator between the faulted phase and ground. No quantitative performance data was given.

Stevens et al [32] review the theoretical performance of the pulse ranging method as compared to the swept frequency ranging technique, concluding that the linear FM technique is more accurate. Design details are given for a linear FM fault locator which they constructed. The results of laboratory tests on a 172.8 mile long lumped

parameter line model are given, with both open and short circuit faults. The accuracy of the fault locator was around 2% for distant faults.

2.4.6.2   Resonance Frequency Measurements

A sine wave transmitted down a faulted line will form a standing wave pattern resulting from interference between the transmitted and reflected signals. As the frequency is varied, the voltage recorded at the terminal station will rise and fall. The distance to the fault can be calculated from the frequency change Δf between voltage maxima and minima.

Figure 2.4 *Resonant Frequency Fault Locator.*

Figure 2.4 illustrates the transmission of a sine wave down a faulted line and the incoming attenuated ($K < V$) reflection time-delayed by $2x/v$. The total voltage at the sending end is

$$v(t) = V \sin(\omega t) + K \sin\left[\omega\left(t - \frac{2x}{v}\right)\right]$$

The rms (root-mean-square) voltage may be calculated to be

$$V_{rms} = \sqrt{\frac{K^2 + V^2}{2} + KV\sin\left(\frac{2\omega x}{v}\right)}$$

A frequency change Δf will change v_{rms} from maximum to minimum when

$$\frac{2(2\pi \Delta f)x}{v} = \pi$$

$$\Rightarrow x = \frac{v}{4\Delta f}$$

This method works for sustained faults and locates faults to within an accuracy of 2% of the line length [1].

2.5   CONCLUSION

For the purposes of this thesis it is considered that accuracy and discrimination are the most important of the evaluation criteria for fault locators listed in Section 2.3.

The impedance measuring method has a lot of problems as discussed in section 2.4.4. While different researchers pursuing the method of fault location by measuring electrical quantities have fixed an individual problem with a particular method, other limitations have always remained.

The accuracies of the fault generated surge methods is compromised for a number of reasons. The type of post-fault transient that occurs on EHV lines depends upon the voltage value when the fault occurs. The DC transient dominates for fault inception at zero voltage, while the high frequency transients dominate when the fault occurs at voltage peaks [6]. Hence the waveforms that the algorithm must work with depend upon the conditions at the time of the fault. Also the surge will have undergone much power line distortion by the time it is measured. In contrast the echo ranging techniques always use a known waveform.

The range accuracy of pulse reflectometry can be improved only by increasing the bandwidth or the transmitted power, while the accuracy of a continuous chirp FM fault locator may also be improved by transmitting a waveform with a higher bandwidth × period product. These reflectometry methods work on de-energised as well as energised lines, so that it is possible to determine if a permanent fault has been cleared without reclosing the mains breakers. Active sensing methods are therefore chosen for further evaluation in this thesis.

However the use of active sensing waveforms requires a power system wide transmission network. Fortunately there is in place just such a communication system used by power utilities, the power line carrier (PLC) system which uses the power lines as transmission media. This PLC net and the EHV lines as a communication channel is considered in detail in the next chapter.

3. EHV POWER LINE CARRIER COMMUNICATION

3.1   INTRODUCTION

After a literature survey of different fault location methods, it was concluded in the previous chapter that active remote sensing techniques using the PLC network were to be investigated further. This chapter provides a brief summary of the power line carrier communication system used on EHV lines. Section 3.2 puts the PLC network in the context of other communications methods used by power utilities and section 3.3 details the features of the PLC communications system. The characteristics of EHV lines (the PLC communication media) at PLC frequencies are summarised in section 3.4, and section 3.5 specifies the requirements of a fault locator using the PLC network. Finally system design equations for successful transmission and reception of signals down EHV lines using the PLC communication network are outlined in section 3.6.

3.2   POWER SYSTEM TELECOMMUNICATIONS

Fault surges, load fluctuations, and the effects of control actions propagate around power networks in milliseconds. To maintain power system stability it is essential that high-speed communication links reliably provide control information at critical points in the power system. The high reliability requirements of this network, (dependable operation is necessary even during conditions of power system collapse), has meant that many power authorities throughout the world have found it necessary to run their own private communications networks. For redundancy enhanced reliability different bearers (communication systems) are used in power system telecommunications and some of these are [33] :

1. Pilot cables. These are overhead and underground cables.

2. Power line carrier (PLC). High frequency ($\leq$ 1 MHz) single sideband modulation signals provide communication services over the high voltage transmission lines.

3. Cable carrier. Cable carrier combines multiple voice channels into groups and supergroups with a bandwidth out to over 1 MHz.

4. VHF and UHF radio. Mobile and fixed links provide for various voice and paging links.

5. Microwave radio. The wide bandwidth of microwave radio systems provides for multiple communication links between stations.

6. Earthwire systems. Cables running down the core of the high voltage overhead earthwire provide communication links - optical fibre especially provides almost unlimited bandwidth.

Typical applications for these communication systems include

1. Rapid clearance of faults.

2. Isolation of faults with the least possible loss of load.

3. Communication with field and operating personnel.

4. Remote control and supervision of the power transmission network.

5. Shedding of load during peak periods.

The next section looks at PLC communication networks as operated in Australia. The characteristics of EHV lines at PLC frequencies are then reviewed and conclusions are drawn for PLC system design based on SNR calculations.

3.3   CARRIER COMMUNICATION SYSTEMS

Electrical utilities have used power line carrier communication channels for over sixty years. International PLC standards are discussed in [34] while in Australia power line carrier is under the jurisdiction of the Department of Communications (DOC).

3.3.1   Frequency Assignment

The services provided by the PLC network can be divided into two categories:

1. Continuous operation providing for telephony and signalling.

2. Intermittent high power protection operation.

Table 3.1 summarises the frequency bands set aside by the DOC licensing authority for power line carrier services [33] - other countries have different allocations but

Table 3.1 *PLC Frequencies Available for Use in Australia*

Frequencies dedicated to continuous power line carrier: 148 to 200 kHz, 405 to 448 kHz, 460 to 484 kHz
Frequencies available for continuous PLC use provided no interference occurs to other services: 80 to 148 kHz
Frequencies available for intermittent PLC services: 200 to 380 kHz

Australia is not atypical. Below 148 kHz special broadcasting permission can sometimes be obtained.

3.3.1.1 Telephony

The useable channel bandwidth is from 300 Hz to between 3.5 kHz and 4 kHz depending upon the manufacturer. This baseband is split up into a voiceband from 300 to between 2400 Hz and 2700 Hz, and a voice frequency (vf) signalling section for the rest of the band [33] [35] which provides the telemetering and control functions [36] listed below.

3.3.1.2 Telemetering and Control

Telemetering A telemeter circuit is a facility by which a measured quantity is converted into electrical form and transmitted to a remote site where the measured quantity can be recovered.

Supervisory Control These services provide for monitoring and controlling functions in a remote station.

Load Frequency Control Monitoring of network loading and frequency stability are telemetered to a central controlling station which provides controlling signals to appropriate plants.

3.3.1.3 Modulation

To maximise the use of the limited bandwidth available single sideband (SSB) modulation is often used on PLC channels. Figure 3.1 illustrates a typical frequency

2580 Hz : telephone signalling
2700 - 3780 Hz : 10 × 120 Hz general purpose signalling channels

11 channels

speech

0.3   2.4   2.58   Frequency   3.78
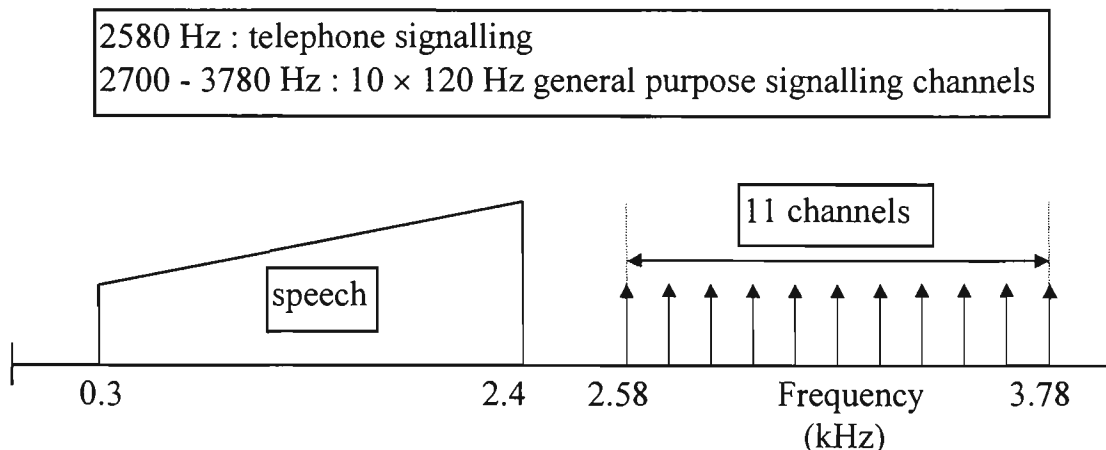   (kHz)

Figure 3.1 *Typical frequency allocation of a single sideband 4 kHz channel conveying telephony and signalling information.*

allocation of a single sideband 4 kHz channel conveying telephony and signalling information.

3.3.2 Network Protection Services

3.3.2.1 Protective Relaying

During fault conditions high-speed relays detect the presence and location of the fault and then use carrier to transmit this information across the power grid. The appropriate circuit breakers are then opened, isolating the impaired line sections. Three different protective relaying methods are employed: carrier blocking schemes, permissive trip relaying and remote trip relaying [36].

Carrier Blocking Schemes These schemes use the transmission of carrier during a fault to prevent the tripping of a circuit breaker in a distant station. Carrier does not have to propagate through the faulted line section. The two carrier blocking schemes used are directional-comparison pilot relaying and phase-comparison pilot relaying.

1(a) Directional-comparison Pilot Relaying. Relays cannot distinguish between a fault near the far end of a line and a fault just beyond the far end of the line. In the latter case carrier is transmitted from the remote station to block the circuit breakers from tripping at the local station.

1(b) Phase-comparison Pilot Relaying. A fault in the neighbourhood of a line protected at each end causes the carrier terminal at each end to send bursts of carrier in phase with the fault current at its local end. Each receiving terminal compares the phase of the fault current at the remote terminal with the local phase. If faults are on the joining line the circuit breakers are tripped while for outside faults the circuit breakers are blocked from tripping.

2. *Permissive Trip Relaying* The local end of a protected line section sends a guard frequency during normal conditions - this changes to a trip frequency when a fault is detected on the line. The circuit breakers at the far end, however, will trip only if the relays there have also detected a fault on the protected line. As the trip signal must travel through a faulted line section high transmit power is used.

3. *Remote Trip Relaying* This occurs when a station with a local fault sends a tripping signal to the remote end to clear power from the line. There is no requirement that the remote end relays should also have detected a fault.

3.3.2.2   Modulation

The high power carrier signals used in protection have either frequency shift or amplitude modulation and have a maximum transmission time of 10 seconds [33]. Frequency bands 2 or 4 kHz wide may be assigned depending upon the function to be performed.

3.3.3   Terminal Equipment

In Australia three types of PLC operation are used in power systems - types A, B and C [33] [35].

3.3.3.1   Type A : Telephony and VF Signalling

This equipment is the most commonly used in power networks and is designed to operate with a 30 dB loss over the length of the interconnecting line. The DOC allows this equipment to put 0.25 W of continuous RF power onto the power lines.

3.3.3.2   Type B : Telephony, VF Signalling and High Speed Protection

For normal operation this equipment operates as for Type A. However for protection signalling functions the speech and vf signalling is removed and replaced by a carrier

modulated by a higher level coded signal. The RF output power can be up to 20 W onto the power line for a maximum of 10 seconds.

3.3.3.3   Type C : Protection

Operation as for protection signalling of Type B. The frequency range of use for this equipment is from 200 to 380 kHz to prevent interference with other PLC services. Transmission times are usually limited to stop radiation from the power lines affecting the performance of Department of Transport radio navigation beacons.   For permissive intertrip or remote trip functions a higher level coded signal is used, while in the case of a blocking signal an unmodulated carrier is transmitted.

3.3.3.4   Separation Filter Group

With wideband carrier systems, where two or more carrier terminals are connected to the same power lines, analogue filters or hybrids are used to prevent cross-coupling between the signals.   In Victoria, the separation filters split the available PLC spectrum into 3 bands (Figure 3.2).   This improves the reliability of the system by isolating the TX/RX equipment on one band from the TX/RX equipment on the other bands.
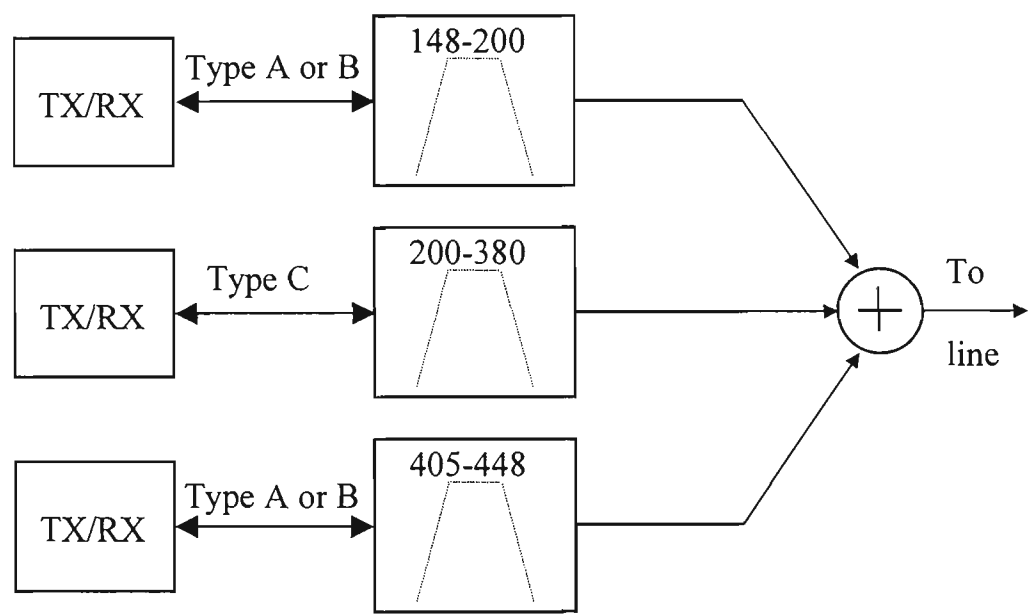
Figure 3.2 *Typical PLC channel combining prior to transmission onto an EHV line.*

3.3.4   Coupling Circuits

The DOC regulations for PLC systems require that the carrier signals be coupled between two phases of the one transmission line or between one phase of one line and

one phase of another line on the same easement [33]. While coupling between a single phase and ground is significantly cheaper than phase to phase coupling, there is a much higher level of radiation from single phase coupling. For this reason this form of coupling is not permitted in Australia.

Radio frequency carrier systems are coupled to the power lines through high voltage capacitors of which there are two types [35]:

1. A capacitive voltage transformer is a series connection of two capacitors connected to a power line which acts as a voltage divider to provide a safe voltage for monitoring on-line mains voltages. These can also double as carrier coupling capacitors.

2. Alternatively a dedicated separate single coupling capacitor can be used.

1 : Coupling capacitor   2 : Arrestor
3 : Drain coil   4 : Grounding switch
5 : Isolation transformer   6 : Tuning Capacitor
7 : Matching transformer

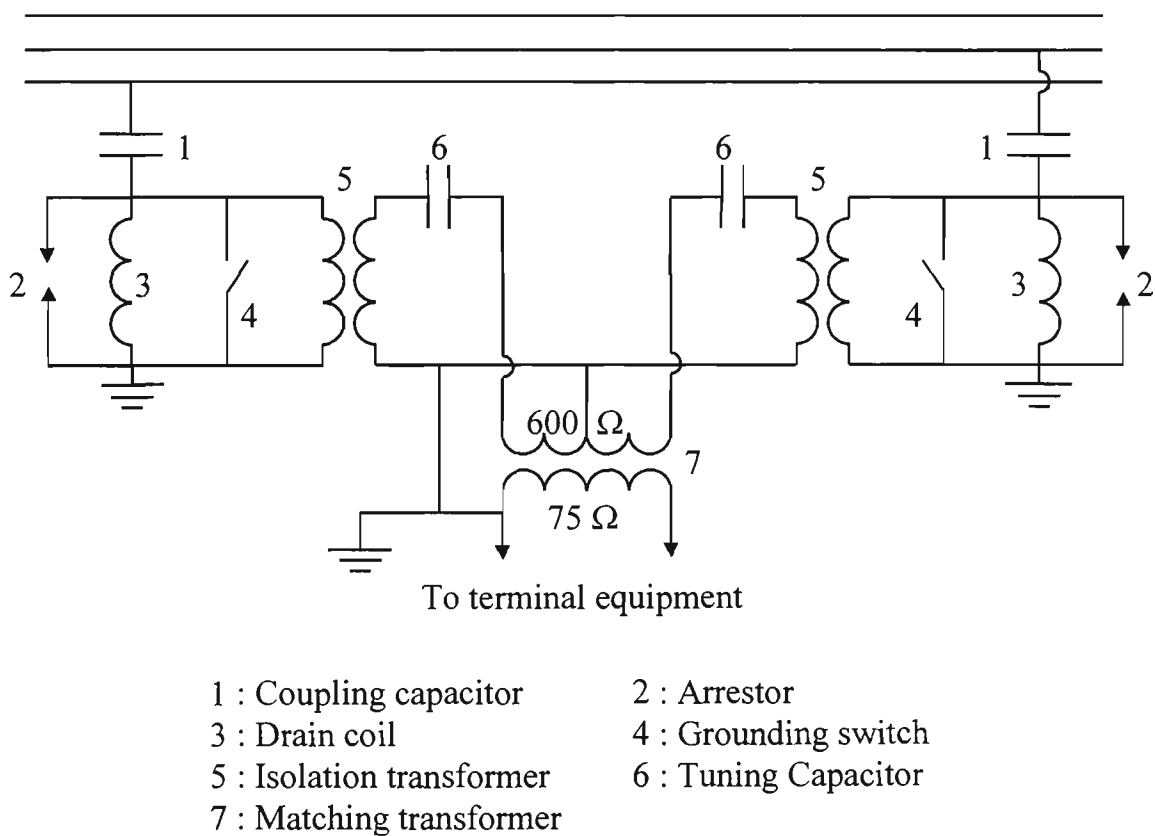Figure 3.3 *Typical coupling equipment schematic for phase-phase coupling.*

For wideband coupling capacitors and CVTs the capacitance is usually 4000 pF or more. Figure 3.3 illustrates a typical phase to phase PLC coupling configuration. The drain coils, typically 1 to 3 mH, are short circuit at power frequencies but high impedance at carrier frequencies. The matching transformer converts from the

unbalanced 75 Ω of the communications room to the balanced 600 Ω of the power lines. The tuning capacitor is used to match the transmitter impedance with the line impedance at the carrier frequency.

3.3.5 Line Traps

The carrier coupling circuitry must be placed on the line side of any protective relays so that the PLC communications is not effected if the relays open. To minimise carrier energy being dissipated in the unknown impedance of the substation, high impedance chokes or line traps are inserted between the substation relay and the carrier coupling point [34]. Figure 3.4 illustrates the circuit for a typical broadband line trap.

Figure 3.4 *Circuit schematic for a broadband line trap.*

At power frequencies the traps have low impedance due to L_1. The traps are tuned to a frequency

$$f_0 = \frac{1}{2\pi\sqrt{L_1C_1}} = \frac{1}{2\pi\sqrt{L_2C_2}}$$

At this frequency the line trap is purely resistive with resistance R. With $R^2 = \omega_0^2 L_1 L_2$ the imaginary impedance of the line trap also has maximum impedance R. Figure 3.5 shows how the impedance of a broadband line trap varies with frequency. Narrow band line traps are also used, attenuating the specific frequencies that are in service on a particular line.

Figure 3.5 *Impedance characteristics of a typical line trap used on EHV lines.* X_r = *real impedance,* X_i = *imaginary impedance.* R = *800* Ω, L_1 = *0.2 mH,* L_2 = *2.0 mH,* C_1 = *3.12 nF* C_2 = *0.312 nF*

3.3.5.1   Frequency Planning

Line traps provide across station attenuation of about 20 dB [33]. This prevents re-using the same frequency on line sections terminating at the same station. Usual practice is to re-use frequencies only when they are separated by two complete line sections. However the high number of services and the limited bandwidth has forced frequencies to be repeated when the stations are separated by only one full line section.

3.4   CHARACTERISTICS OF EHV LINES AT PLC FREQUENCIES

The aim in this section is to give enough detail for PLC communications system design which is summarised in section 3.6.

3.4.1 Line Configurations

In Australia power line carrier sources operate on 22 kV, 33 kV, 66 kV 132 kV, 220 kV and 500 kV lines [33]. Line geometry falls into three main categories.

1. Vertical: three phases one above the other.

2. Flat: three phases horizontal.

3. Triangular: two phases one above the other on one side of the tower and the third phase on the other side of the tower, usually vertically in the middle of the other two phases.

To equalise mutual inductances between different phases of a three phase power system, the lines are cyclically permutated (transposed), at equally spaced intervals over the line length, as illustrated in Fig. 3.6.

Figure 3.6 *Equally spaced transpositions on a typical EHV line.*

3.4.2 Modal Propagation

The mathematics of multi-phase wave propagation at carrier frequencies is called the theory of modal analysis and is treated in detail in chapter 5. Here a brief qualitative description is given [37] [38].

A signal imposed at one end of an n phase power line will separate into n different characteristic modes of propagation along the line. This will happen however the signal is coupled onto the lines because of the cross-coupling between the lines at PLC frequencies. Each mode consists of voltages on each of the lines and has its own propagation constant

$$\gamma_i = \alpha_i + j\beta_i$$

where α_i is the attenuation per unit length, β_i = is the phase shift per unit length of mode i which travels at a speed v_i at frequency f. The manner in which any signal is resolved into its modal components, the modal propagation constants and the line characteristic impedance may all be derived from the theory of modal analysis and so all depend upon

- ♦ the frequency

- ♦ the line geometry

- ♦ the earth resistivity

- ♦ the self and mutual impedances of the lines.

Typically one mode has less attenuation than the other modes which die away as the signal travels down the line. Hence it is possible to talk of an average line propagation speed v and an average line attenuation α. However all modes are regenerated at transpositions and the line ends.

3.4.3 Characteristic Impedance

As discussed in chapter 5 the characteristic impedance of a multi-phase line can be derived from the mathematical theory of modal analysis and so is dependent upon the parameters listed in the previous section. However for design purposes, Table 3.2 summarises typical values for many lines [36].

Table 3.2 *Approximate characteristic impedance of different line types*

Conductor	Phase-to-phase characteristic impedance (Ω)
Single	650-800
2 wire bundle	500-600
4 wire bundle	420-500

3.4.4 Attenuation

Line attenuation depends upon several factors, as listed [36] [37].

1. *Line Geometry* Attenuation increases with d/h, where d and h are the geometric mean spacing and height respectively.

2. *Conductor Parameters* The attenuation depends upon the internal geometry, the construction materials and conductor bundling.

3. *Ground Wires and their Construction* Ground wires have small effect for phase to phase coupling.

4. *Earth Conductivity* The contribution of earth conductivity is calculated by using infinite series developed by Carson [39].

5. *Transpositions* Two to four transpositions attenuate the signal by about 8 dB. There are usually two transpositions per line.

6. *Line Voltage* Higher voltage lines usually have lower loss at carrier frequencies because the higher insulation level reduces leakage and dielectric loss.

7. *Method of Coupling* Phase to phase coupling between adjacent lines has lower attenuation than coupling between outer phases or phase to ground coupling.

8. *Frequency* Attenuation increases exponentially with frequency. Typical values are 0.01 → 0.08 dB/km at 50 kHz to 0.04 → 0.3 dB/km at 200 kHz.

9. *Weather Conditions* Adverse weather can increase attenuation by 15 dB.

10. *Coupling and Shunt Losses* Coupling losses are losses in the resistive components of the line coupling circuitry and are of the order of 3 dB at each end of the line. Shunt losses are due to leakage paths to ground and depend upon the line trap impedance. These losses can vary from 1 to 3 dB - the high values occur at lower values of trap impedance (400 Ω).

The above considerations are generalisations averaged over many different line types. On a given EHV transmission line, reflections, resonances and cross-coupling can produce large effects. Simulation results are presented in chapter 5.

3.4.5 Noise

Power line noise consists of two types, corona noise and impulsive noise [36] [37] [40].

3.4.5.1 Corona Noise

Corona noise, which is always present on power lines, is composed of many individual discharges along the line, particularly during the positive peaks of the mains cycle. Consequently corona noise has strong power frequency harmonics, especially the third harmonic. Corona noise is present in the whole PLC frequency range up to 500 kHz, the amplitude decreasing slowly as the frequency increases. Bundled conductors are used on EHV lines to limit power transmission losses and radio interference caused by corona discharges.

3.4.5.2 Impulse Noise

Impulse noise is caused by switching processes, atmospheric discharge and flashovers, and has the nature of high amplitude voltage spikes superimposed on the always present white corona noise. Each impulse lasts for microseconds producing a wide noise spectrum covering the whole PLC band.

Quasi-peak noise measuring instruments have a circuit with a fast charge time and a slow discharge time. Hence the quasi-peak noise voltage is related to the peak value and also the impulse repetition rate. Typical quasi-peak noise levels in a 3 kHz bandwidth at 140 kHz into 75 Ω are listed in Table 3.3. These are minimal fair weather levels - adverse weather can increase the noise by 25 dB.

Table 3.3 *Typical EHV noise levels measured in communications room*

Line Voltage (kV)	Noise Power in 3 kHz Bandwidth (dBm)
34.5 → 161	-46
230 → 345	-39
500	-37
765	-30

3.5 REQUIREMENTS OF A FAULT LOCATOR USING PLC

A remote sensing system using the PLC network should ideally fulfil the following conditions.

1. It must operate in the high noise environment of power lines and not be affected by the modal distortion inherent in multiconductor propagation at PLC frequencies.

2. It must not displace existing communication channels occupying the limited spectrum.

3. It should be capable of operating over the entire length of the line with high accuracy (to within one tower) and discrimination of multi-path reflections.

4. It must not be affected by the strong in-band interference provided by concurrently operating PLC channels.

3.6 PLC TRANSMIT POWER AND SNR CALCULATIONS

In this section design equations are given for a fault locator that uses the PLC equipment to send a waveform down an EHV line and record signals reflecting back off the line to the sending end [37].

As stated in section 3.4.4 it may be assumed that a signal transmitted down an EHV line suffers 6 dB coupling and shunt losses, both losses being one way, and 8 dB loss through two to four transpositions. We now estimate the attenuation imposed upon a signal when it reflects off a fault on a long line.

Figure 3.7 illustrates a signal reflecting off a single phase-ground fault of resistance R_F. The fault is located in the centre conductor of a horizontal 3-phase system. Using the simplified modal analysis of [38] we may assume that only mode 3 voltages are incident upon the fault. The instantaneous reflected voltage V_r will be on conductor 3 (phase 3) only. However as this phase voltage travels back down the line it will decompose into its modal components, and only the mode 3 component will have sufficiently low attenuation to survive at some distance from the fault.
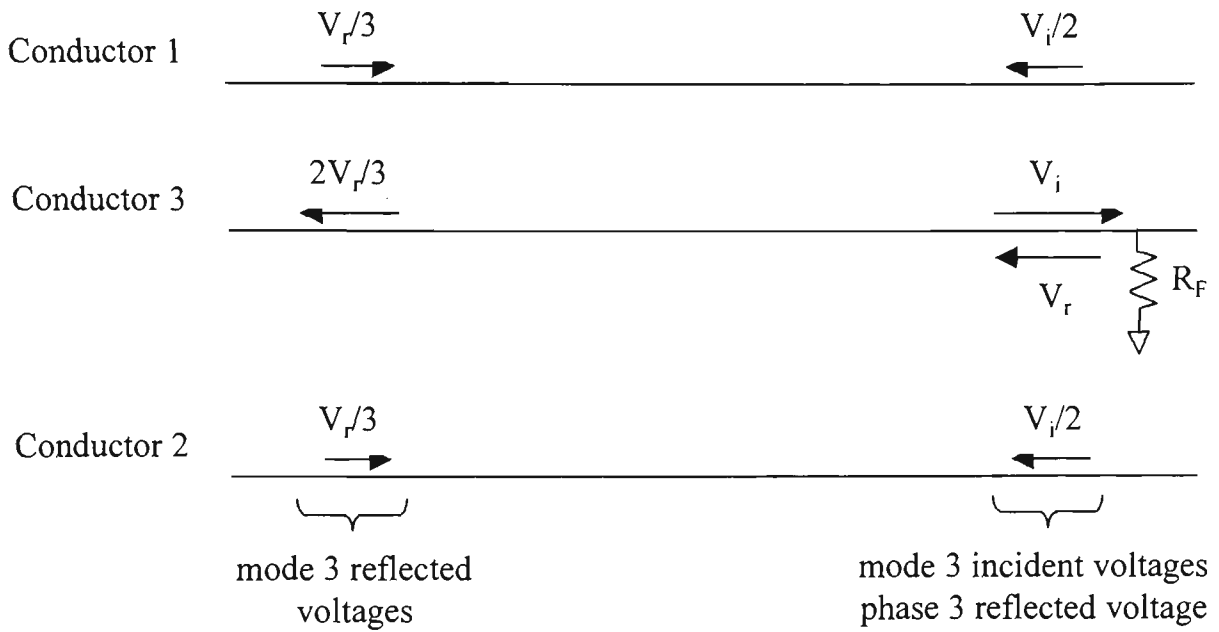
Conductor 1 — $V_r/3$ → ... $V_i/2$ ←

Conductor 3 — $2V_r/3$ ← ... V_i → ... V_r ← R_F

Conductor 2 — $V_r/3$ → ... $V_i/2$ ←

mode 3 reflected
voltages

mode 3 incident voltages
phase 3 reflected voltage

Figure 3.7 *Travelling waves reflecting off a single phase-ground line fault.*

$$\begin{bmatrix} -V_i/2 \\ -V_i/2 \\ V_i \end{bmatrix} = \text{incident phase voltages (mode 3)}$$

$$V_r = \frac{R_f - R_0}{R_f + R_0} V_i = \text{reflected voltage (phase 3 only)},$$

where $R_0 = 300\,\Omega$ = the phase - ground characteristic line impedance

$$\begin{bmatrix} V_r/3 \\ V_r/3 \\ -2V_r/3 \end{bmatrix} = \text{reflected phase voltages (mode 3) at some distance from the fault}$$

Anticipating the notation of Section 5.5.1.1

$$\begin{bmatrix} 0 \\ 0 \\ -V_r \end{bmatrix} = \begin{bmatrix} 1 & 1 & -\frac{1}{2} \\ 1 & -1 & -\frac{1}{2} \\ 1 & 0 & 1 \end{bmatrix} \begin{bmatrix} -V_r/3 \\ 0 \\ -2V_r/3 \end{bmatrix}$$

Combining these equations we can derive the phase 3 signal attenuation of the reflection off the fault as

$$20\log_{10}\left(\frac{\frac{2Vr}{3}}{Vi}\right) = 20\log_{10}\left(\frac{2}{3}\left|\frac{R_f - R_0}{R_F + R_0}\right|\right)$$

This equation is evaluated in Table 3.4 for different fault resistances R_F.

Table 3.4 *Attenuation of phase 3 fault reflection*

Fault Resistance R_F (Ω)	Attenuation of Fault Reflection (dB)
0	3.5
50	6.4
100	9.5

Assuming an average figure of 6 dB signal loss in reflecting off a fault, the received power P_{RX_F} (in dBm) reflected back to the sending end is given by

$$P_{RX\_F} = P_{TX} - 26 - 2\alpha x \qquad \textit{Equation 3.1}$$

where P_{TX} is the transmitted power, α is the attenuation (dB/km) and x is the distance to the fault from the sending end. Also $P_{RX\_F} = SNR + N$, where N is the noise power entering the receiver (in dBm) and SNR is the signal to noise ratio for the fault reflection. Hence

$$P_{TX} = SNR + N + 26 + 2\alpha x \qquad \textit{Equation 3.2}$$

so that the attenuation, line length, noise and the required SNR at the receiver gives the required transmit power.

3.6.1 Pulse Waveforms

Here we look at the performance of the line profiling technique which transmits a short burst of RF down the line and records echoes.

Maximum Range When a single rectangular pulse is used for ranging the maximum range for a given P_{TX}, SNR, α and $N = BN_0$, may be determined from Equation 3.2. Here B is the RF bandwidth and N_0 is the noise power per Hz.

Resolution The resolution and minimum range is determined by the pulse width - to be able to pick out impedance discontinuities close to the transmitter a short pulse width is necessary. In the PLC environment the minimum pulse width will be set by the available bandwidth.

Accuracy The range accuracy of the rectangular pulse waveform is [32]

$$\delta x = \frac{c}{4} \frac{1}{B\sqrt{S/N}}$$
Equation 3.3

where S is the power entering the receiver from the pulse reflecting off the fault and N is the noise power entering the receiver. In the PLC situation the bandwidth B will be set by external constraints so that the only way to increase the accuracy is to increase the transmit power. Existing PLC amplifiers may not be able to provide the necessary peak power and even if they could, the high peak powers would cause interference to other PLC communication channels. The situation can be improved by repeating the transmission and averaging the results, but this lengthens the response time.

3.7 CONCLUSION

Power line carrier exists on most EHV lines. They are currently used for signalling, communication and protection purposes. However the infrastructure used to support PLC applications could also be used to support active fault location techniques with very little additional capital expenditure. Fault location using the PLC system with conventional waveforms requires a high SNR. For a fixed bandwidth the only way to increase the range coverage and accuracy is to increase the transmit power (high peak power amplifiers are expensive and cause interference). To improve maximum range coverage and accuracy without compromising system compatibility, different sensing waveforms which can operate at a lower SNR are required. These different waveshapes are analysed in Chapter 4.

4. PLC TIME DOMAIN REFLECTOMETRY WAVEFORM DESIGN AND SIGNAL PROCESSING

4.1 INTRODUCTION

Following a survey of PLC communications on EHV lines Chapter 3 ended with the conclusion that an active fault location method using the PLC channel must use waveforms that provide satisfactory SNR without interfering with concurrently operating PLC communication links.   This chapter reviews the active sensing waveforms that could be suitable for application on a PLC network and introduces the advantages of spread spectrum signals on EHV lines. Waveform design objectives are listed in section 4.2 and section 4.3 details optimal signal processing techniques for active remote sensing.   Section 4.4 applies these techniques to evaluating the suitability of different waveshapes.   Conventional fault locating waveforms are reviewed in section 4.5 and spread spectrum waveshapes and their advantages are introduced in section 4.6.   Sections 4.7 briefly looks at frequency modulated waveforms and section 4.8 considers in detail ranging with phase coded signals. Finally system design equations for ranging using spread spectrum signals in the PLC environment are detailed in section 4.9 and conclusions are drawn in section 4.9.

4.2 WAVEFORM DESIGN OBJECTIVES

The waveform design considerations are listed below and are common to any radar-like active probing technique [41] [42] [43].   Where appropriate the application of these general criteria to EHV line sounding is highlighted - quantitative PLC system design calculations are detailed in section 4.9.

1. *Signal Energy* From Equation 3.2 the transmit power depends upon the required received SNR of the waveform reflecting off the fault, the noise level, the line attenuation and the line length. For the sensing signal to detect targets, and for the signal processing to accurately estimate target parameters, the total energy in the transmit signal must be above a certain minimum which depends upon these factors.

2. *Accuracy*   This is the error involved in the estimated distance to the fault. An accuracy down to one span is acceptable for EHV lines, because most faults are on or near the pylons.

3. *Resolution*   The resolution is a measure of how close two impedance discontinuities can be and still be distinguished. A resolution down to one span would be ideal.

4. *Sensitivity*   The ability to detect small amplitude variations in a signal reflected from a given point on the line is called the sensitivity of the technique - this is the same as being able to detect a small change in fault resistance.

5. *Dynamic Range*   Signals of many different strengths will enter the remote sensing receiver - the dynamic range gives the ratio of the maximum to minimum signal strength that can be detected by the receiver. In practice this refers to the capacity to measure small signal reflections in the face of high level interference. From section 3.3.3.1 there may be up to 0.25 W of interference from other PLC channels, which sets the maximum signal entering the receiver, and the minimum recordable signal will be determined by the noise floor.

6. *Measurement Time*   The time taken to profile a line is strongly related to the dynamic range. Averaging, for example, takes time, but increases the dynamic range.

7. *Clutter Rejection*   Any undesired reflection entering the receiver is called clutter. Some clutter is desirable for accurate fault location because it can be used for distance calibration.   Reflections from the EHV line transpositions are suitable for this purpose. Clutter can be removed by subtracting the received line profile from that of a healthy line. Any change in line profile from that of the normal line is of interest.

8. *Ambiguities*   Range ambiguities are returns from different ranges that cannot be distinguished and are obviously undesirable. Multiple reflections on the power line are a potential cause of such problems.

9. *Blind Ranges*   If a fault is in a blind range reflections from the fault cannot be discerned. For example if the receiver is turned off while the transmitter is sending out a short pulse.

10. *Range Coverage*   Ideally the technique should be able to detect faults over the whole length of the line. The coverage should not go beyond the line and be affected by faults on other lines into the substation.

11. *Range Sidelobe Level* In any bandlimited system the signal processing can produce spurious reflection peaks or sidelobes. These may be minimised by proper waveform design.

12. *Interference Rejection* The ability of the waveform and signal processing to maintain the integrity of delicate reflections in the face of unwanted noise and interference. The PLC channel is a high noise environment and existing voice, data and protection channels cause strong narrowband interference.

13. *Signal to Noise Ratio* The waveform must be designed for an appropriate SNR to accurately distinguish the line characteristics in the presence of noise and interference.

4.3 SIGNAL PROCESSING CONCEPTS

4.3.1 Matched Filters and the Auto-correlation Function

The following short summary comes from [44].

The (peak instantaneous) signal power to (mean) noise power ratio for an echo returning after a time delay of τ sec may be maximised by processing the received waveform through a matched filter which has a frequency response given by

$$H(f) = \frac{1}{N_i(f)} \frac{R^*(f)}{N_i^*(f)} \exp(-j2\pi f\tau) \qquad \text{\textit{Equation 4.1}}$$

where

   $r(t)$ = received signal

$$R(f) = \int_{-\infty}^{+\infty} r(t)\exp(-j2\pi ft)dt \quad \text{is the Fourier Transform of } r(t)$$

   $N_i(f)$ = noise frequency spectra (assumed stationary)

   * denotes complex conjugate

   τ = delay between transmitted signal and received signal

Clearly, to determine many different values of the unknown parameter τ, a bank of filters would be required. Assuming

   (a) the noise is white

(b) the received signal is an attenuated duplicate of the transmitted signal delayed by a time τ

then the output of the matched filter $y_m(\tau)$ can be shown to be equivalent to the cross-correlation between the received signal and a copy of the transmitted signal, s(t), delayed by time τ :

$$y_m(\tau) = \int_{-\infty}^{+\infty} r(t)\,s(t-\tau)\,dt$$

4.3.2 Optimal Filters for Detection in Clutter

On EHV lines the clutter is stationary so that it is reasonable to assume that the clutter frequency spectrum is identical to the received spectrum. Assuming for the moment that the clutter is the only source of interference

$$N_i(f) = kR(f)$$

Substituting into Equation 4.1 and neglecting time delay, we get that the optimal filter has a frequency response given by

$$H(f) = \frac{K}{R(f)}$$

This is the Urkowitz filter [45]

Manasse [46] showed that when additional noise is present the transfer function of the optimum filter is given by

$$H(f) = \frac{R^*(f)}{\left(\frac{N_0}{2}\right) + k|R(f)|^2}$$

where

$\quad$ $N_0/2$ is the additive noise power spectral density

$\quad$ k is a constant

Rihaczek [47] extended these results concluding that for a clutter to noise ratio of less than 5 dB, the matched filter is nearly the optimum filter, so that the problem of filter design for clutter rejection reduces to the problem of optimal waveform design for

matched filter processing. In massive interference mismatched filtering degrades the resolution.

4.4 WAVEFORM DESIGN USING THE AUTO-CORRELATION FUNCTION

Waveforms are often classified according to the modulation or waveshape. For reflectometry applications the resolution properties of a waveform are of great importance. In the design of radar waveforms [48], the ambiguity function is used to classify waveforms according to their resolving capabilities for a moving target. In line sensing applications the reflecting targets are stationary, so that the resolving properties of the waveform in the presence of Doppler frequency shift are not important. With stationary targets the ambiguity function reduces to the auto-correlation. function

$$\rho(\tau) = \int_{-\infty}^{+\infty} s(t)s*(t-\tau)dt$$

of the transmitted signal, from which the resolving capacity of a waveform can be determined. Typically the auto-correlation function consists of a large peak for $\tau = 0$ which rapidly falls to a low value for $\tau \neq 0$. The width of this peak determines the resolution of the signal.

4.5 TRADITIONAL WAVEFORMS FOR LOCATING FAULTS

The short summary in this section follows [32] [44] [49].

4.5.1 Single Carrier Continuous Wave (CW) Radar

A single sinusoidal waveform is transmitted onto the line. A hybrid transformer (directional coupler) isolates the received signal from the transmitted signal (Fig. 4.1).
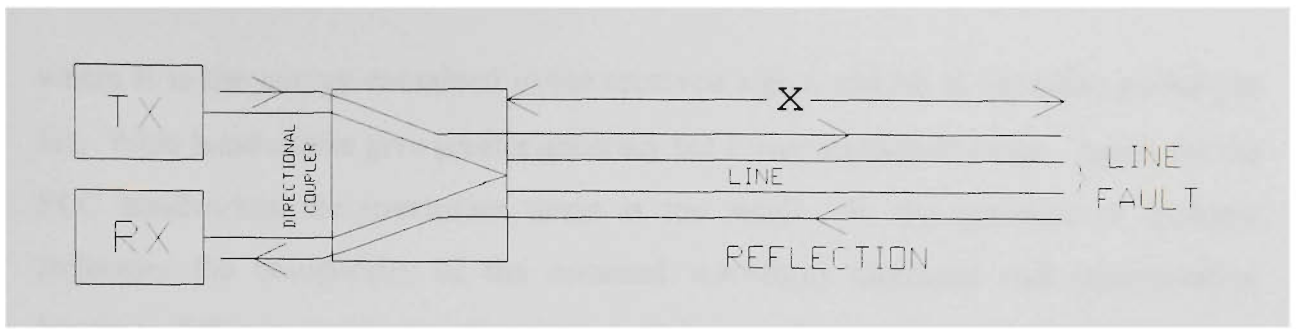
Figure 4.1 *Active sensing of cable fault location.*

The range x is estimated by calculating the phase shift $\Delta\phi$ of the reflected signal relative to the transmitted signal. Assuming that the velocity of propagation is the speed of light c, then the echo travels a distance 2x in time $\Delta\phi/(2\pi f_0)$ to give

$$x = \frac{c\,\Delta\phi}{4\pi\,f_0}$$

The maximum unambiguous range is given by the maximum phase shift of 2π radians which with $f_0 = 40$ kHz gives $x_{max} = 3.8$ km, obviously too low for this application.

4.5.2 Multiple Frequency CW Waveforms

If two continuous sine waves with two different frequencies separated by Δf are transmitted in phase from the sending end, the distance to a reflector may be determined by calculating the phase shift $\Delta\phi$ between the two *reflected* signals. The range is given by

$$x = \frac{c\,\Delta\phi}{4\pi\,\Delta f}$$

and the maximum unambiguous range is again limited by the maximum unambiguous phase shift of 2π to

$$x_{max} = \frac{c}{2\Delta f}$$

The theoretical rms range error is

$$\delta x = \frac{c}{4\pi\,\Delta f\,(2E/N_0)^{1/2}}$$

where E is the energy contained in the received signal and N_0 is the noise power per Hz. Wide bandwidths give greater accuracy but lower maximum range. Again for the PLC bandwidths the maximum range is too small. In the presence of multiple reflectors the complexity of the returned waveform increases and interpretation becomes difficult. Increasing the number of frequencies transmitted reduces the range ambiguities while maintaining accuracy, and the target resolution approaches that obtainable with a pulse of FM-CW waveform.

4.5.3 Repetitive Pulse Waveforms

Substituting $N = BN_0$ and $S = E/T$ into Equation 3.3 it is seen that the conventional rectangular pulse radar with pulse width T and bandwidth B has a theoretical accuracy of

$$\delta x = \frac{c}{2} \sqrt{\frac{T}{4BE/N_0}}$$

Short pulse widths enhance resolution and minimum range performance. In the PLC environment B and hence T will be set by external system constraints. The only way to increase the maximum range coverage and accuracy is to increase the energy transmitted per pulse. High peak powers cause interference and require more expensive transmitter amplifiers to handle the peak signal. Existing PLC transmitter amplifiers might not be able to handle the peak power requirements.

4.6 SPREAD SPECTRUM RANGING TECHNIQUES

4.6.1 Definition of Spread Spectrum

Pulse compression waveforms separate the dependence of range and accuracy performance on broadcast power by spreading the transmitted energy over a longer time interval [50], reducing the peak power rating and cost of the transmitting equipment. By spreading the pulse over a long time interval the low power advantage of the long pulse is combined with the short range performance of the short pulse. Accurate target interrogation depends upon the total energy impinging on the target, not the power.

In addition, the interference to normal PLC operations is reduced and often can be below the natural noise level on the line. Data processing of received echoes contracts the pulse into a shorter duration by means of matched filtering or correlation techniques - the pulse compression ratio is the ratio of the uncompressed to compressed pulse lengths. These spread spectrum signals share the characteristic that the product of waveform bandwidth (B) and waveform period (T_P) must be much greater than unity ($BT_P \gg 1$).

4.6.2 Advantages of Spread Spectrum on EHV Lines

1. The peak power/resolution trade-off of pulse time domain reflectometry is avoided by spreading the transmitted energy over a long time interval.

2. Spread spectrum signals have low power spectral density and so are compatible with narrowband communication links occupying a small part of the spread spectrum bandwidth. In particular spread spectrum will be compatible with already existing narrowband AM and FM power line carrier communication links, together with radio navigation beacons which at present put limitations on PLC communications.

3. Multiple spread spectrum communication links can co-exist inside the same bandwidth together with a spread spectrum fault locator.

4. The correlation techniques used in spread spectrum demodulation perform well in high noise environments.

5. High resolution ranging is possible and multipath effects due to multiple reflections and branches in the transmission line may be distinguished by the correlation method.

6. Wideband signals are less vulnerable to the frequency dependent distorting effects of modal propagation along transmission lines.

7. There is the capability of monitoring the line with or without the presence of the 50 Hz line voltage. Hence clearance of the fault can be determined without closing the main breaker.

8. Reflections/faults on the uncoupled line can be detected by taking advantage of the modal nature of power line propagation. It will be shown later that the

sensitivity is so good that a wide range of fault resistances can be detected even on the uncoupled line.

9. Because of the low power nature of the signal, continuous monitoring of the line is possible without interfering with power or communication networks operating simultaneously.

10. The scheme is insensitive to the variation of the line end source impedances (loading) because of the isolating effects of the line traps.

11. The scheme is not affected by line assymmetry and therefore does not require a fully transposed line as is required by some other schemes. In addition the shunt capacitance of long lines does not effect the accuracy.

The two most common techniques of spread spectrum waveform generation are now described.

4.7 RANGING WITH FREQUENCY MODULATED WAVEFORMS

The most widely used types of frequency modulated waveform are chirp, where the carrier frequency is swept linearly with time, and frequency hopping, where the frequency jumps in a pseudo-random manner [50]. Cable fault location using a chirp waveform has a theoretical accuracy of

$$\delta x = \frac{c}{2 \pi B} \frac{\sqrt{3}}{\sqrt{2E / N_0}}$$

The main problem with this waveform in a power grid network is that it is subject to interference from other chirp generators.

Frequency hopping waveforms have theoretically the same ranging capability as phase modulated waveforms. Historically, direct sequence (phase modulated) waveforms have been more widely used for ranging because of the greater technical difficulty in constructing high hopping-rate synthesisers.

4.8 RANGING WITH PHASE CODED WAVEFORMS

A direct sequence waveform is generated by dividing a long carrier burst into a number of subpulses of equal duration but different phases varying in a periodic manner set by a finite periodic code [50]. Unlike chirp modulation, different direct sequence waveforms can co-exist in the same spectrum since each waveform is identified by its unique repeating code. Spread spectrum modulation methods have been previously proposed for protection signalling links on power lines [51].

The inverse of the time duration of each subpulse is called the chip rate (R_c). The simplest modulation is biphase shift keying (BPSK) where the phase jumps between 0 and 180 degrees [50]. Signal analysis of the received waveform reveals the time delays and magnitudes of the various reflected codes. Each code shift corresponds to a different distance to the impedance discontinuity causing the reflection. The amplitude of the reflected code is related also to the magnitude of the impedance change. As illustrated in Fig. 4.2 the received waveform r(t) consists of leakage from the transmitter through to the receiver together with the sum of all the different return echoes.

Neglecting the signal distortion caused by the line interface and line transfer function, the on-line transmit signal is $A_T s(t)$ and the leakage term is As(t), where A_T and A are scaling factors. Also disregarding the modal distortion of multiconductor propagation we may assume the received echoes to be time delayed scaled copies of the transmit waveform s(t)
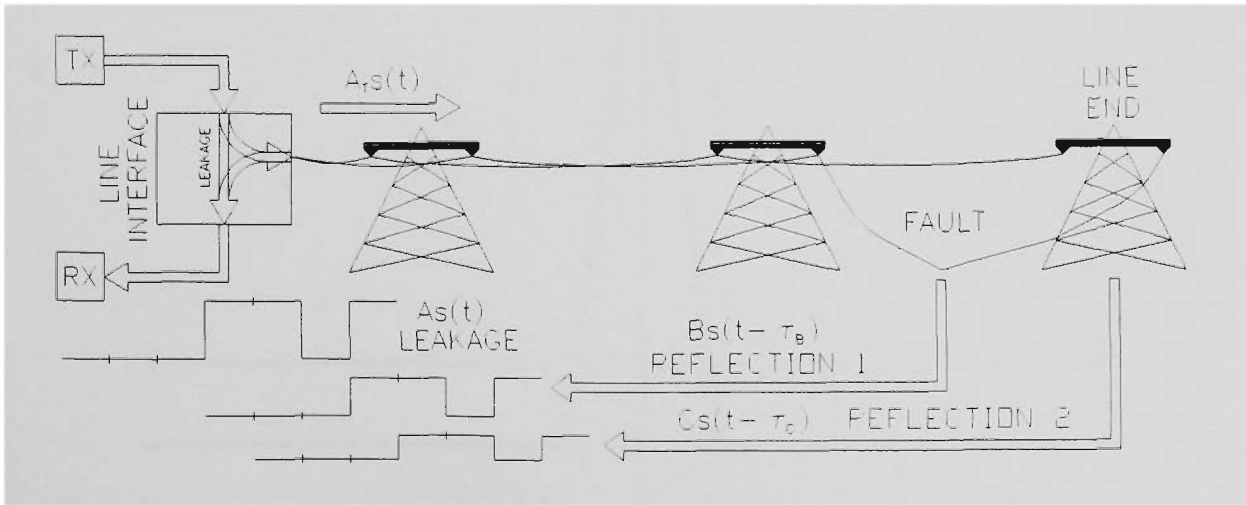

Figure 4.2 *Codes entering the receiver have different time delays and magnitudes.*

$$r(t) = As(t) + Bs(t\text{-}\tau_B) + Cs(t\text{-}\tau_C) + \ .....$$

where B, C,.... are the strengths of the returned signals and τ_B, τ_C, ... are their respective time delays.

4.8.1 Maximal Length Sequence codes

Maximal length sequence (MLS) codes, also known as m-sequences or PN (Pseudo-Noise) codes, are considered for their good auto-correlation function properties as illustrated in Fig. 4.3.

These are repeating sequences of length $L = 2^n - 1$, where n is the length of the shift register used in their generation (see [50] for more details). When used for ranging the sequence period $T_P = L/R_c$ should exceed the round-trip time taken for the smallest recordable (multiple) echo to reach the receiver. Normally $T_P \gg 2D/v$ where D is the line length and $v \approx c$ is the speed of propagation of the wave. This will eliminate range ambiguity problems. The chip rate determines the resolution of the technique and bandwidth occupancy of the signal as illustrated in Table 4.1. Fault positions may be measured to within the distance travelled by the code during one half of a bit period. Shorter duration bit periods (higher chip frequencies) give greater range resolution and clutter rejection at the expense of increased bandwidth.
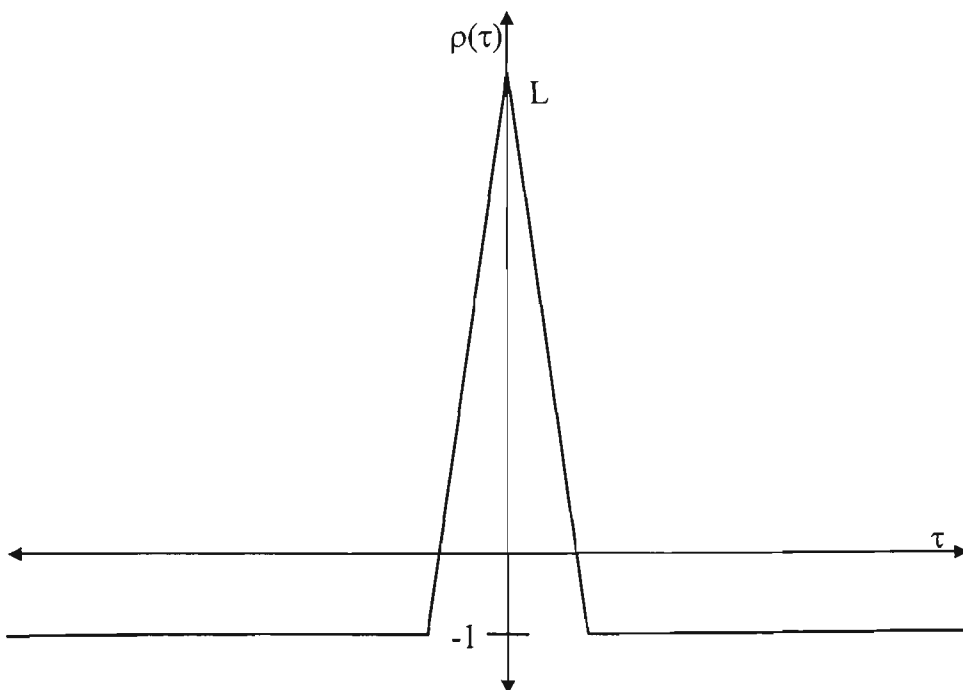

Figure 4.3 *Auto-correlation function of maximal length sequence code of length L*

Table 4.1 *Performance parameters of bandlimited PN code BPSK waveforms used in ranging.*

time resolution	$\approx 1/R_c$
distance resolution	$\approx v/(2R_c)$
bandwidth	$2R_c$
waveform period T_P	$(2^n - 1)/R_c \gg 2D/v$

Figure 4.4(a) shows a block diagram of the signal generation process and Fig. 4.4(b) shows typical waveforms. For clarity the waveforms shown in Fig. 4.4(b) are for a carrier frequency f_0 = 133.33 kHz, a chip rate R_c = 66.67 kHz and a sampling frequency f_s = 2 MHz, giving 30 samples per chip.

PN codes have a $[\sin(x)/x]^2$ power spectral density envelope with spectral nulls at multiples of the chip rate R_c. A pulse shaping filter of bandwidth R_c limits the code spectrum to the mainlobe. The transmit waveform is

$$s(t) = u(t)\sin(2\pi f_0 t)$$
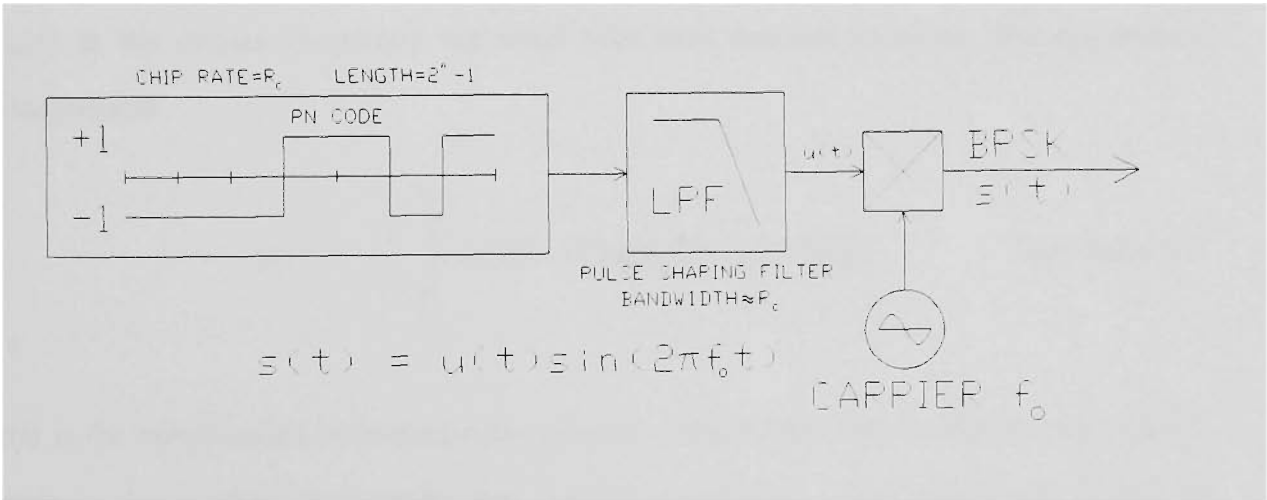
where u(t) is the bandlimited code (lowpass filtered).

Figure 4.4(a) *Generation of the spread spectrum transmitted signal s(t).*

4.8.2 Data Analysis

In our case the transmit waveform $s(t) = u(t)\sin(2\pi f_0 t)$ is periodic with period T_P and so the integration need only be performed over one period. To avoid oscillations in
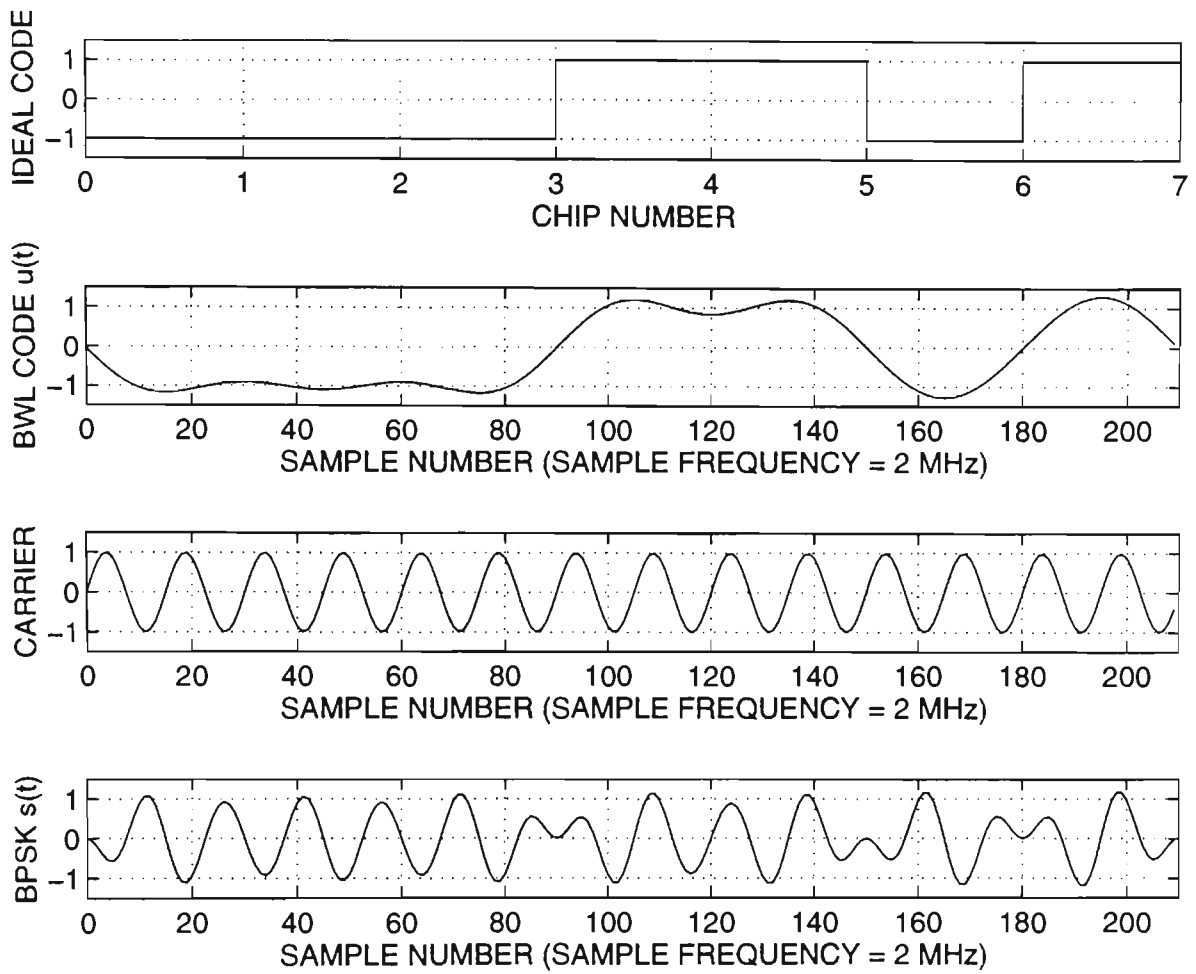
Figure 4.4(b) *Typical waveforms used in generating a mainlobe bandwidth limited (BWL) BPSK remote probing signal.*

$y_m(\tau)$ at the carrier frequency we must take into account in-phase and quadrature components

$$y(\tau) = \frac{2}{T_P} \int_0^{T_P} r(t)\, u(t - \tau)\, \exp[-j2\pi f_0 (t - \tau)]\, dt \qquad \textit{Equation 4.2}$$

$u(t)$ is the bandlimited baseband code which is transmitted and the factor $\exp(-j2\pi f_0 t)$ imposes the in-phase and quadrature carrier components. The magnitude $|y(\tau)|$ of the above equation is the desired output function. The modified receiver processing is illustrated in Fig. 4.5 - the factor $2/T_P$ is a scaling factor that ensures that each peak in the correlation coefficient $|y(\tau)|$ (also called the compressed waveform) is approximately the same magnitude as the magnitude of the corresponding echo in $r(t)$
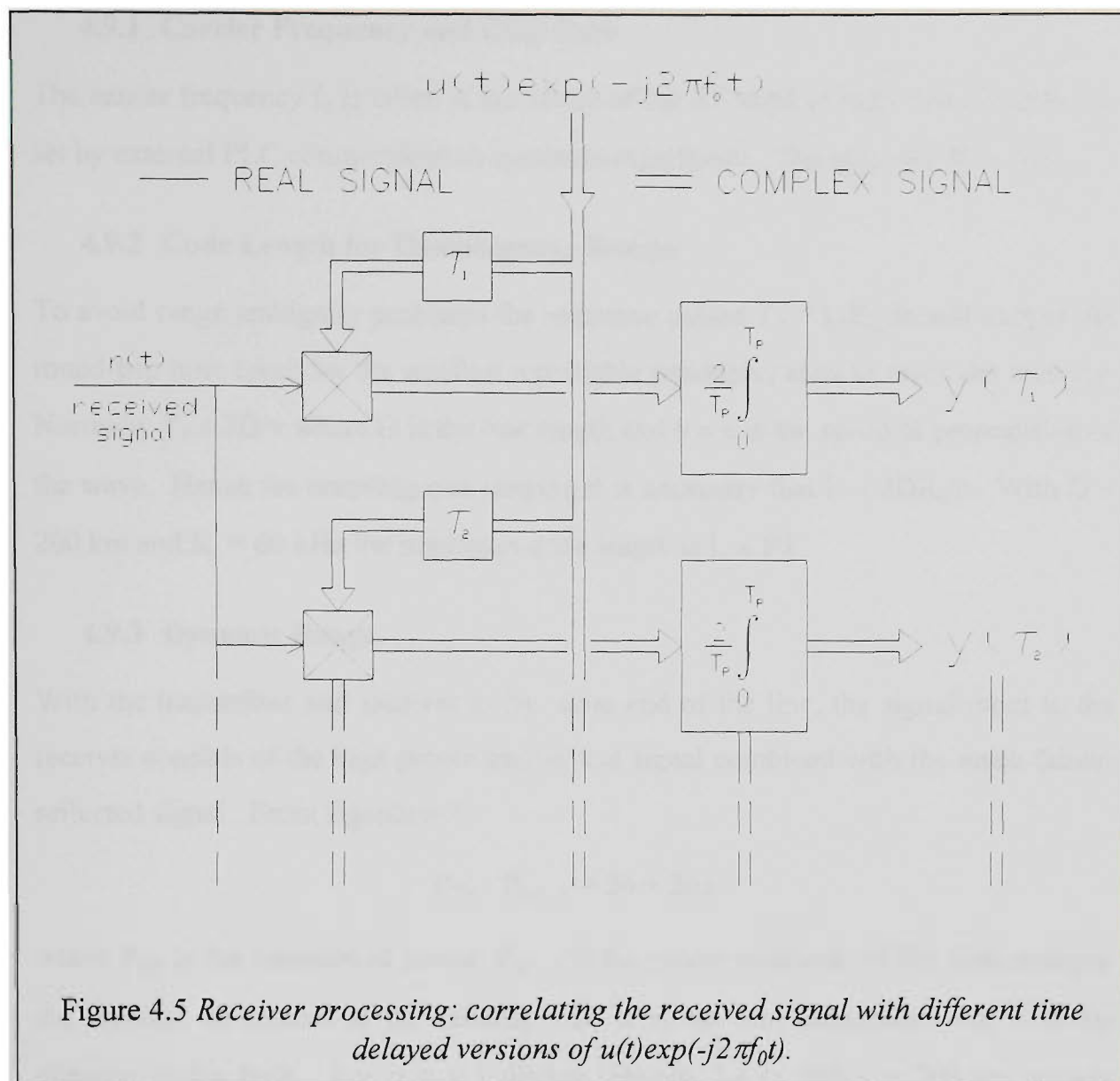
$$u(t)\exp(-j2\pi f_0 t)$$

—— REAL SIGNAL   ═══ COMPLEX SIGNAL

Figure 4.5 *Receiver processing: correlating the received signal with different time delayed versions of u(t)exp(-j2πf₀t).*

causing the peak. This processing is hardware intensive for real time operation but is easily done in software if the processing time is available.

4.9 SPREAD SPECTRUM SYSTEM DESIGN FOR PLC REFLECTOMETRY

In this section design parameters are given for EHV line sounding using direct sequence spread spectrum waveforms. To experimentally investigate the feasibility of spread spectrum fault location a hardware transmitter and receiver is required. For maximum flexibility digital signal processing techniques have been decided upon with D/A and A/D data converters in the transmitter and receiver respectively - hardware memory requirements are derived. For the initial measurements data analysis will be done in none real time on a mainframe.

4.9.1 Carrier Frequency and Chip Rate

The carrier frequency f_0 is taken at the centre of the RF band of bandwidth B which is set by external PLC communication system compatibility. The chip rate $R_c = B/2$.

4.9.2 Code Length for Unambiguous Ranges

To avoid range ambiguity problems the sequence period $T_P = L/R_c$ should exceed the round-trip time taken for the smallest recordable (multiple) echo to reach the receiver. Normally $T_P \gg 2D/v$ where D is the line length and $v \approx c$ is the speed of propagation of the wave. Hence for unambiguous ranging it is necessary that $L \gg 2DR_c/c$. With D = 200 km and R_c = 60 kHz the minimum code length is $L \gg 80$.

4.9.3 Dynamic Range

With the transmitter and receiver at the same end of the line, the signal input to the receiver consists of the high power transmitted signal combined with the much fainter reflected signal. From Equation 3.1

$$P_{TX} - P_{RX\_F} = 26 + 2\alpha x$$

where P_{TX} is the transmitted power, P_{RX_F} is the power reflected off the fault entering the receiver co-located at the sending end, α is the line attenuation and x is the distance to the fault. For α = 0.1 dB/km (section 3.4.4) and x = 200 km we get $P_{TX} - P_{RX\_F}$ = 66 dB, or, in linear voltages

$$V_P/V_{P\_F} = 1995 \approx 2000 \qquad\qquad \textit{Equation 4.3}$$

In order to record the reflected signal with sufficient accuracy in the presence of transmitter feedthrough a 12 bit A/D is required. The fault reflection will then toggle the least significant bit (LSB) of the A/D.

4.9.4 Code Length and Residual Correlation

Figure 4.6 represents a plot of the correlation coefficient $|y(\tau)|$ (from Equation 4.2) vs. time delay τ. The large peak for τ = 0 is due to the transmitted signal coupling directly into the receiver and the smaller peak represents the reflection from the fault.

The magnitude of each peak is proportional to the corresponding voltage entering the receiver, V_P and V_{P_F} respectively (here considered as linear voltages rather than the

logarithmic dBm). Now with an MLS code of length L the code noise floor or residual correlation due to the transmitter feedthrough is V_P/L. In order for the fault reflection to be above the code residual correlation we must have

$$V_{P\_F} \gg \frac{V_P}{L} \Rightarrow L \gg \frac{V_P}{V_{P\_F}}$$

Hence from Equation 4.3 an MLS code of length L $\gg$ 2000 is required.
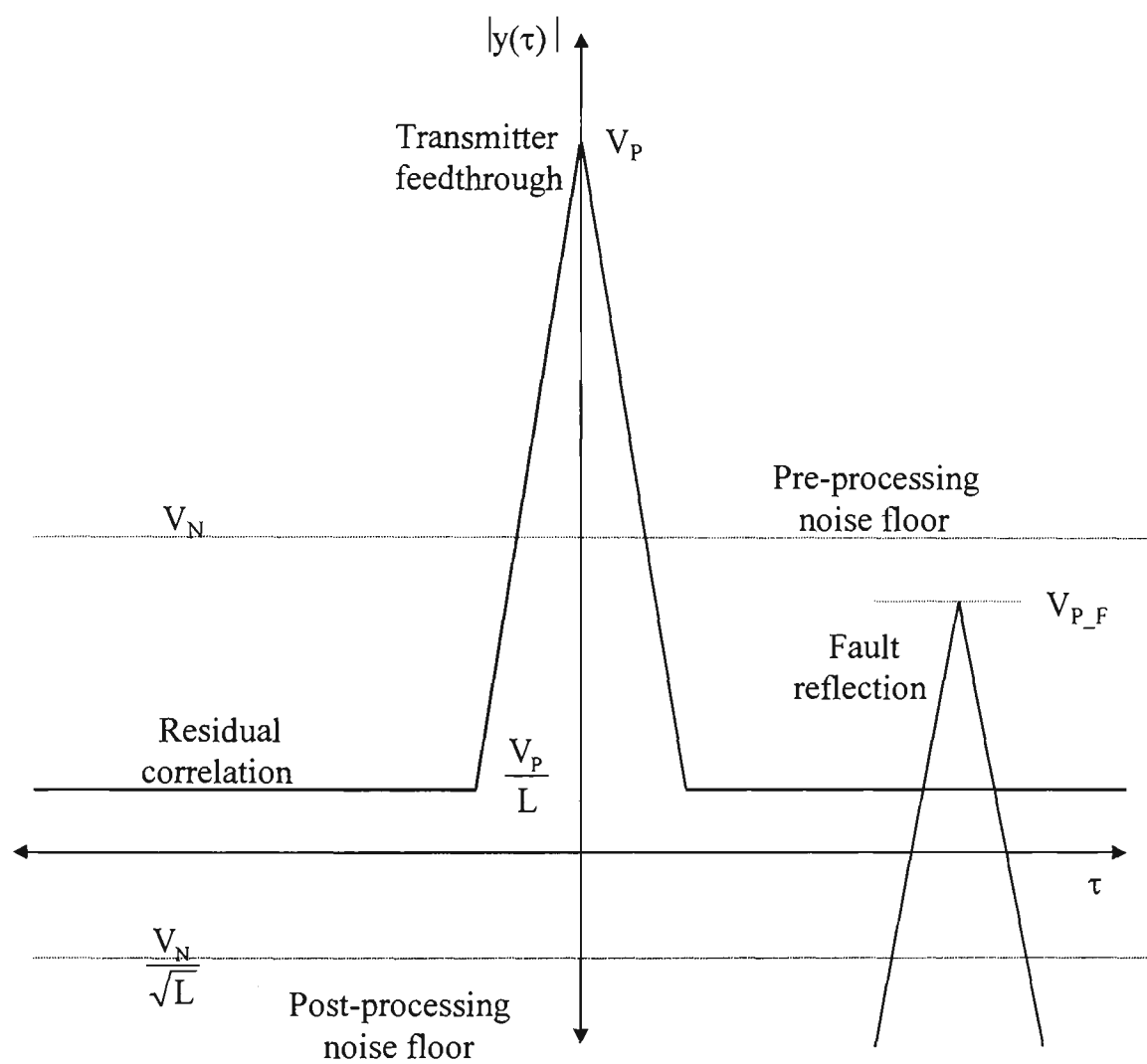

Figure 4.6 *Relative magnitudes of transmitter feedthrough, fault reflection and noise floor.*

4.9.5 Transmit Power and Energy

The post-processing noise floor due to the noise voltage V_N is $V_N/\sqrt{L}$, where V_N is the noise voltage entering the receiver. Referring again to Fig. 4.6 it is seen that we must have

$$V_{P\_F} \gg \frac{V_N}{\sqrt{L}} \qquad \textit{Equation 4.4}$$

Substituting Equation 4.3 into Equation 4.4 we get

$$V_P\sqrt{L} \gg 2000V_N$$

$$\Rightarrow P_{TX} = \frac{\left(V_P/\sqrt{2}\right)^2}{75} \gg \frac{(2000V_N)^2}{150L} \qquad \textit{Equation 4.5}$$

$$\Rightarrow E_{TX} = P_{TX}\frac{L}{R_c} \gg \frac{(2000V_N)^2}{150R_c}$$

where $P_{TX} = \dfrac{\left(V_P/\sqrt{2}\right)^2}{75}$ is the transmit power into the 75 Ω communications room

impedance and E_{TX} is the energy in one period of the transmitted signal.

From Table 3.3 the typical noise level on an EHV line in a 3 kHz bandwidth, as measured in the communications room, may be taken as -35 dBm. With B = 120 kHz, f_0 = 140 kHz and R_c = 60 kHz, N = -35 + 16 = -19 dBm so that V_N = 30.7 mV. Substituting these values into Equation 4.5, with code length L = 2047, the transmit power is $P_{TX} \gg 0.012$ W and the waveform energy $E_{TX} \gg 0.42$ mJ.

4.9.6 Maximum Range

From Equation 3.1 the maximum range is given by (all powers in dBm)

$$X_{max} = \frac{(P_{TX} - P_{RX\_F})_{max} - 26}{2\alpha}$$

With a 12 bit A/D and requiring the fault reflection to toggle the LSB we get $(P_{TX} - P_{RX\_F})_{max} = 6(N_{bit} - 1) = 66$ dB and

$$X_{max} = \frac{20}{\alpha}$$

The range can be increased by improving the A/D dynamic range (more bits or averaging), or reducing the P_{TX} leakage signal by using an effective hybrid (line interface in Fig. 4.2)

4.9.7 Interference Rejection

To combat line noise and PLC channel interference in the receiver we will provide for averaging 4095 code sequence periods to give 36 dB improvement in the SNR. Interference from the transmitted pulse will then be the major factor limiting system performance. Any averaging over and above that necessary to remove the PLC interference will serve to increase the dynamic range of the receiver - this will increase the fault location range.

4.9.8 Sampling Frequency

The minimum sampling frequency is the Nyquist frequency of double the highest frequency in the transmit/receive waveform band. Broadband spread spectrum waveforms require constant group delay filtering - such filters have a poor amplitude fall-off with frequency. Oversampling simplifies the design of the reconstruction and anti-aliasing filters. The sampling frequencies of 2.5 MHz (lower band) and 5 MHz (upper bands) listed in Table 4.2 are for 5th order Bessel filters and give more than 70 dB rejection of aliased frequency components.

4.9.9 Memory Requirements

With a sample frequency f_s the length of memory required for a code of length 2047 is $2047 f_s / R_c$.

4.9.10 Predicted System Performance

In Table 4.2 we predict system performance at three different bandwidths - typical attenuations for a 138 kV line at the given carrier frequencies are taken from [37].

Techniques to further increase the range of the system include

(a) the use of a resistive, inductive or semiconductor hybrid to reduce the magnitude of the transmitted signal entering the receiver

(b) the use of increased dynamic range in the receiver eg. using a 16 bit A/D instead of a 12 bit A/D.

Table 4.2 *System performance at different bandwidths*

	BW1 80 - 200 kHz	BW2 200 - 400 kHz	BW3 80 - 500 kHz
Carrier frequency f_0 (kHz)	140	300	290
Chip rate R_c (kHz)	60	100	210
Attenuation α (dB/km)	0.08	0.15	0.16
Range resolution (km)	2.5 (1%)	1.5 (0.6%)	0.71 (0.3%)
Maximum range (km)	250	133	125
Minimum code length for unambiguous ranging	100	89	175
Sampling frequency f_s (MHz)	2.5	5	5
Memory required for code of length 2047 (kWords)	85.29	102.4	48.74

4.10 CONCLUSION

The objectives of waveform design for reflectometry applications have been detailed and corresponding optimal signal processing techniques (matched filter or correlation techniques) have been given. Spread spectrum signals offer significant advantages over traditional waveforms in the power line environment (cf section 3.5). In particular multiple low power spread spectrum signals can co-exist in the same PLC bandwidth without mutual interference, and transparent to normal PLC and power operation. Accurate line profiling depends upon the total waveform energy rather than the waveform power. With spread spectrum, the energy is spread over a longer time avoiding the high peak powers (causing large interference) required of conventional methods. Also wideband signals are less affected by the frequency dependent distorting effects (resonances, reflections, cross-coupling) inherent in EHV transmission line propagation. These effects will be averaged over the transmission bandwidth and will tend to cancel out.

Design equations have been derived for spread spectrum PLC reflectometry using DSP techniques and performance parameters have been derived. Wider bandwidth codes have higher resolution but lower range due to increased attenuation at higher

frequencies - this will be partly compensated for by the lower noise at higher frequencies. The resolutions in Table 4.2 compare favourably with the 5% resolution attainable with the impedance measuring method currently used by the SECV.

These design equations have ignored the waveform distortion that occurs due to the modal nature of signal propagation down polyphase EHV lines. To investigate these effects, simulation results are presented in chapter 5 for direct sequence waveforms propagating along an EHV line and reflecting off a fault.

5. DIGITAL SIMULATION OF FAULT LOCATION ON EHV LINES USING WIDEBAND SPREAD SPECTRUM TECHNIQUES

LIST OF PRINCIPAL SYMBOLS

The symbols listed below are specific to this chapter. The simulations are for an n = 3 phase line.

Scalar Quantities (real)

$r_k = r(k/f_s)$ = digitised samples of received waveform

v_i = speed of propagation of mode i down line

λ = wavelength

Scalar Quantities (complex)

V_{TX} = Fourier coefficients of direct sequence signal

V_{SS_M} = transform of pre-fault voltage measured at the sending end

V_{S_M} = transform of total fault voltage measured at the sending end

V_{RS_M} = transform of pre-fault voltage measured at the receiving end

V_{R_M} = transform of total fault voltage measured at the receiving end

E_S = transform of voltage input to the line matching unit at the sending end

E_R = transform of voltage out of the line matching unit at the receiving end

Vector Quantities (n × 1)

$\mathbf{V},\mathbf{I}$ = voltage and current transforms

$\mathbf{V_i},\mathbf{V_r}$ = incident and reflected voltage transforms

$\mathbf{V_S},\mathbf{I_S}$ = sending end voltage and current transforms

$\mathbf{V_R},\mathbf{I_R}$ = receiving end voltage and current transforms

$\mathbf{E_F},\mathbf{V_F}$ = transform of total voltages at point of fault

$\mathbf{V_{SS}},\mathbf{I_{SS}}$ = pre-fault sending end voltage and current transforms

$\mathbf{V_{RS}},\mathbf{I_{RS}}$ = pre-fault receiving end voltage and current transforms

$\mathbf{V_{FS}}$ = transform of pre-fault voltage at point of fault

$\mathbf{V_{SF}},\mathbf{I_{SF}}$ = sending end voltage and current transforms due to fault

$\mathbf{V_{RF}},\mathbf{I_{RF}}$ = receiving end voltage and current transforms due to fault

$\mathbf{E_{FF}},\mathbf{V_{FF}}$ = transform of voltages due to fault at point of fault

$\mathbf{I_{FS}},\mathbf{I_{FR}}$ = transform of total currents at point of fault

$\mathbf{I_{FSF}},\mathbf{I_{FRF}}$ = transform of superimposed currents at point of fault

$\mathbf{a_S}$ = transmitter admittance vector

Matrix Quantities (n × n)

γ = propagation constant matrix (diagonal matrix)

$\mathbf{T}$ = transposition matrix

$\mathbf{Z},\mathbf{Y}$ = series impedance and shunt admittance matrices

$\mathbf{Z_0},\mathbf{Y_0}$ = characteristic impedance and admittance matrices

$\mathbf{S}$ = voltage eigenvector matrix

$\mathbf{A_1},\mathbf{B_1},\mathbf{C_1},\mathbf{D_1}$ = matrices defining line section up to point of fault

$\mathbf{A_2},\mathbf{B_2},\mathbf{C_2},\mathbf{D_2}$ = matrices defining line section beyond point of fault

$\mathbf{Y_S}$ = total sending end admittance

$\mathbf{Y_R}$ = total receiving end admittance

$\mathbf{R_F}$ = fault resistance matrix

$\mathbf{U}$ = unit matrix

5.1   INTRODUCTION

In Chapter 4 it was shown that spread spectrum signals offer significant advantages in the PLC environment and introduced reservations about the effect on fault location accuracy of the frequency dependent distortions incurred in signal propagation along EHV lines at PLC frequencies. This chapter presents simulation results for EHV line monitoring using direct sequence spread spectrum waveshapes transmitted and received using the PLC communications network. Section 5.2 overviews the simulation model including waveform generation and data analysis techniques. Section 5.3 details the simulated line interface circuitry and section 5.4 overviews the line model using both transmission parameters and the reflection factor methods. Simulation results from the power line carrier program are detailed in section 5.5 - these show the effects of f_0, R_c, L, x and receiver noise on the correlation function and calculated fault position accuracy and resolution. Finally conclusions are drawn in section 5.6.

5.2   POWER LINE CARRIER FAULT LOCATION SIMULATION MODEL

The simulation program which has been developed can be used to model the steady state voltage distribution established on a polyphase transmission line (both faulted and unfaulted) when any arbitrary periodic waveform is transmitted on a power line carrier (PLC) communication link. The program takes into account line transpositions and models the frequency variation of the line matching units, coupling capacitors, line traps and line parameters. Fig. 5.1 shows the required simulation blocks for sending a periodic BPSK signal down a faulted three phase power line and subsequent data analysis to locate the fault position from the reflected waveform. The transmitted signal and data analysis blocks are both in the time domain, and the DFT/DFT[-1] blocks convert the waveforms to/from the frequency domain for compatibility with the frequency dependent PLC communication model.

5.2.1 Waveform Generation

In this chapter only the maximal length sequence codes [50] are considered because they are simple to generate and the autocorrelation function allows accurate phase measurements. The power spectral density of these codes has a $[\sin(x)/x]^2$ envelope and is bandlimited by the lowpass filter (LPF in Fig. 5.1) so that the direct sequence being transmitted has bandwidth $2R_c$ centred on f_0.

Best results are obtained if the code period is an integral multiple of the carrier period so that the frequency spectrum consists of discrete lines separated by the BPSK repetition frequency R_c/L. Also the sample period should divide the code repetition period into equal intervals, so that the number of sample points in this period is $N_P = (L/R_c)f_s$.

The BPSK Fourier coefficients from the Discrete Fourier Transform (DFT) block are fed into the line interface and power line models which enable the output voltage and phase to be calculated for each separate frequency. The simulation can be performed for both energised and de-energised lines.

5.2.2 Data Analysis

The Fourier coefficients of the required waveform calculated above are treated as phasors and converted to time (DFT^{-1}). This time domain waveform r_k for k = $0,1,..,N_P-1$ is then multiplied by a digitised time shifted copy of the transmitted bandlimited PN code u_k, and this product is passed through a bandpass filter (BPF) centred on f_0 with a bandwidth of R_c/L. This is accomplished by calculating twice the Fourier coefficient at the carrier frequency using the DFT (the subtraction in u_{k-m} is modulo N_P):

$$2\, \Im_{f_0}[r(t_k)u(t_k - \tau_m)] = \frac{2}{N_P} \sum_{k=0}^{k=N_P-1} r_k u_{k-m} \exp(-j2\pi k f_0/f_s) = y(\tau_m)\exp(-j2\pi m f_0/fs)$$

This equation is the discrete form of Equation 4.2, with the $\exp(j2\pi m f_0/f_s)$ term in the summation grouped with $y(\tau_m)$. This does not affect

$$2\left|\Im_{f_0}[r(t_k)u(t_k - \tau_m)]\right| = \left|y(\tau_m)\right| = \left|y(\tau_m)\exp(-j2\pi m f_0/f_s)\right|$$

which in this thesis is referred to as the correlation coefficient and is plotted as a function of sample delay m.

5.2.3 Fault Location Algorithm

This correlation graph consists of a series of peaks, each peak resulting from line reflections - the magnitude of any peak gives the magnitude of the corresponding reflection arriving at the measuring point, and the phase delay of the peak tells us the location of the impedance discontinuity causing the reflection. This may be illustrated by looking at the lattice diagram of Fig. 5.2 which shows the reflection pattern formed on a 100 km double transposed line with a fault at 90 km from the transmitter. The correlation coefficient for the signal at the sending end of an unfaulted line, for example, will consist of peaks corresponding to the signals S0, S1, S2, and so on - the fault will add correlation peaks for the other reflections shown.

Now in general a correlation peak will not line up with a sample delay point so that some form of interpolation is necessary. In the simulation results discussed below the true correlation peak is estimated by fitting a quadratic expression to the point with the local correlation maximum and the two adjacent points. The time delay of the
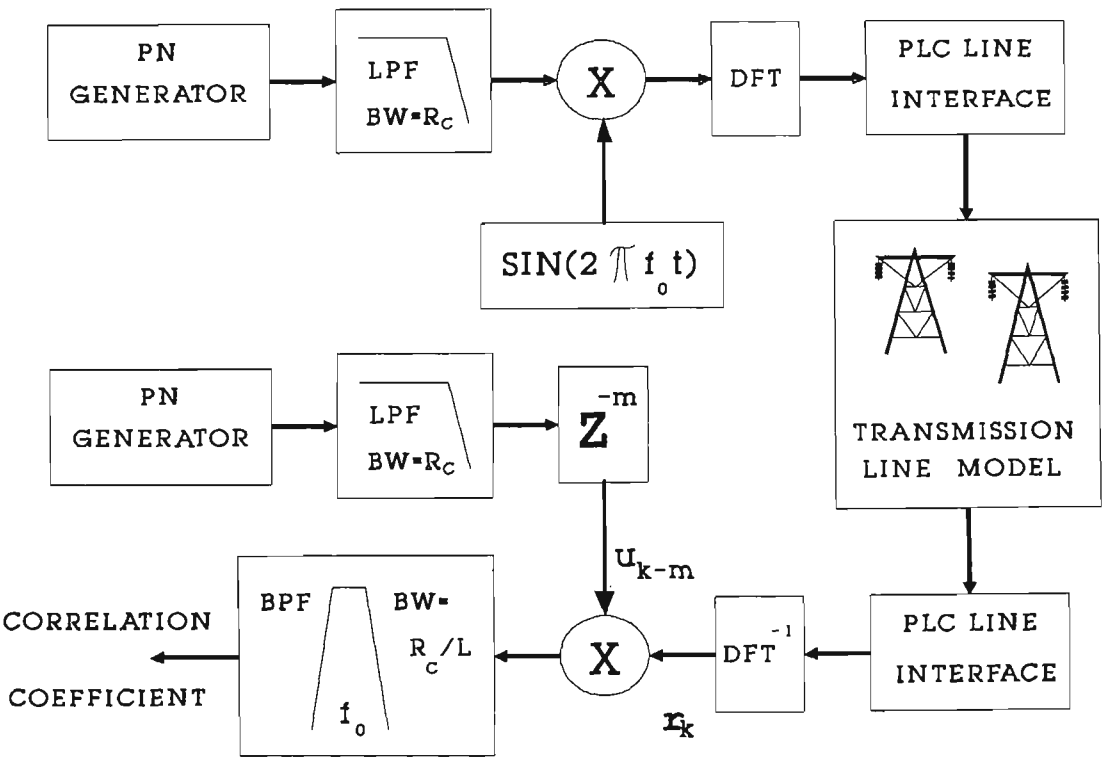

Figure 5.1 *Block diagram of direct sequence fault location simulation.*

quadratic maximum is then taken as the signal phase delay. All fault positions are calculated by comparing the phase delay of the fault reflection with the phase delay of a reference signal which has traversed a known distance. For waveforms at the sending end, for example, the reference may be taken as the primary reflection from the line end (S3 in Fig. 5.2).
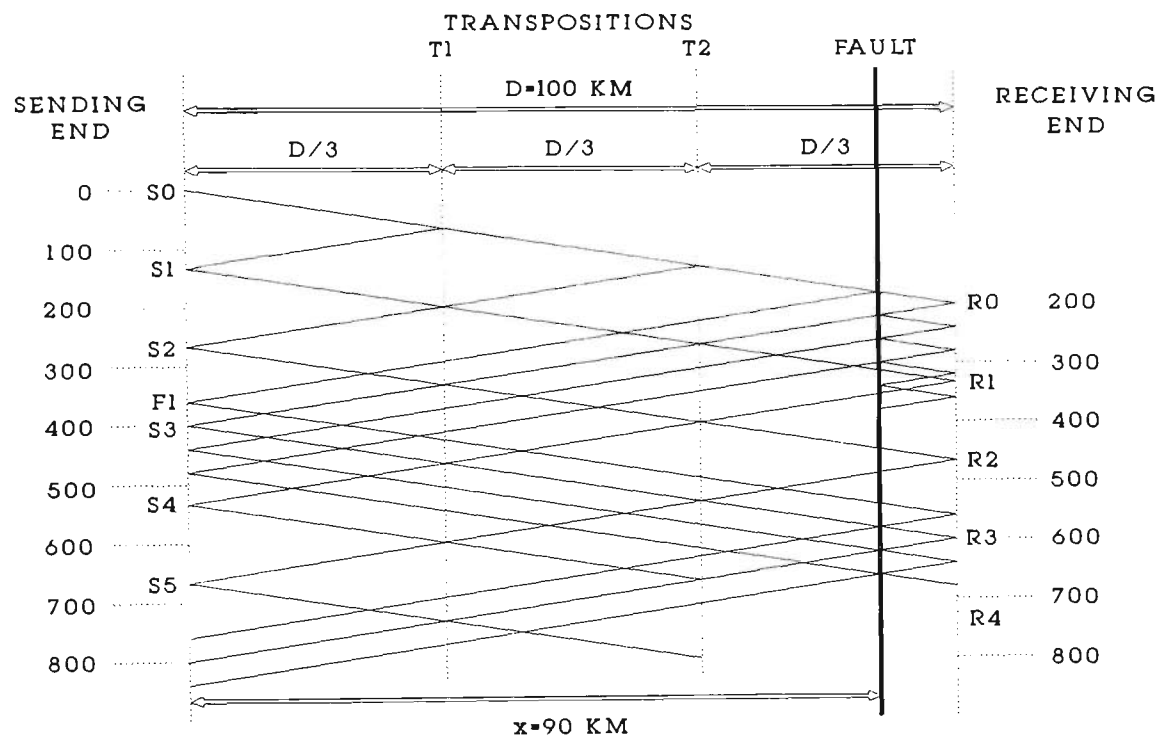

Figure 5.2 *Lattice diagram for 100 km double transposed line with fault at x = 90 km. The numbers at each line end are the sample numbers assuming the signals travel with the speed of light and the sample frequency is 0.6 MHz.*

5.2.4 Spread Spectrum Noise Performance

It is well known [52] that for a b+1 bit A/D converter the variance of the quantisation noise is given by $\sigma^2 = 2^{-2b}/12$. Assuming this noise is uniformly spread over the spectrum from 0 Hz to $f_s/2$ we get that after the BPF of bandwidth R_c/L in Fig. 5.1 the noise variance is

$$\frac{R_c/L}{f_s/2} \frac{2^{-2b}}{12} = \frac{2^{-2b} R_c}{6Lf_s}$$

Hence for given R_c and f_s the quantisation noise power is reduced by a factor L. Similarly, the line noise entering the waveform recorder will be reduced by the same factor. In contracting the bandwidth of the desired signal there is a corresponding increase in the signal-to-noise ratio - this is the essence of the spread spectrum technique.

5.3 PLC LINE INTERFACE

The spread spectrum signal covers a wide frequency range so it is important to model the frequency dependency of the power line carrier interface between the communications room and the EHV lines. For compatibility with existing PLC equipment we are interested in the frequency range 80-520 kHz.

5.3.1 PLC Sending and Receiving End Network Equations

The PLC sending end and receiving end networks are each coupled to the same conductors and are illustrated in Figs. 5.3 and 5.4. The transmitted signal is fed through a resistive hybrid to the line matching unit from which it is coupled to two phases of the transmission line through the CVT capacitors. Voltages measured at the transmitting end are recorded across a 75 ohm resistor connected to the hybrid. At the
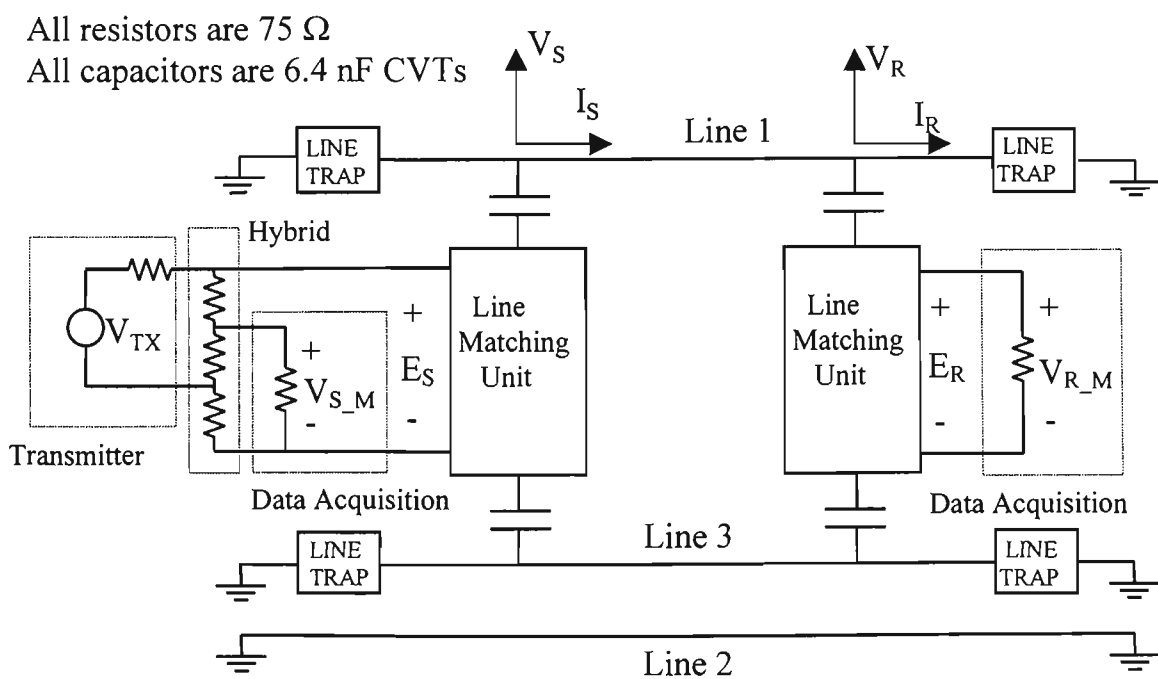

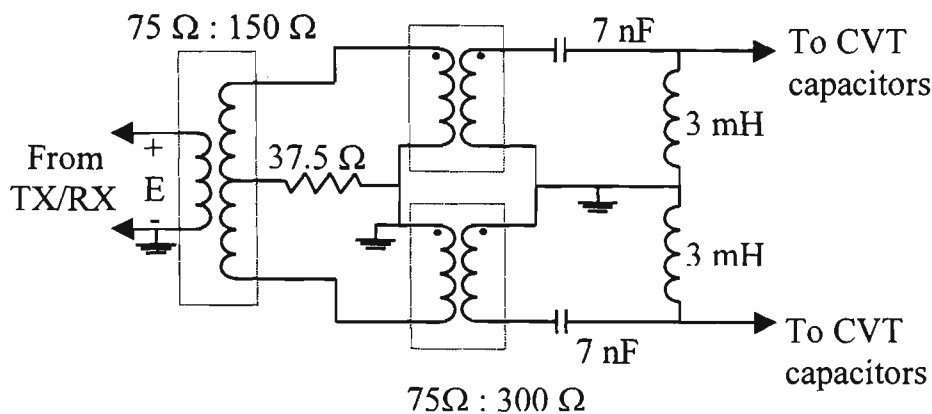Figure 5.3 *PLC transmitting and receiving end network.*

Figure 5.4(a) *Line matching unit.*

receiving end there are similar CVT capacitors coupling into a line matching unit which feeds the line signal to the receiver which is modelled as a 75 ohm resistor. Both ends of the coupled lines are terminated to ground through line traps, and both ends of the uncoupled line are terminated to ground directly. These terminations are typical for de-energised lines.

The PLC networks at the transmitting and receiving ends are represented by admittance matrices

$$\mathbf{Y_S} = \mathbf{Y_{SLMU}} + \mathbf{Y_{SLT}}$$

$$\mathbf{Y_R} = \mathbf{Y_{RLMU}} + \mathbf{Y_{RLT}}$$

where the admittance at the sending end consists of $\mathbf{Y_{SLMU}}$, due to the line matching unit and CVT capacitors, and $\mathbf{Y_{SLT}}$, due to the line traps - similar definitions hold for $\mathbf{Y_{RLMU}}$ and $\mathbf{Y_{RLT}}$ at the receiving end. The admittance value on the uncoupled short
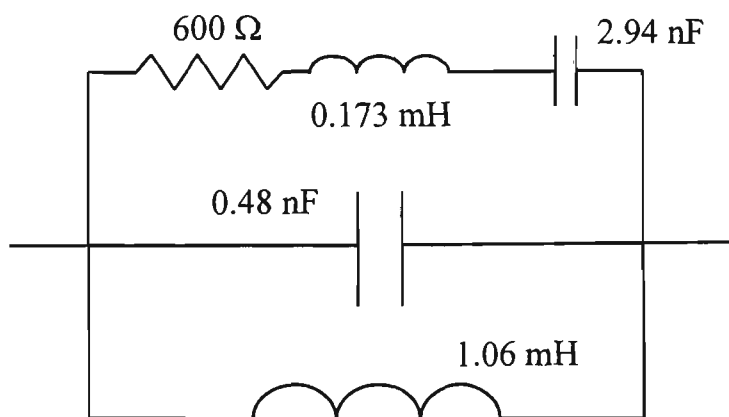

Figure 5.4(b) *Line trap.*

circuit line is represented by a 'large' number. At the sending end the effect of the transmitter may be represented by an admittance vector $\mathbf{a_S}$ to give the boundary condition equations at each end

$$\mathbf{I_S} = -\mathbf{Y_S V_S} + \mathbf{a_S} V_{TX}. \qquad\qquad \textit{Equation 5.1}$$

$$\mathbf{I_R} = \mathbf{Y_R V_R} \qquad\qquad \textit{Equation 5.2}$$

The voltage E_S of Fig. 5.3 is given by $E_S = E_T + E_L$, where

$$E_T = \frac{P_T(s)}{Q_T(s)} V_{TX} \qquad\qquad E_L = \frac{P_L(s)}{Q_L(s)}\left(V_{S1} - V_{S3}\right)$$

where $P_T(s)$, $Q_T(s)$, $P_L(s)$ and $Q_L(s)$ are polynomial functions of the Laplacian operator s, describing the frequency dependency of the circuits in Figs. 5.3 and 5.4(a). V_{S1} and V_{S3} are the phase voltages on the coupled lines at the transmitter CVT capacitors, here taken to be lines 1 and 3.

$$\mathbf{V_S} = \begin{bmatrix} V_{S1} \\ 0 \\ V_{S3} \end{bmatrix}$$

Similar equations hold for the voltage E_R at the receiver end. By analysing the transmitter/hybrid/data acquisition circuitry at the sending end of Fig. 5.3, and the data acquisition circuitry at the receiving end, it can be shown that the voltages measured in the communications rooms at the transmitting and receiving ends are, respectively

$$V_{S\_M} = 0.5 E_S - 0.125 V_{TX}$$

$$V_{R\_M} = E_R$$

5.4   POLYPHASE TRANSMISSION LINE SIMULATION MODEL

The simulation program uses the polyphase transmission line model based on the distributed parameter modal analysis method developed by Wedepohl and others [21] [53] [54]. This uses the line geometry, conductor and earth wire parameters and earth resistivity to derive the impedance per unit length matrix $\mathbf{Z}$ and the admittance per

unit length matrix $\mathbf{Y}$ for any given frequency. Denoting by $\mathbf{V}$ the modified Fourier transform of the voltage on the line Wedepohl showed that the wave equation

$$\frac{d^2 \mathbf{V}}{d x^2} = \mathbf{ZYV}$$

has the solution

$$\mathbf{V} = \exp(-\psi x)\mathbf{V}_i + \exp(\psi x)\mathbf{V}_r \qquad \text{where } \exp(\pm\psi x) \equiv \mathbf{S}\exp(\pm\gamma x)\mathbf{S}^{-1}$$

Here $\mathbf{S}$ is the eigenvector matrix and γ the eigenvalue matrix of the matrix $\mathbf{ZY}$. $\mathbf{S}$ defines the different propagation modes on the polyphase transmission line and the diagonal matrix γ gives the propagation constants for each mode. For any phase voltage vector $\mathbf{V}$, $\mathbf{S}^{-1}\mathbf{V}$ gives the modal components of $\mathbf{V}$. The current on the line is given by

$$\mathbf{I} = \mathbf{Y}_0[\exp(-\psi x)\mathbf{V}_i - \exp(\psi x)\mathbf{V}_r] \qquad \text{where } \mathbf{Y}_0 = \mathbf{Z}^{-1}\mathbf{S}\gamma\mathbf{S}^{-1}$$

is the characteristic admittance of the line. If we consider only the line configuration contribution to $\mathbf{Z}$ and $\mathbf{Y}$ (ignoring the conductor and earth wire terms and with zero earth resistivity) then all the modes collapse into the ideal distortionless mode travelling at the speed of light.

The basic equations describing travelling wave phenomena on a polyphase transmission line may be implemented [55] by either

(1) evaluating the ABCD transmission parameters for the line

or   (2) calculating the forward and backward travelling waves $\mathbf{V}_i$, $\mathbf{V}_r$ using the reflection factor method.

Here we consider both techniques for the steady state case where the mains power has been disconnected and any fault remains as a resistance from the line to ground. Adapting the superposition theorem as applied by Johns and Aggarwal [24], the waveforms generated when a signal is transmitted down a faulted line may be expressed as the sum of two related waveforms. As illustrated in Figs. 5.5 and 5.6 for earth faults the total waveform, (V_{TX}, V_{FS} active, $E_{FF} = -V_{FS}$ on faulted line) is equal to the waveforms generated on a healthy line (V_{TX}, V_{FS} active, E_{FF} removed) added to
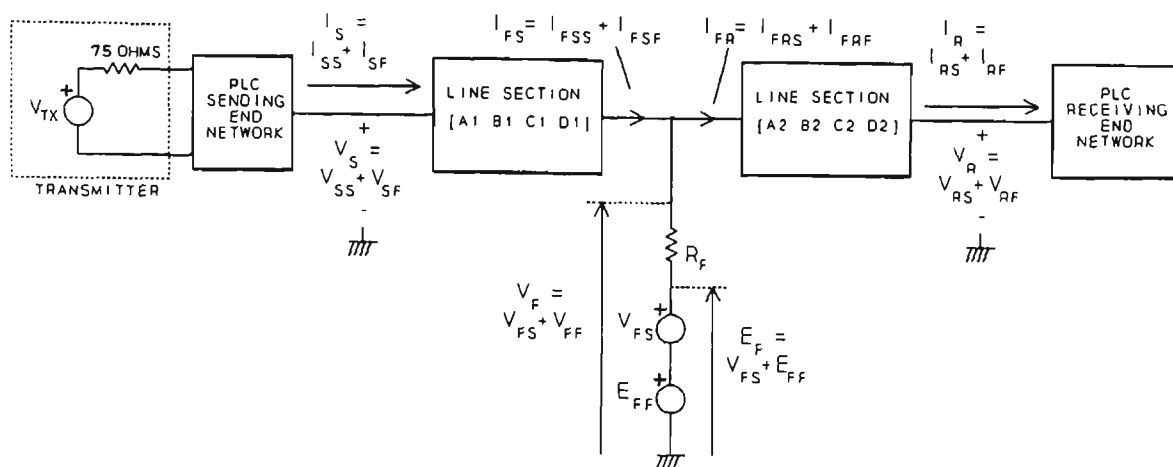
Figure 5.5 *Faulted line,* ABCD *parameter transmission line model illustrating superposition.*
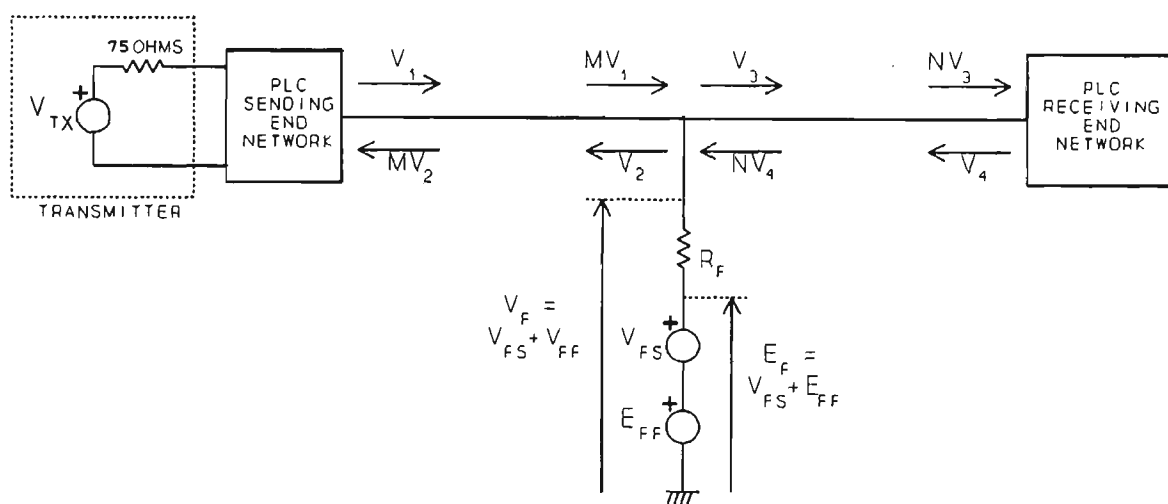

Figure 5.6 *Faulted line, reflection factor model for homogeneous lines illustrating superposition.*

the waveform modification generated by the fault (V_{TX} and V_{FS} removed, $E_{FF} = -V_{FS}$ on faulted line). At the sending end, for example, we have $V_S = V_{SS} + V_{SF}$.

By verifying that superposition holds we can check the internal consistency of the two methods of applying Wedepohl's modal analysis to transmission lines. The simulation studies presented in this paper were for a 100 km horizontal 3 phase line and were programmed on a Cyber 932 mainframe computer with a machine constant ε = 7.1054E-15. With the ABCD parameter method truncation errors limited the accuracy of the above superposition equations to about 1% at frequencies up to 170 kHz - this error increased rapidly at higher frequencies.

In section 5.4.1 below we discuss the application of the ABCD transmission parameters to fault location simulation on a transposed line and in 5.4.2 the same is done for the reflection factor method.

5.4.1 ABCD Parameters

Following Johns and Aggarwal [24] any transmission line (both healthy and with short circuit faults) is modelled as shown in Fig. 5.5. Any section of a homogeneous polyphase transmission line of length x may be represented by the transmission parameter matrix of dimensions 2n × 2n

$$\begin{bmatrix} A(x) & B(x) \\ C(x) & D(x) \end{bmatrix}$$

where

$$A(x) = \cosh(\gamma x) \qquad\qquad B(x) = \sinh(\gamma x)Z_0$$

$$C(x) = Y_0 \sinh(\gamma x) \qquad\qquad D(x) = Y_0 \cosh(\gamma x)Z_0$$

$$\cosh(\gamma x) \equiv S \cosh(\gamma x)S^{-1} \qquad \sinh(\gamma x) \equiv S \cosh(\gamma x)S^{-1}$$

$$Z_0 = S\gamma^{-1}S^{-1}Z \text{ is the characteristic impedance of the line}$$

In Fig. 5.5 homogeneous line sections from the sending end to the fault and from the fault to the receiving end are respectively

$$\begin{bmatrix} A_1 & B_1 \\ C_1 & D_1 \end{bmatrix} = \begin{bmatrix} A(x) & B(x) \\ C(x) & D(x) \end{bmatrix} \qquad \begin{bmatrix} A_2 & B_2 \\ C_2 & D_2 \end{bmatrix} = \begin{bmatrix} A(D-x) & B(D-x) \\ C(D-x) & D(D-x) \end{bmatrix}$$

The transmission line for which simulation results are presented in this paper has two transpositions at equal intervals as illustrated in Fig. 5.7. As described in Appendix 5.7.1 any transposed line can be reduced to the form of Fig. 5.5. It is shown in Appendix 5.7.2 that the steady state pre-fault (ie with $E_{FF} = 0$) voltage V_{FS} at the fault position (due to the transmitted PLC waveform V_{TX}) is

$$V_{FS} = (A_2 + B_2 Y_R)[C + DY_R + Y_S(A + BY_R)]^{-1} a_S V_{TX} \qquad \textit{Equation 5.3}$$
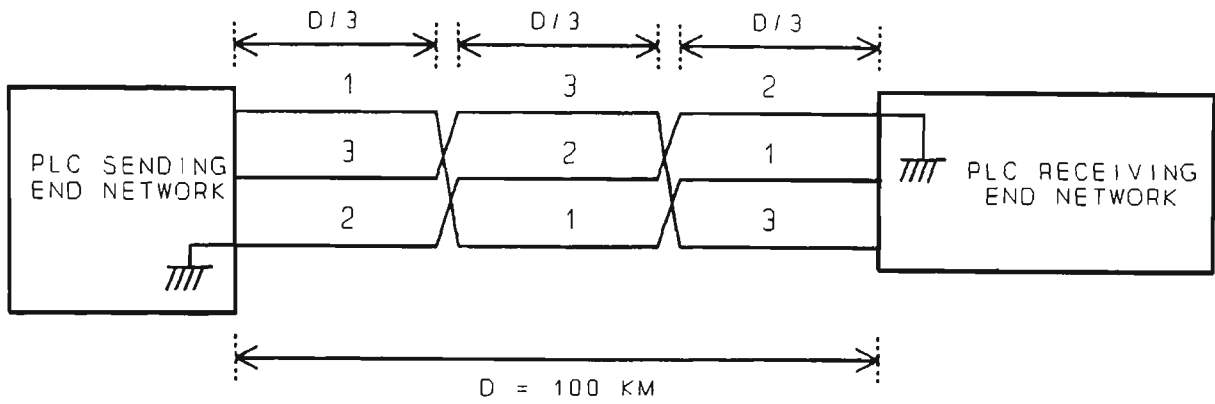
Figure 5.7 *Line transposition scheme showing line numbering.*

The calculations to determine the superimposed waveforms deriving from the fault are as shown in Reference [24]. The total steady state voltage or current at any point is then given by the sum of the unfaulted and superimposed signals.

To check the accuracy of the above calculations the steady state voltages can also be calculated with the transmitter feeding directly into the faulted line. Equations for a typical single phase to ground fault are given in Appendix 5.7.3.

5.4.2 Reflection Factor Method

In evaluating the hyperbolic sinh and cosh functions required for the transmission parameters a positive exponential is added to a negative exponential. For high PLC frequencies and/or long line lengths the exponents become large and excessive truncation errors are incurred. In this case the reflection factor method, illustrated in Fig. 5.6, must be used [55].

This method reduces truncation errors by taking as unknowns the voltages at opposite ends of a homogeneous line travelling in opposite directions. (eg. voltages V_1 and V_2 in Fig. 5.6). For the homogeneous line

$$\mathbf{M} = \exp(-\psi x) \qquad \mathbf{N} = \exp[-\psi(D-x)]$$

and the voltage reflecting off the receiving end is $\mathbf{V_4} = \mathbf{K_r N V_3}$ where $\mathbf{K_r}$ is the reflection factor

$$\mathbf{K_r} = (\mathbf{Y_0} + \mathbf{Y_R})^{-1}(\mathbf{Y_0} - \mathbf{Y_R})$$

$$x$$

$$V_1 \qquad \exp(-\psi x)V_1 \qquad V_3$$

$$\exp(-\psi x)V_2 \qquad V_2 \qquad V_4$$

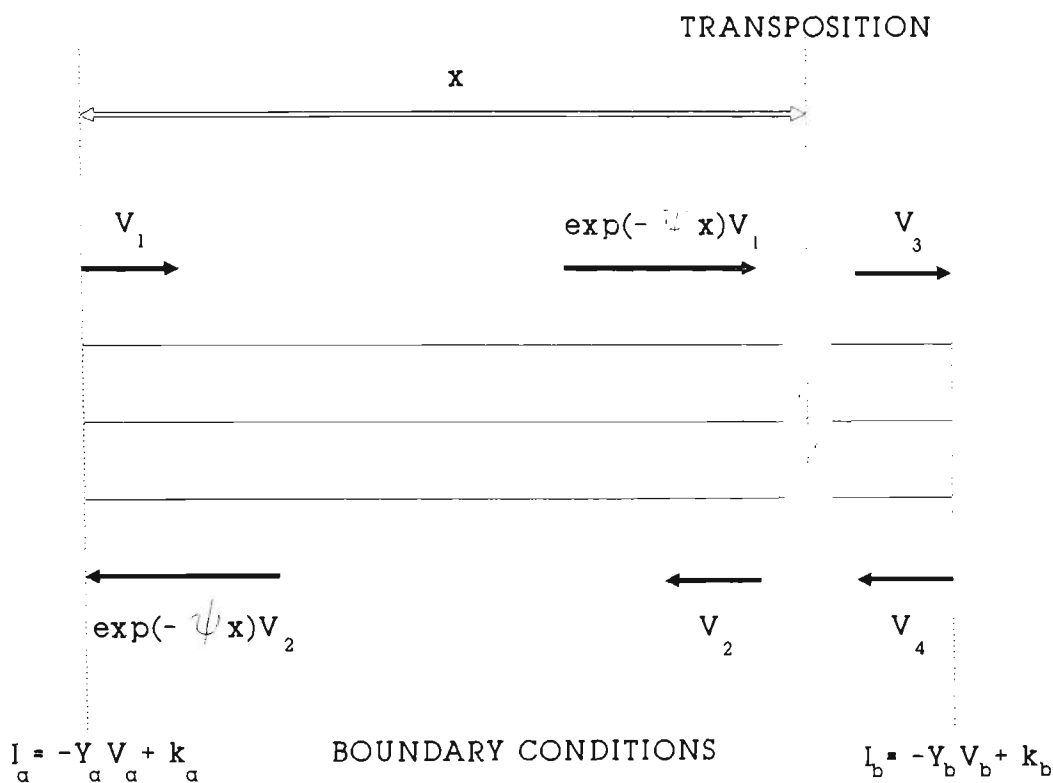$$I_a = -Y_a V_a + k_a \qquad \text{BOUNDARY CONDITIONS} \qquad I_b = -Y_b V_b + k_b$$

Figure 5.8 *Reflection factor boundary conditions with transpositions.*

for receiving end admittance termination Y_R.

It is more complex to take into account the transpositions using the reflection factor method. A boundary condition at one end of a transposed line section can be converted to an equivalent boundary condition at the far end of the line (illustrated in Fig. 5.8) through a process of compression. The reverse process re-expands the line to recover the voltages at line ends - equations are given in Appendix 5.7.4.

With $E_{FF} = 0$ the compression technique may be used to transfer the receiving end boundary condition of Equation 5.2 to an equivalent boundary condition at the transposition closest to the transmitter. The pre-fault signals can then be evaluated as in Appendix 5.7.5.

The fault waveforms are calculated (Appendix 5.7.6) with the voltage sources V_{TX} and V_{FS} short circuited, E_{FF} set equal to $-V_{FS}$ on the faulted line and the end networks of Fig. 5.6 replaced with the equivalent boundary conditions at the ends of the homogeneous line section in which the fault lies.

To obtain the total waveform the end networks of Fig. 5.6 are replaced with the equivalent boundary conditions at the ends of the faulted homogeneous line section,

leaving V_{TX} intact and putting $E_{FF} = -V_{FS}$. The signals are then calculated using the techniques of Appendix 5.7.7.

5.5 FAULT LOCATION SIMULATION STUDIES

Direct sequence spread spectrum fault location has been simulated on a computer model of a 3 phase horizontal line of length 100 km with two transpositions as illustrated in Fig. 5.7. The line geometry is shown in Fig. 5.9 and a full list of line data is included in Appendix 5.7.8. All studies are for a double-ended system and only single phase to ground faults have been simulated.
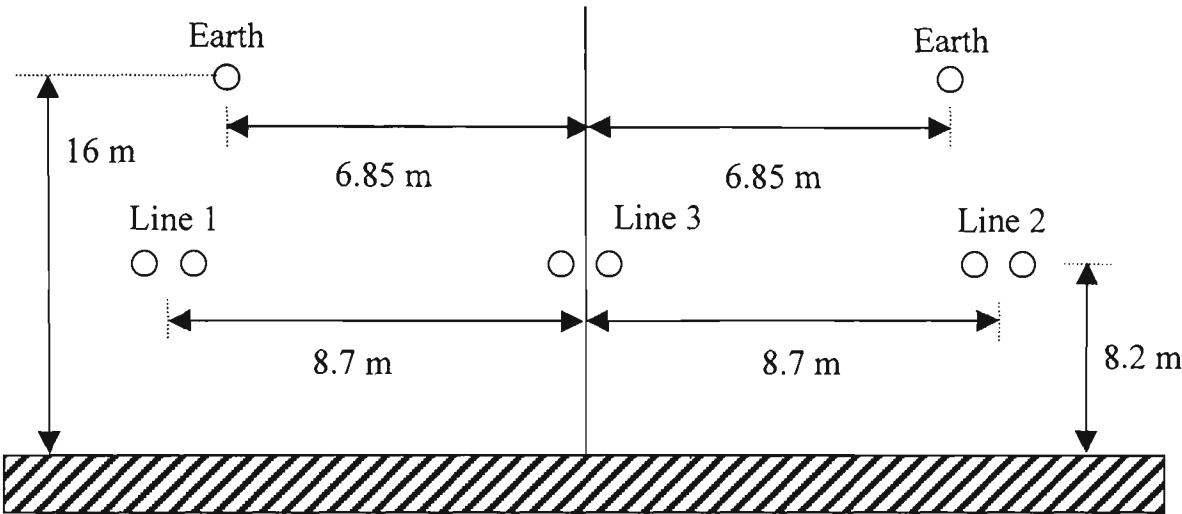
Figure 5.9 *Line geometry and line numbering as viewed from the sending end.*

5.5.1 Discussion of Results

The power line carrier program was used to investigate the effects of f_0, R_c, L, x and receiver noise on the correlation function and calculated fault position accuracy and resolution. The accuracy of the fault location algorithm was compared for waveforms recorded at each end of the line and the results are shown in Table 5.2 at the end of section 5.5.1.3.

Unless otherwise stated the simulation graphs are for a single phase to ground fault with $R_F = 1$ ohm on line 2 at a distance x = 90 km from the transmitter. The lattice diagram showing the main reflections for this fault position is illustrated in Fig. 5.2.

Also the default values for the direct sequence waveform used are $f_0 = 140$ kHz, $R_c = 60$ kHz, $L = 1023$ with a sampling frequency $f_s = 0.6$ MHz.

5.5.1.1   Modal Propagation Characteristics

It is well known [56] that the modal propagation vectors on a horizontal three phase line are approximately independent of frequency and equal to Clarke's diagonal components

$$S = \begin{bmatrix} 1 & -1 & -0.5 \\ 1 & 1 & -0.5 \\ 1 & 0 & 1 \end{bmatrix}$$

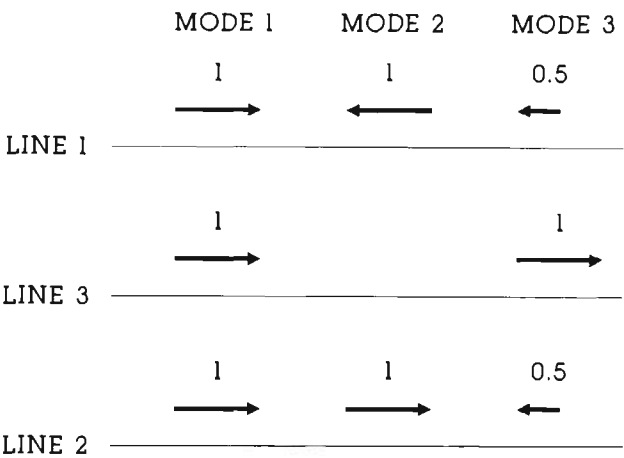These ideal components are illustrated in Fig. 5.10. The attenuation and speed of

Figure 5.10 *Ideal modal components for a horizontal three phase line.*

propagation of each mode at 140 kHz was calculated by the program as

$\alpha_1 = 1.34$ dB/km $\alpha_2 = 0.206$ dB/km $\alpha_3 = 0.0334$ dB/km

$v_1 = 2.73221E8$ m/sec $v_2 = 2.92275E8$ m/sec $v_3 = 2.98593E8$ m/sec

As the different modes propagate along the line they slide past each other, producing interference effects characteristic of a standing wave pattern on a multi-line system.

5.5.1.2   Waveforms Recorded on Unfaulted Lines

In Fig. 5.11(a) the correlation coefficient for the unfaulted line waveform V_{SS_M} (measured at the sending end) is plotted. The large peak S0 corresponds to the transmitter feeding through the hybrid into the waveform recorder - immediately following this peak are 60 kHz side lobe ripples due to the bandwidth restriction of the MLS code. The reflections off the transpositions and the ends are labelled as in Fig. 5.2. The trough S4 is due to cancellation between the reflected waveforms and the residual correlation of the transmitted signal.

We can use the correlation peaks S1, S2, S3 corresponding to primary reflections off impedance discontinuities of known locations (two transpositions and the line end) to calibrate the horizontal axis in terms of distance. In Table 5.1 below the signal speeds calculated from local correlation maxima are recorded.

Table 5.1 *Average signal speeds as calculated from unfaulted line reflections.*

Sending End (x 10^8 m/sec)			Receiving End (X 10^8 m/sec)		
S1	S2	S3	R0-R1	R0-R2	R0-R3
2.97288	2.97271	2.95636	2.95643	2.96901	2.94604

The correlation coefficient for the waveform V_{RS_M}, measured at the receiving end, is shown in Fig. 5.12(a) - again the labels are the same as those in Fig. 5.2. Without synchronous timing between the sending and receiving ends of the line the phase relationship between R0 and the transmitted code is unknown. However, as the distance between line transpositions is known, the measured time delay between the correlation peaks R0 and R1 may be used to determine average signal speeds. Average signal speeds were also calculated using the time delays between R0 and the local minimum R2, and between R0 and the peak R3. The results are summarised in Table 5.1 where it may be seen that the average signal speeds of the different reflections vary by something like 1% - this limits the accuracy with which faults may be located. These speeds lie between the speeds of propagation of mode 2 and mode 3 showing that signal propagation is principally due to the lowest attenuation modes.
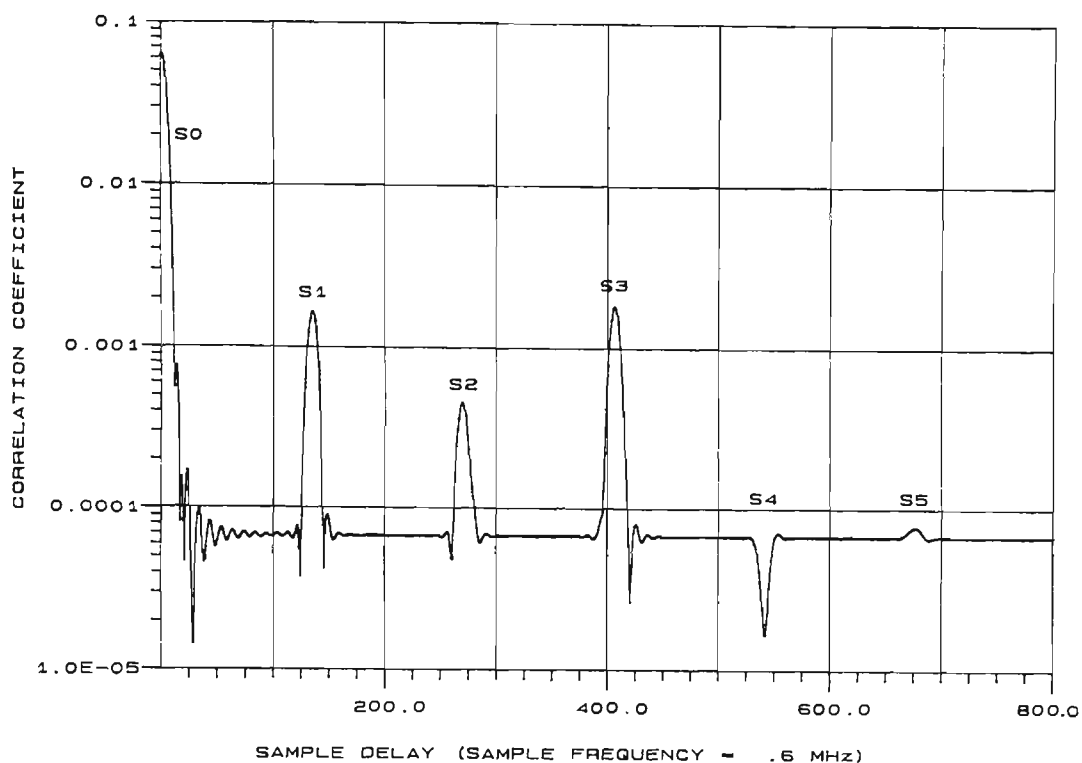
Figure 5.11(a) *Correlation coefficient for V_{SS_M} at sending end for unfaulted line.*
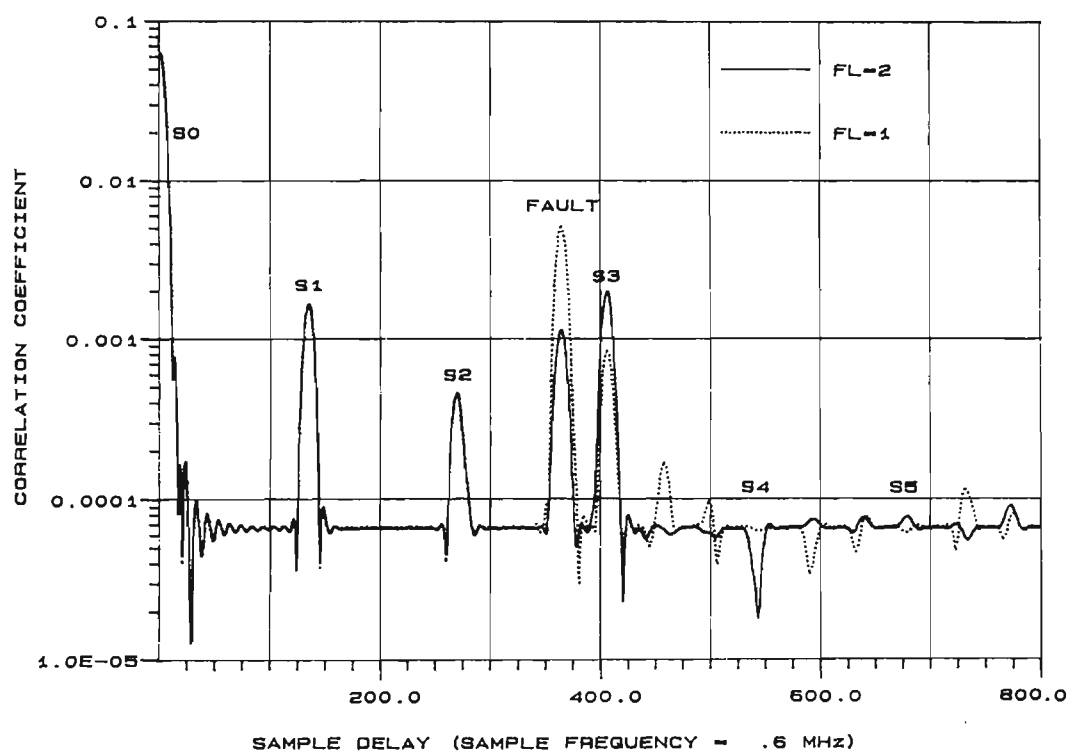

Figure 5.11(b) *Correlation coefficient for V_{S_M} at sending end for a fault at x = 90 km with R_F = 1 ohm on line 2 and line 1 (coupled line).*

Figure 5.11 *Direct sequence parameters : f_0 = 140 kHz, R_c = 60 kHz, L = 1023.*

5.5.1.3 Waveforms Recorded on Faulted Lines

The correlation coefficients for the two waveforms V_{S_M} measured when the fault is on line 2 and line 1 respectively (FL = 2, 1) are illustrated in Fig. 5.11(b). In both cases the primary reflection from the fault is clearly visible and the extra ripples in the graph for sample delays greater than about 420 are due to extra line reflections caused by the fault. When the fault lies on line 1, to which the PLC equipment is coupled, the reflection from the fault is greater than the reflection from the receiving end, while the reverse holds when the fault is on line 2 (uncoupled line).

At the receiving end the two corresponding correlation coefficients for the waveforms V_{R_M} are shown in Fig. 5.12(b). With the fault on line 2 the direct through signal R0 is reduced by 0.6 dB over the unfaulted signal strength - with the fault on line 1 the attenuation of R0 is 5.3 dB greater than the unfaulted attenuation. This latter agrees well with the measurements made in Reference [57]. Like the sending end, the fault reflection is greatest for the fault on the PLC coupled line. Unlike measurements made at the sending end, however, the fault reflections recorded at the receiving end do not unambiguously locate the fault position. Because of the symmetry of line reflections, measurements made at the receiving end could be produced by a fault located either at a distance x or a distance D - x from the sending end. This may be seen in Fig. 5.2 where each signal reflection at the receiving end, from R0 onwards, travels down the line to form a corresponding peak at the sending end, from S3 onwards.

Using S3 as reference in Fig. 5.11(b) the fault position is calculated as x = 89.75 km and from Fig. 5.12(b), with R0-R1 as reference, the fault is estimated to be at x = 90.54 km - these values are tabulated in Table 5.2. The worst case error of 0.42% of line length was for a fault at 55 km when measured at the sending end. The worst case error was slightly larger (0.63% at x = 90 km) for measurements at the receiving end. To investigate the effects of the PLC interface circuitry on the fault location accuracy a simulation run was done with purely resistive line traps and line matching units (CVTs removed) - the corresponding fault position estimates are 90.02 km and 89.99 km respectively. The smearing of the waveform by these frequency selective components appears to be the dominant cause of inaccuracy in the measurements.
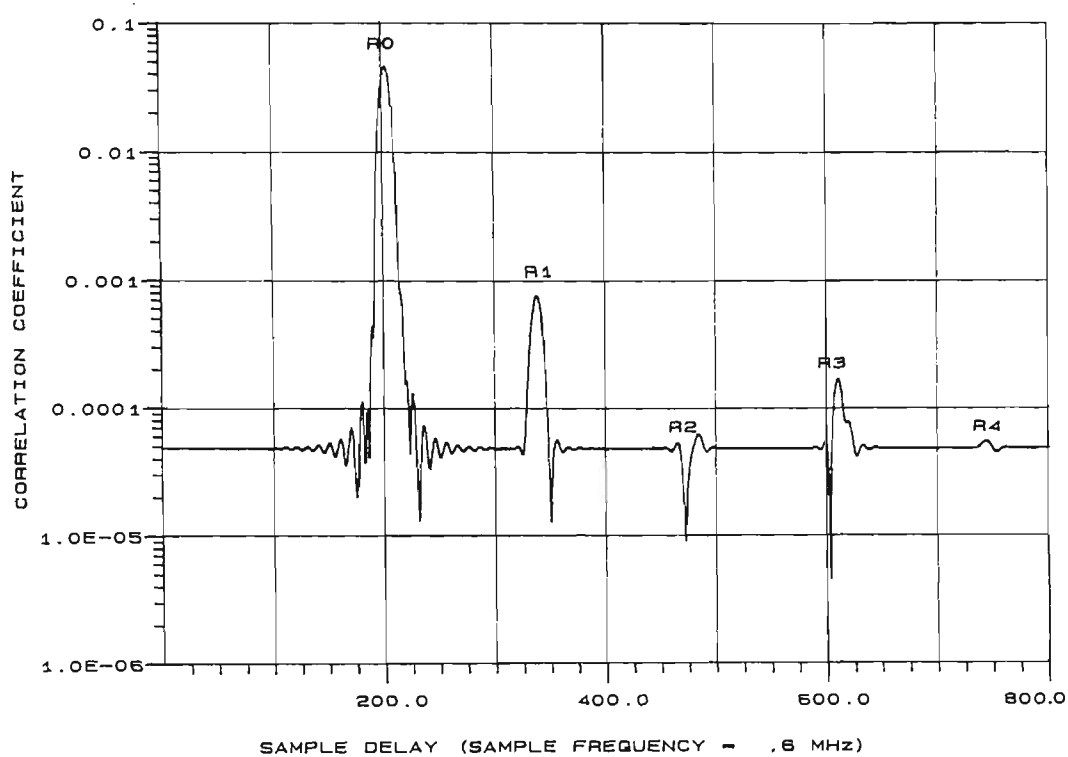
Figure 5.12(a) *Correlation coefficient of* V_{RS_M} *at receiving end for unfaulted line.*
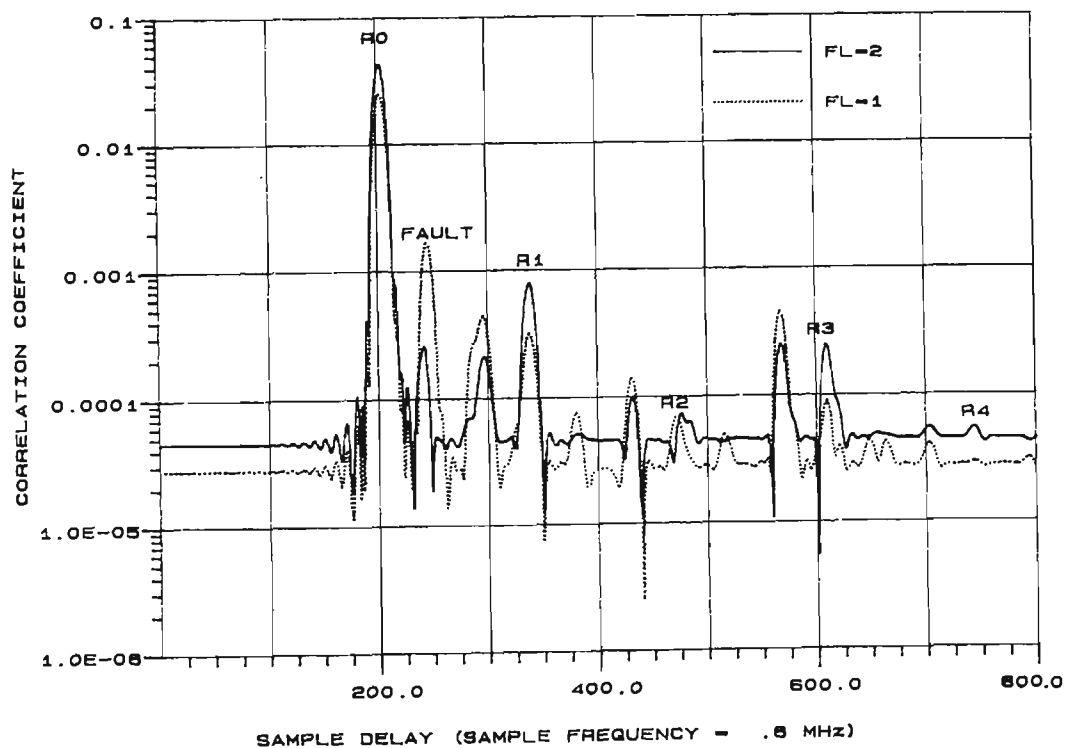

Figure 5.12(b) *Correlation coefficient for* V_{R_M} *at receiving end for a fault at x= 90 km with* R_F *= 1 ohm on line 2 and line 1.*

Figure 5.12 *Direct sequence parameters :* f_0 *= 140 kHz,* R_c *= 60 kHz, L = 1023.*

Table 5.2 *Fault positions as calculated using the faulted line reflections S3 as reference at the sending end, and R0-R1 as reference at the receiving end.*

True fault position (km)	Faulted Line	Fault Resistance (ohms)	Calculated Fault Position(km)	
			Sending End[1]	Receiving End[2]
90	2	1	89.75	90.54
90[3]	2	1	89.75	90.63
90	1	1	89.77	89.68
55	3	1	54.58	54.90
20	3	1	19.97	20.12
2.5[4]	2	1	2.59	3.11

[1] distance from sending end

[2] distance from sending end or distance from receiving end (ambiguous)

[3] 7 bit resolution in waveform recorder

[4] f_0 = 300 kHz, R_c = 220 kHz

5.5.1.4 Voltage Distribution Along Line

As aforementioned, the magnitude of the voltage recorded at the line ends depends upon which line is faulted. To investigate this relationship the true rms voltage distribution along the line when a 140 kHz sine wave is transmitted is plotted in Fig. 5.13, while Figs. 5.14 and 5.15 how the true rms voltage distribution along the line when direct sequence spread spectrum signals are transmitted, the first with f_0 = 140 kHz, R_c = 60 kHz and L = 1023 and the second with f_0 = 300 kHz, R_c = 180 kHz and L = 255.

Looking first at the narrowband signal the characteristic transmission line standing wave pattern with peaks separated by $\lambda/2 \approx 3.0E8/(2.0*140.0E3)$ = 1.07 km is evident. This is the interference pattern resulting from line reflections due to impedance mismatches at the transpositions and at the line ends. In the direct sequence plots, the rapid oscillations in the standing wave pattern of each individual spectral component constituting the broadband waveform sum to zero, leaving only the more gradual variation due to modal propagation and cancellation which is also evident in Fig. 5.13.
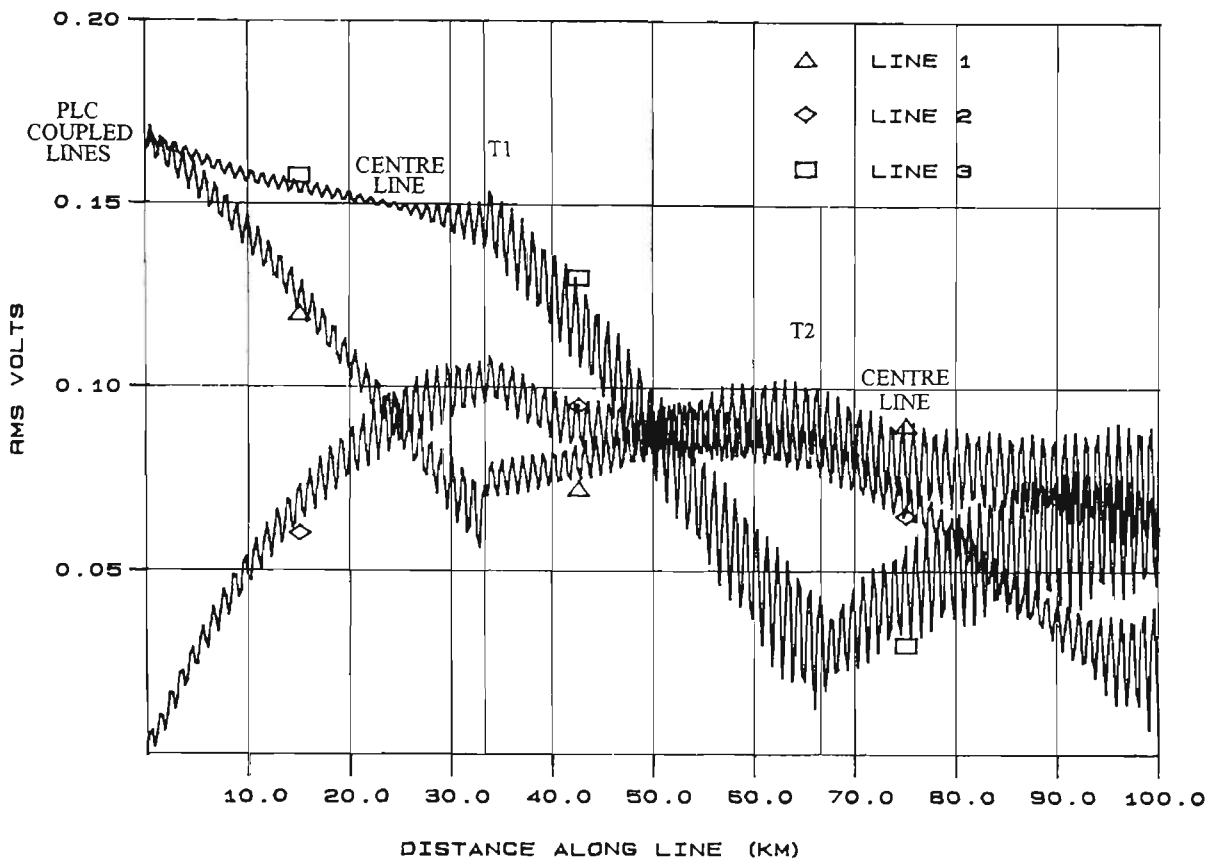
Figure 5.13 *Steady state RMS voltage distribution on all three unfaulted lines when a 140 kHz sinusoid is transmitted.*
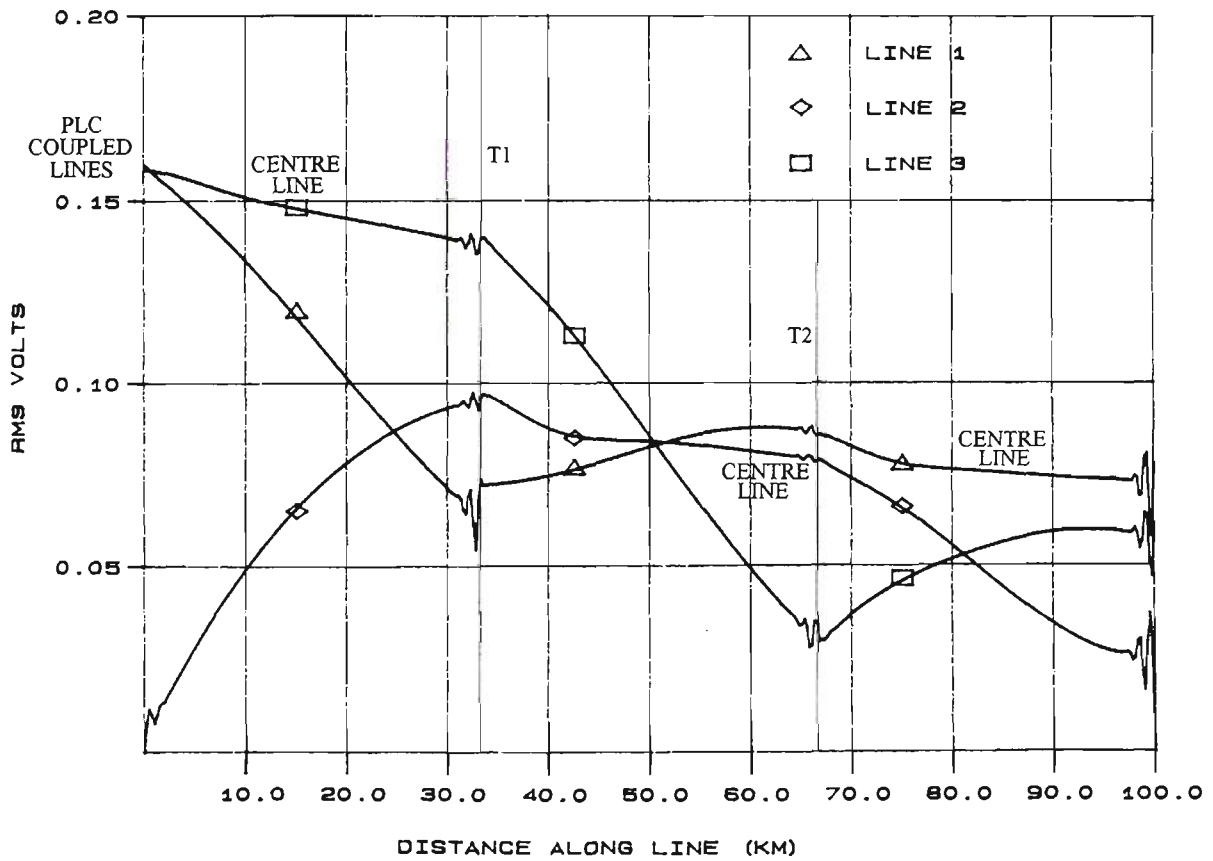

Figure 5.14 *Steady state RMS voltage distribution on all three unfaulted lines when a direct sequence signal with $f_0 = 140$ kHz, $R_c = 60$ kHz and $L = 1023$ is transmitted.*

From the modal characteristics listed in section 6.5.1.1 it is clear that mode 1 decays rapidly - however reflections at the transpositions and the ends will regenerate all the modes. The short lived ripples on each line in Fig. 5.14 at the receiving end and on the transmitter side of each transposition are caused by interference from reflections. Signal propagation on the centre line is principally due to mode 3 and so has less attenuation than waveforms on the outer lines - however on the far side of each transposition on the centre line the rapid decay of mode 1 over about 10 km can be seen. Also modes 2 and 3 slide past each other as they propagate along the line, their relative phases changing by 180° every 50 km - from Fig. 5.10 it may be seen that this will have the effect that the magnitudes of the voltages on the outer lines will be inversely related. This is in fact seen in Fig. 5.14 for the voltages on lines 1 and 2, lines 1 and 3 and lines 2 and 3 for each of the three successive homogeneous line sections.

By the principle of reciprocity the strength of the reflection from a fault at any position on any line is proportional to the magnitude of the prefault voltage at that particular
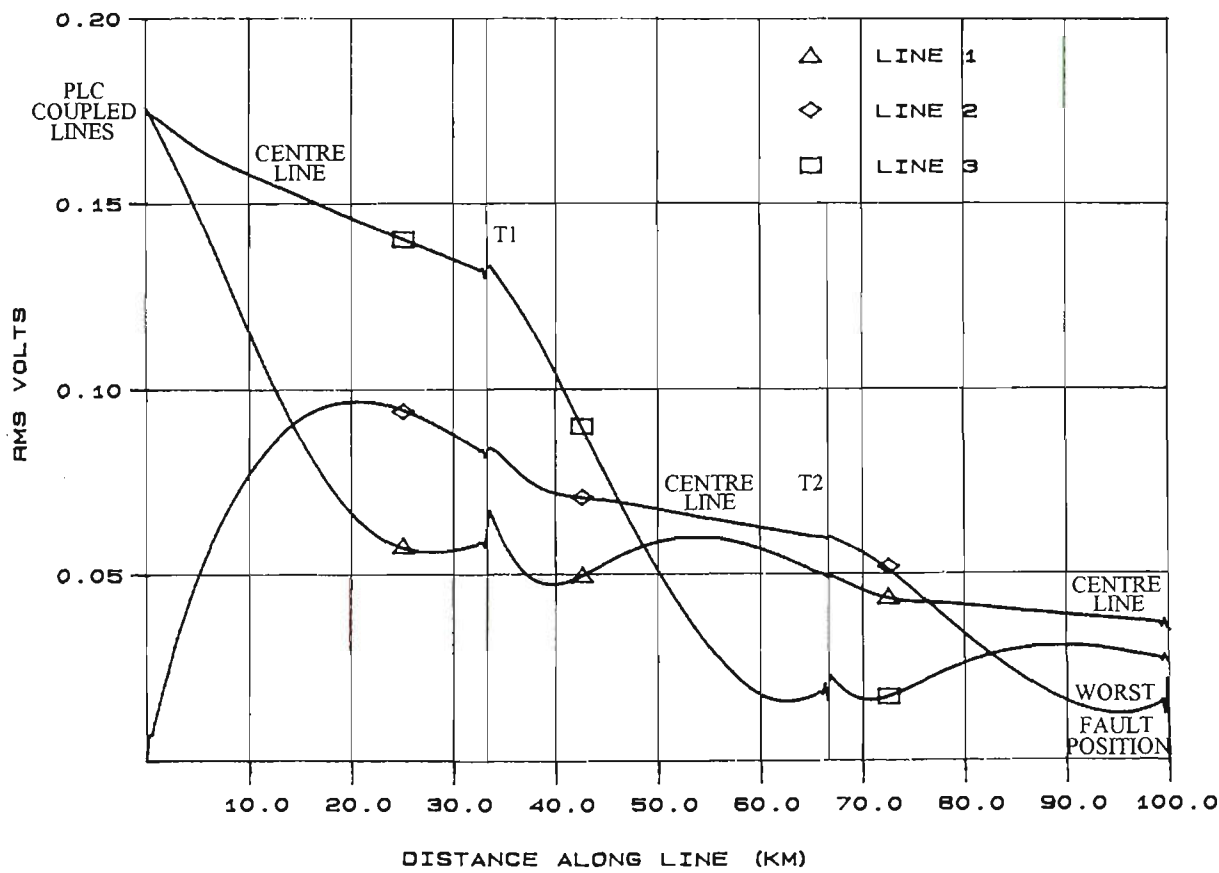

Figure 5.15 *Steady state RMS voltage distribution on all three unfaulted lines when a direct sequence signal with f_0 = 300 kHz, R_c = 220 kHz and L = 255 is transmitted.*

point. In particular from Fig. 5.14 it can be seen that there would be a small reflection from a fault on line 3 near the second transposition and that the graphs in the previous section for a fault on the uncoupled line at x = 90 km are also close to worst case.

Fig. 5.15 illustrates the voltage distribution along the line when the direct sequence signal with f_0 = 300 kHz, R_c = 180 kHz and L = 255 is transmitted. The same modal features as in Fig. 5.14 are evident, the main difference being the increased attenuation at the higher frequencies.

5.5.1.5   Effect of Fault Position

Fig. 5.16 shows the correlation coefficients for the unfaulted and faulted waveforms V_{SS_M} and V_{S_M} - in Fig. 5.16(a) the fault is on line 3 at x = 55 km and in Fig. 5.16(b) the fault is on line 3 at x = 20 km. As the fault moves closer to the sending end, the fault reflection and residual correlation increase. Also reflections from the receiving end and from transpositions on the far side of the fault are attenuated.
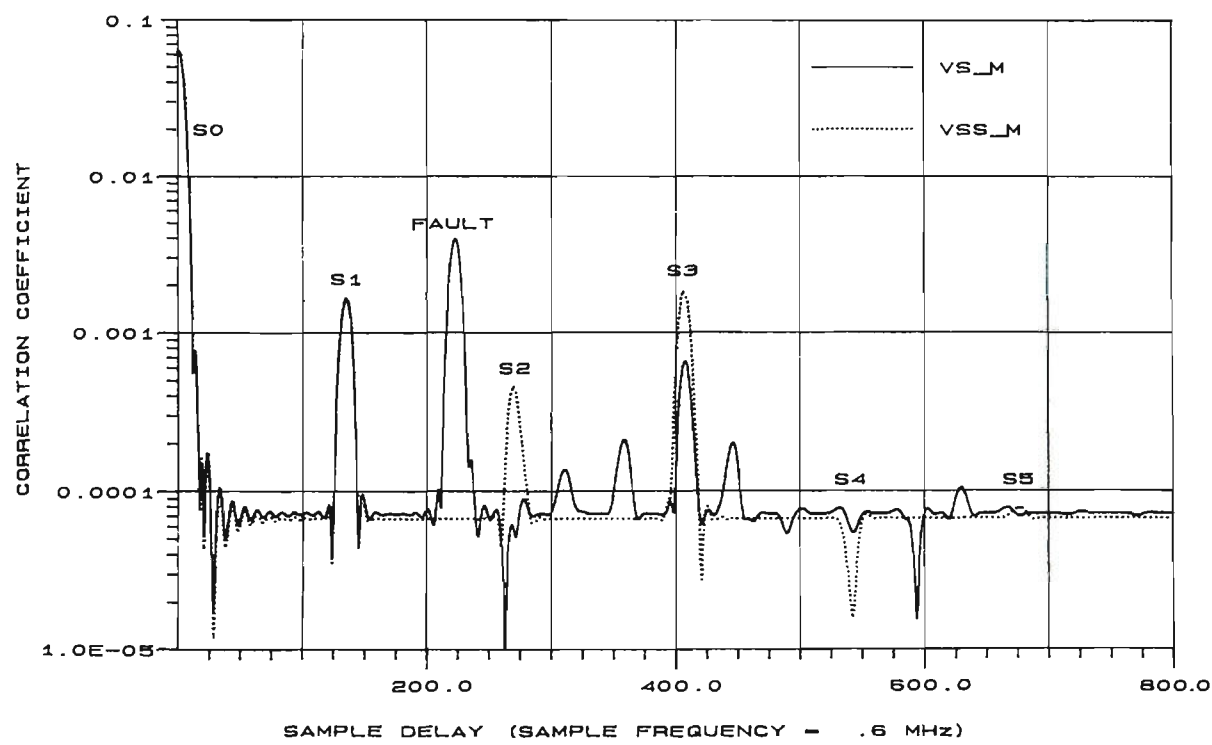

Figure 5.16(a) *Correlation coefficient of V_{S_M} for a fault at x = 55 km on line 3 with R_F = 1 ohm. The correlation coefficient for the unfaulted V_{SS_M} is shown for comparison.*
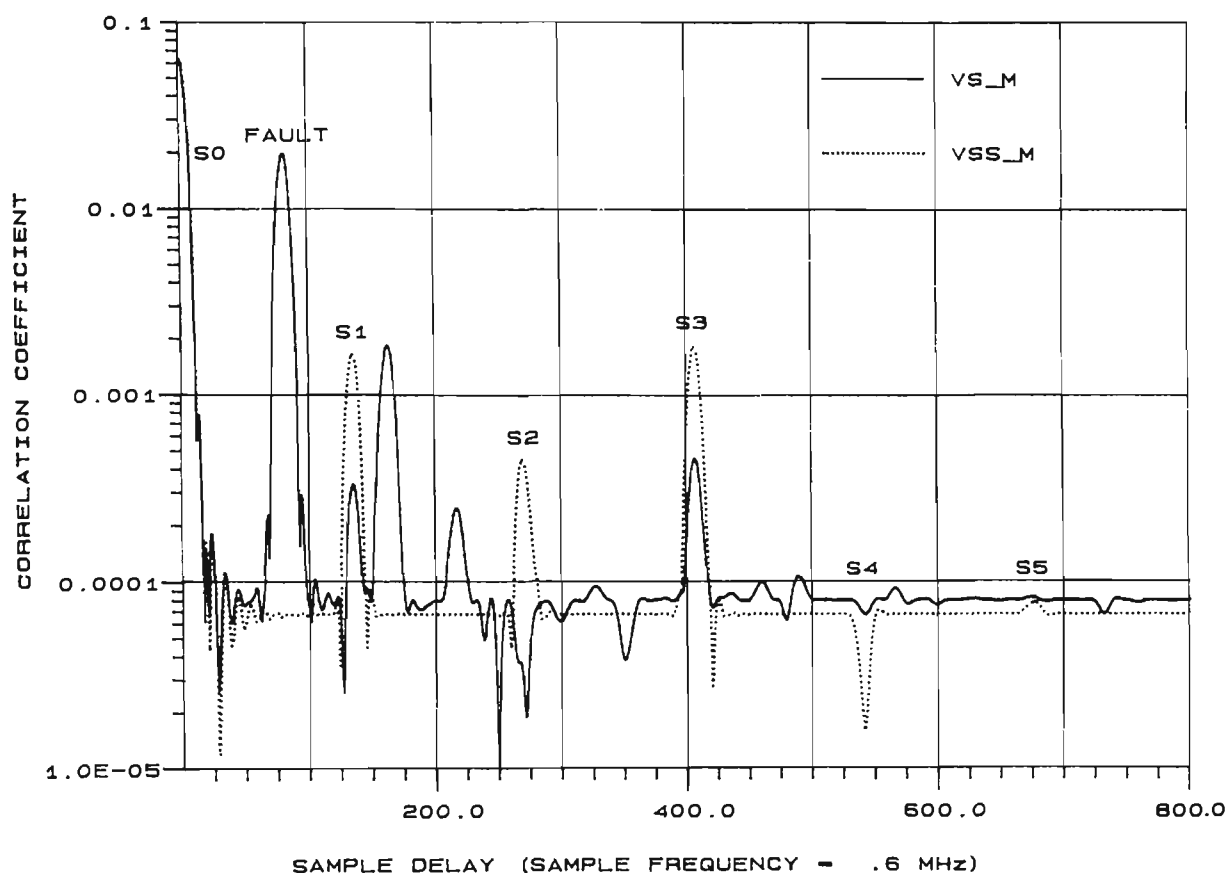
Figure 5.16(b) *Correlation coefficient of V_{S_M} for a fault at x = 20 km on line 3 with R_F = 1 ohm. The correlation coefficient for the unfaulted V_{SS_M} is shown for comparison.*

5.5.1.6   Effect of Faults Near Line Ends

Figs. 5.17(a) and 5.17(b) illustrate the correlation coefficients for V_{SS_M} and V_{S_M} for a fault on line 2 at x = 2.5 km with f_0 = 300 kHz, R_c = 220 kHz and L = 1023. Comparing the unfaulted plot with Fig. 5.11(a) it can be seen that the correlation peaks S0, S1, etc are narrower due to the higher R_c and that the signal attenuations are greater due to the higher frequencies. Because this fault is so close to the sending end, the Gibbs oscillations in the correlation coefficient for the band-limited direct sequence with f_0 = 140 kHz and R_c = 60 kHz obscure the fault reflection. However in Fig. 5.17(a) it can be seen that the higher chip rate compresses the Gibbs oscillations closer together so that in Fig. 5.17(b) the fault reflections are easily discernible.
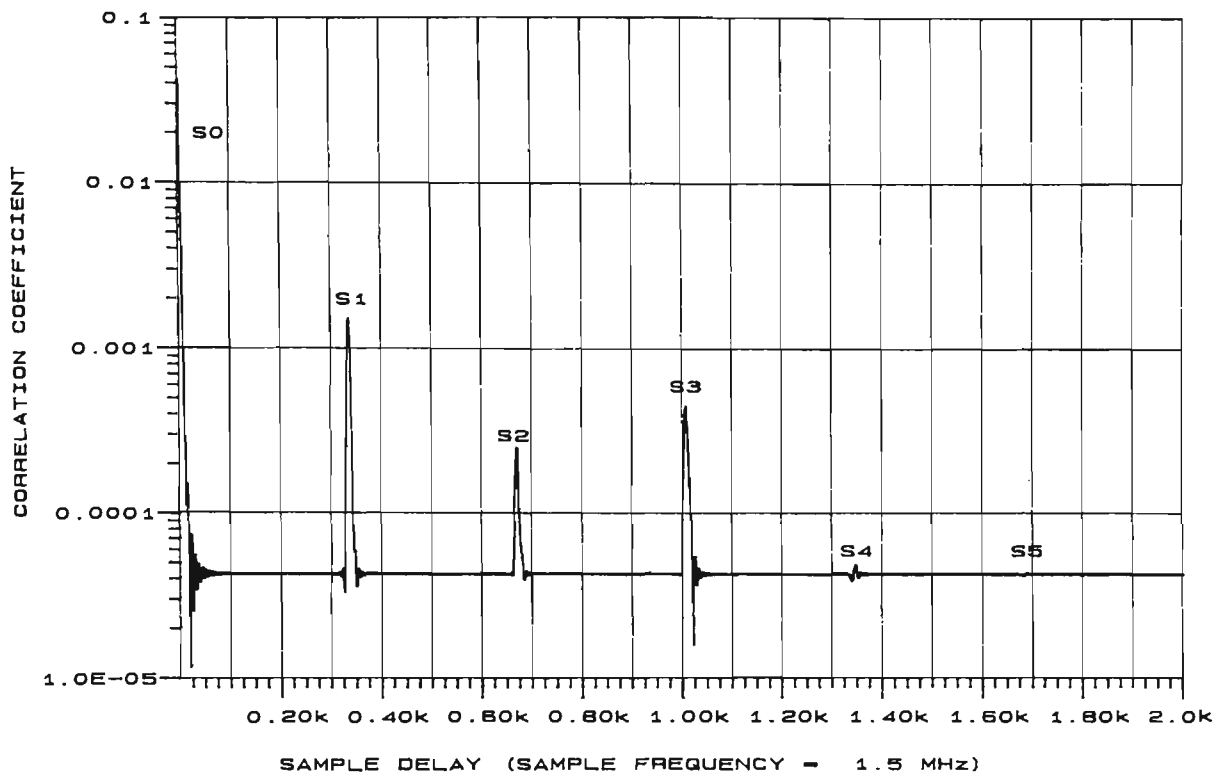
Figure 5.17(a) *Correlation coefficient for V_{SS_M} at sending end for unfaulted line.*
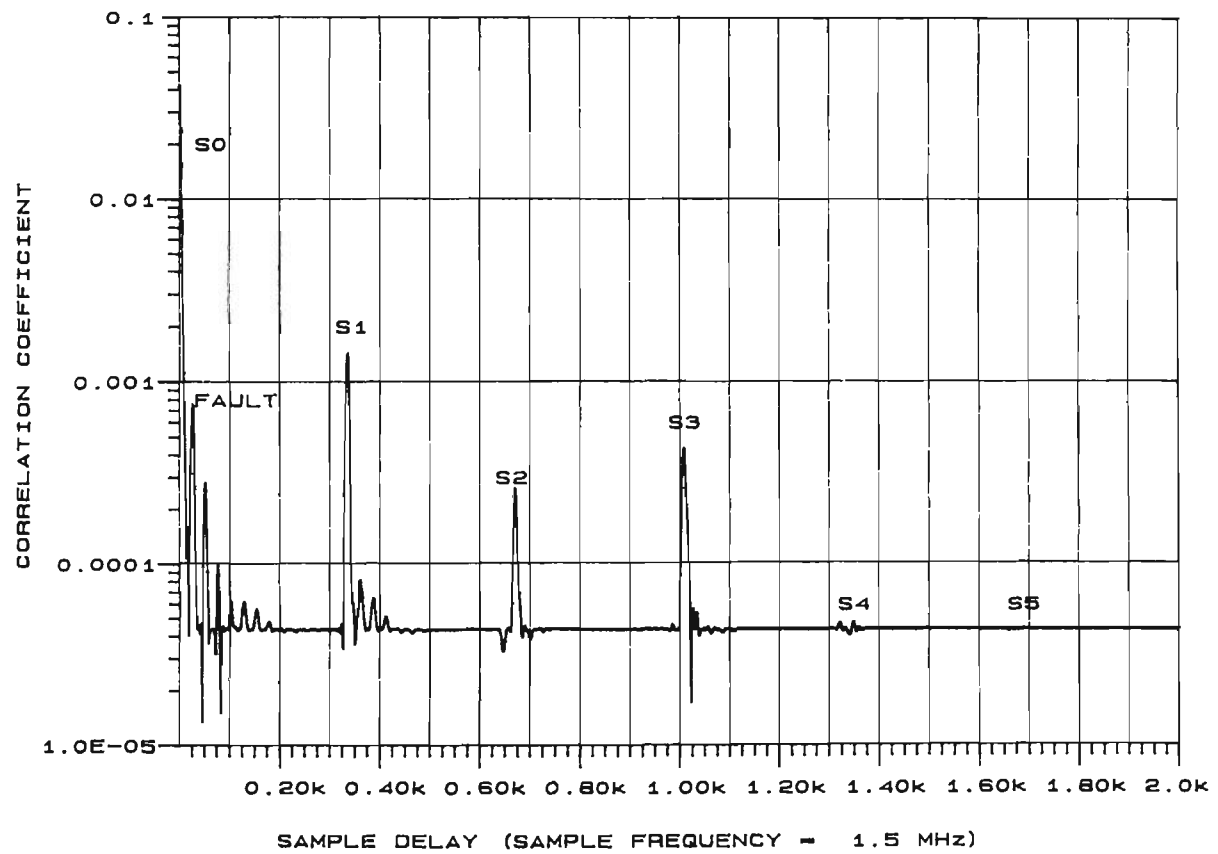

Figure 5.17(b) *Correlation coefficient for V_{S_M} at sending end for a fault on line 2 at* $x = 2.5$ *km with* $R_F = 1$ *ohm.*

Figure 5.17 *Direct sequence parameters :* $f_0 = 300$ *kHz,* $R_c = 220$ *kHz,* $L = 1023$.

5.5.1.7 Effect of Finite Bit Resolution in the Receiver

In Fig. 5.18 are the graphs of the correlation coefficients of V_{SS_M} and V_{S_M} recorded using a 7 bit A/D in the waveform recorder. It may be seen that the reflection from the fault accurately reveals the fault position despite the fact that this signal is toggling only one bit in the receiver. With a 6 bit A/D in the waveform recorder the correlation peak due to the fault reflection was degraded - however the waveform at the receiving end of the line was reproduced accurately. This is because at the sending end direct feedthrough from the transmitter reduces the dynamic range available for the fault waveform.
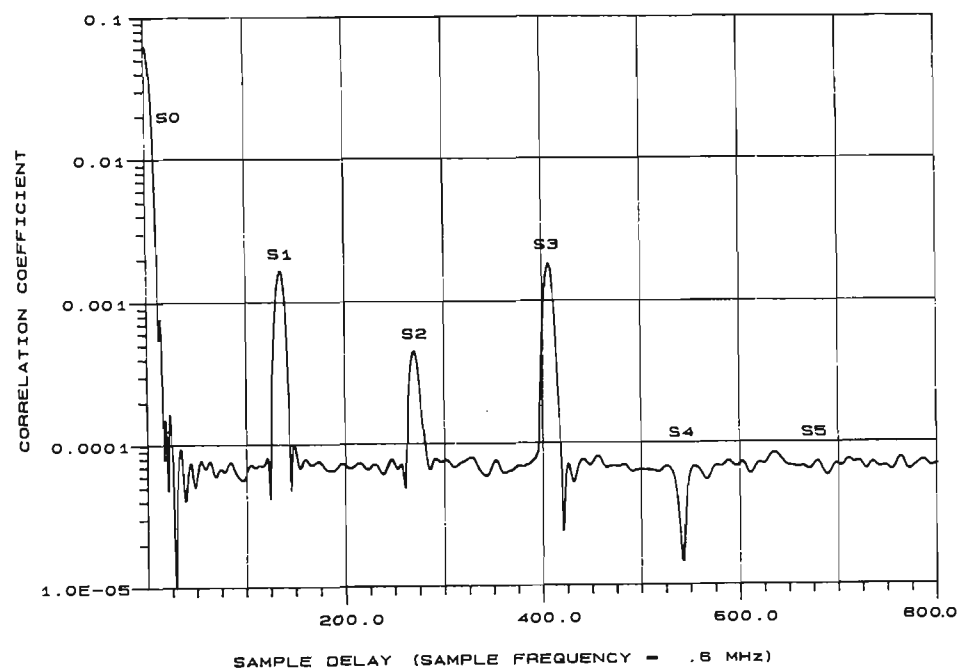

Figure 5.18(a)
Correlation coefficient for V_{SS_M} at sending end for unfaulted line with a 7 bit A/D in the waveform recorder.
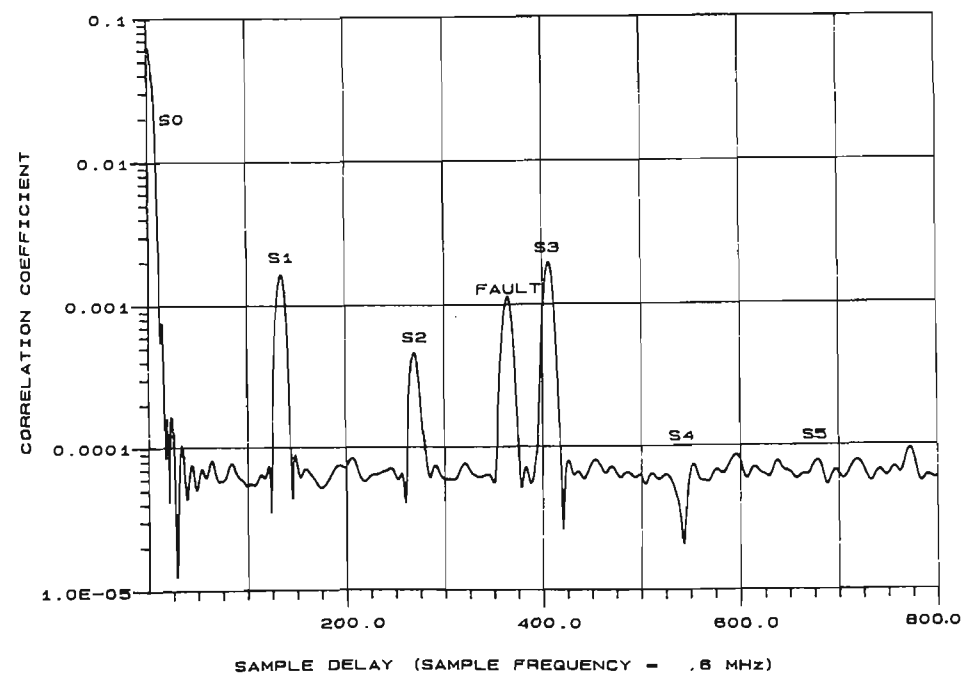

Figure 5.18(b)
Correlation coefficient for V_{S_M} at sending end for a fault on line 2 at x = 90 km with R_F = 1 ohm and a 7 bit A/D in the waveform recorder.

5.6 CONCLUSION

A program to simulate the propagation of power line carrier signals on a polyphase transmission line which takes into account the frequency variation of line and PLC interface parameters must be based on the reflection factor method. For a 100 km double transposed line it was found that using the ABCD transmission parameters produced unacceptably high truncation errors at frequencies above 170 kHz.

When a narrowband PLC signal is transmitted down an EHV system the resultant steady state voltage distribution derives from two distorting influences.

1) Reflections from unmatched terminations and transpositions producing alternate maxima and minima separated by $\lambda/4$.

2) Interference effects due to the different modes of propagation sliding past each other. Mode 1 has high attenuation and so its effects are short lived while modes 2 and 3, the principal propagation modes, produce major voltage fluctuations along the line. Modal interference effects produce more gradual voltage variations along the line than those caused by reflections.

Examinations of the rms voltage distribution when a direct sequence spread spectrum signal is transmitted show that the effects due to 1) above virtually sum to zero over the wideband spectrum but the same modal cancellation effects described in 2) are apparent. By the principle of reciprocity, the pre-fault voltage at any point indicates the strength of the reflection from a fault at the same point. Consequently areas of weak reflection can be identified - these will be different with a different carrier frequency.

Simulations of the direct sequence location of permanent single phase to ground faults indicate that a direct sequence signal with f_0 = 140 kHz, R_c = 60 kHz and L = 1023 operating with an 8 bit A/D in the measuring apparatus would be sufficient to locate worst case faults on the simulated 100 km line with an accuracy of 0.42%. Signals with larger bandwidths provide greater resolution closer to the transmitter but their range is limited because of the higher frequencies involved. The accuracy of 0.42% of the line length obtained from simulations compares favourably with the calculated value of 1% from Table 4.2 (BW1) of the previous chapter. The improved accuracy is

due to the interpolation technique used to estimate the exact position of the correlation maxima.

Modal propagation was initially thought to be the major cause of error, but a simple test that involved eliminating the effect of the coupling equipment and line traps produced an order of magnitude improvement in accuracy from 0.25% to 0.02%. The frequency selective components in the line interface appear to be the dominant source of error - unfortunately, in a practical situation, they cannot be removed!

To experimentally test these simulations and system design predictions we turn now to on-line measurements, which is the subject of the next chapter.

5.7 APPENDICES

This section gives details of derivations of the equations used in the simulation program.

5.7.1 ABCD Parameter Transpositions

Transpositions may be represented by a permutation matrix T which specifies the re-assigned geometrical positions of the lines as they pass through each transposition. If a line segment of length x in a homogeneous line section is represented by the transmission parameter matrix

$$\begin{bmatrix} A(x) & B(x) \\ C(x) & D(x) \end{bmatrix}$$

then a line segment of identical length in the following homogeneous line section has the matrix

$$\begin{bmatrix} T^{-1} & 0 \\ 0 & T^{-1} \end{bmatrix} \begin{bmatrix} A(x) & B(x) \\ C(x) & D(x) \end{bmatrix} \begin{bmatrix} T & 0 \\ 0 & T \end{bmatrix}$$

Similarly the characteristic impedance matrices in the three homogeneous line sections are, in order from the transmitter, Z_0, $T^{-1}Z_0 T$, $T^{-2}Z_0 T^2$.

5.7.2 ABCD Parameters Pre-Fault Conditions

Adapting Equations 5.1 and 5.2 the boundary conditions become

$$I_{SS} = -Y_S V_{SS} + a_S V_{TX} \qquad \textit{Equation 5.4}$$

$$I_{RS} = Y_R V_{RS} \qquad \textit{Equation 5.5}$$

$$\begin{bmatrix} V_{SS} \\ I_{SS} \end{bmatrix} = \begin{bmatrix} A_1 & B_1 \\ C_1 & D_1 \end{bmatrix} \begin{bmatrix} A_2 & B_2 \\ C_2 & D_2 \end{bmatrix} = \begin{bmatrix} A & B \\ C & D \end{bmatrix} \begin{bmatrix} V_{RS} \\ I_{RS} \end{bmatrix} \qquad \textit{Equation 5.6}$$

$$\begin{bmatrix} V_{FS} \\ I_{FRS} \end{bmatrix} = \begin{bmatrix} A_2 & B_2 \\ C_2 & D_2 \end{bmatrix} \begin{bmatrix} V_{RS} \\ I_{RS} \end{bmatrix} \qquad \textit{Equation 5.7}$$

Substituting Equations 5.4 and 5.5 into Equation 5.6 we get

$$[\, C + DY_R + Y_S(A + BY_R)\,]V_{RS} = a_S V_{TX}$$

Solving this equation for V_{RS}, Equation 5.3 can be derived by calculating I_{RS} from Equation 5.5 and substituting V_{RS} and I_{RS} into Equation 5.7.

5.7.3 ABCD Parameters Total Waveform

In this case Equations 5.1 and 5.2 describe the boundary conditions and the transmission parameter equations are

$$\begin{bmatrix} V_S \\ I_S \end{bmatrix} = \begin{bmatrix} A_1 & B_1 \\ C_1 & D_1 \end{bmatrix} \begin{bmatrix} V_F \\ I_{FS} \end{bmatrix} \qquad \textit{Equation 5.8}$$

$$\begin{bmatrix} V_F \\ I_{FR} \end{bmatrix} = \begin{bmatrix} A_2 & B_2 \\ C_2 & D_2 \end{bmatrix} \begin{bmatrix} V_R \\ I_R \end{bmatrix} \qquad \textit{Equation 5.9}$$

Using the notation

$$\begin{bmatrix} A_{r1} & B_{r1} \\ B_{r1} & D_{r1} \end{bmatrix} = \begin{bmatrix} A_1 & B_1 \\ C_1 & D_1 \end{bmatrix}^{-1}$$

$$\begin{bmatrix} V_F \\ I_{FS} \end{bmatrix} = \begin{bmatrix} A_{r1} & B_{r1} \\ C_{r1} & D_{r1} \end{bmatrix} \begin{bmatrix} V_S \\ I_S \end{bmatrix}$$

we get

$$\textit{Equation 5.10}$$

From Fig. 5.5

$$V_F = E_F + R_F(I_{FS} - I_{FR}) \qquad \textit{Equation 5.11}$$

For a single phase to ground fault on line 1 for example, $E_{F1} = 0$, $E_{F2} = V_{F2}$ and $E_{F3} = V_{F3}$. Substituting Equation 5.1 into Equation 5.10

$$V_F = (A_{r1} - B_{r1}Y_S)(C_{r1} - D_{r1})^{-1}I_{FS} + [B_{r1} - (A_{r1} - B_{r1}Y_S)(C_{r1} - D_{r1}Y_S)^{-1}D_{r1}]a_S V_{TX}$$

Substituting Equation 5.2 into Equation 5.9

$$V_F = (A_2 + B_2Y_R)(C_2 + D_2Y_R)^{-1}I_{FR} \qquad \textit{Equation 5.13}$$

Evaluating V_F in terms of I_{FS} - I_{FR} from Equations 5.12 and 5.13 and substituting into Equation 5.11

$$E_F = Z(I_{FS} - I_{FR}) + Q \qquad \textit{Equation 5.14}$$

where

$$Z \equiv [(C_{r1} - D_{r1})(A_{r1} - B_{r1})^{-1} - (C_2 + D_2 Y_R)(A_2 + B_2 Y_R)^{-1}]^{-1} - R_F$$

$$Q \equiv (Z + R_F)[(C_{r1} - D_{r1}Y_S)(A_{r1} - B_{r1}Y_S)^{-1} B_{r1} - D_{r1}]a_S V_{TX}$$

Hence for a single phase to ground fault on line 1 Equation 5.14 becomes

$$\begin{bmatrix} 0 \\ E_{F2} \\ E_{F3} \end{bmatrix} = \begin{bmatrix} Z_{11} \\ Z_{21} \\ Z_{31} \end{bmatrix} [I_{FS1} - I_{FR1}] + \begin{bmatrix} Q_1 \\ Q_2 \\ Q_3 \end{bmatrix}$$

which is easily solved for I_{FS1} - I_{FR1}, E_{F2} and E_{F3}. These values are then substituted into equation 5.11 to solve for V_F. Substituting Equation 5.1 into Equation 5.8

$$V_S = A_1 V_F + B_1 D_1^{-1}(-Y_S V_S + a_S V_{TX} - C_1 V_F)$$

5.7.4 Reflection Factor Transpositions

5.7.4.1 Compression

Fig. 5.8 depicts a line segment of length x with characteristic admittance and impedance matrices Y_c and Z_c respectively, and with a boundary condition on the left hand side given by Equation 5.15. In order to replace this boundary condition/line section/transposition with the equivalent boundary condition on the far side of the transposition, Equation 5.18, the matrix Y_b and vector k_b must be calculated. The equations required are as follows :

$$I_a = -Y_a V_a + k_a \qquad \textit{Equation 5.15}$$

$$I_a = Y_c[V_1 - \exp(-\psi x)V_2] \qquad \textit{Equation 5.16}$$

$$V_a = V_1 + \exp(-\psi x)V_2 \qquad \textit{Equation 5.17}$$

$$I_b = -Y_b V_b + k_b \qquad \textit{Equation 5.18}$$

$$I_b = T^{-1} Y_c T[\exp(-\psi x)V_1 - V_2] \qquad \textit{Equation 5.19}$$

$$\mathbf{V_b} = [\exp(-\psi x)\mathbf{V_1} + \mathbf{V_2}] \qquad \qquad \textit{Equation 5.20}$$

Equations 5.15, 5.16 and 5.17 give $\mathbf{V_2}$ in terms of $\mathbf{V_1}$. Substituting this expression into Equations 5.18, 5.19 and 5.20 gives

$$\mathbf{Y_b} = \mathbf{Y_c}[\mathbf{U} - \exp(-\psi x)(\mathbf{Y_c} + \mathbf{Y_a})^{-1}(\mathbf{Y_c} - \mathbf{Y_a})\exp(-\psi x)]$$

$$[\mathbf{U} + \exp(-\psi x)(\mathbf{Y_c} + \mathbf{Y_a})^{-1}(\mathbf{Y_c} - \mathbf{Y_a})\exp(-\psi x)]$$

$$\mathbf{k_b} = [\exp(-\psi x)\mathbf{Z_c}]^{-1} \{ [\exp(-2\psi x)(\mathbf{Y_c} + \mathbf{Y_a})^{-1}(\mathbf{Y_c} - \mathbf{Y_a}) - \mathbf{U}]$$

$$[\exp(-2\psi x)(\mathbf{Y_c} + \mathbf{Y_a})^{-1}(\mathbf{Y_c} - \mathbf{Y_a}) + \mathbf{U}]^{-1} + \mathbf{U} \} (\mathbf{Y_c} - \mathbf{Y_a})^{-1}\mathbf{k_a}$$

5.7.4.2   Expansion

For the inverse situation assume that $\mathbf{Y_b}$, $\mathbf{k_b}$, $\mathbf{V_3}$ and $\mathbf{V_4}$ are known. From Fig. 5.8

$$\exp(-\psi x)\mathbf{V_1} + \mathbf{V_2} = \mathbf{V_3} + \mathbf{V_4}$$

$$\mathbf{Y_c}[\exp(-\psi x)\mathbf{V_1} - \mathbf{V_2}] = \mathbf{T}^{-1}\mathbf{Y_c}\mathbf{T}(\mathbf{V_3} - \mathbf{V_4})$$

Solving these equations for $\mathbf{V_2}$ in terms of $\mathbf{V_1}$ and substituting into Equations 5.15, 5.16 and 5.17

$$\mathbf{V_1} = (\mathbf{Y_c} + \mathbf{Y_a})^{-1}(\mathbf{Y_c} - \mathbf{Y_a})\exp(-\psi x)\mathbf{V_2} + (\mathbf{Y_c} + \mathbf{Y_a})^{-1}\mathbf{k_a}$$

$$\mathbf{V_2} = 0.5\mathbf{Z_c}[(\mathbf{Y_c} - \mathbf{T}^{-1}\mathbf{Y_c}\mathbf{T})\mathbf{V_3} + (\mathbf{Y_c} + \mathbf{T}^{-1}\mathbf{Y_c}\mathbf{T})\mathbf{V_4}]$$

5.7.5   Reflection Factor Unfaulted Waveforms

Let D_1 be the length of the line from the transmitter to the first transposition and $\mathbf{K_{s1}}$ the reflection factor at the first transposition. Then with $\mathbf{V_1}$ as in Fig. 5.6

$$\mathbf{I_{SS}} = \mathbf{Y_0}[\mathbf{U} - \exp(-\psi D_1)\mathbf{K_{s1}}\exp(-\psi D_1)]\mathbf{V_1}$$

$$\mathbf{V_{SS}} = \mathbf{Y_0}[\mathbf{U} + \exp(-\psi D_1)\mathbf{K_{s1}}\exp(-\psi D_1)]\mathbf{V_1}$$

To solve for $\mathbf{V_1}$ use the boundary condition of Equation 5.1 at the transmitter and then use the expansion method of Appendix 5.7.4 to calculate the voltages at the fault position and at the receiver end.

5.7.6 Reflection Factor Fault Waveforms

Let $\mathbf{K_{t1}}$ be the reflection factor at the transmitter side line end/transposition at distance x_{t1} from the fault and let $\mathbf{K_{r1}}$ be the reflection factor at the line end/transposition on the receiver side at distance x_{r1} from the fault. Assuming the homogeneous line section in which the fault lies has characteristic admittance matrix $\mathbf{Y_c}$ then the equations for Fig. 5.6 become

$$\mathbf{V_{FF}} = [\mathbf{U} + \exp(-\psi x_{t1})\mathbf{K_{t1}}\exp(-\psi x_{t1})]\mathbf{V_2}$$

$$= [\mathbf{U} + \exp(-\psi x_{r1})\mathbf{K_{r1}}\exp(-\psi x_{r1})]\mathbf{V_3}$$

$$\mathbf{I_{FSF}} = \mathbf{Y_c}[\exp(-\psi x_{t1})\mathbf{K_{t1}}\exp(-\psi x_{t1}) - \mathbf{U}]\mathbf{V_2}$$

$$\mathbf{I_{FRF}} = \mathbf{Y_c}[\mathbf{U} - \exp(-\psi x_{r1})\mathbf{K_{r1}}\exp(-\psi x_{r1})]\mathbf{V_3}$$

$$\mathbf{V_{FF}} = \mathbf{E_{FF}} + \mathbf{R_F}(\mathbf{I_{FSF}} - \mathbf{I_{FRF}})$$

Combining these equations solve for $\mathbf{V_2}$ and $\mathbf{V_3}$ and then recover the end voltages using the expansion method of Appendix 5.7.4.

5.7.7 Reflection Factor Total Waveforms

The boundary condition at the sending end, Equation 5.1, when transferred to the faulted section (with characteristic admittance $\mathbf{Y_c}$) can be expressed as

$$\mathbf{Y_c}[\mathbf{V_1} - \exp(-\psi x_{t1})\mathbf{V_2}] = -\mathbf{Y_{t1}}[\mathbf{V_1} + \exp(-\psi x_{t1})\mathbf{V_2}] + \mathbf{a_{t1}}$$

for matrices $\mathbf{Y_{t1}}$ and $\mathbf{a_{t1}}$, while the other equations describing Fig. 5.6 become

$$\mathbf{V_F} = \exp(-\psi x_{t1})\mathbf{V_1} + \mathbf{V_2}$$

$$= [\mathbf{U} + \exp(-\psi x_{r1})\mathbf{K_{r1}}\exp(-\psi x_{r1})]\mathbf{V_3}$$

$$\mathbf{I_{FS}} = \mathbf{Y_c}[\exp(-\psi x_{t1})\mathbf{V_1} - \mathbf{V_2}]$$

$$\mathbf{I_{FR}} = \mathbf{Y_c}[\mathbf{U} - \exp(-\psi x_{r1})\mathbf{K_{r1}}\exp(-\psi x_{r1})]\mathbf{V_3}$$

$$\mathbf{V_F} = \mathbf{E_F} + \mathbf{R_F}(\mathbf{I_{FS}} - \mathbf{I_{FR}})$$

These equations can be solved for $\mathbf{V_1}$, $\mathbf{V_2}$ and $\mathbf{V_3}$ and the other voltages calculated using the expansion method described above in Appendix 5.7.4.

5.7.8 Line Data

Number of conductors = 3

Number of earth wires = 2

Line coordinates (metres) = (-8.7,8.2), (8.7,8.2), (0.,8.2), (6.85,16), (-6.85,16)

Conductor GMR (metres) = 0.0905

Earth wire GMR (metres) = 0.018

Relative magnetic permeability of conductor = 1

Relative magnetic permeability of earth wire = 1

Conductor resistivity (ohms-metres) = 3.21E-8

Earth wire resistivity (ohms-metres) = 3.21E-8

Radius of the outer layer conductor strands (metres) = 0.00125

Radius of the outer layer earth wire strands (metres) = 0.00175

Number of strands in the outer layer of conductors = 30

Number of strands in the outer layer of earth wires = 6

Number of conductors per bundle = 2

Earth resistivity (ohms-metres) = 100.0

Line length (km) = 100.0

Number of transpositions = 2

Transposition matrix $\mathbf{T} = \begin{bmatrix} 0 & 0 & 1 \\ 1 & 0 & 0 \\ 0 & 1 & 0 \end{bmatrix}$

Homogeneous line section lengths (km) = 33.3333, 33.3333, 33.3333

6. EXPERIMENTAL RESULTS OF LINE MONITORING AND FAULT LOCATION USING SPREAD SPECTRUM ON POWER LINE CARRIER

6.1   INTRODUCTION

Chapter 5 simulated the use of existing power line carrier equipment to transmit a spread spectrum waveform down a faulted EHV line. Analysis of the reflections from impedance discontinuities showed that the signals accurately revealed the location of the line fault despite the presence of modal distortions inherent in multiconductor propagation.   This chapter describes prototype hardware designed for on line measurements and presents data obtained on a 330 kV line of length 225 km. Section 6.2 briefly considers signal processing techniques designed to reduce spurious echoes caused by computations based on bandlimited signals.   Section 6.3 reviews the hardware used to obtain the experimental results and section 6.4 presents the signal processing algorithm used to analyse the data.   Finally the hardware results are presented in section 6.5 and conclusions are drawn in section 6.6.

6.2   SIDELOBE REDUCTION

Due to bandwidth limiting by the pulse shaping filter (Fig. 4.4) the compressed waveform has time sidelobes on each side of the main correlation peak.   This is illustrated in Fig. 6.1 which is the correlation coefficient from Equation 4.2 evaluated for the transmitter and receiver in loopback. An MLS code of length 63 with chip rate R_c = 60 kHz was bandlimited to the main lobe using a rectangular window and modulated onto a carrier with frequency f_0 = 140 kHz. The sample rate for the digitised waveforms is f_s = 2 MHz. The central correlation peak has width $2/R_c$ and has been normalised to unit magnitude. The residual correlation is 35.1 dB (20 dB/decade) down from the main correlation peak - this compares with the ideal code self rejection ratio (residual correlation) of $20\log_{10}(63)$ = 36.0 dB. The pulse shaping filter of Fig. 4.4(a) removes the spectral sidelobes of the ideal code which produces a 0.9 dB loss in residual correlation from the ideal.

The highest sidelobe is 31.1 dB down from the main peak. These sidelobes may either be mistaken for true echoes or mask an actual reflection. Two different
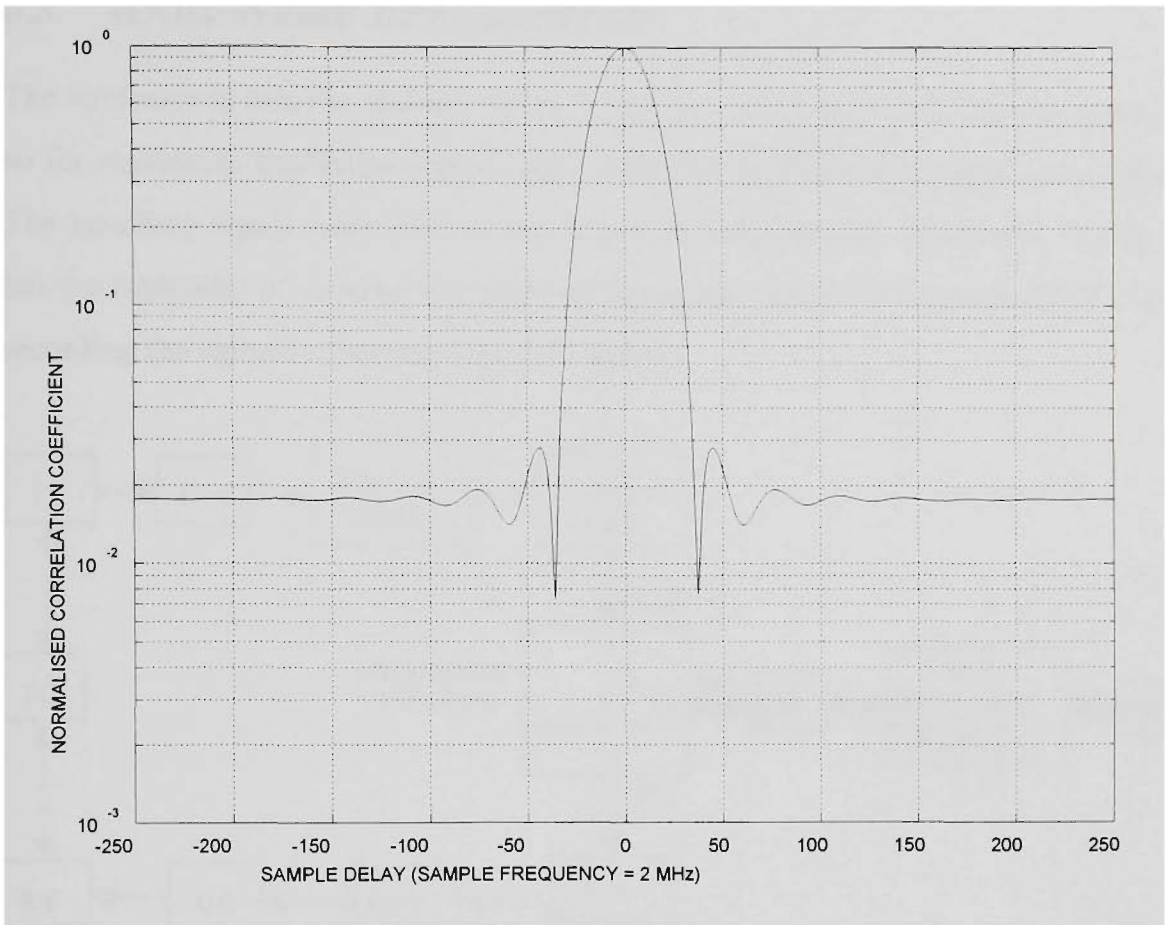

Figure 6.1 *Normalised correlation coefficient for loopback direct sequence waveform. MLS code of length 63 with chip rate R_c = 60 kHz and bandlimited to the main lobe modulating a carrier with frequency f_0 = 140 kHz. Sample frequency f_s = 2 MHz.*

approaches to sidelobe reduction may be used.

(1) Frequency weighting of the bandlimited code u(t) used in the transmitter and as reference waveform in the receiver processing.

(2) Sidelobe suppression filtering of the matched filter output [58].

In traditional radar system design frequency weighting is done only on the reference waveform u(t) used in the correlator [59] - this compromises the integrity of the matched filter processing. Sidelobe reduction comes at the expense of both reduced resolution and reduced signal-to-noise ratio. In the present application no sidelobe reduction techniques were implemented as our prime objective was to obtain the signature of a healthy transmission line with maximum accuracy. Any deviation from

this portrait, including the sidelobes, is of interest and indicates a change in line condition.

6.3 HARDWARE DESCRIPTION

The hardware to test the viability of the proposal was designed as a research tool and so for maximum flexibility digital signal processing (DSP) techniques were selected. The resulting signal transmission and acquisition equipment, illustrated in Fig. 6.2, has the capability of sending any arbitrary repeating waveform down an EHV line and recording the signals reflecting back off the line.
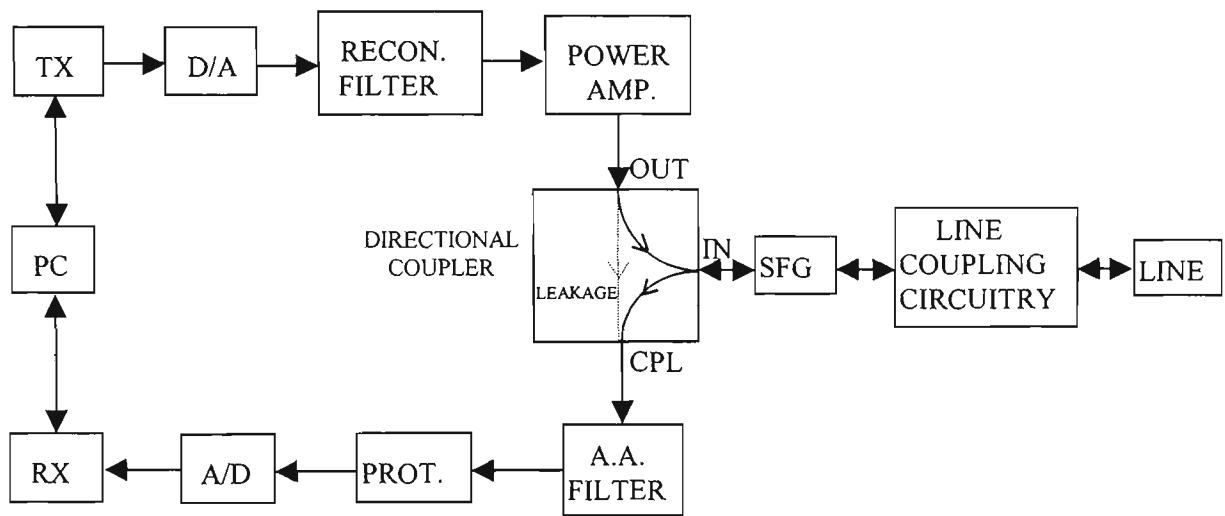

Figure 6.2 *Block diagram of data acquisition hardware.*

Broadcast waveforms were generated in software on a workstation as per Fig. 4.4 and downloaded from a personal computer (PC) to the transmitter memory. Waveform shape, bandwidth, carrier frequency f_0, pulse shaping, chip rate (R_c) and correlation sidelobes are all software controllable. The repetitive nature of the waveform means that only one code length of signal needs to be stored in memory. The digitised samples are read out at a sample rate $f_s = 2$ MHz, converted to analogue form by the 12 bit D/A converter and passed through the 5th order Bessel reconstruction filter before power amplification.

The amplified voltage passes through the directional coupler (or hybrid) and into the separation filter group (SFG) which relays the signal on to the line matching circuitry (LMC) which couples to the line. As explained in section 3.3.3.4 the SFG is used by the SECV to ensure adequate isolation between their different communication

channels, and the LMC (section 3.3.4) matches the 75 Ω communications room equipment to the 600 Ω impedance of the EHV lines. Signals coming back off the line follow the reverse path but travel through the directional coupler into the receiver.

Waveforms entering the receiver first go through a Bessel anti-aliasing filter and protection circuitry before being digitised by a 2 MHz, 12 bit, A/D converter and stored in high speed static RAM. To combat interference from line noise and PLC channels operating simultaneously in the same spectrum, the waveform recorder has the capability to average the incoming waveform up to 4095 times in real-time. The averaging exploits the repetitive nature of the transmitted waveform to give the receiver a wide dynamic range. The received waveforms are downloaded for data analysis which is performed off-line (not real-time) in a workstation environment.

Voltages registered by the receiver consist not only of signals coming off the line but also feedthrough of the emitted waveform from the transmitter through to the recorder. The directional coupler shown connecting the transmitter, the transient recorder and the SFG, increases the isolation between transmitter and receiver, preventing any leakage of the high power signal from overloading the analogue front end and reducing the dynamic range. Even with the isolation of a directional coupler the received signal still contains a large feedthrough leakage component compared to the highly attenuated reflections from the line which must be isolated using subsequent off-line correlation processing.

The PLC channels used by the SECV go up to 500 kHz in frequency. Waveforms at this frequency have a minimum Nyquist sampling frequency of 1 MHz. A sample rate $f_s = 2$ MHz was selected as a compromise between memory size and ease of analogue filter implementation for the reconstruction and anti-aliasing filters.

6.4   DATA ANALYSIS

Data analysis was performed off-line on a workstation. To increase processing speed cross-correlation of the data with the transmitted waveform was performed in the frequency domain according to the following equations

$$G(f_k) = \Im[u(t_i)\exp(-j2\pi f_0 t_i)] \qquad H(f_k) = \Im[r(t_i)] \qquad \textit{Equation 6.1}$$

$$y(t_n) = \frac{2}{N_P}\Im^{-1}[G(f_k)H^*(f_k)] \qquad (i,k,n = 0,1,2,..,N_P - 1) \qquad \textit{Equation 6.2}$$

Here $f_k = kf_s/N_P$ are the discrete frequency increments and $\tau_n = n/f_s$ and $t_i = i/f_s$ are the discrete time increments. $\Im[x(t_i)]$ denotes the Discrete Fourier Transform (DFT) of the digitised time waveform $x(t_i)$ of length $N_P = Lf_s/R_c$ points and $\Im^{-1}$ is the inverse DFT. Also * denotes complex conjugate, and $2/N_P$ is a scaling factor. Equations 6.1 and 6.2 are the frequency domain equivalents of Equation 4.2. In the graphs to follow the correlation coefficient functions $|y(\tau_n)|$ are plotted for each sample delay n between the waveforms s(t) and r(t). The normalised correlation coefficient is scaled so that the largest peak has unit magnitude.

6.5   HARDWARE RESULTS

6.5.1   Background to Experiment

Figure 6.3 is an overview of the EHV circuits running from South Morang Terminal Station to Dederang Terminal Station (SMTS to DDTS) in Victoria, Australia. Line 2 (on which some of the towers are illustrated eg T250, T234 and so on) runs the full 225 km distance in parallel with line 1. The State Electricity Commission of Victoria (SECV) took line 2 of the SMTS-DDTS system out of operation to upgrade a relay. Opportunity was taken of this short maintenance interval to attach the data acquisition equipment to the SFG, with bandwidth 150-200 kHz, connected to the de-energised line in the SMTS. No short circuits were placed on the line and the far end of the PLC communications network in the DDTS was open circuit.

6.5.2   Line Topology and Geography

Lines 1 and 2 are both horizontal, single circuit with two earth wires and have a separation of 110 feet - they cross rivers, distribution circuits (not shown in Fig. 6.3) and a large body of water in Lake Eildon. The two transpositions on line 2 are also highlighted at tower 362 (T362) and tower 168 (T168) - hereafter these are referred to as transposition 1 (T1) and transposition 2 (T2) respectively. In addition three other EHV lines travel for varying lengths in parallel with lines 1 and 2.
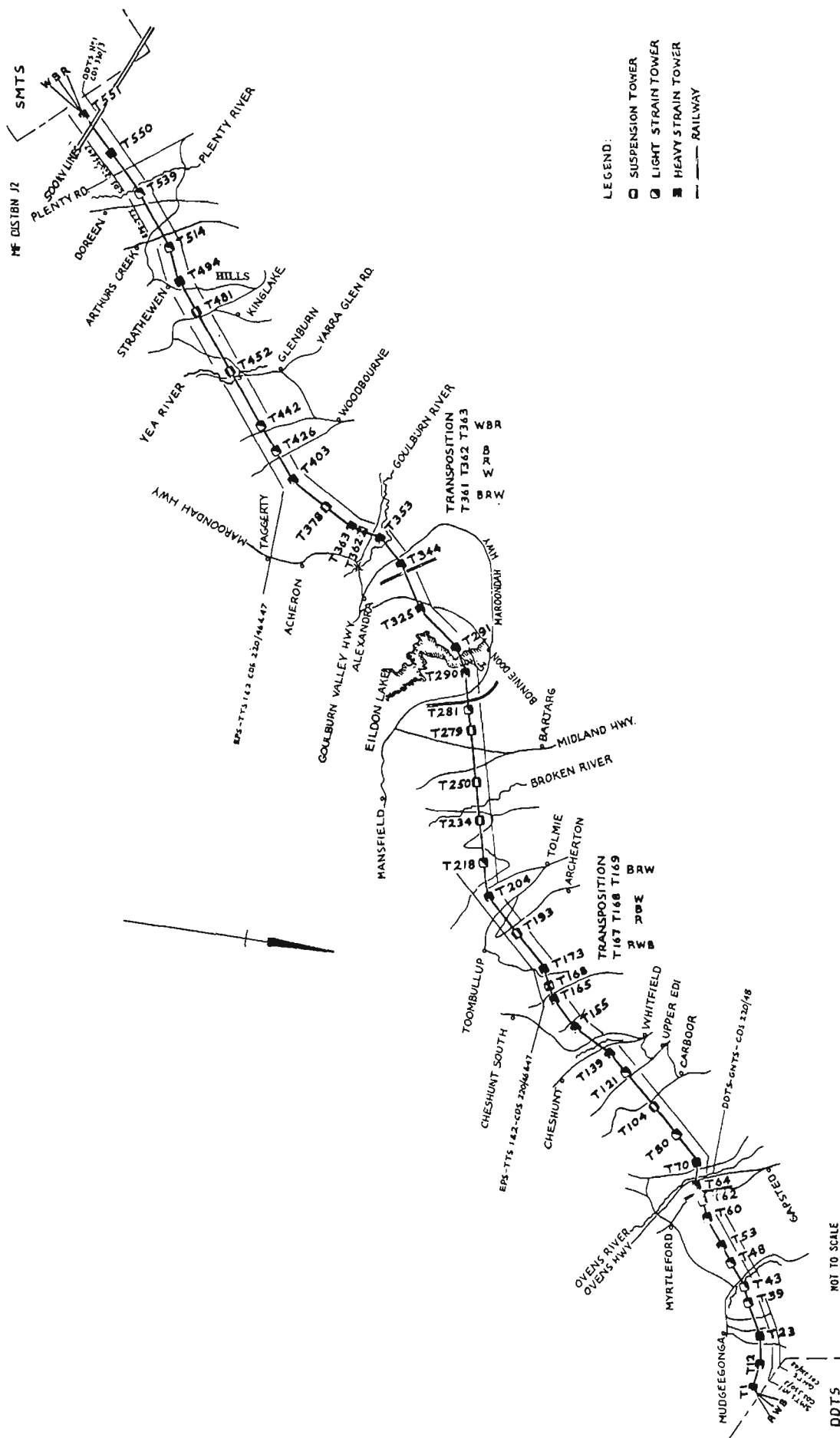
Figure 6.3 *South Morang Terminal Station to Dederang Terminal Station line overview. Reproduced by permission of Power Net Victoria.*

6.5.3   Existing PLC Channels

During the service period all the PLC communication channels were switched off line 2 (open circuit terminations) and diverted to line 1. Table 6.1 lists the single sideband (SSB) PLC channels in operation on this line. The channels have bandwidths of 4 kHz and occur in pairs, one for the GO direction and the other for the RETURN direction. Transmit powers were 1 Watt. It is seen that the last two channel pairs lie within the 150 - 200 kHz band of the spread spectrum line probing signal. Even though these PLC signals were switched to the adjacent line, there was still a considerable amount of interference from these channels because of the high cross-talk coupling between the two lines. All six channel pairs were therefore present as an interference signal to the received spread spectrum waveform. No attempt was made to filter out the four channel pairs outside of the band of the probing signal. These were also coupled into the anti-aliasing filter and A/D converter from line 1, further reducing the available dynamic range of the receiver.

Table 6.1 *PLC channels on line 1 operating during the test. The carrier frequency is listed first (ie the single sideband channels transmit information in the lower sideband).*

GO - TX SMTS-DDTS (kHz)	RETURN - RX DDTS-SMTS (kHz)	Function
84-80	88-84	VFT*
100-96	104-100	data (polling with ping-pong)
120-116	116-112	VFT
136-132	132-128	data
176-172**	172-168	VFT
192-188**	188-184	data

*   VFT = voice frequency tones

** inband channels

6.5.4   PLC Interference Suppression

SECV line measurements have previously shown that there can be up to 10 dB cross-talk between parallel lines sharing the same towers entering a terminal station. This

Table 6.2 *Statistics of noise waveform both with and without averaging.*

	no averaging	averaged 4095 times
peak to peak voltage	1.25 volts	4.54 mV
rms	0.241 volts	0.943 mV

usually prevents frequency re-use [51]. The cross-coupling will be less in this case because the lines do not share the same towers, even so the interference signal produced is still appreciable. The upper plot in Fig. 6.4 shows the interference and noise on line 2 logged with the transmitter idle, and the upper trace in Fig. 6.5 is the windowed frequency spectrum clearly showing the six PLC channel pairs operating on line 1 coupling into line 2. The power spectral density was derived from the 5040 data points using Welch's averaged periodogram method [60], with FFT and Hanning windows of lengths 1024 without overlap. Near end cross-talk is usually the strongest and comes from the six transmitters located at SMTS. The lower trace in Fig. 6.4 and the lower plot in Fig. 6.5 are the equivalent plots with the input waveform averaged N_A = 4095 times. Table 6.2 compares the statistics of the two recorded noise waveforms.
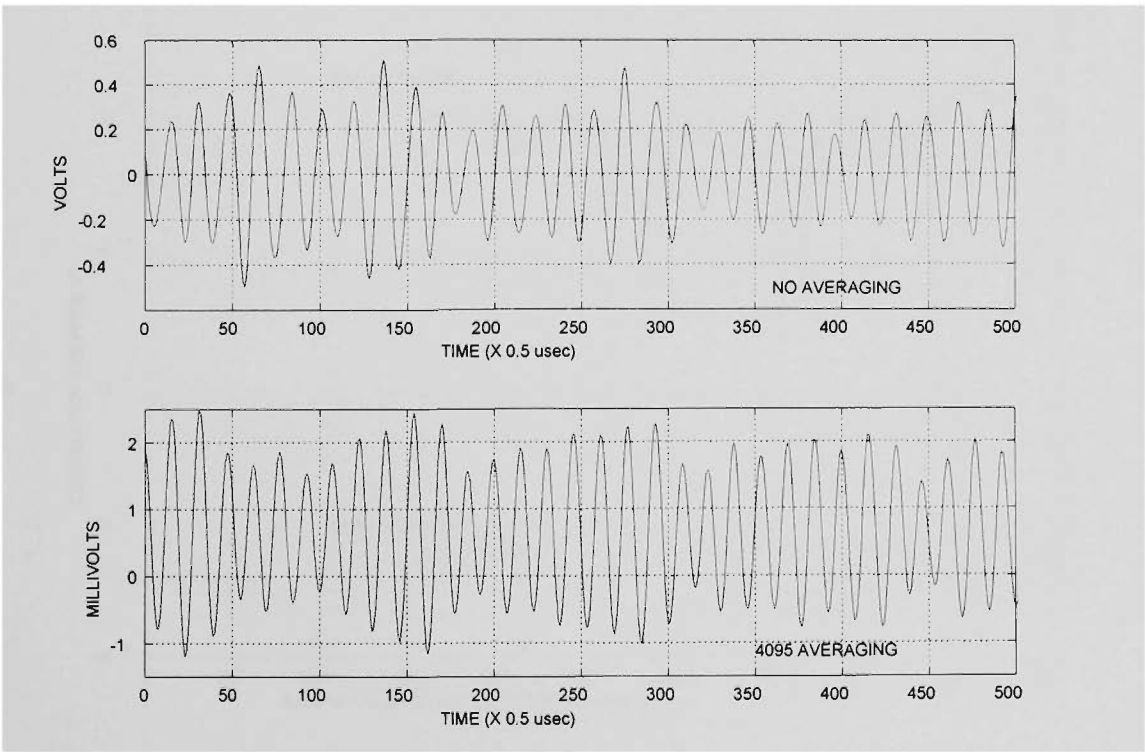

Figure 6.4 *The interference and noise on line 2 logged with the transmitter idle.*
Upper trace : Line noise (time domain) no averaging.
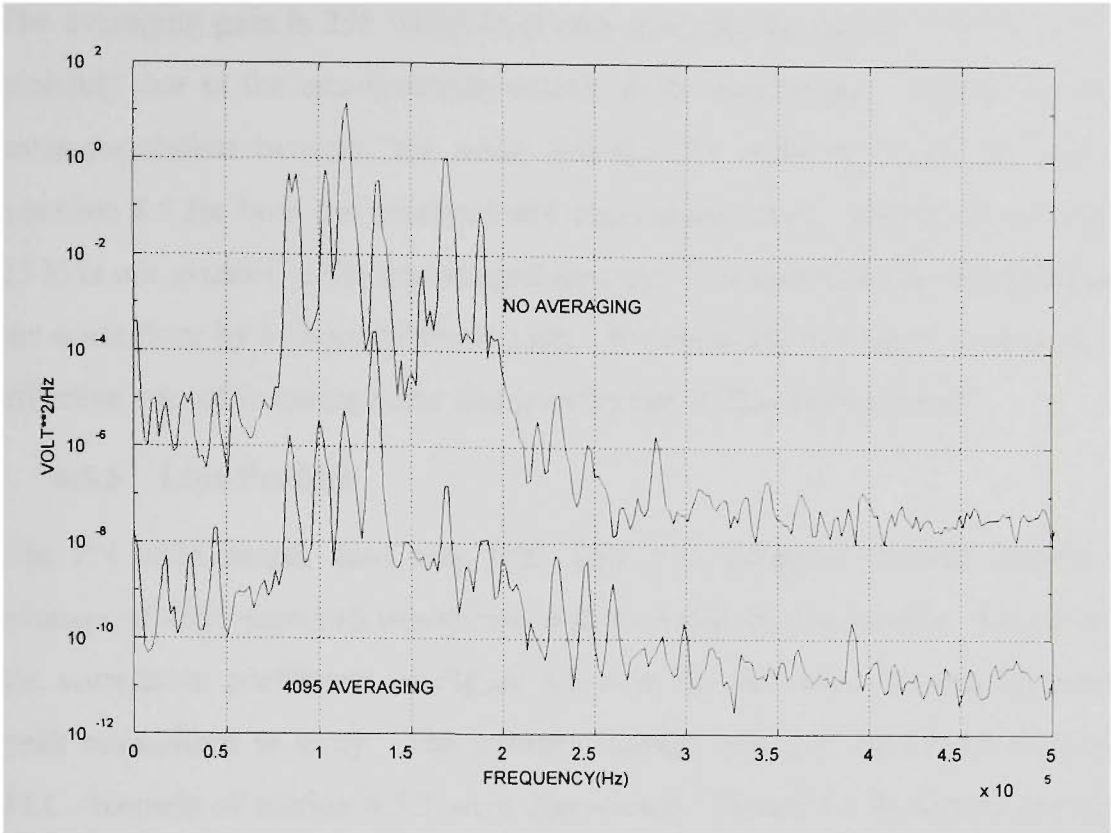*Lower trace : Line noise (time domain) 4095 averaging.*

Figure 6.5 *Windowed spectra of line noise.*
Upper trace : Without averaging.
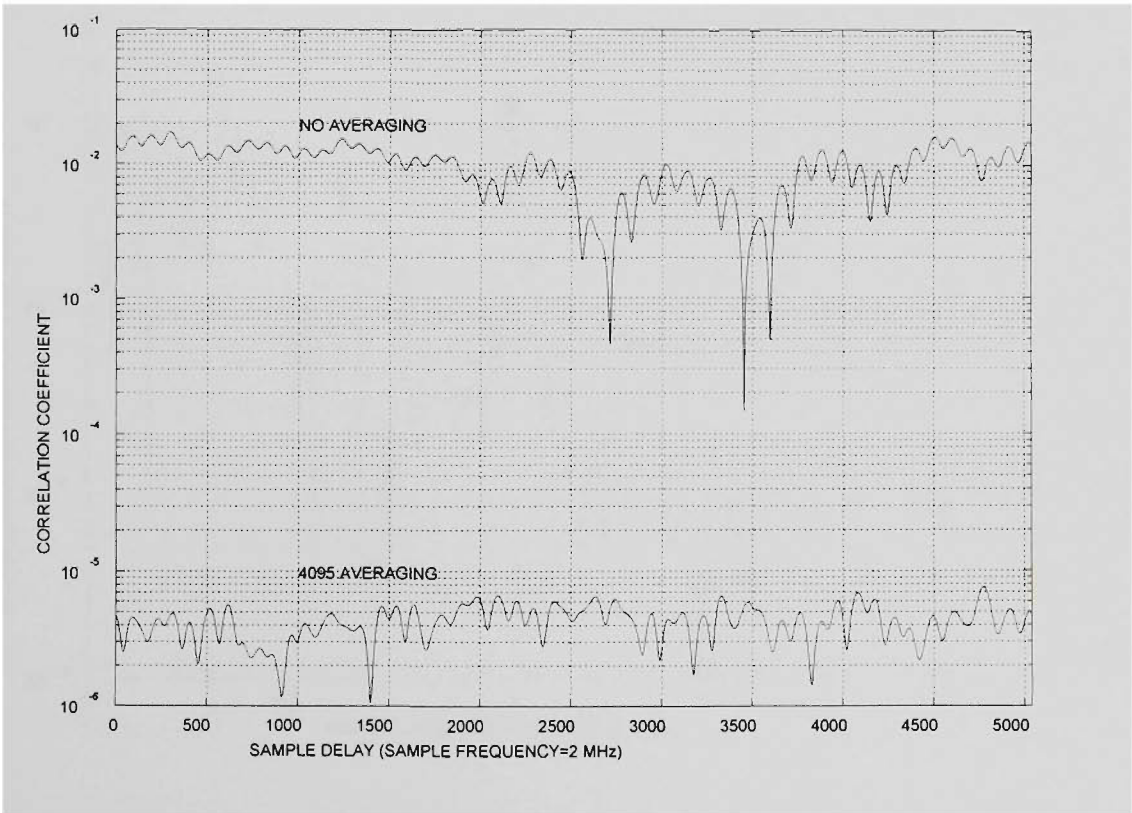*Lower trace : Average of 4095 noise recordings.*

Figure 6.6 *Correlation coefficient of PN code of length 63 with noise and interference (transmitter idle). Top trace is without averaging and bottom trace is with 4095 averaging.*

The averaging gain is 255 which is greater than the theoretical $\sqrt{4095} = 64$ - this is probably due to the non-Gaussian nature of the interference. Figure 6.6 shows the cross-correlation between the noise and the PN code of length 63 according to equation 4.5 for both the averaged and unaveraged cases. Ripples at the chip rate of 25 kHz are evident in the unaveraged case and it is seen that the averaging improves the noise floor by a factor of about 2500. We conclude that signal averaging is a very effective way of reducing noise and interference in this environment.

6.5.5   Line Profiles

The PN code length used was 1023 with two different transmit powers and the average of 4095 received waveforms was recorded by the receiver. Figure 6.7 shows the correlation coefficient of Figure 4.5 with the maximum transmitter feedthrough peak normalised to unity. The transmit voltage was 2.4 volts (0.08 W) and all the PLC channels of section 6.5.2 were operational. Figure 6.8 illustrates the correlation coefficient with a higher transmit voltage of 8.7 V (1 W) and with the major inband
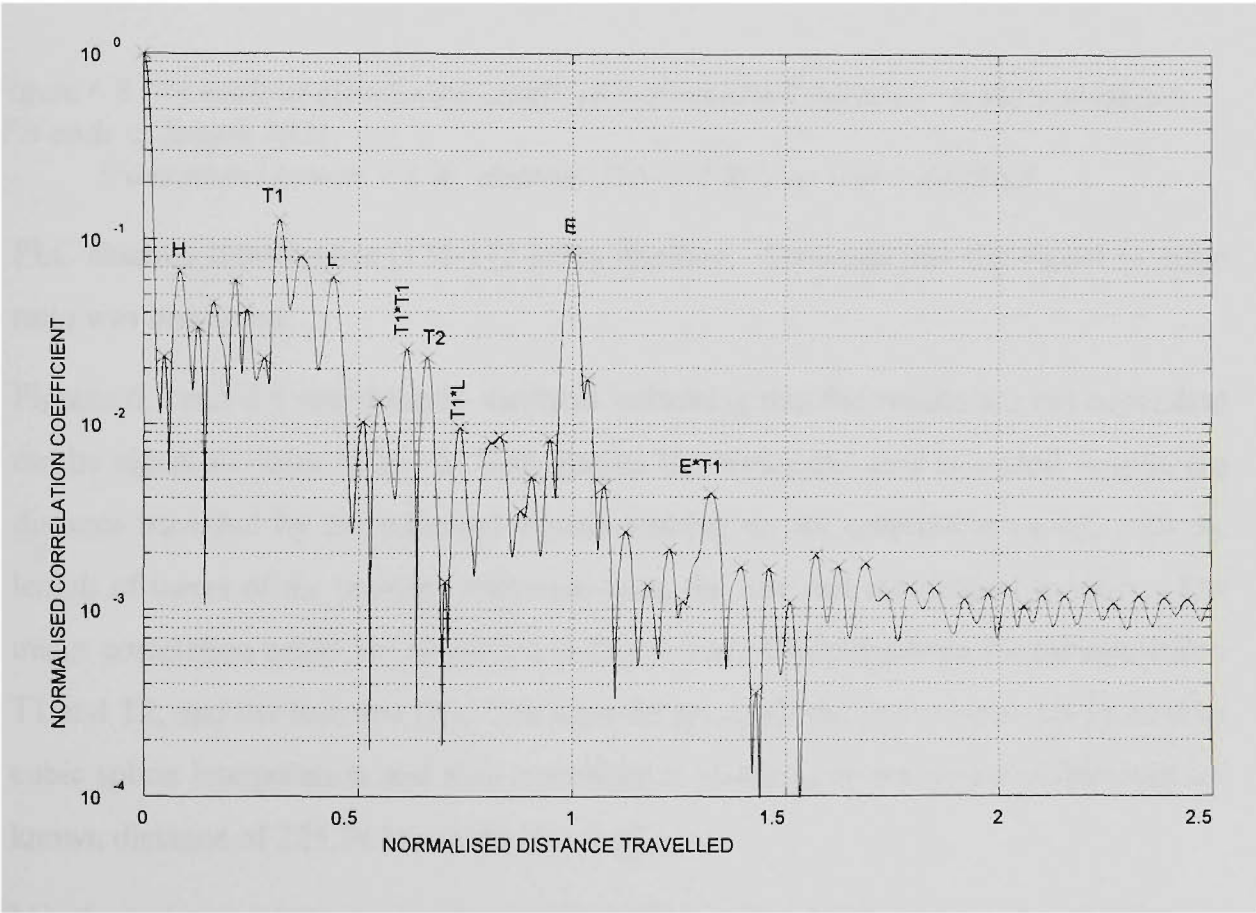

Figure 6.7 *Normalised correlation coefficient of received signals with the transmitted PN code of length 1023.*

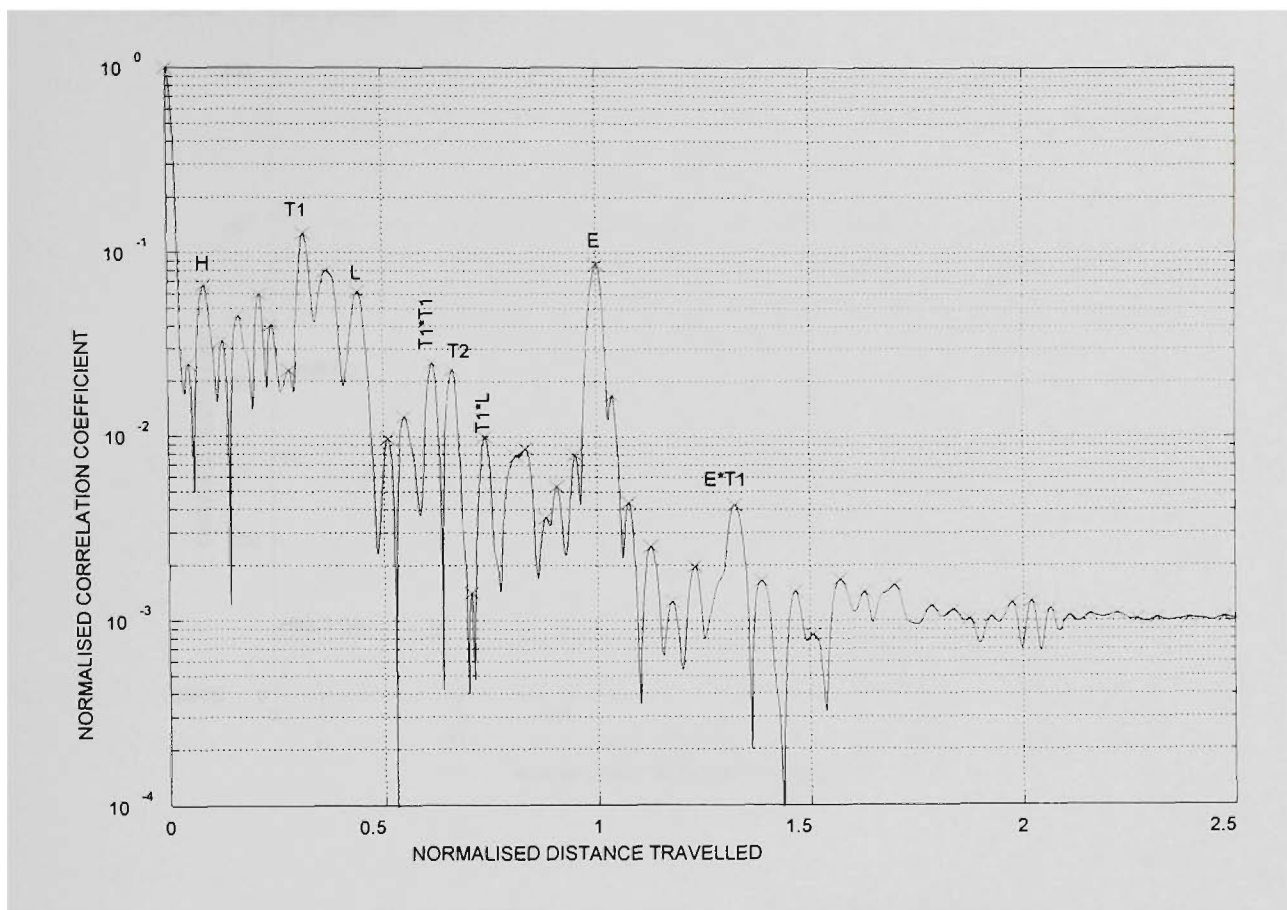*Transmitted power = 0.08 W, all channels on line 1 operational.*

Figure 6.8 *Normalised correlation coefficient of received signals with the transmitted PN code of length 1023.*

Transmitted power = 1 W, channel 176-172 kHz on line 1 disabled.

PLC channel interference (176-172 kHz) disabled. Consequently the signal to noise ratio was improved.

Figures 6.7 and 6.8 are virtually identical indicating that the results are not dependent on the signal to noise ratio. In both graphs the horizontal axis is scaled to give the distance travelled by the reflected signals making up the correlation peaks, with the length of travel of the primary reflection from the line end normalised to unity. The major correlation peaks are identified in Fig. 6.9 as reflections from the transpositions T1 and T2, and the line end (E). The time delays to all the peaks were determined by cubic spline interpolation and then converted to distance by interpolation between the known distance of 225.34 km to the line end.

In order to interpret the many other peaks in Figs. 6.7 and 6.8 a lattice diagram for line 2 is drawn in Fig. 6.9. The lattice diagram shows all signal paths with up to 3 reflections. The main reflections are the transpositions (T1 and T2), the line end (E)
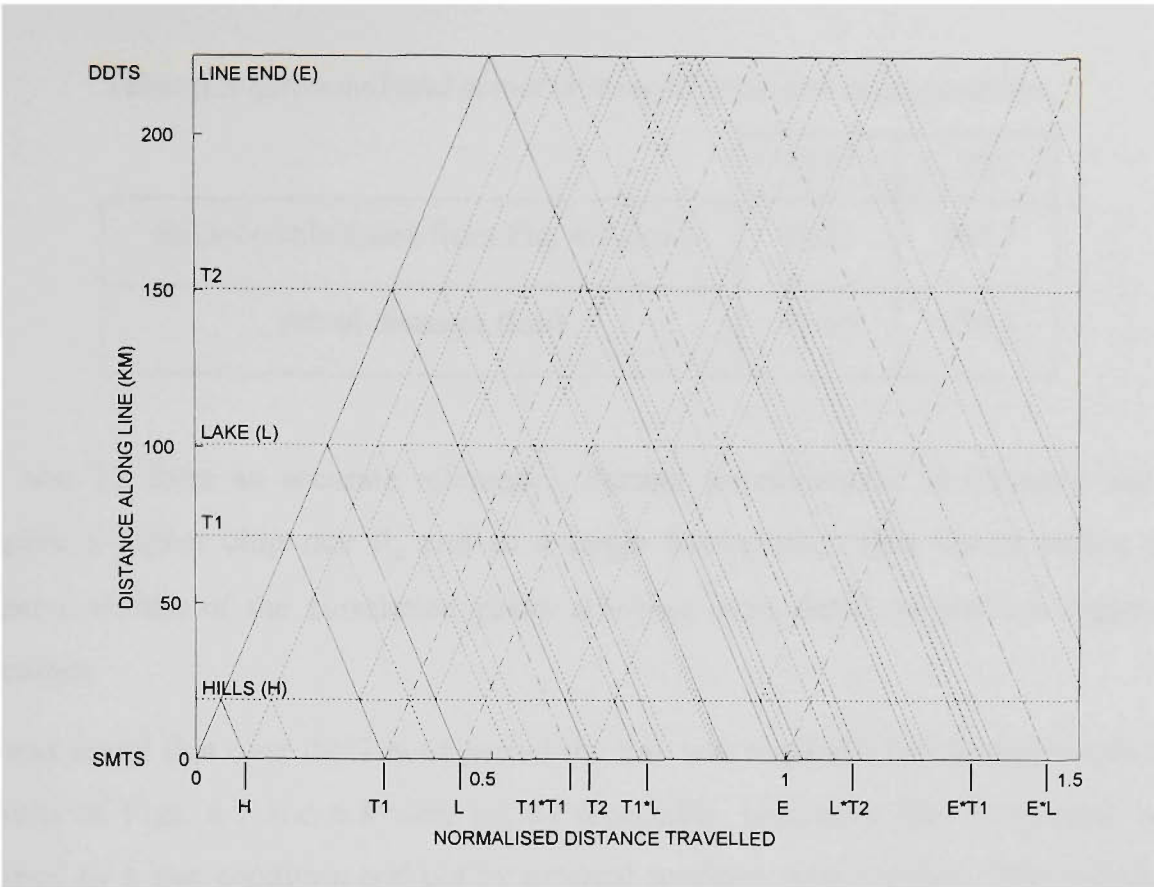
Figure 6.9 *Lattice diagram for SMTS-DDTS line.*

and a reflection from the transmission path over Lake Eildon (L). These are shown as solid lines. The major signal paths involving more than one reflection are shown as dashed (---) lines. Most of the major correlation peaks can be identified from these four main reflections. The remaining peaks can be attributed to other impedance changes, such as the change in ground constants when the lines pass over a range of wooded hills (H) and other geographical or physical conditions.

The lattice diagram shows that a change in line conditions at one point (such as a fault) will produce a number of peaks in the correlation output caused by the various reflection combinations. It is the first peak that determines the distance. This effect is illustrated in the simulations of chapter 5 where the first correlation peak caused by a fault had an amplitude comparable to that of a transposition near the line end. The distance to the fault was easily measured. Unfortunately for this test the line concerned was not out of service long enough to attach a short, but the transpositions can be easily detected indicating that the method would have no trouble in discerning a fault. Table 6.3 shows the predicted and actual distance to the two transpositions. The accuracy is 0.71% of the line length but would improve for a fault condition since

Table 6.3 *Estimated and actual distances to the line transpositions.*

	T1	T2
distance calculated from Fig. 6.7 (km)	71.21	148.7
actual distance (km)	71.65	150.3

T1 and T2 form an accurate reference. Further improvements in accuracy would require a higher chip rate R_c and so a larger bandwidth. This would reduce the relative widths of the correlation peaks allowing more detail as well as improved accuracy.

It was found that over the 2 hour period the line was available for measurements the results of Figs. 6.7 and 6.8 were highly repeatable, indicating that every peak was caused by a line condition and not by external spurious noise signals. The technique could therefore be used for monitoring small long term impedance changes in the line by comparing the correlation plot to a previous correlation template. This method could be of benefit in long term line diagnostics.

The incoming line reflections after the primary reflection from the line end are around 60 dB down from the transmitter feedthrough signal which is close to the bandwidth limited MLS code self rejection ratio of $20\log_{10}(1023) = 60.2$ dB [50]. This indicates that considerably more interference could be tolerated which raises the possibility of using spread spectrum line monitoring techniques with existing PLC equipment operating on the same line. Alternatively the amount of averaging can be reduced or eliminated which will give a faster response time.

6.6 CONCLUSION

This chapter has described the use of direct sequence spread spectrum waveforms at power line carrier frequencies for remote line diagnostics. The technique is suitable for both energised and de-energised lines because it uses an active probing signal.

The proposed method is sensitive enough to detect impedance discontinuities due to faults, transpositions and the line end; in addition large geographical anomalies appear as strong reflection peaks. Using the line end as a distance reference, the distance to

the first transposition was measured to within 0.5 km and the distance to the second transposition was measured to within 1.6 km. If the technique was to be used for fault location greater accuracy could be obtained because the transpositions as well as the line end could be used as a distance reference. Greater resolution and accuracy could be obtained by using a wider bandwidth spread spectrum probing signal. In this experiment the bandwidth was limited to 50 kHz by a line separation filter used by the existing PLC equipment. Bandwidths up to 450 kHz could be obtained if the line separation filters were bypassed.

This performance was achievable in the face of strong interference from PLC channels operating concurrently on an adjacent parallel line in the same bandwidth as the probing signal. This robustness required the application of interference suppression techniques in this case the use of an averaging capability in the receiver. The use of a much longer code would be equally effective. Long codes increase the data analysis time and averaging requires a longer data acquisition interval.

In the results shown here the processing was done off-line on a computer workstation. However real-time operation is possible with the use of modern digital signal processing components and typical data acquisition and processing times are listed in Table 6.4. The numbers in Table 6.4 are for N_P (the number of samples in a code period) = 2^{16} and f_s = 1.6 MHz. These figures are similar to the conservative design used in obtaining the above on-line results.

The acquisition time is determined by the signal transmission time needed to get the required number of averages ($T_P \times N_A = LN_A/R_c$).

The processing time is dependent upon the number of samples in a code period ($N_P = T_P f_s = Lf_s/R_c$), the particular algorithm implemented, and the performance of the DSP processor. From [61] the time required to evaluate the circular correlation of Equations 6.1 and 6.2, using Fast Fourier Transform (FFT) routines, is

$$T_{circ} = 2k_{ct}N_P\log_2(N_P) + k_m N_P$$

where k_{ct} and k_m are constants depending on the speed of the particular processor being used. k_{ct} is related to the time it takes for a single FFT butterfly operation and k_m depends also on the time required for a complex multiply operation. While this

equation assumes that N_P is a power of 2, similar processing times are achievable provided that N_P has many factors. The approximate processing times listed in Table 6.4 are for the Texas Instruments TMS320C30 floating point digital signal processor running at 20 MFLOPS and are based on the radix-2 complex FFT routine listed in [62]. These processing times would be reduced using a split radix or higher radix algorithm, and using a real FFT for the forward transform $H(f_k) = \Im [r(t_i)]$ of equation 6.1.

The table values for the processing and acquisition times are very conservative because of the large oversampling rate used in the measurements. It should be possible to reduce the sampling frequency closer to the Nyquist limit of 2 × signal bandwidth = 2 × 200 = 400 kHz.

Table 6.4 *Data acquisition and processing times on a 20 MFLOPS TMS320C30 processor, both with and without averaging, for $N_P = 2^{16}$ data points and sample frequency $f_s = 1.6$ MHz.*

	4095 averaging	no averaging
data acquisition time	167.73 sec	40.96 msec
data processing time	0.49 sec	0.49 sec
total response time	168.2 sec	0.53 sec

The method is flexible in that both low speed and high speed operation is possible. The former can tolerate strong interference, while the latter requires little interference (ie PLC channels switched off) so that the averaging and code length requirements can be reduced.

Separate lines entering a terminal station may be probed simultaneously by using different codes on each line. Provided the cross-correlation discrimination between the codes is sufficient to compensate for the cross-talk across the lines the method will be applicable to these network grids.

Most of the faults which occur on EHV line are of a transient nature [3]. Although these faults permit circuit reclosure, often damage is caused to cables or insulators. Code design for the detection and localisation of these transient arcing faults is the subject of Chapter 7.

7. CODE SELECTION FOR HIGH SPEED EHV POWER LINE CHANNEL SOUNDING USING SPREAD SPECTRUM

7.1 INTRODUCTION

EHV power lines convey electrical energy over hundreds of km from generating source to consumers and are also a transmission medium for voice and data communications channels between terminal stations via modulated power line carrier (PLC) waveforms in the frequency range 80 to 500 kHz. In Chapters 5 and 6 it was shown that the PLC infrastructure can also be used for detecting and locating faults using techniques borrowed from radar. The proposed method involved transmitting a signal from one end of the line and monitoring the magnitude and delay time of reflections of that signal caused by impedance changes in the line. It was shown using simulation that faults on either of the three phases would cause a large reflection that could be easily distinguished. Other features such as line transpositions and changes in ground constants also caused reflections. Measurements confirmed that reflections from the former were significant and could be used as a known reference point for fault location purposes.

PLC systems have a transmit power restriction based on the capability of the existing amplifiers and so traditional pulsed radar techniques (narrow pulse duration of high peak power) are not suitable. Direct sequence spread spectrum techniques based on periodic m-sequence spreading codes do not require the high peak power and were chosen for the measurements in Chapter 6. A disadvantage with this technique is that the codes are continuously transmitted and so the receiver (which is co-located) must identify the weak reflected signals in the presence of the strong transmitted signal. A directional coupler (hybrid) can be used to provide some isolation between the transmit and receive signals, but trans-hybrid leakage cannot be avoided and the signal into the receiver is still dominated by the transmitted signal. Codes with low auto-correlation properties are required to remove the self-interference effect of the transmitted signal. M-sequences have an auto-correlation function that falls to 1/L (L

= code length) of its peak value within 1 chip period of the maximum; long codes therefore have excellent auto-correlation properties.

Unfortunately, long codes take a long time to transmit, and the correlation processing in the receiver also takes a long time. They are not suitable for high speed operation. Shorter length sequences can lead to a quicker response time but the self-interference produced by the residual correlation limits the receiver's sensitivity irrespective of the signal to noise ratio of the received signal. The detection and location of faults could be jeopardised, particularly if the change in line impedance is small. This situation might arise if the fault impedance is significantly greater than zero. Additionally if the fault is intermittent over one code period then the residual correlation rises in an unpredictable fashion. Short codes are less likely to be affected by intermittent operation.

Section 7.2 considers the effect of finite fault impedance and intermittent operation (conduction duty cycle) using a simulated 100 km line based on the Wedepohl model [55]. If the fault impedance is increased to 300 ohms the signal returned to the receiver is reduced by over 8 dB. Such a return signal might not be identified at the receiver if a short m-sequence is being used to enable high speed operation. To overcome this loss of sensitivity, reduced residual correlation codes are analysed in section 7.3 and their effect on the output correlation coefficient are observed using both simulation (section 7.3) and measurement (section 7.4).

Finally, compatibility of the codes with other PLC services will be discussed in section 7.5, since it is important that interference into PLC channels sharing the same spectrum (although not necessarily on the same link) should be minimised. This is likely to occur if the modulated codes have a flat spectrum.

7.2 SIGNAL PROCESSING AND RESIDUAL CORRELATION

In this chapter for the data analysis we use a slightly modified form of Equations 6.1 and 6.2 for DFT processing.

$$y(\tau_n) = 2\frac{K_0}{N_P}\Im^{-1}\{\Im[u(t_i)\exp(-j2\pi f_0 t_i)]\Im^*[r(t_i)]\} \quad (i,n = 0,1,..,N_P -1) \quad \textit{Equation 7.1}$$

Here $\tau_n = n/f_s$ and $t_i = i/f_s$ are the discrete time increments, $\Im[x(t_i)]$ denotes the Discrete Fourier Transform (DFT) of the digitised time waveform $x(t_i)$ of length $N_P = Lf_s/R_c$ digitised points, * denotes complex conjugate, $\Im^{-1}$ is the inverse DFT and K_0 is a scaling factor which depends upon the code being used. In the graphs to follow the magnitude $|y(\tau_n)|$, the correlation coefficient, is plotted for each sample delay, n, between the waveforms s(t) and r(t).

Simulation results for a single circuit 100 km long horizontal line with equally spaced transpositions at 33.33 km and 66.66 km from the transmit end are discussed in Chapter 5. It is shown that a direct sequence waveform at PLC frequencies modulated by an MLS code of length 1023 will accurately locate line transpositions and faults. All three phases at the line ends are shorted to ground at the 50 Hz power frequency - the PLC coupled lines go to earth through line traps which have high impedance at PLC frequencies. Further simulation results are now discussed for a single phase to ground fault 90 km from the transmit end on the line which is not coupled to the two
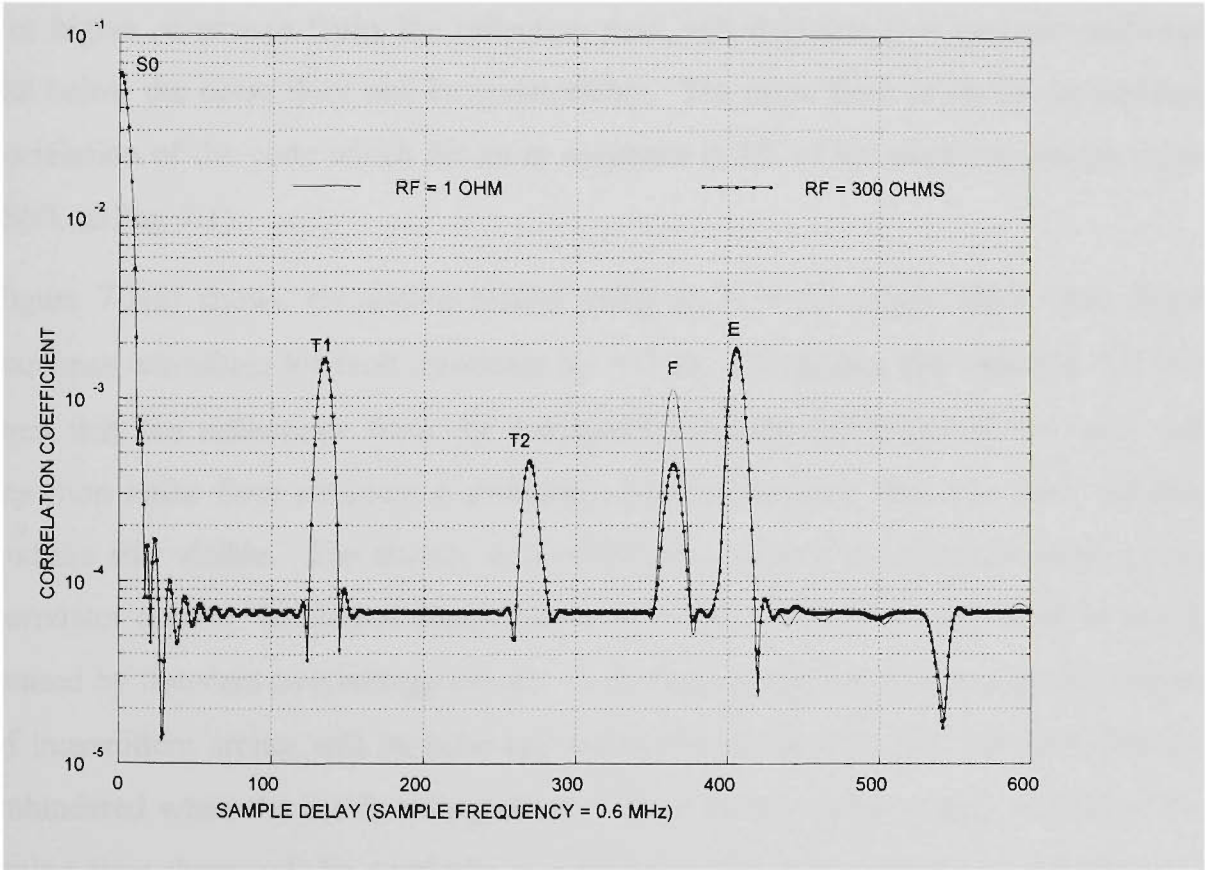
Figure 7.1 *Simulation line profiles of a faulted 100 km 3 phase line (fault resistances $R_F = 1\ \Omega$ and $R_F = 300\ \Omega$) using MLS code direct sequence waveforms. $f_0 = 140$ kHz, $R_c = 60$ kHz and L = 1023.*

phase differential PLC communication network. The sensing waveforms are direct sequence waveforms derived from MLS codes of different lengths. The carrier frequency is 140 kHz and the chip rate is 60 kHz. . For the MLS codes discussed in this section $K_0 = 1$.

Figure 7.1 shows simulation results using an $L = 1023$ length MLS code direct sequence waveform for different fault resistances $R_F = 1\ \Omega$ and $R_F = 300\ \Omega$. The large peak for zero sample delay is the leakage from the transmitter into the receiver and near this peak the sidelobe ripples at the chip rate are discernible. These are due to the bandlimiting of the code by the pulse shaping filter (Fig. 4.4(a)). The reflections from the transpositions (T1 and T2) are clearly visible as is the reflection from the line end (E). The reflections from the different resistance faults, labelled 'F', are of similar magnitude to the reflections from the transpositions and line end - the higher fault resistance reduces the reflected signal by a factor of 8.3 dB. Using the known distance covered by the reflection (E) the fault is measured as 89.7 km from the sending end with $R_F = 1\ \Omega$ and 89.75 km from the sending end with $R_F = 300\ \Omega$. For higher resistance faults the reflection peak will decrease in magnitude and may fall below the noise floor and be undetectable. The noise floor is set by the residual correlation of the code which for an m sequence is 1/L of the peak correlation value (S0/L in Fig. 7.1).

Figure 7.2(a) shows simulation results using an $L = 63$ length MLS code direct sequence waveform for fault resistance $R_F = 1\ \Omega$. Comparing this with Fig. 7.1 it is seen that the reflections from the transpositions have fallen below the code self rejection noise floor (residual correlation), while reflections from the fault and line end are still visible. The shorter code effectively reduces the dynamic range of the correlator output. Insulation deterioration on a high voltage line can result in arcing caused by transient overvoltage events. A probing signal passing through this region of intermittent arcing will be reflected during the arcing time but will pass through unhindered when the arc is extinguished. If the code is long enough to enclose the arcing time there will be aperiodic correlation in the data analysis of Equation 7.1 which will produce high sidelobes and residual correlation. For example, Figure 7.2(b) illustrates the degradation in this compressed waveform ($L = 63$) when $R_F = 1$
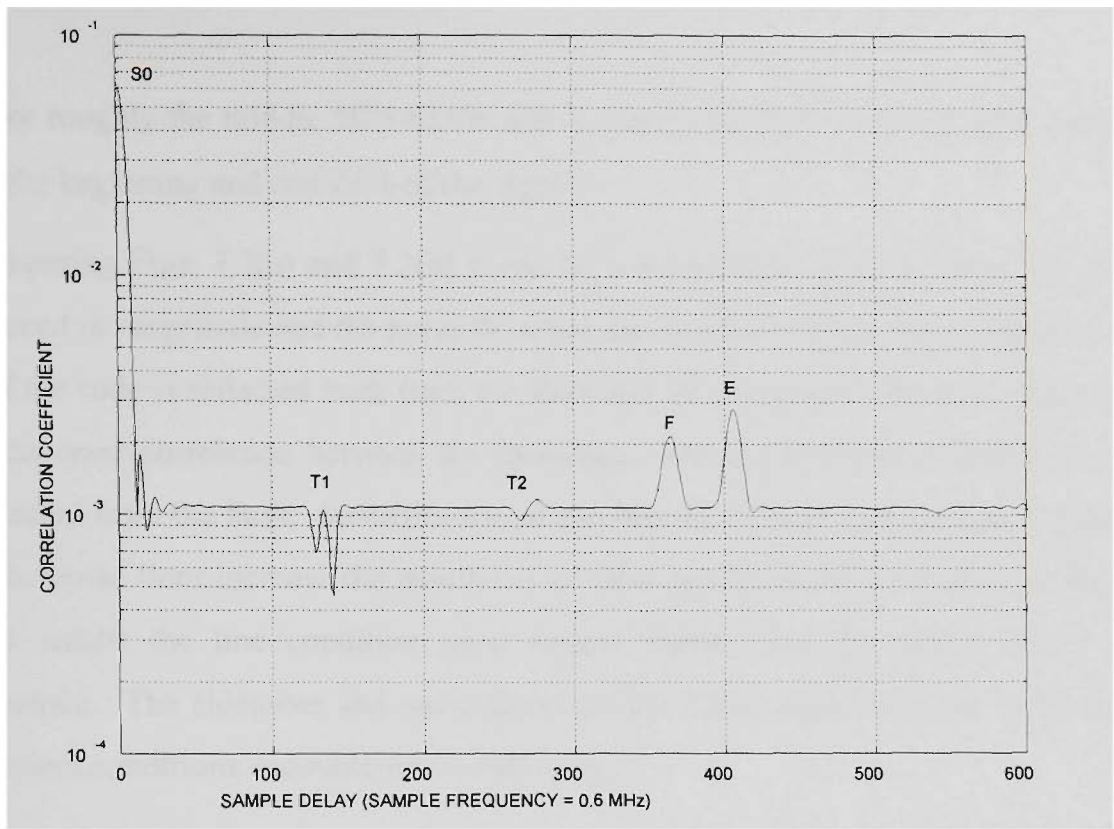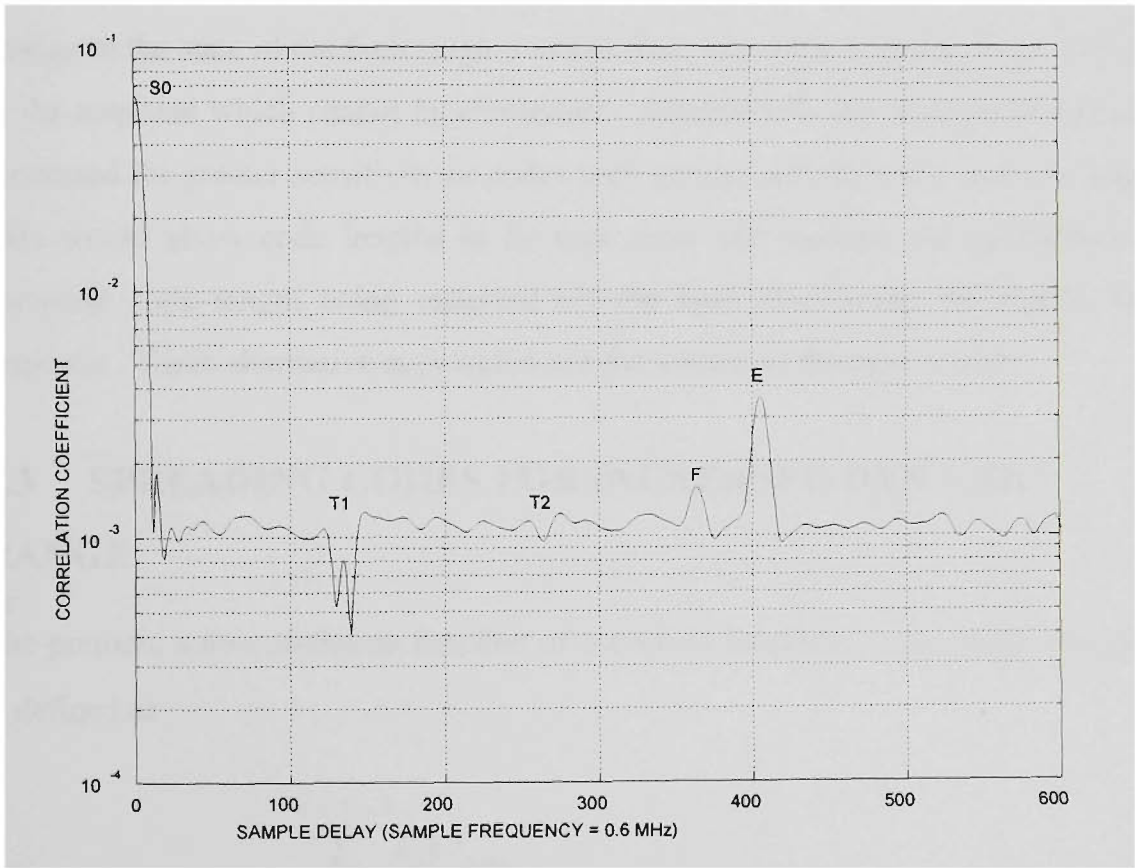
Figure 7.2(a) *Permanent fault.*

Figure 7.2(b) *Periodic intermittent fault, duty cycle ≈ middle 50% of code length.*

Figure 7.2 *Simulation line profiles of a faulted 100 km 3 phase line with fault resistances $R_F = 1 \ \Omega$ using MLS code direct sequence waveforms. $f_0 = 140 \ kHz$, $R_c = 60 \ kHz$ and $L = 63$.*

Ω for roughly the middle 50% of the active signal and $R_F = \infty$ (ie no fault condition) for the beginning and end 25% of the signal.

Comparing Figs. 7.2(a) and 7.2(b) it can be seen that the reflection from the fault is reduced in magnitude and the noise floor has increased and is no longer smooth. Only half the code is reflected back from the fault and the increase in the noise floor is due to the cross-correlation between the spreading code and the central half of the code reflected from the fault. Identification of the fault is difficult and the added sidelobes in the noise floor increase the possibility of false prediction of the fault position. For best results the line condition must remain stable over the period of the code sequence. The sidelobes and noise floor in Fig. 7.2(b) could be even worse for the transient conditions encountered on real lines.

To maintain dynamic range in the presence of these partial correlations longer code lengths could be used which would increase the processing time. This would reduce the residual noise floor, but the longer code periods are more likely to be affected by a change in the state of the fault (high Z to low Z or vice versa), giving rise to the ripple in the response which cannot be eliminated. Alternatively the m-sequences could be processed for greater sensitivity or codes with greater self rejection could be applied. This would allow code lengths to be kept short and increase the probability of a complete code length being reflected off the fault eliminating the ripples in the response. These alternative approaches are the subject of the next section.

7.3   SPREADING CODES FOR INCREASED DYNAMIC RANGE

The periodic auto-correlation function of a code of length L, $\{..,c_{L-1},c_0,c_1,..,c_{L-1},c_0,..\}$, is defined as

$$\rho(m) = \frac{\sum_{n=0}^{n=L-1} c_n c^*_{n+m}}{\sum_{n=0}^{n=L-1} |c_n|^2} \qquad m = 0,1,2,...,L-1 \qquad \textit{Equation 7.2}$$

where * denotes complex conjugate. The peak correlation is $\rho(0) = 1$. For high resolution channel sounding it is desirable that the spreading code has zero residual correlation, $\rho(m) = 0$ for $m \neq 0$ - a code with such an auto-correlation function is called orthogonal and has the greatest sensitivity to small reflections. Three methods of obtaining zero residual correlation are now presented.

7.3.1 DC Processing of MLS Codes

The well known binary maximal length sequence (MLS) codes, $c_i \in \{-1,+1\}$, generated by a shift register of length n with multiplicative feedback, have a length L $= 2^n - 1$ and a residual correlation of $-1/L$. This residual correlation may be reduced to 0 by subtracting the DC level of the code from the auto-correlation function of Equation 7.2:

$$\rho_{DC}(m) = \frac{\displaystyle\sum_{n=0}^{n=L-1} (c_n - 1)c^*_{n+m}}{\displaystyle\sum_{n=0}^{n=L-1} |c_n|^2} \qquad m = 0,1,2,\ldots,L-1$$

The peak correlation is $1 + \dfrac{1}{L}$ and so the value of the scaling constant K_0 in Equation 7.1 is set to $\dfrac{L}{L+1}$.

7.3.2 MLS Orthogonal Codes

The MLS orthogonal codes [63] are derived from the MLS codes by replacing each code value -1, +1 with complex numbers A_{-1}, A_{+1} respectively. Provided the complex numbers are chosen correctly the resulting code is orthogonal. Here we consider only real codes where the MLS code values are replaced by

$$A_{+1} = \frac{L+1-2\sqrt{L+1}}{L-3}$$

$$A_{-1} = -1$$

The residual correlation is 0 and the peak correlation $\rho(0) = 1$, giving $K_0 = 1$ in Equation 7.1.

7.3.3 Complementary Codes

Complementary codes are two codes (a,b) of the same length L that have the property that the sum of their auto-correlation functions satisfies

$$\rho_a(m) + \rho_b(m) = 0 \text{ for } m \neq 0$$

$$\rho_a(0) + \rho_b(0) = 2$$

Examples of these codes include Golay codes [64] and the complex polyphase generalisations [65]. Here we consider the Golay codes with $a_i, b_i \in \{-1,+1\}$, which require scale factor $K_0 = 0.5$ for signal processing in Equation 7.1. Denote by a^N_n and b^N_n the nth elements of the complementary Golay codes of length $L = 2^N$. One way of generating Golay codes of length 2^{N+1} is by concatenating codes of length 2^N as follows.

$$a^0 = \{1\}$$

$$b^0 = \{1\}$$

$$a^{N+1} = a^N + b^N$$

$$b^{N+1} = a^N - b^N$$

where the + and - refer to concatenation. These equations generate the sequence of Golay codes

$$a^0 = \{1\} \qquad\qquad b^0 = \{1\}$$

$$a^1 = \{1,1\} \qquad\qquad b^1 = \{1,-1\}$$

$$a^2 = \{1,1,1,-1\} \qquad\qquad b^2 = \{1,1,-1,1\}$$

$$a^3 = \{1,1,1,-1,1,1,-1,1\} \qquad\qquad b^3 = \{1,1,1,-1,-1,-1,1,-1\}$$

For the complementary codes the correlation coefficient is evaluated from

$$y(\tau) = y_a(\tau) + y_b(\tau)$$

where

$$y_a(\tau) = \int_0^{T_P} r_a(t) u_a(t-\tau) \exp[-j2\pi f_0(t-\tau)] \, dt$$

$$y_b(\tau) = \int_0^{T_P} r_b(t) u_b(t-\tau) \exp[-j2\pi f_0(t-\tau)] \, dt$$

$u_a(t)$ is the bandlimited Golay a^N code and $r_a(t)$ is the received waveform when the direct sequence waveform constructed from the a^N code is transmitted. Similar definitions hold for $u_b(t)$ and $r_b(t)$.). Each integral is evaluated using Equation 7.1. The sensitivity of Golay codes and their suitability for detecting and locating arcing faults is considered in the next section.

7.3.4 Simulation Results

The crest factors of the different band-limited direct sequence waveforms are very similar and rather large (1.96 for the MLS and Golay codes and 2.11 for the MLS orthogonal code considered). Also the bandwidth limiting to $2R_c$ causes low-level oscillations in the correlation coefficient. There are signal processing algorithms to reduce these correlation sidelobes at the expense of reduced resolution and signal to noise ratio. In our case sidelobe reduction techniques are not so important since a difference technique is used to analyse the results. Any deviation of a line profile, including sidelobes, from a previously obtained template of the healthy line is of interest.

Figure 7.3 shows simulation results using Golay code (length = 512) direct sequence waveforms for the same 100 km line, both with and without a fault 90 km from the transmit end. The carrier frequency is 133.33 kHz and the chip rate is 66.66 kHz. The horizontal axis has been normalised to a line of unit length (d = 1). The fault is a single phase to ground fault with a resistance of 1 ohm on the line which is not coupled to the two phase differential PLC communication network. The reflections from the transpositions (T1 and T2) are clearly visible as is the reflection from the line end (E). The reflection from the fault is labelled (F) and using the known distance covered by the reflection (E) the fault is measured as 89.7 km from the sending end.
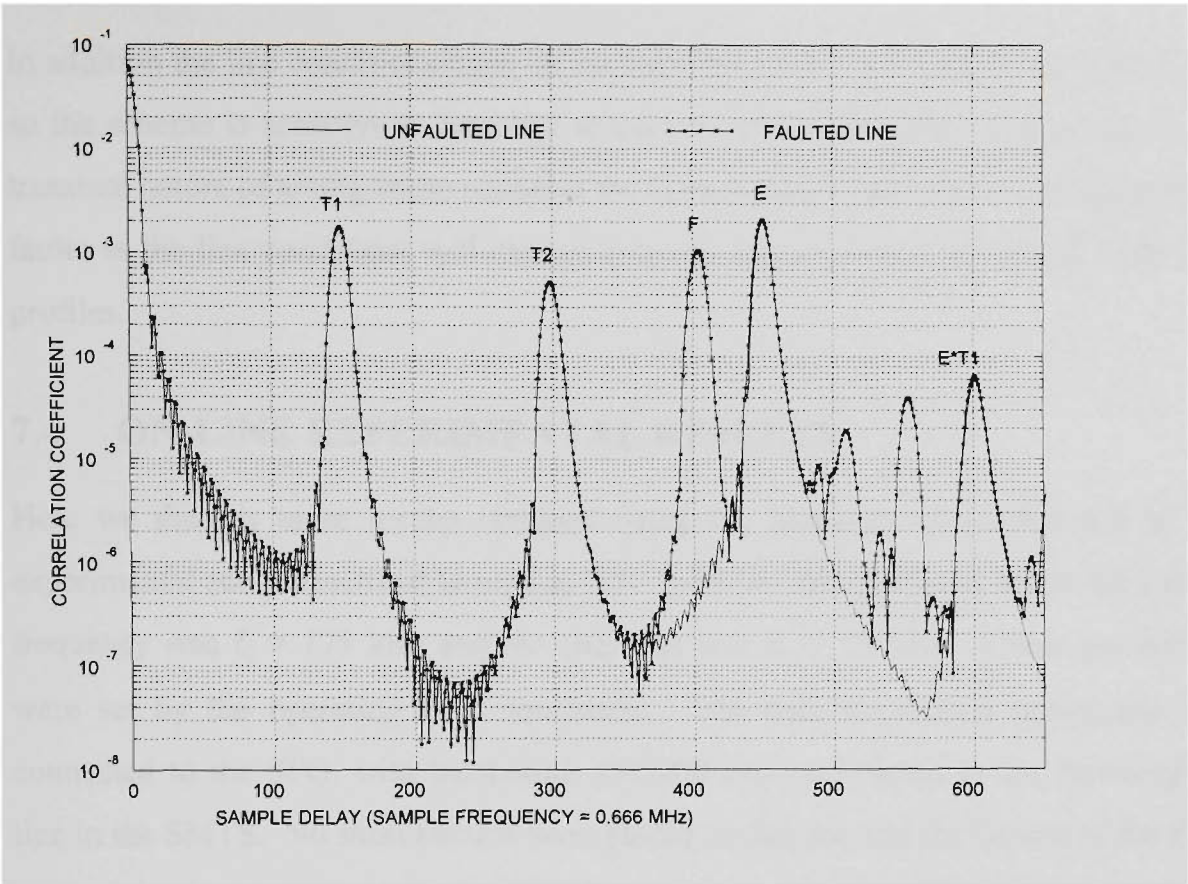
Figure 7.3 *Simulation line profiles of a 100 km 3 phase line (faulted, $R_F = 1 \, \Omega$, and unfaulted) using Golay code direct sequence waveforms. $f_0 = 133.33$ kHz, $R_c = 66.66$ kHz and L = 512.*

The MLS waveform of Fig. 7.2 and Golay waveform both give the same fault location estimate for $R_F = 1 \, \Omega$ - this is to be expected as the waveforms occupy the same frequency spectrum and both are subject to distortion by the 3 phase line return transfer function. Looking at the large peaks in Figs. 7.1 and 7.3 at zero delay it is seen that the bandlimited distorted MLS code has a self rejection ratio of 3 decades and the bandlimited Golay codes have a self rejection ratio of over four decades. Consequently the Golay codes are more sensitive to small reflections. As the fault impedance increases the fault peak will disappear below the MLS residual noise level of Fig. 7.2 while still being visible on the Golay plot of Fig. 7.3. This can also be seen for the multiple reflections from the fault, line end and transpositions, with d > 1, where the large peaks in the Golay code plots appear as small ripples in the MLS code graph.

For line probing the transmission of the b^N sequence must wait until any reflections from the previously transmitted a^N sequence have died down - otherwise there will be cross interference between the a^N and b^N codes. The response time is therefore longer.

In addition the line conditions must be the same for both the a^N and b^N sequences and so the scheme is sensitive to transient changes in line conditions. Consequently the transient nature of arcing faults excludes the Golay codes as suitable for locating these faults as the line conditions will change between the successive a^N and b^N code line profiles.

7.4   ON-LINE EXPERIMENTAL RESULTS

Here we discuss more results obtained using the hardware of section 6.3 in the experimental setup described in section 6.5. In the results discussed below the carrier frequency was $f_0 = 175$ kHz and the chip rate was $R_c = 25$ kHz. These parameters were set by the operating PLC equipment. The data acquisition equipment was connected to the SFG, with bandwidth 150-200 kHz, connected to the de-energised line in the SMTS. No short circuits were placed on the line and the far end of the PLC communications network in the DDTS was open circuit. The spread spectrum transmit power was 0.08 W.

Twelve SSB, 4 kHz bandwidth PLC communications circuits (six transmit, six receive), each with a transmit power of 1 Watt, were still operational on line 1 (section 6.5.3). Many of these were transmitting on frequencies within the measurement band (150-200 kHz). The high interference from these channels was effectively removed by the receiver averaging (section 6.5.4). Without averaging the noise signal coming into the receiver was 0.24 volts rms - with averaging the received direct sequence signal of 0.028 volts rms was easily recovered and the smallest peaks in the graphs discussed below correspond to return reflections as small as 30 μV rms, far less than 500 μV which corresponds to 1 LSB of the A/D converter.

The on-line results are graphed in Fig. 7.4 with the large transmitter feedthrough peak normalised to unity (normalised correlation coefficient) and the horizontal axis scaled to unit line length from the reflection off the line end.

Fig. 7.4(a) shows results for the MLS code of length 63 (MLS6) using the normal processing of Equation 7.1. Clearly evident is the large peak due to leakage in the directional coupler from the transmitter through to the receiver at zero distance (d = 0), and the reflections from the line transpositions T1 and T2 and the line end E.

Again the horizontal axis has been scaled so that the reflections correspond to a line of unit length. Impedance discontinuities where the line passes over hills (H) and a large lake (L) also cause large reflections. The residual correlation for $d > 1$ is about 0.018 which corresponds to the self rejection ratio of the bandlimited code.

Figure 7.4(b) shows results for the same MLS6 data using the DC processing of section 3.1 ($u(t_i)$ replaced by $u(t_i) - 1$ in Equation 7.1). Below are listed the major differences compared to Fig. 7.4(a).

1. The reflection T2 has halved in magnitude and the 3 peaks immediately before T2 are increasing in magnitude with distance (ending in T1*T1, the double reflection off T1).
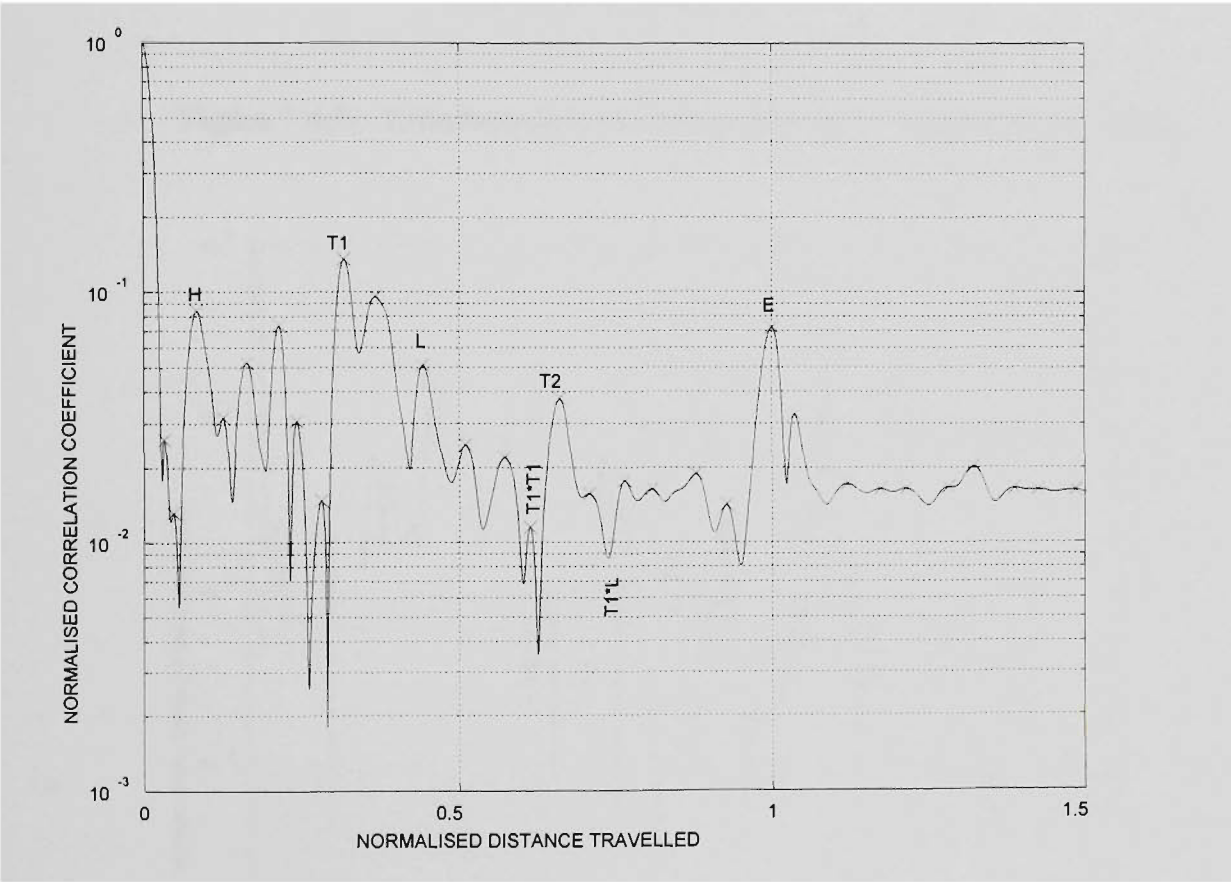

Figure 7.4(a) *Transmitted MLS code of length 63, normal processing.*

Figure 7.4 *Normalised correlation coefficients of received signals with transmitted power = 0.08 W.*
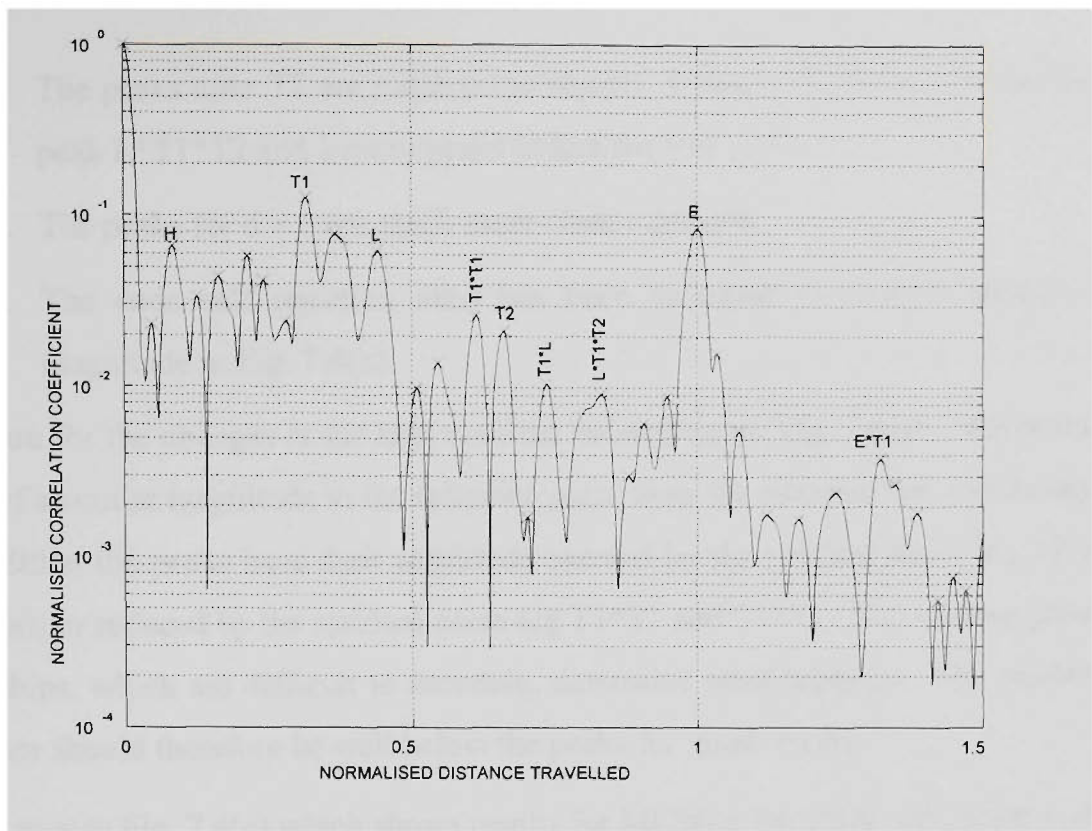
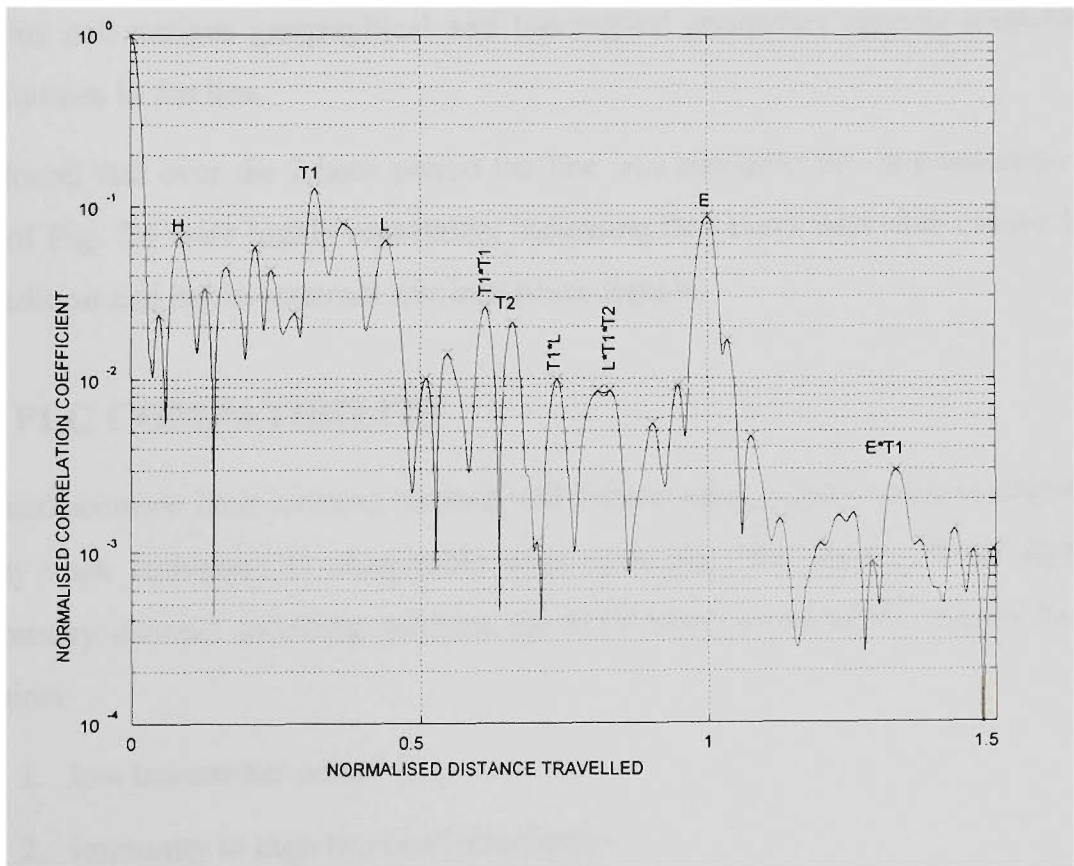Figure 7.4(b) *Transmitted MLS code of length 63, modified processing.*

Figure 7.4(c) *Transmitted MLS orthogonal code of length 63.*

Figure 7.4 *Normalised correlation coefficients of received signals with transmitted*
power = 0.08 W.

2. The peaks after T2 are much more sharply defined - T1*L and the double peak L*T1*T2 and 2 more peaks before the line end E.

3. The peaks for d > 1 are much more clearly defined.

4. The code self rejection ratio has been increased to over 3 orders of magnitude in Fig. 7.4(b).

The reason for the changes is the high residual noise floor of Fig. 7.4(a). When this floor is of a similar magnitude to the reflected peaks then the potential for interference exists. Either the peaks have their amplitude boosted by the residual noise (eg T2 in Fig. 7.4(a)) or reduced by the residual noise (eg T1*T1 and T1*L). The relative phase relationships, which are difficult to ascertain, determine what happens. The residual noise floor should therefore be well below the peaks for good results.

Turning now to Fig. 7.4(c) which shows results for MLSO6, the MLS orthogonal code of length 63, it is seen that this graph is very similar to Fig. 7.4(b) supporting the results discussed previously. The unlabelled peaks are caused by further multiple reflections and various geographical and topological anomalies causing impedance discontinuities in the line.

It was found that over the 2 hour period the line was available for measurements the results of Fig. 7.4 were highly repeatable, indicating that every peak was caused by a line condition and not by external spurious noise signals.

7.5   PLC COMPATIBILITY

A fast and accurate fault location method will reduce outage times and it is important that any such technique is compatible with operating PLC links. Time domain reflectometry channel sounding methods for EHV lines are therefore subject to two constraints

1. low transmitter power

2. immunity to high levels of interference

Periodic wideband spread spectrum signals are ideally suited to these restrictions.

All these periodic codes have spectral nulls at the code repetition frequency and in any practical system only bandlimited codes are transmitted, typically the main lobe or less.

Figures 7.5(a) to 7.5(c) show the main lobe double-sided power spectra of, respectively, the MLS and MLS orthogonal codes of length 63 and the Golay complementary codes of length 32. In each case the power spectrum $|X(n)|^2$ is derived from the periodic Fourier equations

$$X(n) = 0.5(a_n - jb_n) \qquad n = ...,-2,-1,0,1,2,... \quad \text{where}$$

$$a_0 = \frac{1}{L} \sum_{i=0}^{i=L-1} c_i$$

$$a_n = \frac{2}{n\pi} \sin\left(\frac{n\pi}{L}\right) \sum_{i=0}^{i=L-1} c_i \cos\left(\frac{(2i+1)n\pi}{L}\right)$$

$$b_n = \frac{2}{n\pi} \sin\left(\frac{n\pi}{L}\right) \sum_{i=0}^{i=L-1} c_i \sin\left(\frac{(2i+1)n\pi}{L}\right)$$
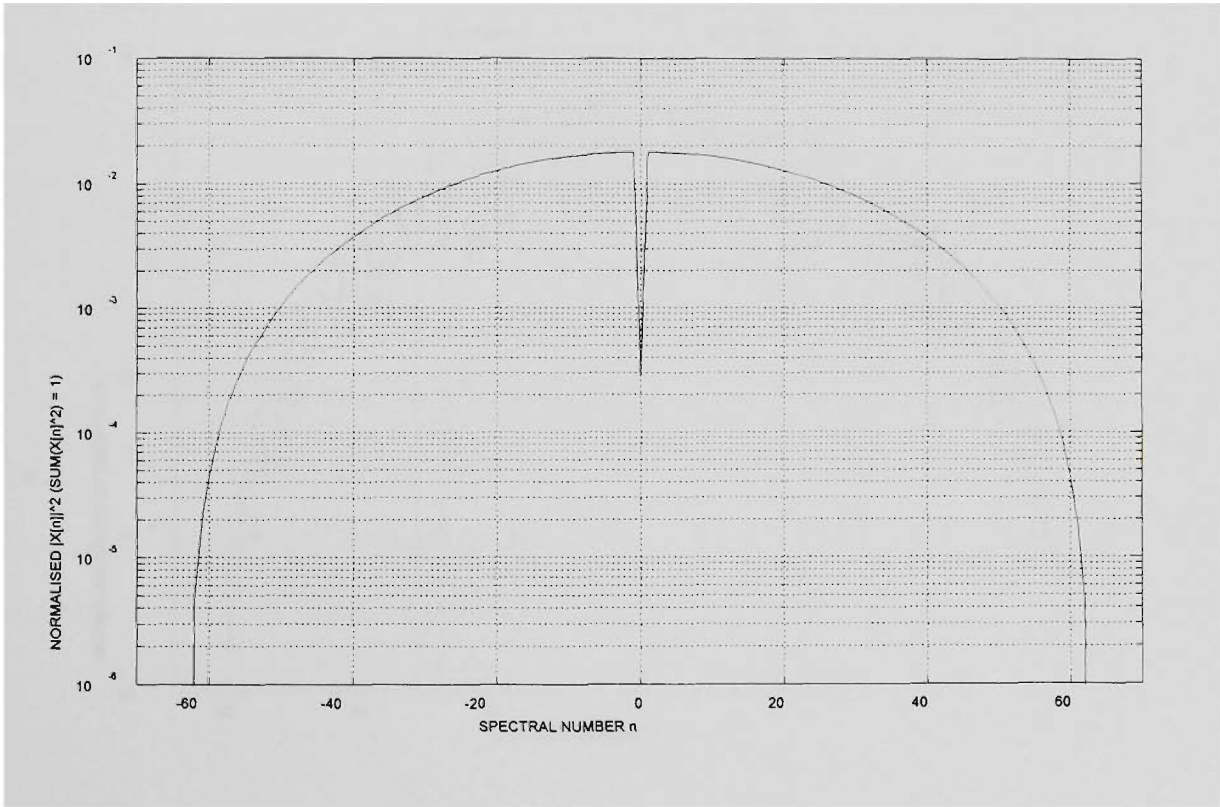

Figure 7.5(a) *MLS code of length 63.*

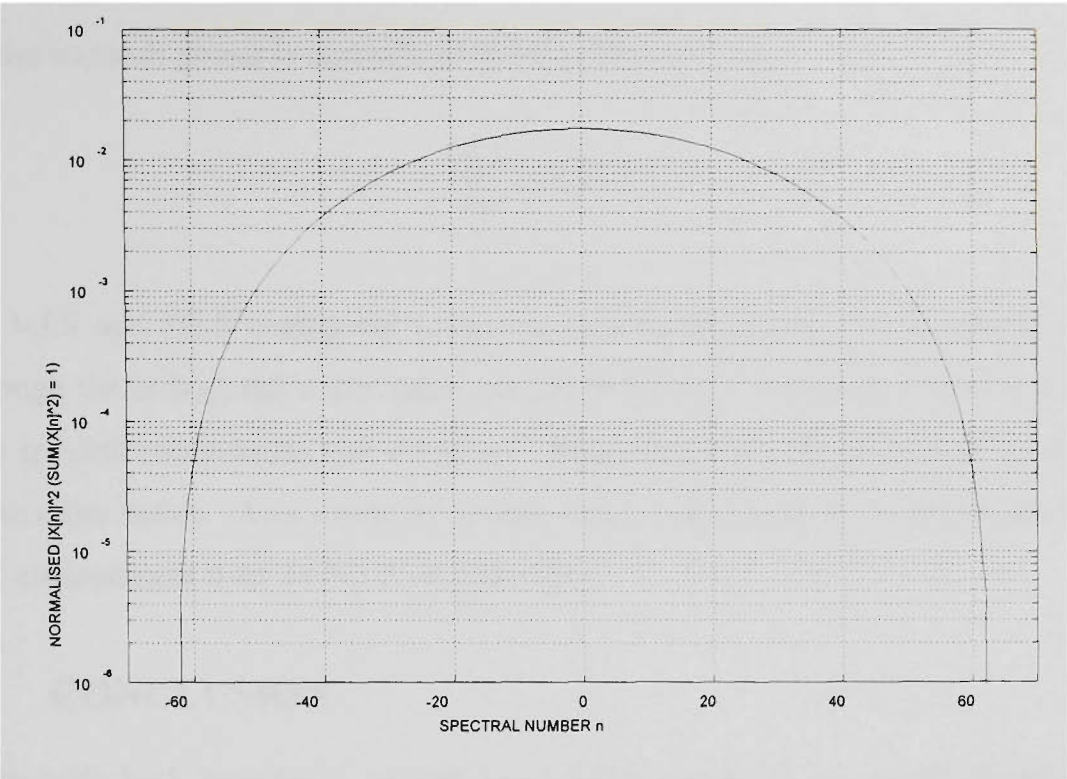Figure 7.5 *Main lobe double-sided normalised power spectral densities.*

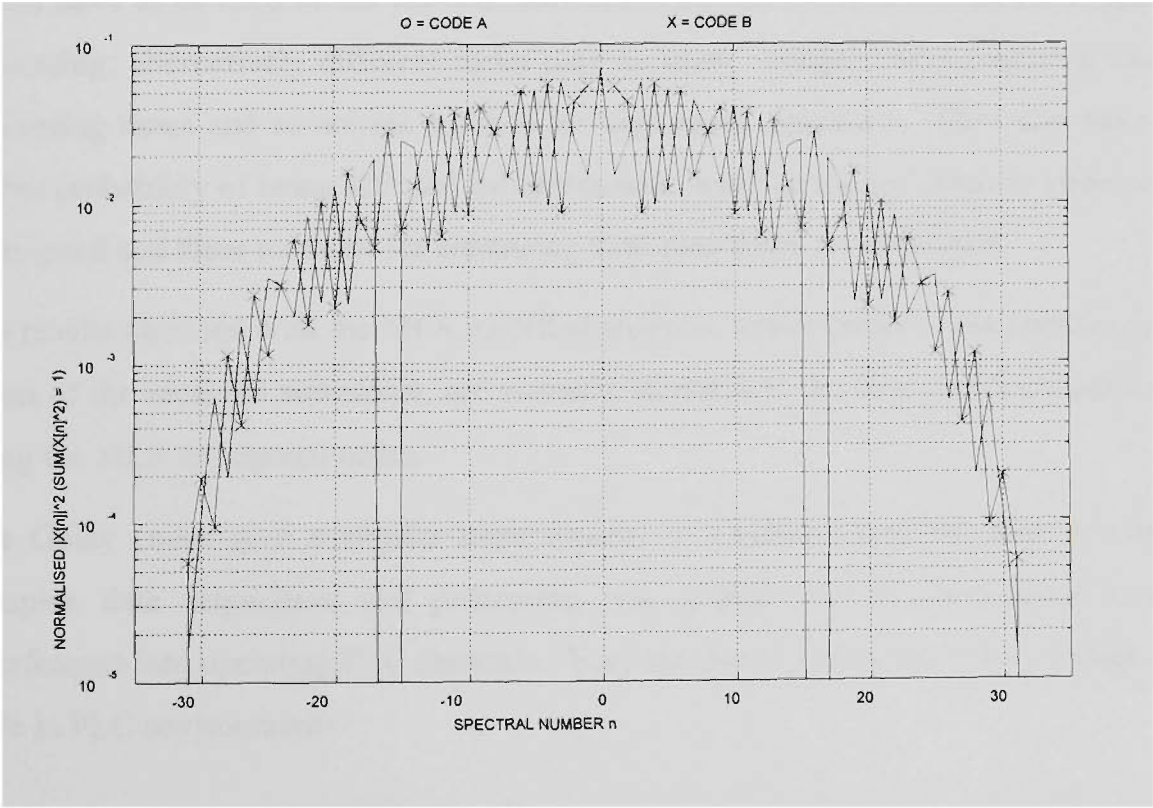Figure 7.5(b) *MLS orthogonal code of length 63.*

Figure 7.5(c) *Golay code of length 32.*

Figure 7.5 *Main lobe double-sided normalised power spectral densities.*

and the transmit power is normalised to unity for each code.

$$\sum_{n=-L}^{n=L} |X(n)|^2 = 1$$

The MLS and MLS orthogonal codes have almost the same power spectral density although the orthogonal codes have a much larger DC component. The Golay codes have spectral components that are up to 3 times the power of the spectral components of the other codes. As a result the Golay codes could cause more interference in the PLC environment than the MLS related codes.

7.6   CONCLUSION

Faults with high impedance or with intermittent operation can cause problems with PLC channel sounding systems using MLS codes.

The MLS codes have a residual correlation equal to the reciprocal of the code length L which can limit the sensitivity of the code to small reflections. Either longer codes would have to be used or the residual correlation can be reduced by modified signal processing; alternatively different codes may be used. Longer codes require greater processing times and so are not suitable for high speed operation. They also have a higher probability of being affected by intermittent fault conditions. Shorter codes are high speed and three methods for enhancing their sensitivity are described.

The results obtained with the MLS modified analysis, which removes the residual DC offset of the received waveform, are virtually identical to the line profiles measured using the MLS orthogonal codes.

The Golay codes give a similar improvement in residual noise but require more complex data acquisition and processing and produce up to three times more interference into operating PLC channels. They are therefore less suitable as a ranging code in PLC environments.

Channel sounding using PLC is sensitive enough to detect impedance discontinuities due to faults, transpositions and the line end; in addition, large geographical anomalies appear as strong reflection peaks. High speed operation with short codes is feasible

provided interference from other PLC services is low and so averaging is not needed. This would be possible if existing PLC communication channels were replaced by alternate communication bearers such as radio or optic fibre.

8. CONCLUSION

8.1 RECAPITULATION

Electrical authorities require fast and accurate fault locators to protect the quality of supply and reduce outage times. Fault location methods are a major research topic worldwide and no single fault location method satisfies the requirements of an ideal fault locator. The approach taken in this thesis is the novel application in the PLC environment of low power spread spectrum signals for remote sensing purposes.

A classification and review of the different fault location methods developed over the last fifty years was presented in Chapter 2. Many researchers have tried to overcome the limitations of the reactance ratio measuring method and the fault generated surge methods with varying degrees of success. It was decided that active fault location methods were advantageous because clearance of the line can be verified without closing the mains breakers.

Active fault location requires a transmission network that provides global coverage of the power network. Chapter 3 provides an overview of the PLC communication system which uses the EHV lines as transmission media. While currently used for signalling, communication and protection purposes, the PLC hardware could also be used for locating faults with little additional outlay. The theory of modal analysis is introduced, which describes the characteristics of signal propagation along EHV lines at PLC frequencies. Noise and attenuation properties of typical EHV lines are given and system design equations for a fault locator using the PLC system are derived. A fault locator using pulse waveforms requires short pulses for good resolution and minimum range performance, but high peak powers (causing interference) for probing long lines accurately. For compatibility with existing PLC services, an accurate fault locator must use alternative waveforms.

Chapter 4 introduces waveform design objectives for accurate fault location on EHV lines and covers optimal signal processing techniques. Traditional waveforms are reviewed and their disadvantages noted. Spread spectrum waveshapes are introduced which avoid the peak power/resolution trade-off by spreading the transmitted energy over a long time interval, reducing the peak power and cost of the transmitting

equipment. Spread spectrum waveforms combine the low power advantage of the long pulse with the good resolution properties of the short pulse. The low power density of spread spectrum signals ensures that existing narrowband PLC communication links, occupying a small part of the spread spectrum bandwidth, can operate undisturbed while spread spectrum line monitoring is taking place. In addition multiple spread spectrum communication links could operate in the same bandwidth as a spread spectrum fault locator. Direct sequence spread spectrum signals derived from the MLS codes were chosen for their ease of implementation and good correlation properties. Finally, at the end of Chapter 4, system design equations for a spread spectrum fault locator are derived. Predicted system performance depends upon the bandwidth used and varied from a 1% fault location accuracy over a 250 km range (BW = 80-200 kHz) to a 0.71% fault location accuracy over a 125 km range (BW = 80-500 kHz). These accuracies compare favourably with the 5% accuracy obtainable with the widely used reactance ratio measuring fault location method. This spread spectrum fault locator system design is original and was published as a conference paper [66].

The predicted accuracies at the end of Chapter 4 ignore the modal distortion that occurs as signals propagate down EHV lines. Chapter 5 gives details of a program that was written to simulate PLC spread spectrum fault location which takes into account the frequency variation of the PLC interface and line parameters. Plots of steady state voltage distribution along the 100 km long simulated line showed that spread spectrum signals have the slow voltage variation characteristic of modal propagation, but the faster oscillations due to standing waves, typical of narrowband signals, cancelled out over the spread spectrum bandwidth. Areas of weak reflection could be identified, giving worst case fault positions. Using MLS codes of length 1023, direct sequence signals located single phase to ground faults at different positions along the line with an accuracy of 0.42% of line length. When the frequency selective components of the PLC line interface were removed, the fault location accuracy improved by an order of magnitude. This indicates that the line interface is the main source of error in fault location using this technique. These simulation results are original and have been published in a journal article [67].

Chapter 6 describes prototype hardware designed for on-line measurements and presents results obtained on a 330 kV line of length 225 km. The spread spectrum bandwidth was limited to 50 kHz (150-200 kHz) by a line separation filter used by the existing PLC equipment. Six PLC channels were operating on an adjacent line causing massive interference to the incoming reflections. Received signals were averaged 4095 times neutralising the effects of noise and interference. Direct sequence signals based on MLS codes of length 1023 were sent down the line with two different transmit powers, 0.08 W and 1 W. Both line profiles were virtually identical and peaks due to reflections from impedance discontinuities (caused by the line end, the transpositions and geographical features) were clearly identifiable. Using the line end as a distance reference, the first transposition was located to within 0.5 km (0.22% of line length) and the second transposition to within 1.6 km (0.71% of line length). These accuracies would be improved if an actual fault was on the line since the transpositions could be used as a distance reference. A wider PLC bandwidth would also improve resolution and accuracy. Additionally, if the PLC channels were not operating, averaging would not be required and shorter code lengths could be used, reducing the data acquisition and response times. These experimental results agree well with the simulated and calculated results of Chapter 5 and Chapter 4 respectively. These results are original and have been published in a journal article [68].

For high speed operation and for the location of transient faults short code lengths are necessary. However short MLS codes suffer from a high residual correlation. The final chapter looks at data processing and code selection for reduction of the code residual correlation noise floor. Golay codes and MLS orthogonal codes are introduced, both of which have zero residual correlation in the non-bandlimited case. On-line results using an MLS code of length 63 with a transmit power of 0.08 W were analysed in the normal manner, and also with the code DC offset removed from the auto-correlation function. These two profiles were then compared with an on-line profile measured using an MLS orthogonal code of length 63. The noise floor was reduced by well over one order of magnitude for the two low residual correlation cases. The lower noise floor exposed many low level reflection peaks. This verified that the sensitivity of MLS codes with normal processing is limited by code self noise

rather than noise from external sources. High speed operation using short code lengths is therefore possible provided low residual noise codes or processing are used. and external noise is not dominant. Other PLC services are a major source of external noise and therefore have to be switched off during the measurement period..

8.2 FUTURE WORK

This Thesis has a number of weaknesses which warrant further research. Some of these are listed below.

1. The technique has not been tested on a line experiencing a fault condition. Further on-line tests are necessary.

2. A major source of error appears to be the line interface. Signal processing techniques such as equalisation and deconvolution can be used to eliminate this error.

3. The technique has not been tested on more complicated line structures. The application of the technique to teed line and distribution networks should be investigated.

4. The effect of transients and arcing faults on the correlator output has not been fully investigated. Only one simulation has been performed where the fault is intermittent over the period of the code. More work needs to be done in this area.

5. The performance of different codes (eg polyphase codes) and different modulations (eg SSB, frequency hopping) needs to be investigated.

8.3 ACKNOWLEDGEMENTS

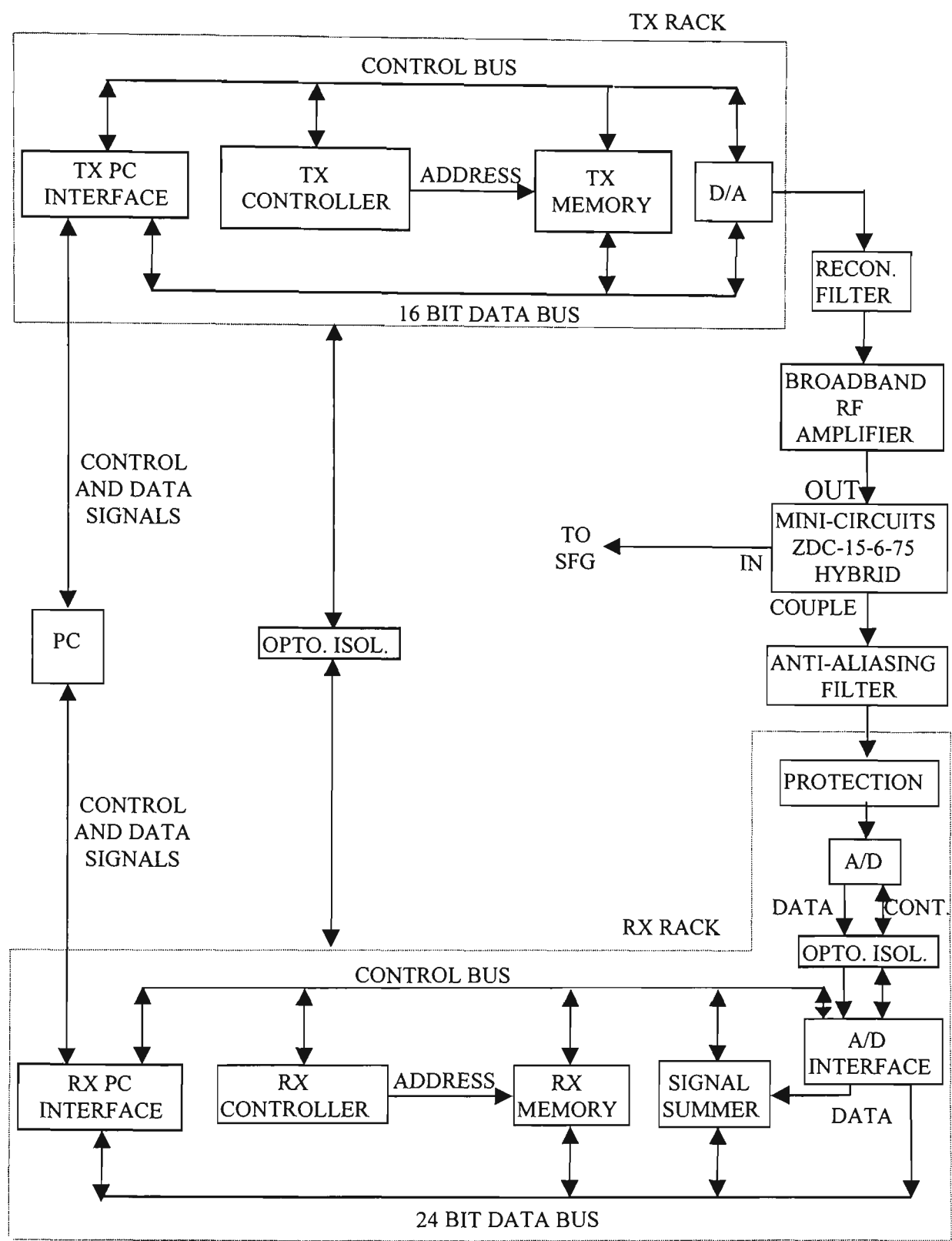# APPENDIX : HARDWARE DESIGN

Figure A1. *Block diagram of the transmit and receive hardware which was bought or constructed for the on-line measurements.*

Figure A1 illustrates the spread spectrum transmit/receive hardware designed for connection to the SECV PLC circuitry. This hardware was used to obtain the on-line measurements described in Chapters 6 and 7 and consists of four main components.

1. Personal computer (PC) for downloading waveforms to the transmitter and uploading waveforms from the receiver. This is done via a plug-in digital I/O card in the PC interfacing to data transfer cards in the TX and RX racks. These data transfer cards are under programmable logic control.

2. Transmit rack.

3. Receive rack.

4. Reconstruction filter, power amplifier, hybrid or directional coupler, and anti-aliasing filter.

Figure A1 shows the external (ie from the TX front panel to the RX front panel via co-ax) communication lines between the TX controller board and the RX controller board. Each communication line is terminated in an opto-isolator to prevent ground loops. These communication links provide for the following features.

1. The RX can run off the same clock as the TX.

2. After the TX has sent a number of waveforms set by the user a signal is sent to the RX to start recording. This allows a steady state signal to be built up on the line before the RX starts recording.

3. When the RX has finished recording a signal is sent to the TX to stop transmitting.

Transmitter Figure A2 shows the transmitter rack with the transmitter memory board and the D/A board (in the open RF shielded box) displayed. The transmitter memory consists of 128 K × 16 bits of 100 nsec static RAM. The transmitter controller can address up to 16 Megawords of memory and can send up to 4095 waveforms before the 'START_RX' command is sent to the RX. The 12 bit D/A is ECL driven for low glitch energy. The transmitter has a maximum D/A conversion rate of 5 Msamples/sec.

Receiver Figure A3 shows the receiver rack with the RX memory board displayed. This consists of 128 K × 24 bit of 35 nsec static RAM. The receiver controller can

address up to 16 Megawords of memory. There is fast protection (op-amp clamping circuitry) on the sensitive A/D input (2 V p-p maximum) and opto-isolation between the 5 MHz 12 bit A/D and the A/D interface card. The signal summer board consists of a 24 bit wide full binary adder. During each sample cycle of averaging there is a READ/WRITE cycle for the memory - data is read from memory, added to the latest
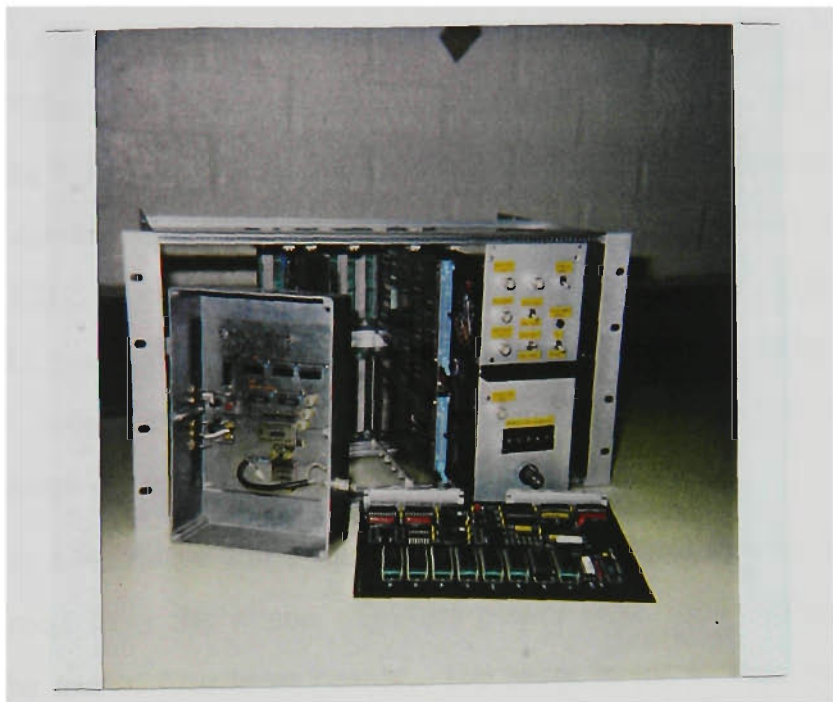

Figure A2 *Transmitter rack showing transmitter memory board (128K × 16 bits) and 5 MHz ECL driven D/A board in open RF shielded box.*
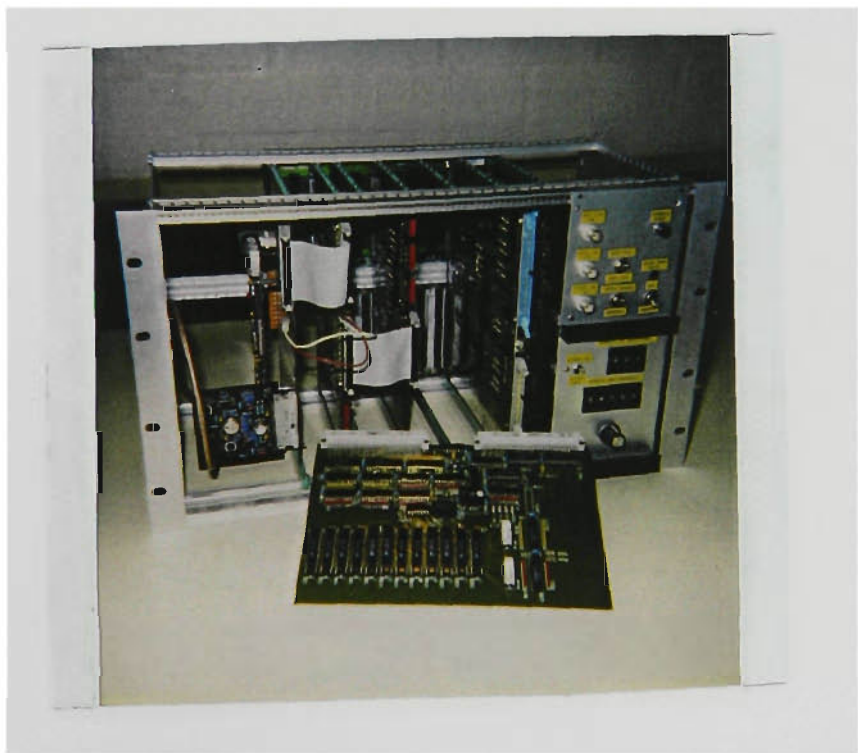

Figure A3 *Receiver rack showing receiver memory board (128K × 24 bits).*

Hardware Design

incoming sample, and the previous sum is written back to memory. The 24 bit wide processing allows 4095 summations of the 12 bit data without overflow. The RX has a maximum speed of 5 MHz without averaging, or 4 MHz with averaging. 24 bit wide data with READ/WRITE cycles at a 4 MHz sample rate gives a data transfer rate of 192 Mbits/sec.

Reconstruction Filter, Broadband RF Amplifier, Mini Circuits ZDC-15-6-75 Hybrid, Anti-aliasing Filter These components are illustrated in Fig. A4. The reconstruction and anti-aliasing filters were analogue Bessel filters - the reconstruction filter was 5th order and the anti-aliasing filter was 9th order (5th order would have sufficed). The Mini Circuits ZDC-15-6-75 Directional Coupler, with a frequency response from 20 kHz to 35 MHz, was used for TX/RX isolation. The RF Amplifier was a home made Stereo Power Amplifier (Playmaster Pro Series One) modified to give a wider frequency response out to 1 MHz.

Power Supplies, Grounding For a single system ground at the SFG all power supplies were run isolated from the mains. Ground planes were used throughout and this necessitated the use of four layer boards. The noise in the system was held to less than 1 LSB (0.5 mV) allowing the signal to use the full system dynamic range. The design and construction of this equipment was a major time consuming component of this research.
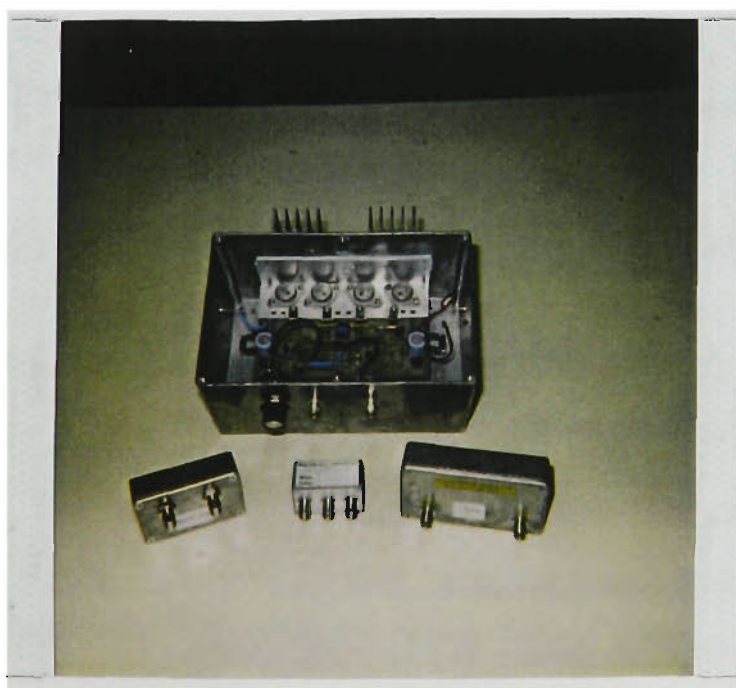

Figure A4 *RF power amplifier in open RF shielded box. In the front are, clockwise, the reconstruction filter, the Mini-Circuits 75 Ω directional coupler and the anti-aliasing filter.*

REFERENCES

1. S T. W. Stringfield, D. J. Marihart and R. F. Stevens, *Fault Location Methods for Overhead Lines*, AIEE Trans., Vol. 76, pp 518-529, Aug. 1957.

2. M. Sant and Y. G. Paithankar, *Online Digital Fault Locator for Overhead Transmission Lines*, Proc. IEE, Vol. 126, No. 11, pp 1181-1185, Nov. 1979.

3. *Bibliography and Summary of Fault Location Methods*, AIEE Committee report; AIEE Trans., 1955, PAS-74, pp 1423-1428.

4. H. T. Gooding, *Cable Fault Location on Power Systems*, Proc. IEE, Vol. 113, No. 1, pp 111-119, January 1966.

5. S. E. Westlin, J. A. Bubenko, *An Accurate Method for Fault Location on Electric Power Transmission Lines*, IFAC Symposium 1977, Melbourne, 21-25 February 1977.

6. M. Vitins, *A Correlation Method for Transmission Line Protection*, IEEE Trans. Power App. Sys., Vol PAS-97, No. 5, pp 1607-1615, Sept/Oct. 1978.

7. A. Wiszniewski, *Accurate Falt Impedance Locating Algorithm*, IEE Proc., Vol. 130, Pt. C, No. 6, pp 311- 314, November 1983.

8. Gale P. F., Crosley P. A., Xu Bingyin, Ge Haozhong, Cory B. J., Barker J. R. G., *Fault Location Based on Travelling Waves*, Proc. IEE International Conference on Development in Power System Protection, UK, 1992, pp 54-59.

9. L. Eriksson, M. Saha and G. Rockefeller, *An Accurate Fault Locator with Compensation for Apparent Reactance in the Fault Resistance Resulting from Remote-End Infeed*, IEEE Trans. Power App. Sys., Vol PAS-104, No. 2, pp 424-436, Feb. 1985.

10. T. Takagi, Y. Yamakoshi, M. Yamaura, R. Condow and T. Matsushima, *Development of a New Type Fault Locator Using the One-Terminal Voltage and Current Data*, IEEE Trans., Vol. PAS-101, No. 8, August 1982, pp 2892-2898.

11. T. Takagi, Y. Yamakoshi, J. Baba, K. Uemura and T. Sakaguchi, *A New Algorithm of an Accurate Fault Location for EHV/UHV Transmission Lines : Part*

1 - Fourier Transformation Method, IEEE Trans. Power App. Sys., Vol. PAS-100, No. 3, pp 1316-1323, March 1981.

12. Gill G. Richards and Owen T. Tan, *An Accurate Fault Location Estimator for Transmission Lines*, IEEE Trans. Power App. Sys., Vol. PAS-101, No. 4, pp 945-949, April 1982.

13. D. J. Lawrence and D. L. Waser, *Transmission Line Fault Location Using Digital Fault Recorders*, IEEE Trans. Power Deliv., Vol. 3, No. 2, pp 496-502, April 1988.

14. Sachdev, M. S. and Agarwal R., *Accurate Fault-Location Estimates from Digital Impedance Relay Measurements*, 3rd Conference Developments in Power System Protection, IEE Conference Publication No. 249, pp 180-184, April 1985.

15. Cook V., *Fundamental Aspects of Fault Location Algorithms Used in Distance Protection*, IEE Proc., Vol. 133, Pt. C, No. 6, pp 359-368, September 1986.

16. Johns A. T. and Jamali S., *Accurate Fault Location Technique for Power Transmission Lines*, IEE Proc., Vol. 137, Pt. C, No. 6, pp 395-402, Nov. 1990.

17. Aggarwal R. K., Cory D. V., Johns A. T. and Kalam A., *A Practical Approach to Accurate Fault Location on Extra High Voltage Teed Feeders*, IEEE PES 1992 Summer Meeting, Seattle, WA, July 12-16, pp 1-8, 1992.

18. Johns A.T., Moore P. J. and Whittard R., *New Technique for the Accurate Location of Earth Faults on Transmission Systems*, IEE Proc.-Gener. Transm. Distrib., Vol. 142, No. 2, pp 119-127, March 1995.

19. Stevens R. F. and Stringfield T. W., *A Transmission Line Fault Locator Using Fault Generated Surges*, AIEE Trans., Vol. 67, pp 1168-1179, 1948.

20. Cossley P. A. and McLaren P. G., *Distance Protection Based on Travelling Waves*, IEEE Trans. Pow. App. Sys., Vol. PAS-102, No. 9, pp 2971-2983, Sept. 1983.

21. Wedepohl L. M., *Application of matrix methods to the solution of travelling-wave phenomena in polyphase systems*, Proc. IEE, Vol. 110, No. 12, pp 2200-2212, December 1963.

22. Christopoulos C., Thomas D. W. P., and Wright A., *Signal Processing and Discriminating Techniques Incorporated in a Protective Scheme Based on Travelling Waves*, IEE Proc., Vol. 136, Pt. C, No. 5, pp 279-288, Sept 1989.

23. Agrawal, Pramod, *An Investigation into a Method of Detecting the Fault Induced High Frequency Voltage Signals of EHV Transmission Lines for Protection Applications*, IEEE Trans. Pow. Deliv., Vol. 6, No. 1, pp 119-126, January 1991.

24. Johns A. T. and Aggarwal R. K., *Digital simulation of faulted e.h.v. transmission lines with particular reference to very-high-speed protection*, Proc. IEE, Vol 123, No. 4, pp 353-359, April 1976.

25. Agrawal, Pramod, *Performance of the Pramod Johns Scheme for UHS Protection of EHV Transmission Lines under Arcing Fault Conditions*, IEEE Trans. Pow. Deliv., Vol. 6, No. 1, pp 127-133, January 1991.

26. T. Takagi, Y. Yamakoshi, J. Baba, K. Uemura and T. Sakaguchi, *A New Algorithm of an Accurate Fault Location for EHV/UHV Transmission Lines : Part II - Laplace Transformation Method*, IEEE Trans. Power App. Sys., Vol. PAS-101, No. 3, pp 564-573, March 1982.

27. *EMTP Users Manual*, Bonneville Power Administration, Branch of System Engineering, Portland, Oregon, November 1977.

28. A. O. Ibe and B. J. Cory, *A Travelling Wave-Based Fault Locator for Two and Three Terminal Networks*, IEEE Trans. Pow. Sys., Vol. PWRD-1, No. 2, pp 283-288, April 1986.

29. Ranjbar A. M., Shirani A. R. and Fathi A. F., *A New Approach for Fault Location Problem on Power Lines*, IEEE Trans. Pow. Deliv., Vol. 7, No. 1, pp 146-151, January 1992.

30. Leslie J. R., Kidd K. H., *The "Linascope" - An Echo Ranging Fault Locator for High Voltage Lines*, AIEE Trans, Vol. 67, pp 1162-1167, 1948.

31. L. R. Spalding, C. C. Diemond, *A Transient Fault Locator for High-Voltage Transmission Lines*, AIEE Trans., Vol. 68, pp 1005-1012, 1949.

32. D. Stevens, G. Ott, W. Pomeroy and J. Tudor, *Frequency-Modulated Fault Locator for Power Lines*, IEEE Trans. Power App. Syst., Vol. PAS- 95, No. 5, pp 1760-1768, Sept./Oct. 1972.

33. *Communications Systems*, J. L. Needham, Transmission Development Department, SECV.

34. Podszeck H.-K., *Carrier Communication over Power Lines,* Springer-Verlag, Berlin-Heidelberg-New York, 1972.

35. *Power Line Carrier and Microwave Systems for Power Authorities*, in-house SECV Technical Report.

36. M. Swingle and H. I. Dobson, *Power Line Carrier Systems*, Chapter 14, *Communication System Engineering Handbook*, D. H. Hamsher (Editor), McGraw-Hill, New York, 1967.

37. GEC, *PLC Guide*, Virginia, 1976/1977.

38. *Brown Boveri Review*, Vol. 64, August 1977, Baden Switzerland.

39. Carson J. R., *Wave Propagation in Overhead Wires with Ground Return*, Bell Syst. Tech. Jour., 1926, Vol. 5, pp 539-554.

40. *Summary of an IEEE Guide for Power Line carrier Communications*, A Report by the Power System Communication Committee, IEEE Trans. Pow. App. Sys., Vol. PAS-99, No. 6, Nov/Dec 1980.

41. Newton S., *A New Technique in OTDR*, Electronic and Wireless Word, May and June, 1988.

42. G. W. Deley, *Waveform Design*, Chapter 3, *Radar Handbook*, M. I. Skolnik (Editor), McGraw-Hill.

43. E. C. Farnett, T. B. Howard and G. H. Stevens, *Pulse-compression Radar*, Chapter 20, *Radar Handbook*, M. I. Skolnik (Editor), McGraw-Hill.

44. Skolnik, Merrill I., *Introduction to Radar Systems*, 2nd edition, McGraw-Hill Kogakusha, 1980.

45. Urkowitz H., *Filters for Detection of Small Radar Signals in Clutter*, J. Appl. Phys., Vol. 24, No. 8, pp 1024-1031, Aug. 1953.

46. Nathanson F. E., Reilly J. P. and Cohen M. N., *Radar Design Principles*, McGraw-Hill, 2nd edition, 1991.

47. Rihaczek A. W., *Optimum Filters for Signal Detection in Clutter*, IEEE Trans. AES, Vol. AES-1, No. 3, pp 297-299, Dec. 1965.

48. Rihaczek A. W., *Radar Waveform Selection - A Simplified Approach*, IEEE Trans. AES, Vol. AES-7, No. 6, pp 1078-1086, November 1971.

49. M. I. Skolnik, *Theoretical Accuracy of Radar Measurements*, Transactions I.R.E., Vol. ANE-7, No. 4, Dec 1960, pp 123-129.

50. R. C. Dixon, *Spread Spectrum Systems*, Second Edition, John Wiley and Sons, 1984.

51. Faulkner M., *A New Modulation for Power Protection Signalling*, IREECON International Electronics Convention, Sydney, 1987.

52. Oppenheim A. V. and Schafer R. W., *Digital Signal Processing*, Prentice-Hall, 1975.

53. Galloway R. H., Shorrocks W. B. and Wedepohl L. M., *Calculation of electrical parameters for short and long polyphase transmission lines*, Proc. IEE, Vol. 111, No. 12, pp 2051-2059, Dec. 1964.

54. Bickford J. P., Mullineux N. and Reed J. R., *Computation of power system transients*, IEE Monograph series 18, Published by Peter Peregrinus Ltd. Lond. and NY on behalf of IEE, 1980.

55. Wedepohl L. M., *Electrical characteristics of polyphase transmission systems with special reference to boundary-value calculations at power-line carrier frequencies*, Proc. IEE, Vol. 112, No. 11, pp 2103-2112, Nov. 1965.

56. Naredo J. L., Romero R., Silva J. L. and Moreno P., *Application of Approximated Modal Analysis Methods for PLC System Design*, IEEE Trans. Pow. Deliv., Vol. PWRD-2, No. 1, January 1987.

57. Jones D. E., *Power Line Carrier Operation During Line Faults*, Ontario Hydro Research News, Vol. 12, pp 21-25, 1960.

58. Rohling H., Plagge W., *Mismatched Filter Design for Periodical Binary Phased Signals*, IEEE Trans., Vol. AES-25, No. 6, pp 890-896, November 1989.

59. Rabiner L. R. and Gold B., *Theory and Application of Digital Signal Processing*, Prentice-Hall, 1975.

60. Welch, Peter D., *The Use of Fast Fourier Transform for the Estimation of Power Spectra : A Method Based on Time Averaging over Short, Modified Periodograms*, IEEE Trans. Audio Electroacoust., Vol. AU-15, pp 70-73, June 1967.

61. Stockham, Thomas G., *High Speed Convolution and Correlation*, 1966 Spring Joint Computer Conference, AFIPS Conf. Proc., Vol. 28, pp 229-233, 1966.

62. Papamichalis, P. (Ed.), *Digital Signal Processing Applications with the TMS320 Family*, Vol. 3, Chapter 4, Appendix A1, Texas Instruments, 1990.

63. Tetsuo Kirimoto, Yoshimasa Oh-Hashi and Takashi Hotta, *Orthogonal Periodic Sequences with Two Complex Numbers Derived from M-Sequences*, Electronics and Communication in Japan, Part 3, Vol. 74, No. 5, 1991, pp 57 - 64.

64. Golay, Marcel J. E., *Complementary Series*, IRE Transactions on Information Theory, April 1961, pp 82-87.

65. Budisin S. Z., *New Complementary pairs of Sequences*, Electronic Letters, Vol. 6, No. 13, 21st June, 1990, pp 881-883.

66. Taylor V., Faulkner M. and Kalam A., *Fault Location on EHV Lines Using Wideband Spread Spectrum Techniques*, Conf. Proc., Intnl. Conf. Pow. Sys. Prot., 13-14 Sept. 1989, Singapore, pp 142-161.

67. Taylor V., Faulkner M., Kalam A. and Haydon J., *Digital Simulation of Fault Location on EHV Lines Using Wideband Spread Spectrum Techniques*, IEE Proc. - Gener. Transm. Distrib., Vol. 142, No. 1, January 1995, pp 73-80.

68. Taylor V., Faulkner M., *Experimental Results of Line Monitoring and Fault Location Using Spread Spectrum on Power Line Carrier*, IEE Proc. - Gener. Transm. Distrib., Vol. 143, No. 5, September 1996, pp 427-434.

REPRINTS OF PAPERS

TAYLOR, VICTOR ALEXANDER

Tutor,
Department of Electrical & Electronic Engineering,
Footscray Institute of Technology, Australia

B. Sc. (Hons) 1973, Melbourne University, Australia
Grad. Dip. Applied Sci. 1980, Footscray Institute
of Technology, Australia
B.E. (Elec.) 1987, Footscray Institute of Technology,
Australia

1981 - 1987, Lab. Technician, F.I.T., Australia
1988, Technical Officer, F.I.T., Australia
1988 - 1989, Tutor, F.I.T., Australia

FAULKNER, MICHAEL

Senior Lecturer,
Department of Electrical & Electronic Engineering,
Footscray Institute of Technology, Australia

B. Sc. Eng. 1970, London University, UK
M.E. 1979, University of New South Wales, Australia

1979 - Present, Senior Lecturer, Footscray Institute
of Technology, Australia

KALAM, AKHTAR

Senior Lecturer/Course Director for Masters Program,
Department of Electrical & Electronic Engineering,
Footscray Institute of Technology, Australia

B.Sc. 1969, St. Xavier's College, India
B.Sc.Eng 1973, Aligarh Muslim University, India
M.S. 1975, University of Oklahoma, U.S.A.
Ph.D. 1981, University of Bath, U.K.

1973 - 1974, Sales Engineer, J.K. & Brothers, India
1975 - 1976, Sales Engineer, Ingersoll-Rand, India
1976 - 1978, Asst. Lecturer, University of
Technology, Baghdad
1982 - 1984, Lecturer, Capricornia Institute,
Australia
1984 - till date, Senior Lecturer, Footscray
Institute of Technology, Australia

Publications: 2 books

FAULT LOCATION ON EHV LINES USING WIDEBAND SPREAD SPECTRUM TECHNIQUES

TAYLOR, Victor

Tutor

FAULKNER, Michael

Senior Lecturer

HAYDEN, John

Communications Engineer, State Electricity Commission of Victoria, Melbourne, Victoria, Australia.

KALAM, Akhtar

Senior Lecturer

V. Taylor, M. Faulkner and A. Kalam are with the Department of Electrical and Electronic Engineering, Footscray Institute of Technology, Melbourne, Victoria, Australia.

ABSTRACT

This paper describes current investigations into the feasibility of spread spectrum fault location using digital signal processing techniques. Specifications for a prototype data acquisition system have been derived from transmission line characteristics and the design is outlined. The frequency range for operation has been set at 80 kHz to 200 kHz for compatibility with the existing power line carrier frequency network.

Main Key Words: spread spectrum, fault location

1.0 INTRODUCTION

Power line protection systems use relays and fault locators operating on an impedance measuring principle to determine when a fault has occurred and its approximate position along the line. In these systems the presence of the line voltage is necessary for the impedance measurements.

Faults will also cause a discontinuity in the characteristic impedance

of the line. This discontinuity will act as a reflection point for signals. The position of this reflection point can be sensed using reflectometer or radar-like techniques. Time domain reflectometer equipment is used by telecommunications authorities for determining the position of breaks in underground cables. This equipment sends a pulse down the line and then measures the times and amplitudes of the reflections. A disadvantage of this technique is that very high peak powers are required if resolution is to be maintained in a high noise environment.

Radar-like techniques which use a wideband chirp or spread spectrum signal require lower transmission power levels and are more likely to be suited to a power line environment. This project aims to investigate the feasibility of using radar-like spread spectrum techniques as a means of accurately locating the position of a power line fault by determining:

1) The best wave shape for transmission and its required receiver structure.

2) The expected range resolution of the system.

3) The trade-off relationships between the system detection time, the noise handling capability and the circuit complexity (cost).

4) The compatibility of such a system with existing PLC and PSL equipment, and any proposed spread spectrum PSL system [5].

2.0 SPREAD SPECTRUM WAVEFORMS

2.1 Definition

The distinguishing feature of a spread spectrum waveform is that the signal occupies a bandwidth greater than the minimum necessary to transmit the basic information being sent. This bandwidth spreading is often accomplished by means of a periodic code. Examples of spread spectrum techniques used in communications and ranging include

1) pulsed-FM or chirp modulation where a carrier is transmitted whose frequency is swept over a wide band during a given time interval.

2) time hopping, where carrier bursts are transmitted, the duration of each burst being governed by a periodic code sequence.

3) frequency hopping, where the frequency of the sine wave carrier shifts in a periodic fashion through a finite sequence of discrete

frequencies, the proportion of time at each frequency being set by a code sequence.

4) direct sequence, where a sine wave carrier is phase inverted by a pseudorandom code.

Chirp modulation has been used almost exclusively in radar and frequency swept signals have been applied to fault location on transmission lines [1], [2].

Time hopping has been used in communications and cable fault location [3].

Frequency hopping systems are usually used for communications rather than ranging because of the difficulty in constructing rapid hopping fast settling frequency synthesisers required for high resolution ranging. It has been suggested that high speed coherent frequency hoppers would be suitable for ranging [4].

Direct sequence systems are widely used for both communications and ranging and are the main focus of what follows. The long range accuracy of direct sequence ranging has led to navigational use in aircraft and space vehicles.

2.2 Advantages of Spread Spectrum

1. The peak power/resolution trade-off of pulse time domain reflectometry is avoided by spreading the transmitted energy over a long time interval.

2. Spread spectrum signals have low power spectral density and so are compatible with narrowband communication links occupying a small part of the spread spectrum bandwidth. In particular spread spectrum will be compatible with already existing narrowband AM and FM power line carrier communication links, together with radio navigation beacons which at present put limitations on PLC communications.

3. Multiple spread spectrum communication links can co-exist inside the same bandwidth together with a spread spectrum fault locator.

4. The correlation techniques used in spread spectrum demodulation perform well in high noise environments.

5. High resolution ranging is possible and multipath effects due to multiple reflections and branches in the transmission line may be distinguished by the correlation method.

6. Wideband signals are less vulnerable to the frequency dependent

distorting effects of modal propagation along transmission lines.

7. There is the capability of monitoring the line without the presence of the 50 Hz line voltage. Hence clearance of the fault can be determined without closing the main breaker.

3.0 SPREAD SPECTRUM RANGING

3.1 Direct Sequence Ranging

Fig. 1 depicts a code $p(t)$ with a bit rate of 60 kHz (called chip rate R_c - 60 kHz) modulating a carrier of frequency f_0 - 140 kHz to produce a direct sequence signal; because of the 180 degree phase shifts this is called a biphase modulated carrier (BPSK).
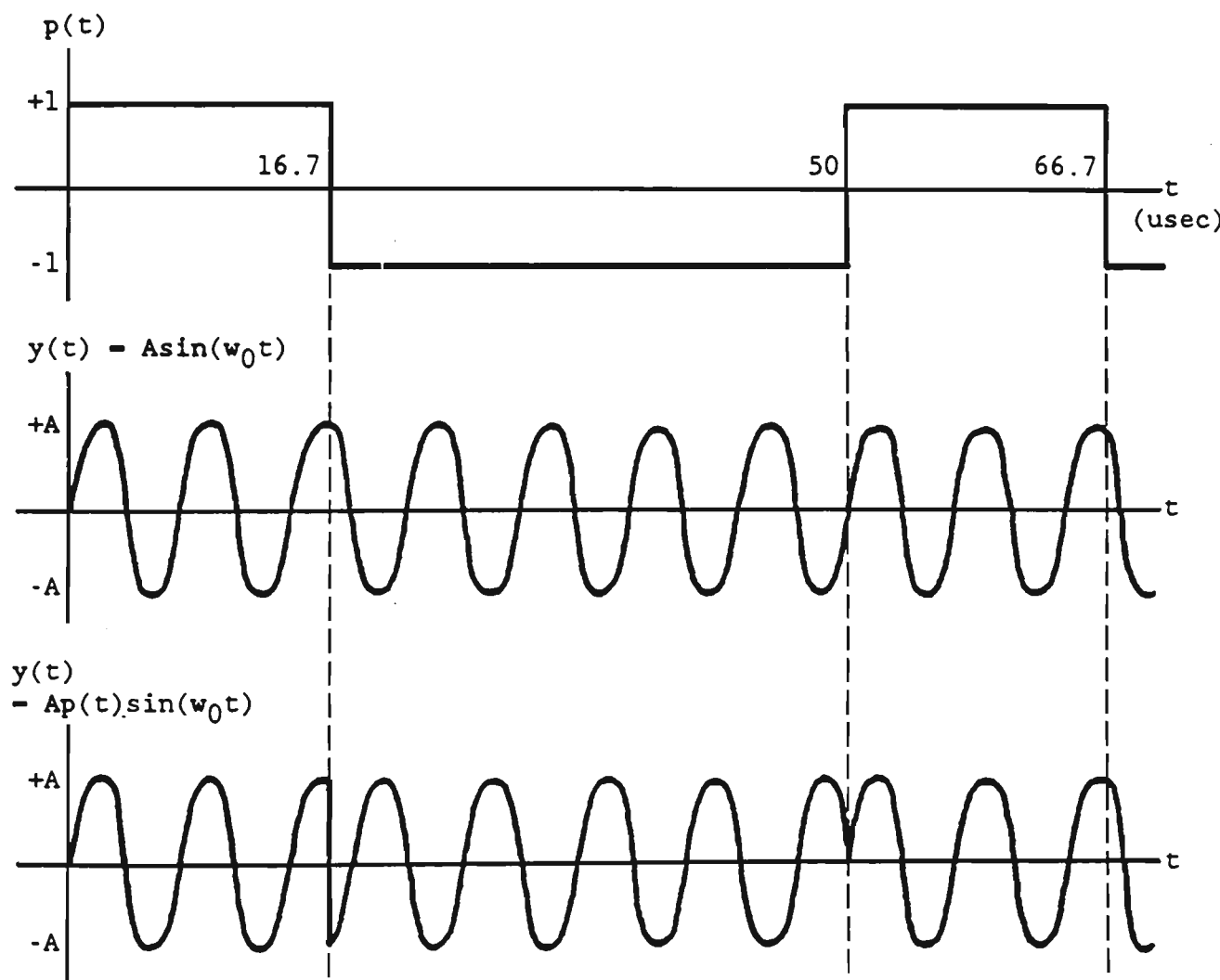

Figure 1. Code $p(t)$ with R_c - 60 kHz modulating a carrier with frequency f_0 - 140 kHz to produce a direct sequence waveform.

When this signal is transmitted down a transmission line it will reflect

back from the impedance discontinuity caused by any fault on the line (Fig. 2(a)). Using signal processing techniques the relative phase of the transmitted code $p_T(t)$ and the received reflected code $p_R(t)$ may be determined. As shown in Fig. 2(b) the number of code bits or chips in phase difference between the transmitted and received codes represents the time taken for the code to travel to the fault and back. Knowing the velocity v of signal propagation along the transmission line we can calculate the distance to the fault as in pulse or chirp echo ranging.
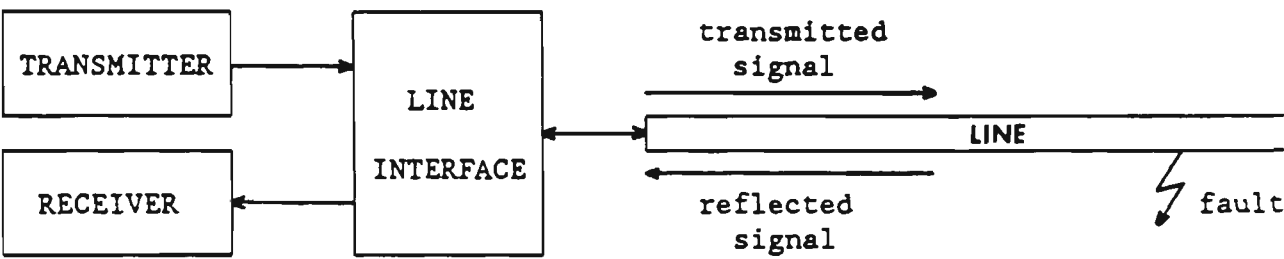

<u>Figure 2(a).</u> Transmission line fault locator.

distance of fault from transmitter = $(v/2)(3.5/R_c)$
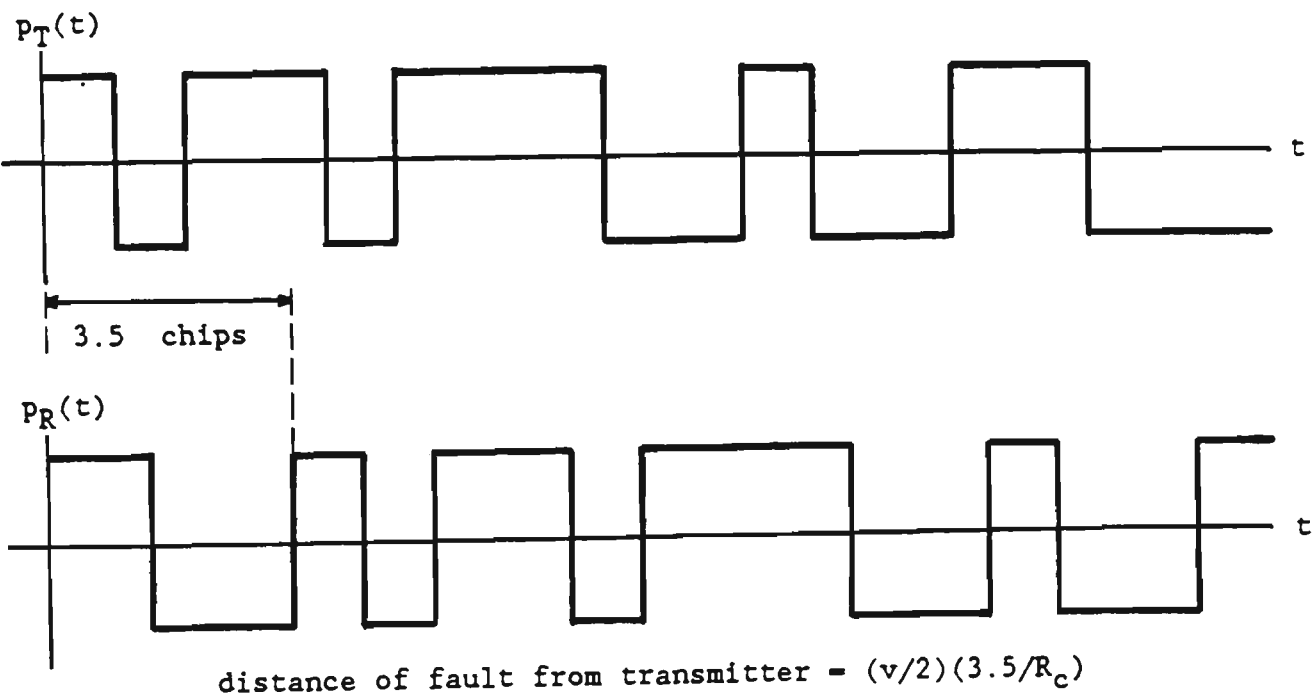
<u>Figure 2(b).</u> Phase shift between transmitted and reflected codes gives fault location.

3.4 Code Requirements

Ranging codes have four basic requirements.

<u>3.4.1 Synchronisation :</u> The receiver takes the reflected signal and slides a copy of the transmitted code past the reflected code until the two

codes are aligned giving the range determining phase shift. With long codes this can be a time consuming process but this time is reduced with proper selection of codes.

3.4.2 Sensitive autocorrelation function : The autocorrelation function of a code is a measure of the similarity between a code and a phase shifted version of itself. It is desirable that the autocorrelation function for ranging codes has a high value for zero phase shift and rapidly falls to (near) zero as the phase shift increases. This property increases range resolution in the face of noise, bandwidth limitation, and waveform distortion due to modal propagation and fault reflection.

3.4.3 Low cross-correlation : Cross-correlation is a measure of the similarity between two different code sequences. Spread spectrum communications systems use codes with low cross-correlation to send different messages occupying the same bandwidth along a channel. Provided the ranging codes have low cross-correlation with any communication codes used, then ranging and communications can co-exist in the same bandwidth - indeed the ranging code can also be used for communications [6]. Similarly, if ranging codes on one line have low cross-correlation with ranging codes used on a nearby line, then ranging measurements can take place simultaneously on both lines.

3.4.4. Minimum code length : For unambiguous range estimates the maximum amount of slip between transmitted and received codes must be less than the length of the code. This means that the modulated carrier must stretch out for twice the maximum length of the line under investigation before the code starts to repeat - this requirement sets the minimum code length.

3.5 Ranging Codes

3.5.1 MLS (PN) codes : A linear code generator consists of a shift register and circuitry to EX-OR selected bits of the shift register and feed the result into the shift input of the shift register. Maximal linear sequence (MLS) codes are by definition the longest codes that can be generated by a shift register of given length. For a shift register of length n the MLS codes are of length $N = 2^n - 1$ and have the following properties.

1. MLS codes contain 2^{n-1} 1s and $2^{n-1} - 1$ 0s.

2. If a window of width n is slid along an MLS code then each of the

2^{n-1} non-zero binary n-tuples is seen exactly once (to avoid difficulties at the ends imagine the code is circular).

The above properties ensure that in the short term a long maximal sequence looks like random numbers. However in the long term the sequence is periodic and hence is called a pseudonoise (PN) sequence.

3. The most important property of any PN sequence

$$A = \{a_0, a_1, \ldots, a_{N-1}\}$$

is the behaviour of its auto-correlation function $R_A(i)$. As illustrated in Fig. 3, $R_A(0) = N$ and $R_A(i) = -1$, for $0 < i < N$.
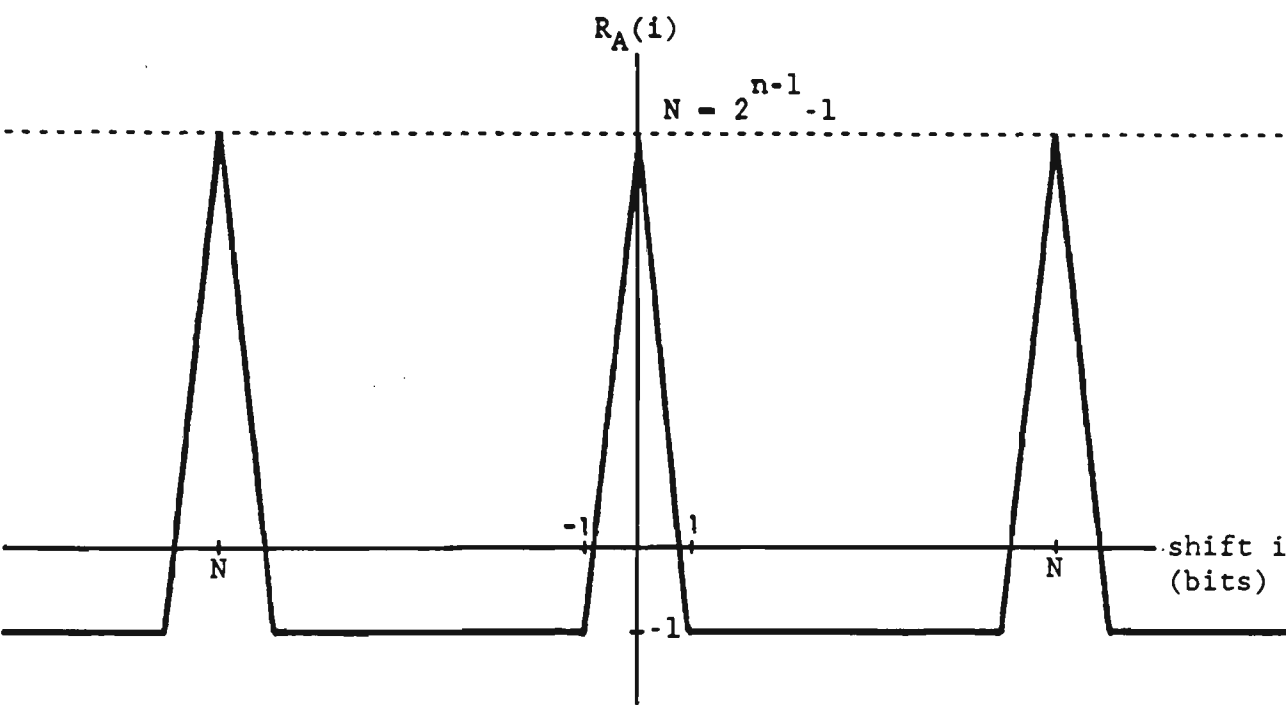

Figure 3. Autocorrelation function of PN sequence with length N. The index of discrimination of a code is shown in Equation (1).

$$\frac{R_A(0)}{\max_{0 < i < N} R_A(i)} = N \quad \text{for PN sequences.} \qquad \ldots (1)$$

Codes with a large index of discrimination are desirable for communication and ranging because the relative phase shift of two versions of the code may be determined more accurately.

3.5.2 Golay codes : Golay codes occur in complementary pairs and have the following property - if A and B are an N bit complementary code pair then

$R_A(0) = R_B(0) = N$

$R_A(i) = -R_B(i)$ for $0 < i < N-1$ ... (2)

$R_A(i) + R_B(i) = 2N \delta(i)$ for $i = 0,1,...,N-1$

Hence while both A and B have some autocorrelation sidelobes, when the autocorrelations are added the sidelobes cancel and a high central peak is left. This property of Golay codes has been used to advantage in optical time domain reflectometry spread spectrum fault location [7].

3.5.3 JPL codes : The JPL (Jet Propulsion Laboratory) ranging codes are constructed by modulo 2 addition of two or more PN sequences whose lengths are relatively prime to one another. While the resulting code may be very long, synchronisation proceeds by synchronising on the individual (shorter) codes, greatly reducing the time required for synchronisation [8], [9].

3.5.4 Hybrid system : This modified direct sequence ranging technique uses a short quickly searched code for fine range resolution. Ambiguity in range is resolved by modulating with a digital pattern whose bit rate equals the PN sequence repetition rate and whose period exceeds the propagation delay of the largest range to be measured [10].

3.6 Range Resolution

The basic range resolution capability is to within the distance travelled by the signal down the cable during one half a chip period. The higher the chip rate the greater the number of chips delay between the transmitted and received signal and hence the greater the resolution. However, many direct sequence systems can resolve range to within one tenth of a chip period.

Fig. 4 illustrates the power spectral density $G_A(f)$ of a PN sequence with chip rate R_c and length N modulating a carrier of frequency f_0. The spectrum of this BPSK waveform consists of a suppressed carrier and discrete lines separated by R_c/N with a $[sin(x)/x]^2$ envelope. As N increases the spectral lines move closer together, approximating white noise.

Here we see a range/resolution trade-off as higher chip rates give better resolution but require wider bandwidth. RF bandwidth restriction degrades the autocorrelation function (Fig. 5) and hence will lead to

degraded range resolution. Many PN ranging systems transmit only the main lobe with bandwidth $2R_c$ which contains 90% of the direct sequence power.
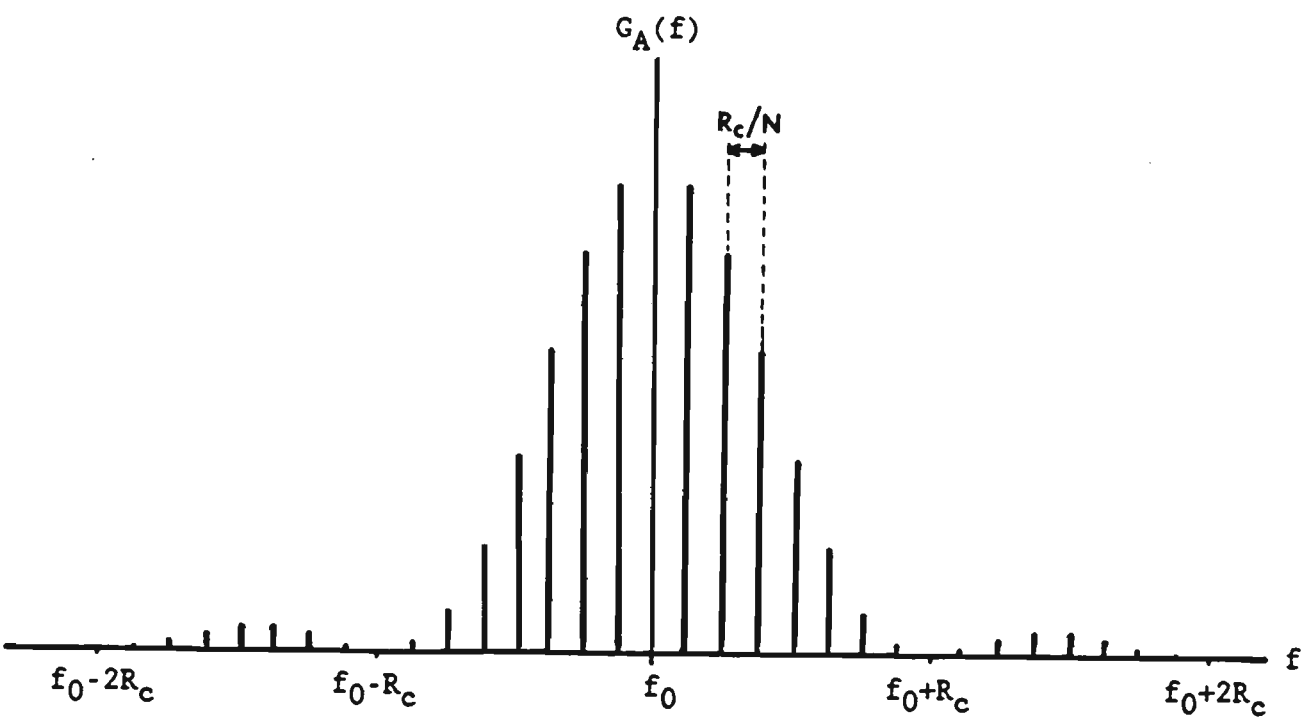

Figure 4. Power spectral density of PN sequence of length N and chip rate R_c, biphase modulating a carrier of frequency f_0.
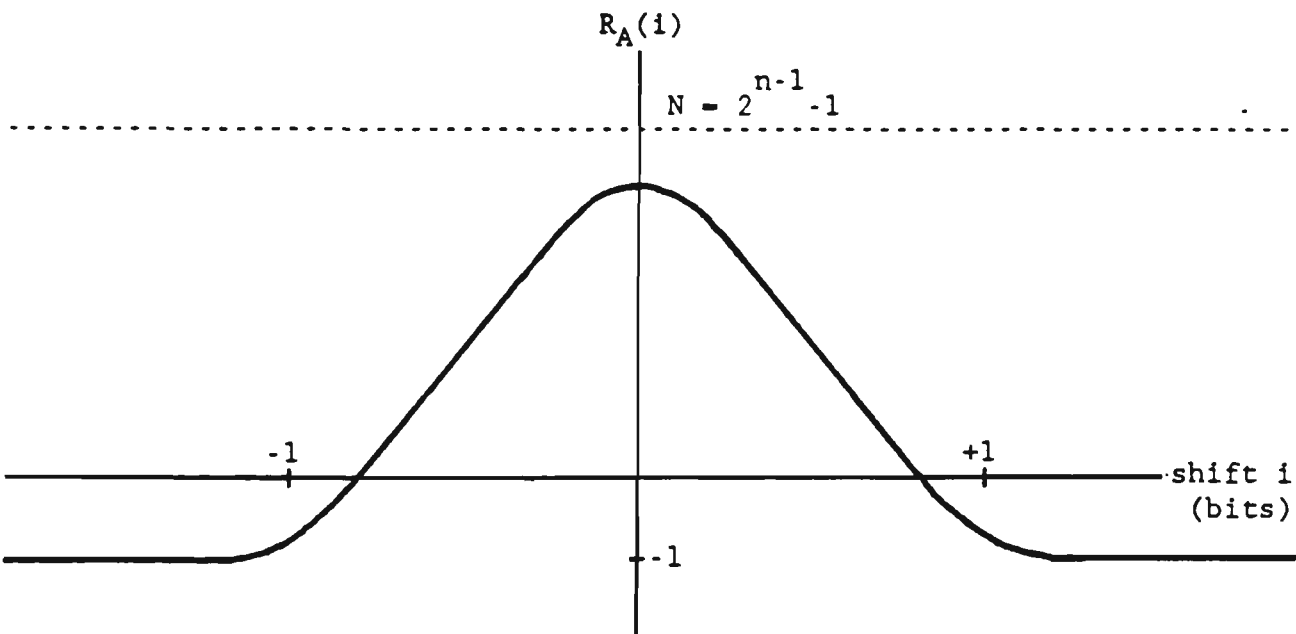

Figure 5. PN autocorrelation function with bandwidth restriction.

4.0 SECV POWER LINE CARRIER SYSTEM

Power authorities worldwide maintain communication links over transmission lines for the operation of voice communication channels and the sending of protective relaying, telemetering and control signals. These high frequency links transmit single sideband AM and FM signals and are known as power line carrier (PLC).

4.1 Coupling Methods

Fig. 6 shows a typical PLC coupling to a transmission line. In Australia, Department of Communications regulations require the carrier signals to be injected between two phases of the one transmission circuit or, alternatively, betwen one phase of one line and one phase of another line on the one easement.

Connection of the carrier equipment to the power line is achieved either by using the capacitor section of the capacitive voltage transformers or by using a separate h. v. capacitor. From the low voltage side of the CVT there is a drain coil to ground which provides a low impedance path at the 50 Hz power frequency but which has significant impedance at PLC frequencies. The drain coil protects the communication system from overvoltages.

The coupling capacitors are connected to the line matching unit (LMU) shown in Fig. 7. The LMU converts from the 600 ohm balanced power line signal to the 75 ohm unbalanced signal output from the communications room.

To isolate the carrier signal on the power line from the local station bus, line traps are installed between the coupling capacitors and the local station switchgear (Fig. 8). These line traps have tuning packs to set the line traps to the particular carrier frequencies used on that line.

4.2 PLC Frequencies

The LMU in the switchyard is connected to a separation filter group (SFG) inside the communications room. This consists of a combination of four lowpass or highpass filters which splits PLC communications into three frequency bands : 80 - 200 kHz, 200 - 400 kHz and 400 - 500 kHz.

151

Figure 6. Typical PLC line interface used by the SECV

Figure 7. Line matching unit.

C.C.: coupling capacitor
DR: drain coil
g: protective device
k: knife switch

P: protective device

1 mH

line   line

0.0005 μF

600 Ω   0.003 μF
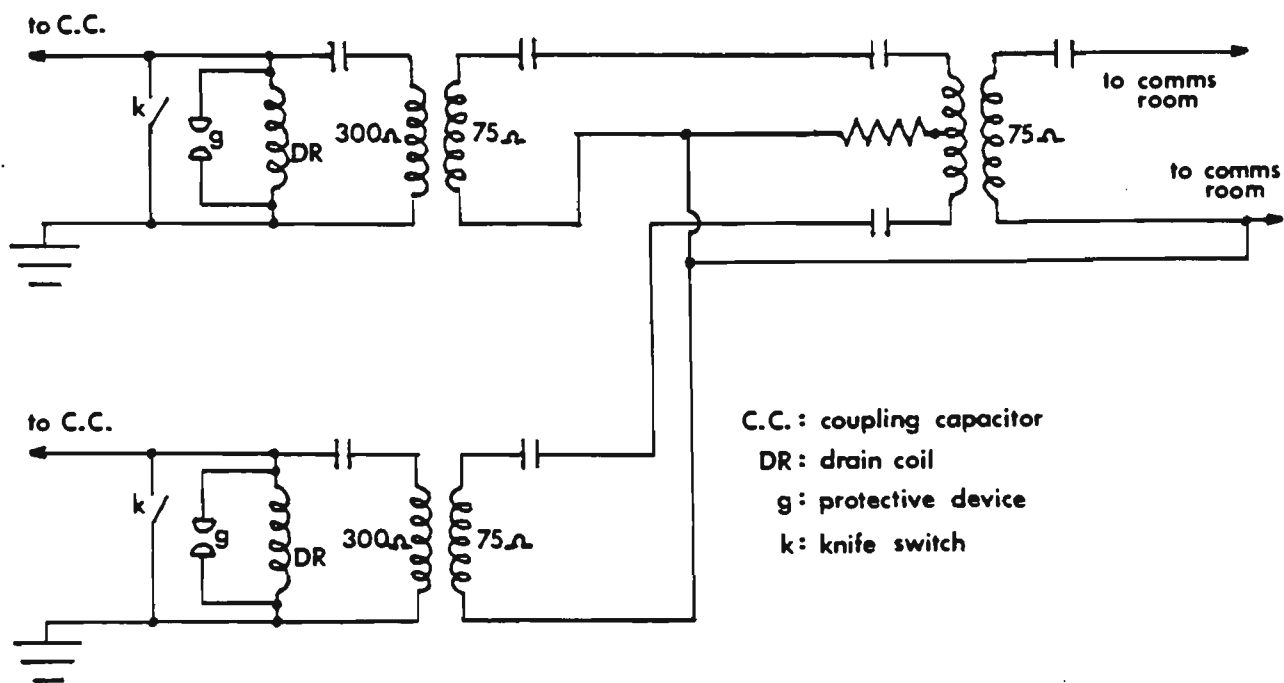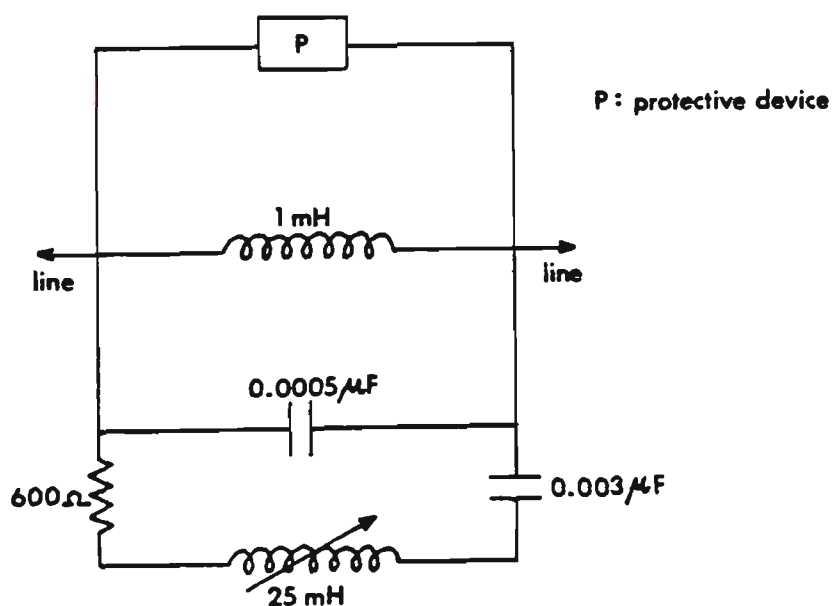
25 mH

Figure 8. Line trap with tuning pack. Resistive component of impedance is at least 600 ohm from 80 - 480 kHz.

153

5.0 SYSTEM DESIGN

To experimentally investigate the feasibility of spread spectrum fault location a spread spectrum transmitter and receiver is being constructed. For maximum flexibility digital signal processing techniques have been decided upon with D/A and A/D data converters in the transmitter and receiver respectively. For the initial measurements data analysis will be done in none real time on a mainframe.

5.1 Predicted System Performance

With the transmitter and receiver at the same end of the line, the signal input to the receiver consists of the high power transmitted signal combined with the much fainter reflected signal. Attenuation of the reflected signal can easily reach 50 dB so that in order to record the reflected signal with sufficient accuracy we will need a 12 bit A/D.

To combat line noise in the receiver we will provide for averaging 4095 code sequence periods to give 36 dB improvement in the SNR. Interference from the transmitted pulse will then be the major factor limiting system performance.

Basic system design equations are as follows:

1) From [11] we assume 6 dB coupling and shunt losses (one way) - also we estimate 6 dB signal loss in reflecting off the fault. Hence

$$P_{RX} = P_{TX} - 18 - 2ad \qquad \ldots (3)$$

where P_{TX} is the transmitted power (dB), P_{RX} is the received power (dB), a is the attenuation (dB/km) and d is the distance (km) to the fault from the transmitter/receiver. Maximum range is calculated by requiring a ratio of 50 dB of transmitted voltage to received reflected voltage. This gives approximately 4 bits of reflected voltage at the A/D and implies 16 dB of one way attenuation so that

$$d_{max} = (P_{TX} - P_{RX} - 18)/2a = 16/a \qquad \ldots (4)$$

2) Assuming signals propagate along the transmission line with the speed of light c

$$\text{range resolution} = c/(2R_c) \qquad \ldots (5)$$

3) Minimum code length $= 2d_{max}/(c/R_c)$ $\qquad \ldots (6)$

4) With a sample frequency f_s the length of memory required for a code of length 1023 is $1023f_s/R_c$ $\qquad \ldots (7)$

In Table 1 we predict system performance at three different bandwidths

- typical attenuations for a 138 kV line at the given carrier frequencies are taken from [11].

Wider bandwidth codes have higher resolution but lower range due to increased attenuation at higher frequencies - this will be partly compensated for by the lower noise at higher frequencies. The resolutions in Table 1 compare favourably with the 5% resolution attainable with the impedance measuring method currently used by the SECV.

Techniques to further increase the range of the system include

  (a) the use of a resistive, inductive or semiconductor hybrid to reduce the magnitude of the transmitted signal entering the receiver

and (b) the use of increased dynamic range in the receiver eg. using a 16 bit A/D instead of a 12 bit A/D.

Table 1. System performance at different bandwidths.

	BW$_1$ 80 - 200 kHz	BW$_2$ 200 - 400 kHz	BW$_3$ 80 - 500 kHz
carrier f_0 (kHz)	140	300	290
chip rate R_c (kHz)	60	100	210
attenuation a (dB/km)	0.08	0.15	0.16
f_s (MHz)	2.5	5	5
range resolution (km)	2.5	1.5	0.71
range (km)	200	107	100
minimum code length	80	72	140
memory required for code of length 1023 (kWords)	42.625	51.15	24.36

5.2 Data Analysis

Fig. 11 illustrates the data analysis process that will be carried out on the mainframe computer. The data consists of L - Nf_s/R_c digitised samples of one complete received code sequence length - these points consist of some of the transmitted signal together with the reflected signal and noise.

Implementation of the software hybrid will probably rely on a template

recording made without any fault present on the line. Perhaps simply subtracting the template from the recorded data will be sufficient or perhaps an adaptive algorithm will be necessary to implement the hybrid.

The sequence of points $x_0, x_1, \ldots, x_{L-1}$ resulting from the hybrid processing is multiplied by the L digitised points of the circularly shifted generating PN (for example) sequence, $a_m, a_{m+1}, \ldots, a_{m+L-1}$ where $0 <= m <= L - 1$ and $+$ denotes addition modulo L. The DFT of this product is calculated at the carrier frequency f_0

$$X_m[\exp(jw_0 t)] = \sum_{k=0}^{k=L-1} x_k a_{k+m} \exp[-j(2 \ kf_0/f_s)] \qquad \ldots (6)$$

$L = Nf_s/R_c$ data points   (transmitted signal
                              $+$ reflected signal
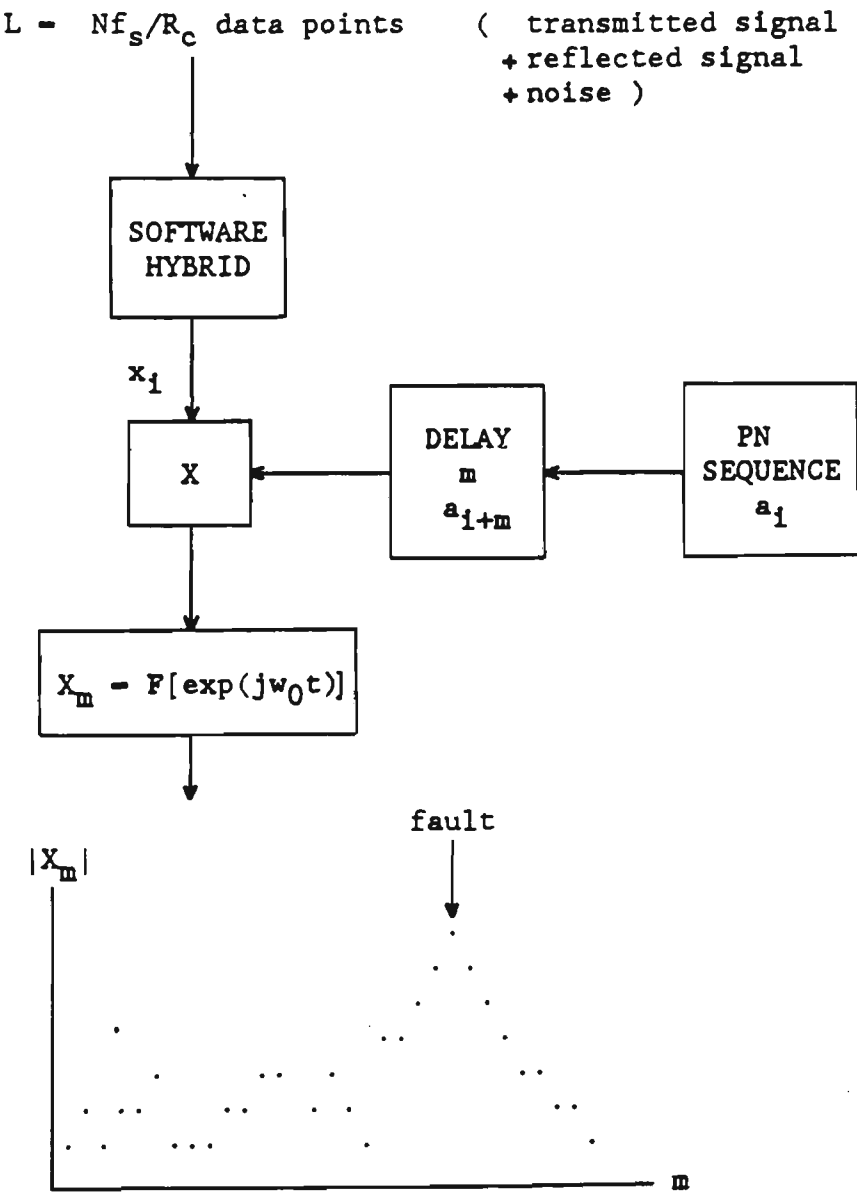 $+$ noise)

Figure 9. Data analysis on the mainframe.

A graph of $|X_m|$ versus m should reveal peaks corresponding to impedance discontinuities on the line. Hopefully the m axis can be calibrated for distance from known reflection points on the line (line transpositions or branches).

Taking the DFT is equivalent to passing the signal through a very narrow bandpass filter and is a noise reducing process. With a PN code of length 1023 the correlation process has a voltage index of discrimination of 60 dB. If this figure is realised in practice it is possible that the correlation process will reveal the fault location even without first removing the transmitted signal.

5.3 Signal Processing Hardware

Fig. 10 illustrates the block diagram of the system being constructed using the Eurocard format for modular development and expansion.

The waveform to be sent out is software generated and then downloaded into battery backed up static RAM in the waveform transmitter. A transmitter controller board is then used to transmit in a periodic manner the waveform stored in the RAM - this goes out through a D/A converter to a reconstruction filter, is amplified by a broadband amplifier and then goes through an interface to the LMU and onto the line.

The amplifier output, together with any reflected waveform after it has passed through an anti-aliasing filter, is fed back into the receiver front end. After a set number of cycles through the TX RAM the receiver is triggered and, under control of a receiver controller board, an A/D samples a full code sequence length cycle of the incoming waveform and the samples are stored in the receiver static RAM. The receiver will also have the capability to average up to 4095 incoming waveform cycles.

The received waveform is then downloaded from the receiver RAM onto floppy disc for analysis on a mainframe computer.

5.3.1 Sampling Rate : Initial tests will be in the range $BW_1 = 80 - 200$ kHz but we also anticipate operation in the frequency ranges $BW_2 = 200 - 400$ kHz and $BW_3 = 80 - 500$ kHz, corresponding to the PLC frequency bands. For BW_2 and BW_3 we sample at 5 MHz (Nyquist frequencies 800 kHz and 1 MHz respectively) and we sample at 2.5 MHz for BW_1 (Nyquist frequency = 400 kHz) - these rates apply to both the transmitter and receiver. Oversampling simplifies the design of the reconstruction and anti-aliasing filters. Fourth order Bessel filters have been chosen for their constant
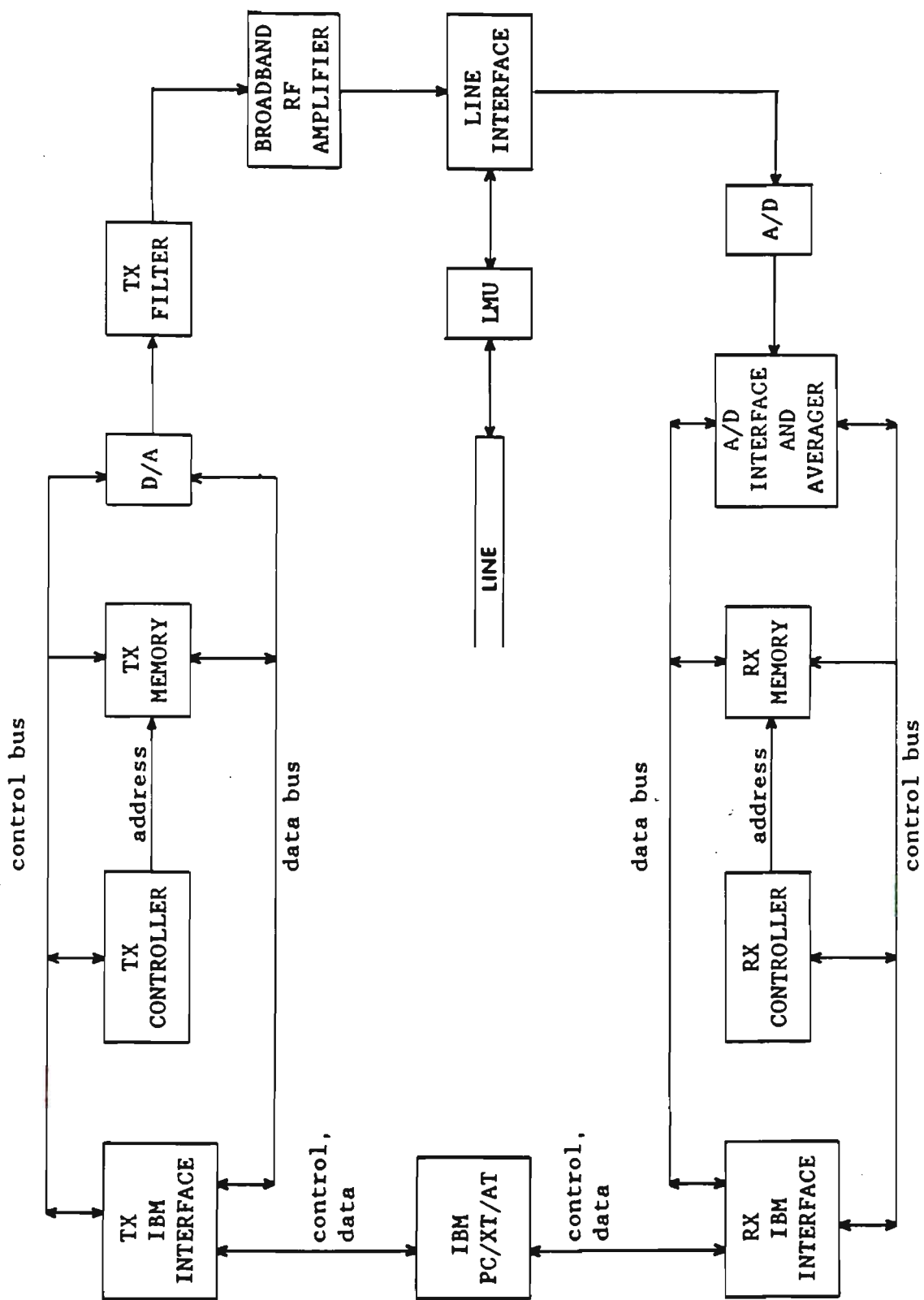
Figure 10. Data acquisition system block diagram.

158

group delay characteristic.

5.3.2 Dynamic Range : Power line noise figures in [11] indicate that in fair weather there may be as little as -24 dBm of noise on a 138 kV line in BW_1 = 80 - 200 kHz. Assuming 47 dBm (50 Watts) of power output from the amplifier, we see that a 12 bit D/A in the transmitter is justified. The large transmitted signal component going into the input to the receiver necessitates a 12 bit A/D.

5.4 Line Interface

Fig. 11 illustrates two possible line interfaces. Without the hybrid the transmitted and reflected signals are attenuated equally and fed to the receiver - the transmitted signal component would be removed using software as the start of the data analysis.

In order to reduce the transmitted signal entering the receiver a high power wideband resistive hybrid may be constructed out of three 75 ohm resistors - however this has the disadvantage of dissipating half the transmitted and received powers. Assuming that the resistive hybrid attenuates the transmitted signal fed back to the receiver by 10 dB and that 50 W. of power is output from the RF amplifier, then the hybrid increases the ranges in Table 1 by about 10%.
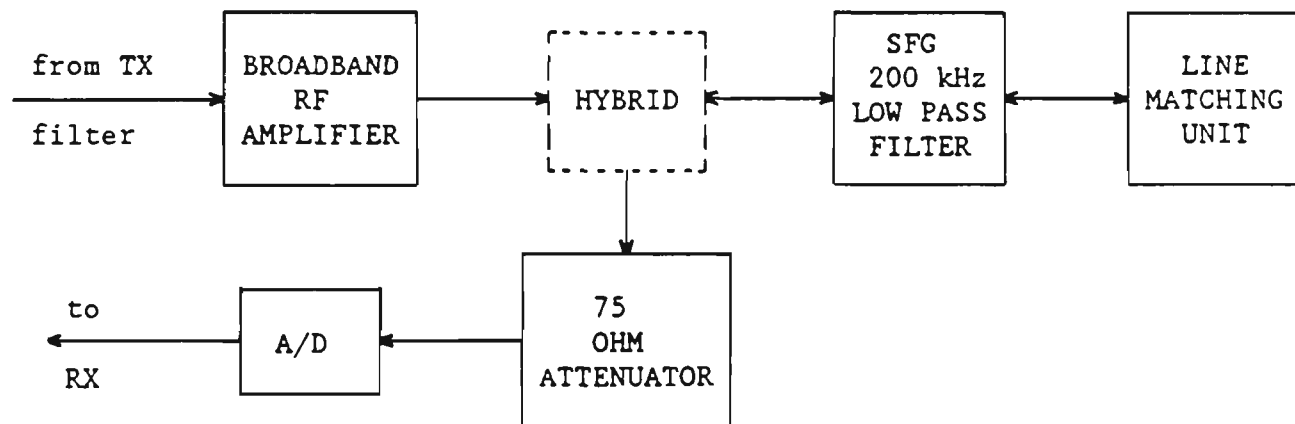

Figure 11. Line interface for BW_1 = 80 - 200 kHz. with attenuator, and with (possibly) a hybrid.

The configurations of Figs. 10 and 11 have both the transmitter and receiver located at the same end of the line under investigation which requires the operation of either a hardware or software hybrid. This complication could be overcome by having the receiver at the opposite end of the line to that of the transmitter. While the received signal is

reduced in strength, this is compensated for by by not having a strong transmitting signal feeding straight into the receiver.

6.0 CONCLUSION

The design of a data acquisition system to investigate the possibility of using wideband spread spectrum techniques to locate faults on transmission lines has been outlined. Spread spectrum signals have low density power spectra and hence have low mutual interference with many other types of communication methods; also correlation techniques perform well in high noise environments. Existing power line carrier and signalling equipment will be used. Analysis shows that ranges up to 200 km can be expected, with range resolution from 2.5 km to 0.71 km depending upon the available bandwidth. A subsequent paper will detail the electronic design of the data acquisition system which is under construction.

7.0 ACKNOWLEDGEMENTS

REFERENCES

1. D. Stevens, G. Ott, W. Pomeroy and J. Tudor, "Frequency-modulated fault locator for power lines", IEEE Trans. Power App. Syst., Vol. PAS-95, no. 5, pp. 1760-1768, Sept./Oct. 1972.

2. G. Hjipieris, G. Macrae and S. Thomas, "A Transmission Line Test System", Proceedings MIOP '88 Microwaves and Optoelectronics Conference, 1A-1/1-6, 2-4 March, 1988, Wiesbaden, West Germany.

3. L. E. Roemer, Chiou-Shiun Chen, M. S. Hostetler, "Cepstral Processing Using Spread Spectra for Cable Diagnostics", IEEE Trans. Instr. Meas., Vol. IM-30, no. 1, March, 1981.

4. R. C. Dixon, "Spread Spectrum Systems", Second Edition, John Wiley and Sons, 1984.

5. M. Faulkner, 'A New Modulation for Power Line Protection Signalling', IREECON International, September 1987.

6. R. B. Ward, "Digital Communications on a Pseudonoise Tracking Link Using Sequence Inversion Modulation", IEEE Trans. Comm. Tech., Vol. COM-15, No. 1.

7. F. Sischka, S. Newton, M. Nazarathy, "Complementary Correlation Optical Time Domain Reflectometry", Hewlett-Packard Journal, December 1988.

8. S. W. Golomb (editor), "Digital Communications with Space Applications", Englewood Cliffs, N. J., Prentice-Hall, 1964.

9. R. C. Titsworth, "Optimal Ranging Codes", IEEE Trans. Space Electron. Telem., vol. SET-10, pp.19-30, Mar. 1964.

10. R. C. Dixon, " A Spread Spectrum Ranging Technique for Aerospace Vehicles", reprinted in 'Spread Spectrum Techniques', R. C. Dixon (editor), IEEE Press, 1976.

11. Power Line carrier Application Guide, General Electric Products Section, Lynchburg, Virginia.

Digital simulation of fault location on EHV lines using wideband spread spectrum techniques

V. Taylor
M. Faulkner
A. Kalam
J. Haydon

Indexing terms: Digital simulation, Fault location on power lines

Abstract: Spread spectrum techniques perform well in high-noise environments such as power lines, and their use in radar ranging is well known. Existing power line carrier (PLC) equipment may be used to transmit a direct sequence signal down a faulted EHV line. The fault position may then be calculated from correlation analysis of the reflected waveforms. This fault-location process has been simulated on a digital computer by taking into account the frequency variation of the PLC interface and line parameters over the spread spectrum bandwidth. The effect of waveform characteristics and fault location are examined for a 100 km double transposed line with a single phase to ground fault. Results indicate that permanent faults may be located to within 0.5 km.

List of symbols

f_0 = carrier frequency
R_c = code bit (chip) rate
L = code length
f_s = sample frequency
N_p = number of sample points in digitised waveforms
y_k = sampled line model output $(k = 0, 1, \ldots, N_P - 1)$
p_k = sampled bandlimited code $(k = 0, 1, \ldots, N_P - 1)$
S_i, R_i = reflections at sending and receiving end $(i = 0, 1, \ldots)$
F_1 = primary fault reflection at sending end
D = line length
T = transposition matrix
V, I = voltage and current transforms
Z, Y = series impedance and shunt admittance matrices
Z_0, Y_0 = characteristic impedance and admittance matrices
S = voltage eigenvector matrix
V_i, V_r = incident and reflected voltage transforms

V_S, I_S = sending end voltage and current transforms
V_R, I_R = receiving end voltage and current transforms
E_F, V_F = transform of total voltages at point of fault
V_{SS}, I_{SS} = prefault sending end voltage and current transforms
V_{RS}, I_{RS} = prefault receiving end voltage and current transforms
V_{FS} = transform of prefault voltage at point of fault
V_{SF}, I_{SF} = sending end voltage and current transforms due to fault
V_{RF}, I_{RF} = receiving end voltage and current transforms due to fault
E_{FF}, V_{FF} = transform of voltages due to fault at point of fault
V_{TX} = transmitted PLC signal
Y_S = total sending end admittance
Y_R = total receiving end admittance
a_S = transmitter admittance vector
x = distance to fault from sending end
R_F = fault resistance matrix
γ = propagation constant matrix

1 Introduction

Electricity supply authorities worldwide are subject to increasing power supply demands, so that there is always a need for quicker and more accurate fault-location methods to improve the quality of supply and to decrease outage times. Some faults, such as those due to high-voltage breakdown, require the presence of the mains voltage to be observable, and others, called permanent faults (e.g. a conductor shorted to ground), can be measured on de-energised lines [1]. More than 50 years of research into both types of faults [2, 3] have produced two different approaches to remote sensing of the fault position: passive and active sensing.

1.1 Passive sensing

These fault-location methods are based on the measurement of waveforms that exist immediately after fault inception. Typically these signals consist of a steady-state power frequency sinusoid, together with transient high-frequency components and an exponentially decaying DC value. Some algorithms are based on power frequency lumped parameter transmission line models, and

they require filtering to extract the steady-state fault signals. Later research attempted to incorporate the high-frequency transient travelling waves by using more sophisticated line models.

The performance of reactance-measuring devices have been improved by compensating for nonzero fault resistance and nonzero fault reactance due to double end feed lines, load current and remote end feed [4–7]. In Reference 5 faults on a 71.2 km long trnsmission line were located to within 1 km.

The Newton–Raphson method is applied in Reference 8 to estimate the power frequency voltages and currents using a least-squares method; faulted transmission line equations are solved for R_F and x. In Reference 9 the Newton–Raphson method is used to solve equations derived using steady-state superposition on a lossless faulted line. The s-domain lumped parameter circuit representation of a transmission line may be transformed into the z-domain for sampled data analysis. This method is used in Reference 10 were field tests on a 167.5 mile long line with a fault at $x = 112$ miles estimated the fault location at $x = 110.9$ miles.

A lumped parameter model of the line is derived using least-squares analysis on voltage and current measurements in Reference 11; the fault-location algorithm also estimates R_F and does not require filtering of the high-frequency transients. However, the model neglects shunt capacitance and so is limited to lines less than 50 miles long. The superposition theorem using the Laplace transform is applied in Reference 12, whereas Reference 13 models the line using the telegraph equations. Correlation techniques have been used in References 14 and 15 to measure the time delay between voltage surges generated by the fault, from which the fault location is calculated.

1.2 Active sensing

In these methods the fault is located by measuring signals that result from sending a known waveform down the line; in particular we look at the radar-like techniques based on the analysis of travelling waves. Pulse echo ranging and FM fault-location equipment is described in References 16, 17 and 18. The range accuracy of pulse reflectometry can be improved only by increasing the transmitted power, whereas the accuracy of a continuous chirp FM fault locator may also be improved by transmitting a waveform with a higher bandwidth X period product. These reflectometry methods work on de-energised as well as energised lines, so that it is possible to determine if a permanent fault has been cleared without reclosing the mains breakers.

This paper considers the transmission of a direct sequence spread spectrum as an active sensing waveform.

2 Spread spectrum waveforms and ranging

A direct sequence [19] spread spectrum signal consists of a sinewave carrier multiplied by a periodic code which jumps in a noise-like manner (hence pseudonoise or PN) between $+1$ and -1. This waveform is also described as biphase shift-keyed (BPSK). Spread spectrum modulation methods have been previously proposed for protection signalling links on power lines [20].

The use of direct sequence waveforms for ranging is well known [21], and is illustrated in Fig. 1 to find transmission line faults [22]. A BPSK signal is transmitted down the line and the signal reflected from the fault is recorded. If the speed of propagation of the signal along

the line is known, then, by measuring the phase shift (time delay) between the transmitted and received codes, the distance to the fault may be calculated.
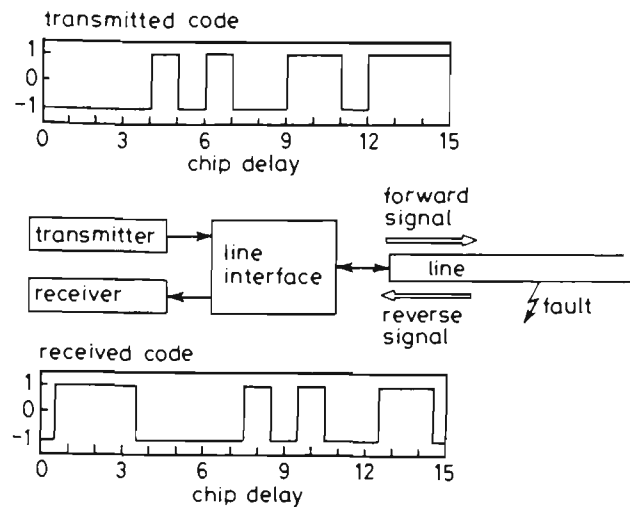

Fig. 1   Transmission line fault locator

For unambiguous range measurements the code should be long enough to stretch over twice the line length. Fault positions may be measured to within the distance travelled by the code during one-half of a bit period. Shorter-duration bit periods (higher chip frequencies) give greater range resolution at the expense of increased bandwidth.

3 Power line carrier fault location simulation model

The simulation program which has been developed can be used to model the steady-state voltage distribution established on a polyphase transmission line (both faulted and unfaulted) when any arbitrary periodic waveform is transmitted down the power line carrier (PLC) communications links. The program takes into account line transpositions and models the frequency variation of the line matching units, coupling capacitors, line traps and line parameters. Fig. 2 illustrates the simulation of
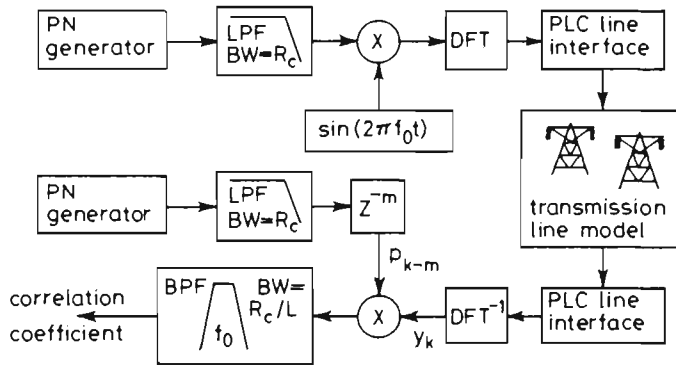

Fig. 2   Direct sequence fault-location simulation

sending a periodic BPSK signal down a faulted three-phase power line, the measurement of reflected waveforms and subsequent data analysis to locate the fault position.

The transmitted signal and data analysis blocks are in the time domain. The line model and PLC interface are frequency-dependent and are described in the frequency domain. The discrete Fourier transform (DFT) is used to change the transmitted waveform to the frequency domain, and the inverse discrete Fourier transform (DFT^{-1}) changes the received signal back to the time domain.

74

3.1 Waveform generation

In this paper only the maximal length sequence codes [19] are considered, because they are simple to generate and the autocorrelation function allows accurate phase measurements. The power spectral density of these codes has a $sinc^2$ envelope, and, as indicated in Fig. 2, the code is band-limited by the lowpass filter (LPF) so that after mixing with the carrier frequency f_0 the direct sequence BPSK waveform being transmitted has a bandwidth of $2R_c$ centred on f_0.

The best results are obtained if the code period is an integral multiple of the carrier period, so that the frequency spectrum consists of discrete lines separated by the BPSK repetition frequency R_c/L. The DFT requires a sampled version of the transmitted waveform. The Nyquist condition states that the sample rate f_s must be more than twice the highest transmitted frequency $(R_c + f_0)$. The sample period should also divide the code repetition period into equal intervals, so that the number of sample points in this period is $N_P = (L/R_c)f_s$. N_P is the size of the data window used for both the DFT and DFT^{-1} routines.

The BPSK Fourier coefficients from the discrete Fourier transform (DFT) block are fed into the line interface and power line models which enable the output voltage and phase to be calculated from each separate frequency. The simulation can be performed for both energised and de-energised lines.

3.2 Data analysis

The Fourier coefficients of the required waveform calculated above are treated as phasors and converted to time (DFT^{-1}). This time-domain waveform y_k for $k = 0, 1, \ldots, N_P - 1$ is then multiplied by a digitised time-shifted copy of the transmitted bandlimited PN code p_k, and this product is passed through a bandpass filter (BPF) centred on f_0 with a bandwidth of R_c/L. This is accomplished by calculating the Fourier coefficient at the carrier frequency using the DFT (the subtraction in p_{k-m} is modulo N_P, since the waveform is repeated every N_P samples)

$$Y_m [\exp (j2\pi f_0 t]$$
$$= (2/N_P) \sum_{k=0}^{k=N_P-1} [y_k p_{k-m} \exp (-j2\pi k f_0/f_s)]$$
$$\text{for } m = 0, 1, \ldots, N_P - 1$$

The magnitude of this Fourier coefficient, which in this paper is referred to as the correlation coefficient, is then plotted as a function of sample delay m, measured in sample periods $1/f_s$).

3.2.1 Fault-location algorithm:
This correlation graph consists of a series of peaks, each peak resulting from line reflections; the magnitude of any peak gives the magnitude of the corresponding reflection arriving at the measuring point, and the phase delay of the peak tells us the location of the impedance discontinuity causing the reflection. This may be illustrated by looking at the lattice diagram of Fig. 3, which shows the reflection pattern formed on a 100 km double transposed line with a fault at 90 km from the transmitter. Reflections are caused by the transpositions, line ends and faults. The correlation coefficient for the signal at the sending end of an unfaulted line, for example, will consist of peaks that correspond to the signals S0, S1, S2, and so on; the fault will add correlation peaks for the other reflections shown.

In general, a correlation peak will not line up with a sample delay point, and so some form of interpolation is necessary. In the simulation results discussed below the
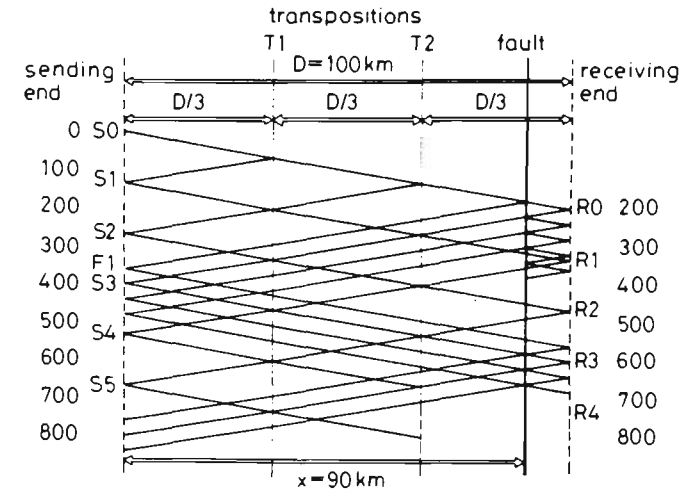

Fig. 3 *Lattice diagram for 100 km double transposed line with fault at x = 90 km. The numbers at each line end are the sample numbers, assuming that the signals travel with the speed of light and the sample frequency is 0.6 MHz*

true correlation peak is estimated by fitting a quadratic expression to the point with the local correlation maximum and the two adjacent points. The time delay of the quadratic maximum is then taken as the signal phase delay. All fault positions are calculated by comparing the phase delay of the fault reflection with the phase delay of a reference signal that has traversed a known distance. For waveforms at the sending end, for example, the reference may be taken as the primary reflection from the line end (S3 in Fig. 3).

4 PLC line interface

The spread spectrum signal covers a wide frequency range, so it is important to model the frequency dependency of the power line carrier interface between the communications room and the EHV lines. For compatibility with existing PLC equipment we are interested in the frequency range 80–200 kHz.

4.1 PLC sending and receiving end network equations

The PLC sending end and receiving end networks are each coupled to the same conductors, and are illustrated in Figs. 4 and 5. The transmitted signal is fed through a resistive hybrid to the line matching unit from which it is coupled to two phases of the transmission line through the CVT capacitors. Voltages measured at the transmitting end are recorded across a 75 Ω resistor connected to the hybrid. At the receiving end there are the same CVT capacitors coupling into a line matching unit, which feeds the line signal to the receiver, which is modelled as a 75 Ω resistor. Both ends of the coupled lines are terminated to ground through line traps, and both ends of the uncoupled line are terminated to ground directly. These terminations are typical for de-energised lines.

The PLC networks at the transmitting and receiving ends are represented by the admittance matrices Y_S and Y_R, respectively. Each matrix is composed of components due to the line matching units and CVT capacitors. The admittance value on the uncoupled short circuit line is represented by a 'large' number. At the sending end the

IEE Proc.-Gener. Transm. Distrib., Vol. 142, No. 1, January 1995

75

electr... of the transmitter may be represented by an admittance vector a_S, to give the boundary condition equations at each end

$$I_S = -Y_S V_S + a_S V_{TX}$$

$$I_R = Y_R V_R$$

unit length matrix Y for any given frequency. Denoting by V the modified Fourier transform of the voltage on the line, Wedepohl showed that the wave equation
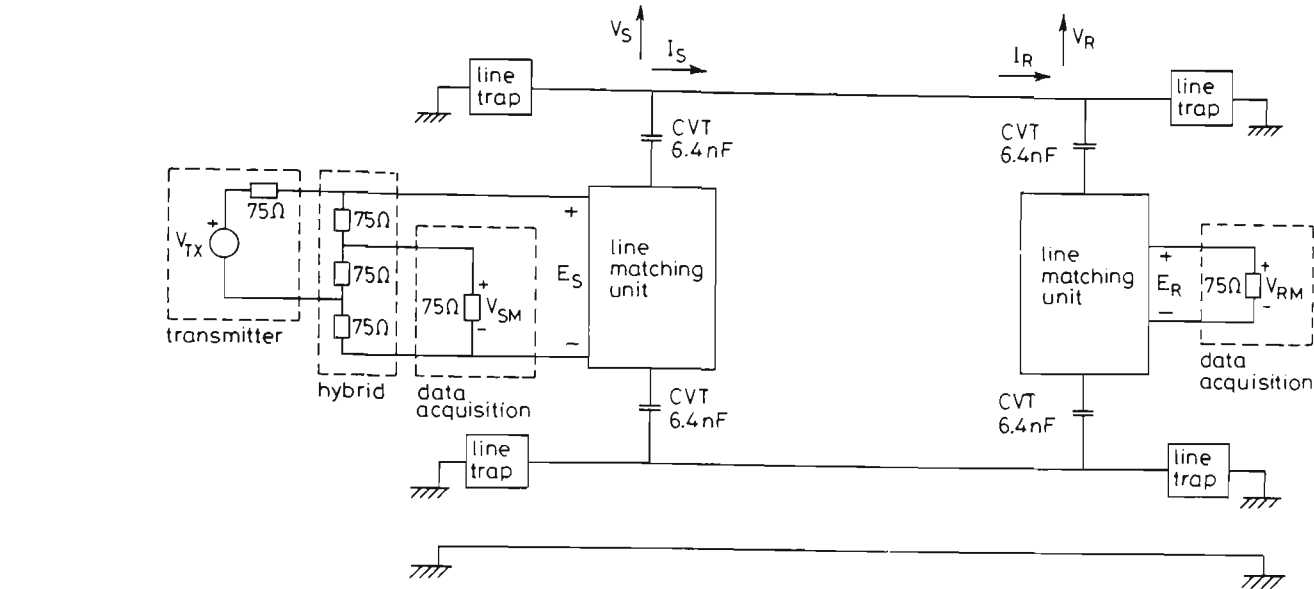
$$\frac{d^2 V}{dx^2} = ZYV$$

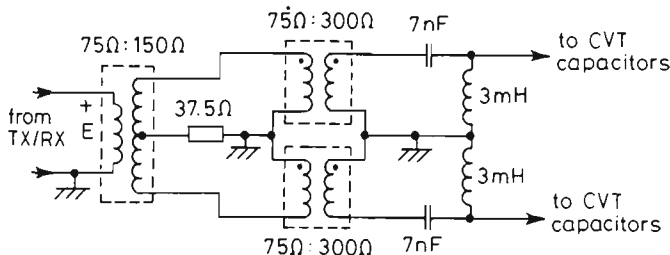**Fig. 4** *PLC transmitting and receiving end network*
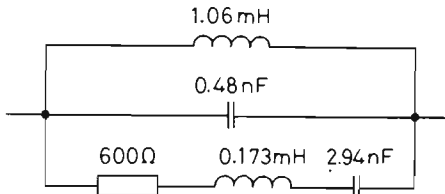

Fig. 5A *Line matching unit*

Fig. 5B *Line trap*

The voltage E_S of Fig. 4 is given by $E_S = E_1 + E_2$, where

$$E_1 = \frac{P(s)}{Q(s)} V_{TX} \qquad E_2 = \frac{M(s)}{N(s)} (V_{L1} - V_{L2})$$

where $P(s)$, $Q(s)$, $M(s)$ and $N(s)$ are polynomial functions of the Laplacian operator s, and V_{L1} and V_{L2} are the phase voltages on the coupled lines at the transmitter CVT capacitors. Similar equations hold for the voltage E_R at the receiver end, so that the voltages measured in the communications rooms at the transmitting and receiving ends are, respectively

$$V_{SM} = 0.5E_S - 0.125V_{TX}$$

$$V_{RM} = E_R$$

5 Polyphase transmission line simulation model

The simulation program uses the polyphase transmission line model based on the distributed parameter modal analysis method developed by Wedepohl and others [24, 25]. This uses the line geometry, conductor and earth wire parameters and earth resistivity to derive the impedance per unit length matrix Z and the admittance per

has the solution

$$V = \exp(-\psi x)V_i + \exp(\psi x)V_r,$$

$$\exp(-\psi x) \equiv S \exp(-\gamma x)S^{-1}$$

Here S is the eigenvector matrix and γ is the eigenvalue matrix of the matrix ZY; S defines the different propagation modes on the polyphase transmission line. The diagonal matrix γ gives the propagation constants for each mode. For any phase voltage vector V, $S^{-1}V$ gives the modal components of V. The current on the line is given by

$$I = Y_0[\exp(-\psi x)V_i - \exp(\psi x)V_r] \qquad Y_0 = Z^{-1}S\gamma S^{-1}$$

Y_0 is the characteristic admittance of the line.

The basic equations that describe travelling wave phenomena on a polyphase transmission line may be implemented [26] by either: evaluating the ABCD transmission parameters for the line; or calculating the forward and backward travelling waves V_i and V_r using the reflection factor method.

Here we consider the steady-state case in which the mains power has been disconnected and any fault remains as a resistance from the line to ground. By adapting the superposition theorem as applied by Johns and Aggarwal [27], the waveforms generated when a signal is transmitted down a faulted line may be expressed as the sum of two related waveforms. As illustrated in Fig. 6 for earth faults, the total waveform (V_{TX} and V_{FS} active, $E_{FF} = -V_{FS}$ on the faulted line) is equal to the waveforms generated on a healthy line (V_{TX} and V_{FS} active, E_{FF} removed) added to the waveform modification generated by the fault (V_{TX} and V_{FS} removed, $E_{FF} = -V_{FS}$ on the faulted line). At the sending end, for example, we have $V_S = V_{SS} + V_{SF}$.

The simulation studies presented in this paper were for a 100 km horizontal three-phase line and were programmed on a Cyber 932 mainframe computer with a machine constant $\varepsilon = 7.1054 \times 10^{-15}$. With the ABCD parameter method, truncation errors limited the accuracy of the above superposition equations to about 1% at fre-

76

IEE Proc.-Gener. Transm. Distrib., Vol. 142, No. 1, January 1995

5.1 Reflection factor method

In evaluating the hyperbolic sinh and cosh functions required for the transmission parameters a positive exponential is added to a negative exponential. For high PLC
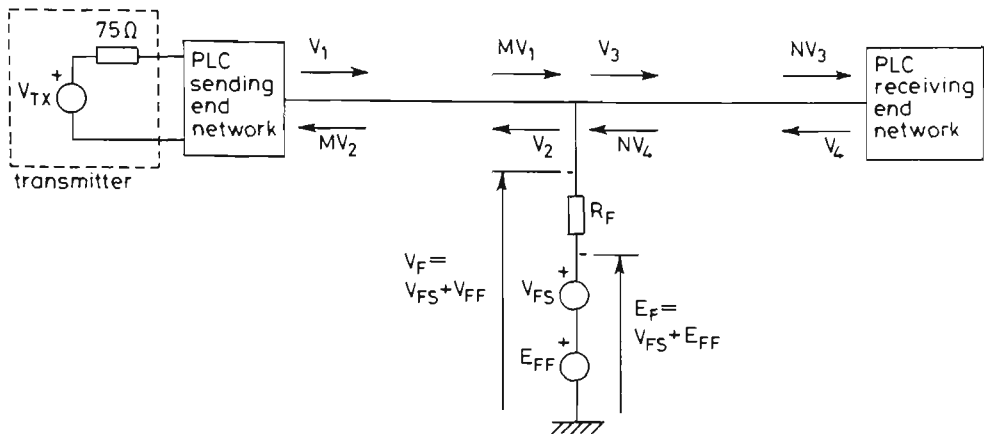

Fig. 6 *Faulted line reflection factor model for homogeneous lines, illustrating superposition*

frequencies and/or long line lengths the exponents become large and excessive truncation errors are incurred. In this case the reflection factor method, illustrated in Fig. 6, must be used [26]. This method reduces truncation errors by taking as unknowns the voltages at opposite ends of a homogeneous line travelling in opposite directions (e.g. voltages V_1 and V_2 in Fig. 6). For the homogeneous line

$$M = \exp(-\psi x) \quad N = \exp[-\psi(D - x)]$$

and the voltage reflecting off the receiving end is $V_4 = K_r NV_3$ where K_r is the reflection factor

$$K_r = (Y_0 + Y_R)^{-1}(Y_0 - Y_R)$$

for receiving end admittance termination Y_R.

It is more complex to take into account the transpositions using the reflection factor method. A boundary condition at one end of a transposed line section can be converted to an equivalent boundary condition at the far end of the line through a process of compression. The reverse process re-expands the line to recover the voltages at line ends.

With $E_{FF} = 0$ the compression technique may be used to transfer the receiving end boundary condition of eqn. 2 to an equivalent boundary condition at the transposition closest to the transmitter. The prefault signals can then be evaluated.

The fault waveforms are calculated with the voltage sources V_{TX} and V_{FS} short-circuited, E_{FF} set equal to $-V_{FS}$ on the faulted line and the end networks of Fig. 6 replaced with the equivalent boundary conditions at the ends of the homogeneous line section in which the fault lies.

The total waveform is calculated with the end networks of Fig. 6 replaced with the equivalent boundary conditions at the ends of the faulted homogeneous line section, leaving V_{TX} intact and putting $E_{FF} = -V_{FS}$.

6 Fault-location simulation studies

Direct sequence spread spectrum fault location has been simulated on a computer model of a three-phase horizontal line of length 100 km with two transpositions, as illustrated in Fig. 7; a full list of line data is included in the Appendix. All studies are for a double-ended system and only single phase to ground faults have been simulated.

6.1 Discussion of results

The power line carrier program was used to investigate the correlation function and calculated fault positions for faults with distinct resistances on different lines at various positions from the line ends. The accuracy of the fault-location algorithm was compared for waveforms recorded at each end of the line.

Unless otherwise stated, the simulation graphs are for a single phase to ground fault with $R_F = 1\,\Omega$ on line 2 at a distance $x = 90$ km from the transmitter. The lattice diagram showing the main reflections for this fault position is seen in Fig. 3. The parameters for the direct sequence waveform used are $f_0 = 140$ kHz, $R_c = 60$ kHz and $L = 1023$, with a sampling frequency $f_s = 0.6$ MHz.

6.1.1 Modal propagation characteristics: It is well known [28] that the modal propagation vectors on a horizontal three-phase line are virtually independent of frequency and are equal to Clarke's diagonal components

$$S \approx \begin{bmatrix} 1 & -1 & -\frac{1}{2} \\ 1 & 1 & -\frac{1}{2} \\ 1 & 0 & 1 \end{bmatrix}$$

The attenuation and speed of propagation of each mode at 140 kHz was calculated by the program as

$$\alpha_1 = 1.34\,\text{dB/km} \qquad \alpha_2 = 0.206\,\text{dB/km}$$

$$v_1 = 2.73221 \times 10^8\,\text{m/s} \quad v_2 = 2.92275 \times 10^8\,\text{m/s}$$

$$\alpha_3 = 0.0334\,\text{dB/km}$$

$$v_3 = 2.98593 \times 10^8\,\text{m/s}$$

As the different modes progate along the line they slide past each other, producing interference effects characteristic of a standing wave pattern on a multiline system.

6.1.2 Waveforms recorded on unfaulted lines: In Fig. 8A the correlation coefficient for the unfaulted line waveform V_{SSM} is plotted. The large peak S0 corresponds to the transmitter feeding through the hybrid into the waveform recorder; immediately after this peak are 60 kHz side lobe ripples due to the bandwidth restriction of the MLS code. The reflections from the transpositions and the ends are labelled as in Fig. 3. The floor level of the graph ($\approx 6.7 \times 10^{-5}$) is set by the residual correlation of the MLS code. For a code length of 1023 the floor level is $\approx 1/1023$ of the correlation maximum, which in this case is S0. The trough S4 is due to cancellation between the reflected waveforms and the residual correlation of the transmitted signal.

We can use the correlation peaks S1, S2 and S3, corresponding to primary reflections off impedance discontinuities of known locations (two transpositions and

IEE Proc.-Gener. Transm. Distrib., Vol. 142, No. 1, January 1995

77

the ~~~~~~~~~~~~~~~~~~~~~~~~~~axis in terms of distance. In Table 1 the signal speeds calculated from local correlation maxima are recorded. It may be seen
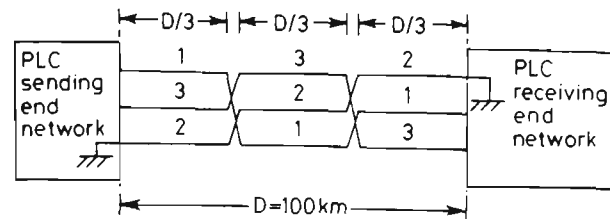

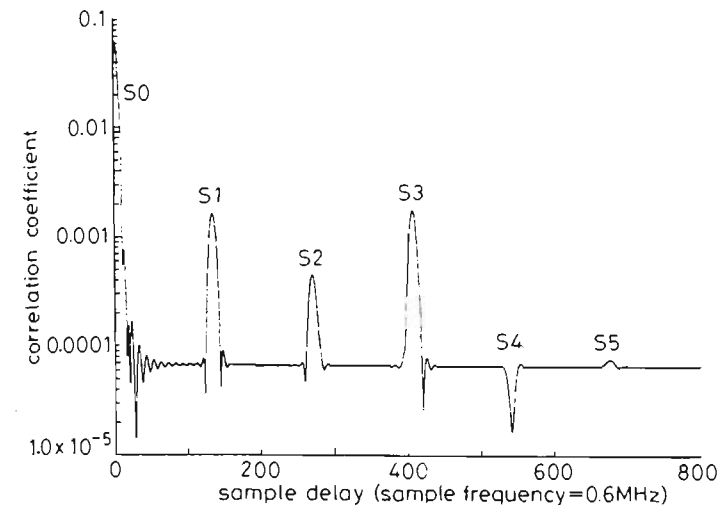**Fig. 7**   *Line transposition scheme, showing line numbering*

Fig. 8A   *Correlation coefficient for V_{SSM} at sending end for unfaulted line. Direct sequence parameters: $f_0 = 140\ kHz$, $R_c = 60\ kHz$, $L = 1023$*
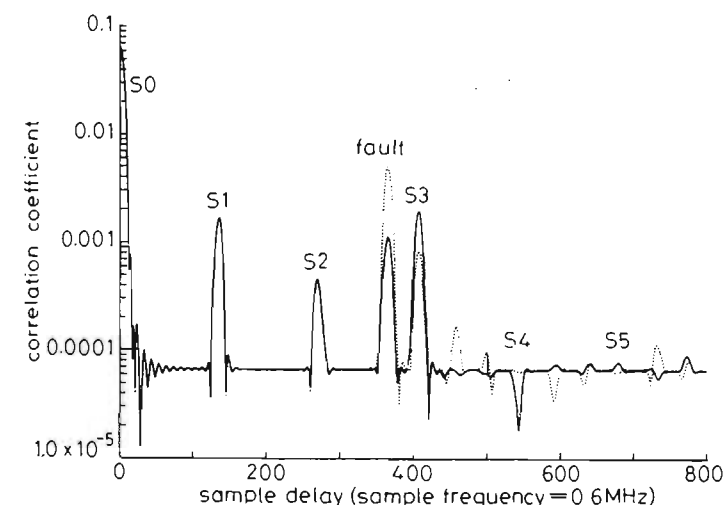

Fig. 8B   *Correlation coefficient for V_{SM} at sending end for fault at $x = 90\ km$ with $R_F = 1\ \Omega$ on line 2 and line 1*

——— FL = 2
········ FL = 1

Table 1:   Average signal speeds ($\times 10^8$ m/s) as calculated from unfaulted line reflections

S1	S2	S3
2.97288	2.97271	2.95636

that the average signal speeds of the different reflections vary by something like 1%; this limits the accuracy with which faults may be located. These speeds lie between the speeds of propagation of mode 2 and mode 3; this shows that signal propagation is principally due to the lowest attenuation modes.

6.1.3 Waveforms recorded on faulted lines: The correlation coefficients for the two waveforms V_{SM} measured when the fault is on line 2 and line 1, respectively ($FL = 2, 1$), are illustrated in Fig. 8B. In both cases the primary reflection from the fault is clearly visible and the

extra ripples in the graph for sample delays greater than about 420 are due to extra line reflections caused by the fault. When the fault lies on line 1, to which the PLC equipment is coupled, the reflection from the fault is greater than the reflection from the receiving end, whereas the reverse holds when the fault is on line 2 (uncoupled line).

By using S3 as the reference in Fig. 8B, the fault position on line 2 is calculated as $x = 89.75$ km (see Table 2).

Table 2: Fault positions calculated using the faulted line reflections S3 as reference at the sending end

True fault position	Faulted line	Fault resistance	Calculated fault position
km		Ω	km
90	2	1	89.75
90	1	1	89.77

To investigate the effects of the PLC interface circuitry on the fault-location accuracy a simulation run was performed with purely resistive line traps and line-matching units (CVTs removed); the corresponding fault position estimate was 90.02 km. We conclude that the PLC interface circuitry has a degrading effect on the accuracy of the measurements.

6.1.4 Voltage distribution along line: As mentioned above, the magnitude of the voltage recorded at the line ends depends on which line is faulted. To investigate this relationship, the true r.m.s. voltage distribution along the line when a 140 kHz sinewave is transmitted is plotted in Figs. 9a and b shows the true r.m.s. voltage distribution along the line when the direct sequence spread spectrum signal is transmitted.

Looking first at the narrow-band signal, the characteristic transmission line standing wave pattern with peaks separated by $\lambda/2 \approx c/(2 \times f_0) = 3.0 \times 10^8/(2.0 \times 140.0 \times 10^3) = 1.07$ km is evident. This is the interference pattern that results from line reflections owing to impedance mismatches at the transpositions and at the line ends. In the direct sequence plots, the rapid oscillations in the standing wave pattern of each individual spectral component that constitutes the broad-band waveform sum to zero, leaving only the more gradual voltage variation due to modal propagation and cancellation, which is also evident in Fig. 9a.

From the modal characteristics listed in Section 6.1.1, it is clear that mode 1 decays rapidly; however, reflections at the transpositions and the ends will regenerate all the modes. The short-lived ripples on each line in Fig. 9b at the receiving end and on the transmitter side of each transposition are caused by interference from reflections. Signal propagation on the centre line is principally due to mode 3 [28] and so has less attenuation than waveforms on the outer lines; however, on the far side of each transposition on the centre line the rapid decay of mode 1 over about 10 km can be seen. Modes 2 and 3 slide past each other as they propagate along the line, their relative phases changing by 180° each 50 km; this will have the effect that the magnitudes of the voltages on the outer lines will be inversely related. This is in fact seen in Fig. 9b for the voltages on lines 1 and 2, lines 1 and 3 and lines 2 and 3 for each of the three successive homogeneous line sections.

By the principle of reciprocity, the strength of the reflection from a fault at any position on any line is proportional to the magnitude of the prefault voltage at that particular point. In particular, from Fig. 9b it can be seen

78

that th███████████████████████fault on line 3 near the second transposition, and that the graph in the preceding section for a fault on the uncoupled line at $x = 90\ km$ is close to its worst case.
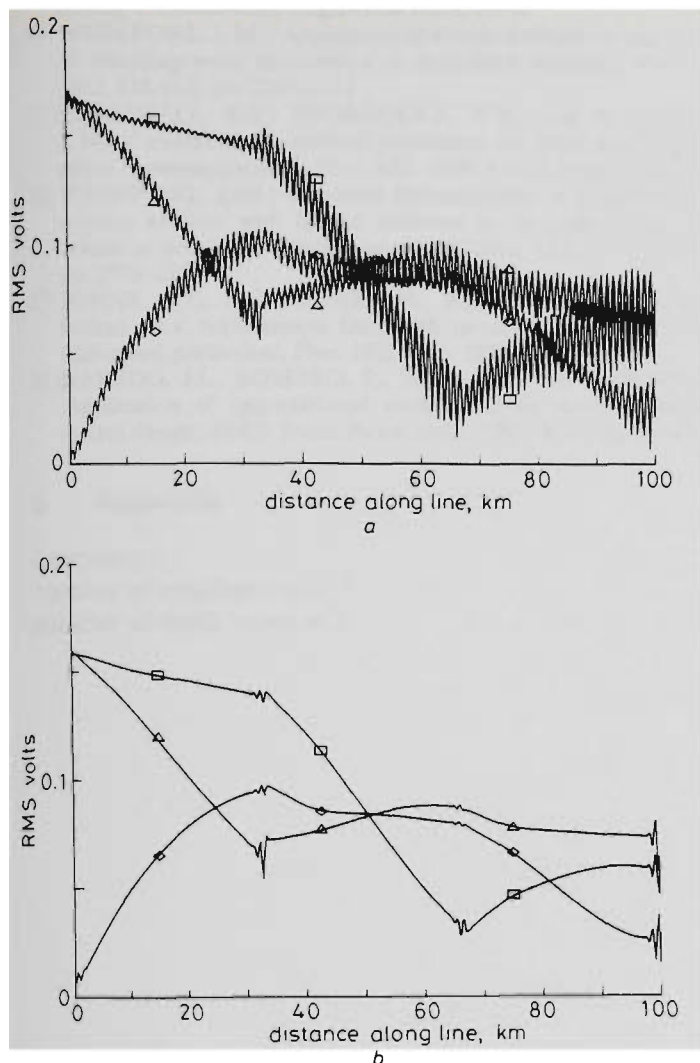

Fig. 9   *Steady-state RMS voltage distribution on all three unfaulted lines*

a When a 140 kHz sinusoid is transmitted
b When a direct sequence signal with $f_0 = 140$ kHz $R_c = 60$ kHz and $L = 1023$ is transmitted
△ line 1
◇ line 2
□ line 3

7   Conclusions

A program to simulate the propagation of power line carrier signals on a polyphase transmission line which takes into account the frequency variation of line and PLC interface parameters must be based on the reflection factor method. For a 100 km double transposed line it was found that use of the ABCD transmission parameters produced unacceptably high truncation errors at frequencies above 170 kHz.

When a narrow-band PLC signal is transmitted down an EHV system, the resultant steady-state voltage distribution is derived from two distorting influences. The first influence is reflections from unmatched terminations and transpositions that produce alternate maxima and minima, separated by $\lambda/4 \approx c/(4 \times f_0)$. The second influence is of interference effects due to the different modes of propagation sliding past each other. Mode 1 has high attenuation, and so its effects are short-lived, whereas modes 2 and 3, the principal propagation modes, produce major voltage fluctuations along the line. Modal interference effects produce more gradual voltage variations along the line than those caused by reflections.

Examinations of the r.m.s. voltage distribution when a direct sequence spread spectrum signal is transmitted show that the effects due to the first influence above virtually sum to zero over the wideband spectrum, but the same modal cancellation effects as described in the second influence are apparent. By the principle of reciprocity, the prefault voltage at any point indicates the strength of the reflection from a fault at the same point. Consequently, areas of weak reflection can be identified.

Simulations of the direct sequence location of permanent single phase to ground faults indicate that a direct sequence signal with $f_0 = 140$ kHz, $R_c = 60$ kHz and $L = 1023$ would be sufficient to locate worst-case faults on the simulated 100 km line with any accuracy of 0.5 km.

8   References

1 STRINGFIELD, T.W., MARIHART, D.J., and STEVENS, R.F.: 'Fault location methods for overhead lines', *AIEE Trans.*, 1957, **76**, pp. 518–529
2 AIEE COMMITTEE: 'Bibliography and summary of fault location methods', *AIEE Trans.*, 1955, **74**, pp. 1423–1428
3 GOODING, H.T.: 'Cable fault location on power systems', *Proc. IEE*, 1966, **113**, (1), pp. 111–119
4 SANT, M., and PAITHANKAR, Y.G.: 'Online digital fault locator for overhead transmission lines', *Proc. IEE*, 1979, **126**, (11), pp. 1181–1185
5 TAKAGI, T., YAMAKOSHI, Y., YAMAURA, M., CONDOW, R., and MATSUSHIMA, T.: 'Development of a new type fault locator using the one-terminal voltage and current data', *IEEE Trans., Power Appar. Syst.*, 1982, **101**, (8), pp. 2892–2898
6 WISZNIEWSKI, A.: 'Accurate fault impedance locating algorithm', *IEE Proc. C*, 1983, **130**, (6), pp. 311–314
7 ERIKSSON, L., SAHA, M., and ROCKEFELLER, G.: 'An accurate fault locator with compensation for apparent reactance in the fault resistance resulting from remote-end infeed', *IEEE Trans. Power Appar. Syst.*, 1985, **104**, (2), pp. 424–436
8 WESTLIN, S.E., and BUBENKO, J.A.: 'An accurate method for fault location on electric power transmission lines'. *IFAC Symposium*, Melbourne, Australia, 1977
9 TAKAGI, T., YAMAKOSHI, Y., BABA, J., UEMURA, K., and SAKAGUCHI, T.: 'A new algorithm of an accurate fault location for EHV/UHV transmission lines: Part 1 — Fourier transformation method'. *IEEE Trans. Power Appar. Syst.*, 1981, **100**, (3), pp. 1316–1323
10 LAWRENCE, D.J., and WASER, D.L.: 'Transmission line fault location using digital fault recorders', *IEEE Trans. Power Deliv.*, 1988, **3**, (2), pp. 496–502
11 RICHARDS, G.G., and TAN, O.T.: 'An accurate fault location estimator for transmission lines', *IEEE Trans. Power Appar. Syst.*, 1982, **101**, (4), pp. 945–949
12 TAKAGI, T., YAMAKOSHI, Y., BABA, J., UEMURA, K., and SAKAGUCHI, T.: 'A new algorithm of an accurate fault location for EHV/UHV transmission lines: Part II — Laplace transformation method'. *IEEE Trans. Power Appar. Syst.*, 1982, **101**, (3), pp. 564–573
13 IBE, A.O., and CORY, B.J.: 'A travelling wave-based fault locator for two and three terminal networks', *IEEE Trans. Power Syst.*, 1986, **1**, (2), pp. 283–288
14 ROBERTS, F.F.: 'New methods for locating cable faults, particularly on high frequency cables', *J. IEEE*, 1946, **93**, (26), pp. 385–404
15 SPALDING, L.R., and DIEMOND, C.C.: 'A transient fault locator for high-voltage transmission lines', *AIEE Trans.*, 1949, **68**, pp. 1005–1012
16 STEVENS, D., OTT, G., POMEROY, W., and TUDOR, J.: 'Frequency-modulated fault locator for power lines', *IEEE Trans., Power Appar. Syst.*, 1972, **95**, (5), pp. 1760–1768
17 VITINS, M.: 'A correlation method for transmission line protection', *IEEE Trans. Power Appar. Syst.*, 1978, **97**, (5), pp. 1607–1615
18 CHRISTOPOULOS, C., THOMAS, D.W.P., and WRIGHT, A.: 'Signal processing and discriminating techniques incorporated in a protective scheme based on travelling waves', *IEE Proc. C*, 1989, **136**, (5), pp. 279–288
19 DIXON, R.C.: 'Spread spectrum systems' (John Wiley and Sons, 1984), 2nd edn.
20 FAULKNER, M.: 'A new modulation for power line protection signalling', *IREECON International*, Sydney, Australia, 1987
21 GOLOMB, S.W. (Ed.): 'Digital communications with space applications' (Prentice-Hall, Englewood Cliffs, 1964)

IEE Proc.-Gener. Transm. Distrib., Vol. 142, No. 1, January 1995

79

, and KALAM, A.: 'Fault location on EHV lines using wideband spread spectrum techniques'. International Conference on *Power System Protection*, Singapore, 1989, pp. 142–161

23 OPPENHEIM, A.V., and SCHAFER, R.W.: 'Digital signal processing' (Prentice-Hall, Englewood Cliffs, 1975)

24 WEDEPOHL, L.M.: 'Application of matrix methods to the solution of travelling-wave phenomena in polyphase systems', *Proc. IEE*, 1963, **110**, (12), pp. 2200–2212

25 GALLOWAY, R.H., SHORROCKS, W.B., and WEDEPOHL, L.M.: 'Calculation of electrical parameters for short and long polyphase transmission lines', *Proc. IEE*, 1964, **111**, (12), pp. 2051–2058

26 WEDEPOHL, L.M.: 'Electrical characteristics of polyphase transmission systems with special reference to boundary-value calculations at powerline carrier frequencies', *Proc. IEE*, 1965, **112**, (11), pp. 2103–2112

27 JOHNS, A.T., and AGGARWAL, R.K.: 'Digital simulation of faulted e.h.v. transmission lines with particular reference to very-high-speed protection', *Proc. IEE*, 1976, **123**, (4), pp. 353–359

28 NAREDO, J.L., ROMERO, R., SILVA, J.L., and MORENO, P.: 'Application of approximated modal analysis methods for PLC system design', *IEEE Trans. Power Deliv.*, 1987, **2**, (1), pp. 57–63

9 Appendix

Line data

number of conductors = 3
number of earth wires = 2

line coordinates
$$= (-8.7; 8.2), (8.7, 8.2), (0.0, 8.2), (6.85, 16), (-6.85, 16), \text{ m}$$

conductor GMR = 0.0905 m
earth wire GMR = 0.018 m
relative magnetic permeability of conductor = 1
relative magnetic permeability of earth wire = 1
conductor resistivity = 3.21×10^{-8} Ωm
earth wire resistivity = 3.21×10^{-8} Ωm
radius of the outer layer conductor strands = 0.00125 m
radius of the outer layer earth wire strands = 0.00175 m
number of strands in the outer layer of conductors = 30
number of strands in the outer layer of earth wires = 6
number of conductors per bundle = 2
earth resistivity = 100.0 Ωm
line length = 100.0 km
number of transpositions = 2

$$\text{transposition matrix } T = \begin{bmatrix} 0 & 0 & 1 \\ 1 & 0 & 0 \\ 0 & 1 & 0 \end{bmatrix}$$

homogeneous line section lengths = 33.3333, 33.3333, 33.3333 km

80

IEE Proc.-Gener. Transm. Distrib., Vol. 142, No. 1, January 1995

Line monitoring and fault location using spread spectrum on power line carrier

V. Taylor
M. Faulkner

Abstract: Signals transmitted over the power line carrier system are used to locate faults and other impedance mismatches on EHV power lines. The compatibility and sensitivity performance requirements for doing this are summarised. Conventional remote sensing waveshapes are reviewed and direct-sequence spread-spectrum modulation is proposed for this application. Optimal signal processing techniques are outlined and frequency domain correlation techniques are detailed. Prototype hardware has been constructed and on-line results are presented for a 225 km 330 kV line. Line reflections were identified within an accuracy of 1.6 km even though the channel bandwidth was limited to 50 kHz by external constraints. It is shown that accuracy is dependent on channel bandwidth, signal-to-noise ratio and waveform energy. It is suggested that a further increase in accuracy is possible by referencing the received signal to known impedance discontinuities such as the transpositions. Fault location accuracy down to one span should be possible using this technique, which will work on both energised and de-energised lines.

List of symbols

δR = error in range estimate
c = speed of light
T = pulse width of rectangular pulse
B = RF bandwidth of line probing signal
E = energy contained in received signal
N_0 = noise power per Hz
T_p = period of spread spectrum signal
R_c = chip (bit) rate
v = speed of propagation of signal down line
D = line length
L = code length
$s(t)$ = transmitted signal

$u(t)$ = bandlimited code
f_0 = carrier frequency
$r(t)$ = received signal
τ = time delay between received signal and transmitted signal
$R(f)$ = the Fourier transform of $r(t)$
$N_i(f)$ = noise frequency spectra
$y_m(\tau)$ = matched filter output
$y(\tau)$ = correlator output with quadrature components
$|y(\tau)|$ = correlation coefficient
t_i, τ_i = discrete time samples
f_k = discrete frequencies
$\mathbf{F}$ = discrete fourier transform (DFT)
$\mathbf{F}^{-1}$ = inverse DFT
N_A = number of times waveform is averaged in receiver
T_{circ}, k_{ct}, k_m = microprocessor computation times

1 Introduction

This paper describes a remote sensing scheme that uses the power line carrier (PLC) communications network to transmit a waveform down an EHV line and to receive echoes reflecting off power-grid impedance discontinuities. It is capable of locating impedance changes on EHV power lines with high accuracy and good sensitivity. The scheme uses a direct-sequence spread-spectrum waveform, which has the potential for operation without affecting existing PLC transmissions.

Spread-spectrum modulation, traditionally used in military applications, is a method of sending information down a channel over a wide bandwidth with low-power spectral density. These broadband signals cannot be detected by users of the same spectrum and so are ideal for noninvasive probing of power grids.

A previous paper [1] simulated the use of existing power line carrier equipment to transmit a spread-spectrum waveform down a faulted EHV line. Analysis of the reflections from impedance discontinuities showed that the signals accurately revealed the location of the line fault despite the presence of modal distortions inherent in multiconductor propagation. This paper describes prototype hardware designed for online measurements and presents data obtained on a 330 kV line of length 225 km.

1.1 Compatibility and performance goals
A remote sensing system using the PLC network should ideally fulfil the following conditions:

IEE Proc.-Gener. Transm. Distrib., Vol. 143, No. 5, September 1996

427

(i) ... must not displace existing communication channels occupying the limited spectrum available. The transmitted signal must not cause any appreciable interference to these channels

(ii) It must not be affected by the strong in-band interference provided by concurrently operating PLC channels

(iii) It must operate in the high noise environment of power lines and not be affected by modal distortion

(iv) It should have high sensitivity to variations in line parameters to allow identification of the various anomalies causing reflections

(v) It should have fast response to (possibly transient) deviations in line conditions

(vi) It should be capable of operating on both electrified and dormant lines, hence the clearance of faults may be verified without reclosing the circuit breakers

(vii) It must resolve closely spaced reflections, preferably to within one span

(viii) It should be capable of operating over the entire length of the line with high accuracy and discrimination of multipath reflections

2 Time domain reflectometry waveform design

This Section reviews some of the major ranging schemes that could be suitable for application on a PLC network. The following short summary follows [2–4].

2.1 Repetitive pulse waveforms
The conventional rectangular pulse radar with pulse width T and bandwidth B has a theoretical accuracy of

$$\delta R = \frac{c}{2} \sqrt{\frac{T}{4BE/N_0}}$$

High peak powers are required for greater maximum range coverage, and short pulse widths and wide bandwidths enhance both resolution and minimum range performance. High peak powers cause interference and require more expensive transmitter amplifiers to handle the peak signal. Existing PLC transmitter amplifiers might not be able to handle the peak power requirements.

2.2 Pulse compression waveshapes
Pulse compression waveforms separate the dependence of range performance on broadcast power by spreading the transmitted energy over a longer time interval, reducing the peak power rating and cost of the transmitting equipment. In addition, the interference to normal PLC operations is reduced and often can be below the natural noise level on the line. Data processing of received echoes contracts the pulse into a shorter duration by means of matched filtering or correlation techniques (the pulse compression ratio is the ratio of the uncompressed to compressed pulse lengths). These spread-spectrum signals share the characteristic that the product of waveform bandwidth (B) and waveform period (T_p) must be much greater than unity ($BT_p \gg 1$). The two most common techniques of waveform generation are described as follows.

2.2.1 Frequency modulation: The most widely used types of frequency modulated waveform are chirp,

where the carrier frequency is swept linearly with time, and frequency hopping, where the frequency jumps in a pseudorandom manner. Cable fault location using a chirp waveform has a theoretical accuracy of

$$\delta R = \frac{c}{2} \frac{\sqrt{3}}{\pi B (2E/N_0)^{1/2}}$$

The main problem with this waveform in a power grid network is that it is subject to interference from other chirp generators. Frequency hopping waveforms have theoretically the same ranging capability as phase modulated waveforms. Historically, direct-sequence waveforms have been more widely used for ranging because of the greater technical difficulty in constructing high hopping-rate synthesisers.

2.2.2 Phase modulation (direct sequence): A direct sequence waveform is generated by dividing a long carrier burst into a number of subpulses of equal duration but different phases varying in a periodic manner set by a finite periodic code [5]. Unlike chirp modulation, different direct-sequence waveforms can coexist in the same spectrum since each waveform is identified by its unique repeating code. The online results presented in this paper are for this modulation. The following Section describes their operation.
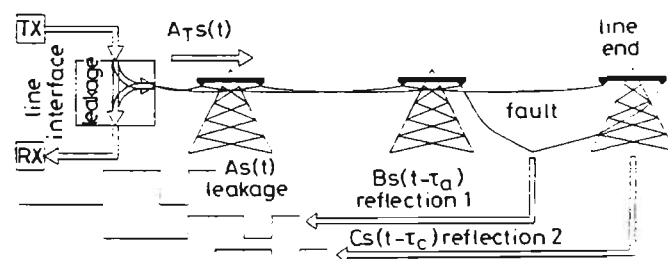

Fig. 1 *Codes entering receiver have different time delays and magnitudes*

2.3 Ranging with direct-sequence spread spectrum
The inverse of the time duration of each subpulse is called the chip rate (R_c). The simplest modulation is biphase shift keying (BPSK) where the phase jumps between 0 and 180° [1]. Signal analysis of the received waveform reveals the time delays and magnitudes of the various reflected codes. Each code shift corresponds to a different distance to the impedance discontinuity causing the reflection. The amplitude of the reflected code is related also to the magnitude of the impedance change. As illustrated in Fig. 1 the received waveform $r(t)$ consists of leakage from the transmitter through to the receiver together with the sum of all the different return echoes. Neglecting the signal distortion caused by the line interface and line transfer function, the online transmit signal is $A_T s(t)$ and the leakage term is $As(t)$, where A_T and A are scaling factors. Also disregarding the modal distortion of multiconductor propagation one may assume the received echoes to be time delayed scaled copies of the transmit waveform $s(t)$

$$r(t) = As(t) + Bs(t - \tau_B) + Cs(t - \tau_C) + \cdots$$

where B, C, ... are the strengths of the returned signals and τ_B, τ_C ... are their respective time delays.

Maximal length sequence (MLS) codes, also known as PN (pseudo noise) codes, are considered in this paper. These are repeating sequences of length $L = 2^n - 1$ where n is the length of the shift register used in their generation (see [5] for more details). When used

428

IEE Proc.-Gener. Transm. Distrib., Vol. 143, No. 5, September 1996

for JR_c should exceed the round-trip time taken for the smallest recordable (multiple) echo to reach the receiver. Normally $T_p \gg 2D/v$ where D is the line length and $v \simeq c$ is the speed of propagation of the wave. This will eliminate range ambiguity problems. The chip rate determines the resolution of the technique and bandwidth occupancy of the signal as illustrated in Table 1.

Table 1: Performance parameters of bandlimited PN-code BPSK waveforms used in ranging

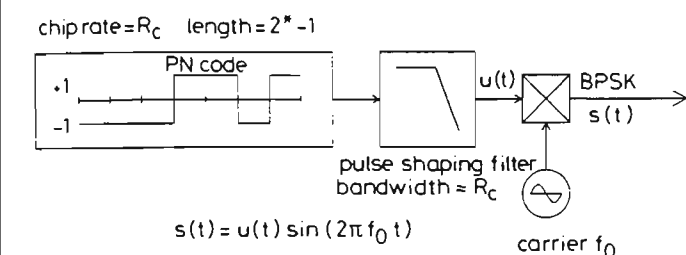|	
time resolution	$\simeq 1/R_c$
distance resolution	$\simeq v/(2R_c)$
bandwidth	$2R_c$
waveform period T_P	$(2n-1)/R_c \gg 2D/v$

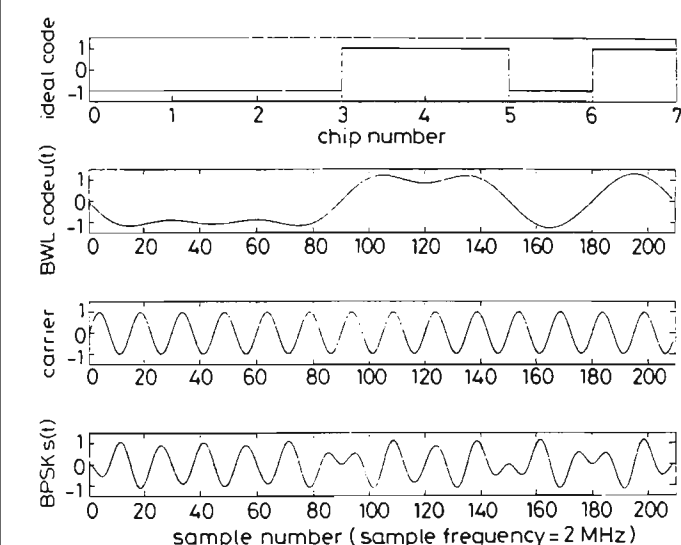**Fig.2** *Generation of spread-spectrum transmitted signal s(t)*

Fig.3 *Typical waveforms used in generating a mainlobe bandwidth limited (BWL) BPSK remote probing signal*

Fig. 2 shows a block diagram of the signal generation process. For clarity the waveforms shown in Fig. 3 are for a carrier frequency $f_o = 133.33\,\text{kHz}$, a chip rate $R_c = 66.67\,\text{kHz}$ and a sampling frequency $f_s = 2\,\text{MHz}$, giving 30 samples per chip. PN codes have a $[\sin(x)/x]^2$ power spectral density envelope with spectral nulls at multiples of the chip rate R_c. A pulse shaping filter of bandwidth R_c limits the code spectrum to the mainlobe. The transmit waveform is $s(t) = u(t)\sin(2\pi f_o t)$, where $u(t)$ is the bandlimited code (lowpass filtered). In this paper, a PN code length of 1023 was used at a chip rate of 25kHz. The code was BPSK modulated on to a carrier frequency of 175kHz giving a transmitted signal $s(t)$ that occupied a bandwidth of 50kHz located in the spectrum between 150 and 200kHz.

2.4 Optimal signal processing

Radar performance parameters relevant to the analysis of data include the following two cases (from [2]).

2.4.1 Maximisation of probability of identification of authentic echoes:
The (peak instantaneous) signal power to (mean) noise power ratio for an echo returning after a time delay of τ seconds may be maximised by processing the received waveform through a matched filter which has a frequency response given by

$$H(f) = \frac{1}{N_i(f)} \frac{R^*(f)}{N_i^*(f)} \exp(-j2\pi f\tau)$$

where

$r(t)$ = received signal

$$R(f) = \int_{-\infty}^{+\infty} r(t)\exp(-j2\pi ft)dt \quad \text{is the Fourier}$$

transform of $r(t)$

$N_i(f)$ = noise frequency spectra (assumed stationary)

* denotes complex conjugate

τ = delay between transmitted signal and received signal

Clearly, to determine many different values of the unknown parameter τ, a bank of filters would be required. Assuming the noise is white and the received signal is an attenuated duplicate of the transmitted signal delayed by a time τ, the output of the matched filter $y_m(\tau)$ can be shown to be equivalent to the cross-correlation between the received signal and a copy of the transmitted signal delayed by time τ:

$$y_m(\tau) = \int_{-\infty}^{+\infty} r(t)s(t - \tau)dt$$

where $s(t)$ = transmitted signal. The transmit waveform $s(t) = u(t)\sin(2\pi f_o t)$ is periodic with period T_p and so the integration need only be performed over one period. To avoid oscillations in $y_m(\tau)$ at the carrier frequency one must take into account in-phase and quadrature components

$$y(\tau) = \frac{2}{T_p} \int_0^{T_p} r(t)u(t - \tau)\exp[-j2\pi f_0(t - \tau)]dt \quad (1)$$

$u(t)$ is the bandlimited baseband code which is transmitted and the factor $\exp[-j2\pi f_0(t-\tau)]$ imposes the in-phase and quadrature carrier components. The magnitude $|y(\tau)|$ of the above equation is the desired output function. The factor $2/T_p$ is a scaling factor that ensures that each peak in the correlation coefficient $|y(\tau)|$ (also called the compressed waveform) is approxi-
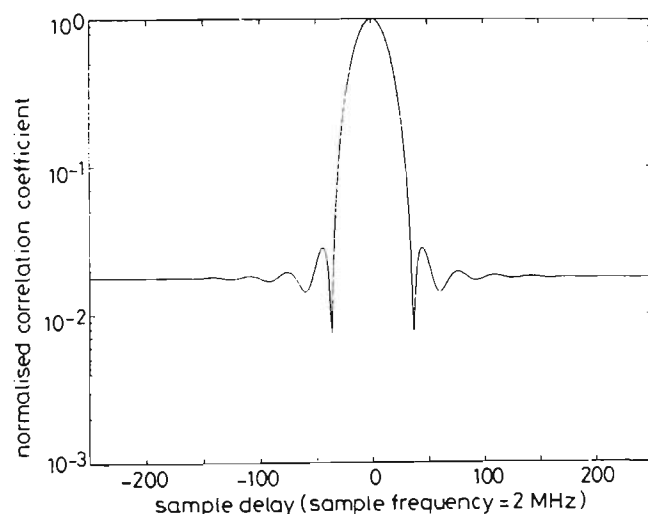

Fig.4 *Normalised correlation coefficient for loopback direct sequence waveform*

MLS code of length 63 with chip rate $R_c = 60\text{kHz}$ and bandlimited to main lobe modulating carrier with frequency $f_o = 140\text{kHz}$; sample frequency $f_s = 2\text{MHz}$

IEE Proc.-Gener. Transm. Distrib., Vol. 143. No. 5. September 1996

429

corresponding echo in $r(t)$ causing the peak. This processing is hardware intensive for real-time operation but is easily done in software if the processing time is available.

2.4.2 Minimisation of probability of erroneous identification of echoes:
Due to bandwidth limiting by the pulse-shaping filter the compressed waveform has time sidelobes on each side of the main correlation peak. This is illustrated in Fig. 4 which is the correlation coefficient from eqn. 1 evaluated for the transmitter and receiver in loopback. An MLS code of length 63 with chip rate $R_c = 60\text{kHz}$ was bandlimited to the main lobe using a rectangular window and modulated onto a carrier with frequency $f_0 = 140\text{kHz}$. The sample rate for the digitised waveforms is $f_s = 2\text{MHz}$. The central correlation peak has width $2/R_c$ and has been normalised to unit magnitude.

The residual correlation is 35.1dB (20dB/decade) down from the main correlation peak: this compares with the ideal code self-rejection ratio (residual correlation) of $20\log_{10}(63) = 36.0\text{dB}$. The pulse-shaping filter of Fig. 2 removes the spectral sidelobes of the ideal code which produces a 0.9dB loss in residual correlation from the ideal. The highest sidelobe is 31.1dB down from the main peak. These sidelobes may either be mistaken for true echoes or mask an actual reflection. Two different approaches to sidelobe reduction may be used:

(i) Frequency weighting of the bandlimited code $u(t)$ used in the transmitter and as reference waveform in the receiver processing

(ii) Sidelobe suppression filtering of the matched filter output [6]

In traditional radar system design, frequency weighting is done only on the reference waveform $u(t)$ used in the correlator: this compromises the integrity of the matched filter processing [7]. Sidelobe reduction comes at the expense of both reduced resolution and reduced signal-to-noise ratio. In the present application this was not done as the prime objective was to obtain the signature of a healthy transmission line with maximum accuracy. Any deviation from this portrait, including the sidelobes, is of interest and indicates a change in line condition.
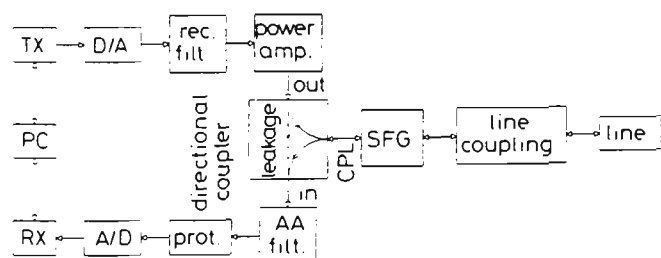

Fig.5 *Block diagram of data acquisition hardware*

3 Hardware description

The hardware to test the viability of the proposal was designed as a research tool and so for maximum flexibility digital signal processing (DSP) techniques were selected. The resulting signal transmission and acquisition equipment, illustrated in Fig. 5, has the capability of sending any arbitrary repeating waveform down an EHV line and recording the signals reflecting back off the line.

Broadcast waveforms were generated in software as per Fig. 2 and downloaded from a personal computer to the transmitter memory: carrier frequency f_0, pulse shaping, chip rate (R_c) and correlation sidelobes are all software controllable. The repetitive nature of the waveform means that only one code length of signal needs to be stored in memory. The transmitted signal is read out at high speed, converted to analogue form by the D/A converter and passed through the reconstruction filter before power amplification.

The amplified voltages pass through the directional coupler (or hybrid) and into the separation filter group (SFG) which relays the signals on to the line-matching circuitry (LMC) which couples to the line. The SFG is used by the SECV to ensure adequate isolation between their different communication channels and the LMC matches the 75Ω communications room equipment to the 600Ω impedance of the EHV lines. Signals coming back off the line follow the reverse path but travel through the directional coupler into the receiver.

The waveform recorder has real-time averaging capability to combat interference from line noise and PLC channels operating simultaneously in the same spectrum. The averaging exploits the repetitive nature of the transmitted waveform to give the receiver a wide dynamic range. Waveforms entering the receiver first go through an antialiasing filter and protection circuitry before being digitised by a fast A/D converter and stored in high-speed memory. The received waveforms are downloaded for data analysis which is performed offline in a workstation environment.

Voltages registered by the receiver consist not only of signals coming off the line but also feedthrough of the emitted waveform from the transmitter through to the recorder. The directional coupler shown connecting the transmitter, transient recorder and SFG, increases the isolation between transmitter and receiver, preventing any leakage of the high-power signal from overloading the analogue front end and reducing the dynamic range. Even with the isolation of a directional coupler the received signal still contains a large feedthrough leakage component compared to the highly attenuated reflections from the line which must be isolated using subsequent offline correlation processing.

The PLC channels used by the SECV go up to 500kHz in frequency. Waveforms at this frequency have a minimum Nyquist sampling frequency of 1MHz. A sample rate $f_s = 2\text{MHz}$ was selected as a compromise between memory size and ease of analogue filter implementation for the reconstruction and antialiasing filters.

3.1 Data analysis
Data analysis was performed offline on a Sun workstation. To increase processing speed cross-correlation of the data with the transmitted waveform was performed in the frequency domain according to the following equations

$$G(f_k) = \mathbf{F}[u(t_i)\exp(-j2\pi f_0 t_i)], \quad H(f_k) = \mathbf{F}[r(t_i)] \quad (2)$$

$$y(\tau_n) = \frac{2}{N_p}\mathbf{F}^{-1}\{G(f_k)H^*(f_k)\} \quad (3)$$

$$(i, k, n = 0, 1, 2, \ldots, N_p - 1)$$

Here, $f_k = kf_s/N_p$ are the discrete frequency increments and $\tau_n = n/f_s$ and $t_i = i/f_s$ are the discrete time increments. $\mathbf{F}(x(t_i))$ denotes the discrete Fourier transform
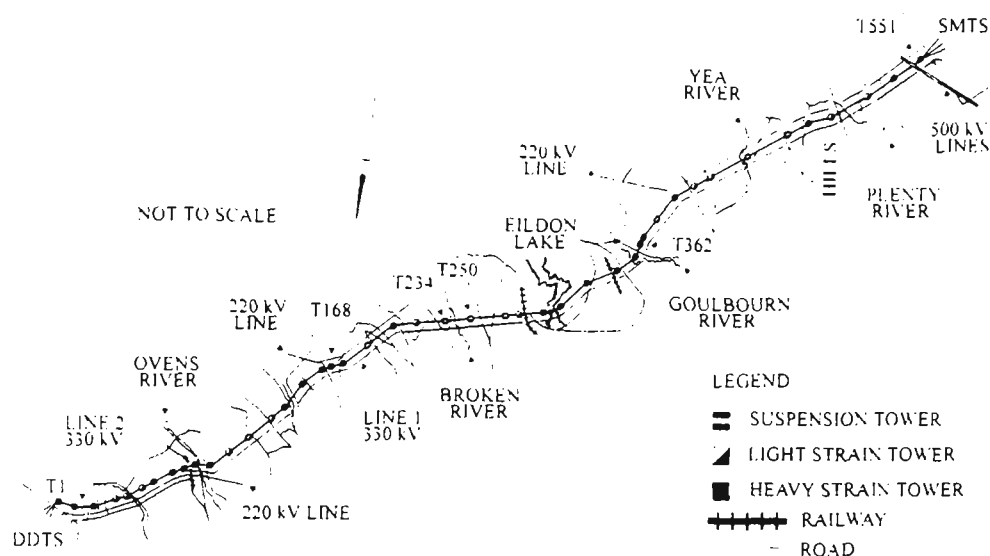
Fig.6 *South Morang Terminal Station to Dederang Terminal Station line overview*
Reproduced by permission of Power Net Victoria

(DFT) of the digitised time waveform $x(t_i)$ of length N_p = Lf_s/R_c points and F^{-1} is the inverse DFT. Also * denotes complex conjugate, and $2/N_p$ is a scaling factor. In the graphs to follow the correlation coefficient functions $|y(\tau_n)|$ are plotted for each sample delay n between the waveforms $s(t)$ and $r(t)$. The normalised correlation coefficient is scaled so that the largest peak has unit magnitude.

4 Hardware results

Fig. 6 is an overview of the EHV circuits running from South Morang terminal station to Dederang terminal station (SMTS to DDTS) in Victoria, Australia. Line 2 (on which some of the towers are illustrated e.g. T250, T234 and so on) runs the full 225km distance in parallel with line 1. The State Electricity Commission of Victoria (SECV) took line 2 of the SMTS–DDTS system out of operation to upgrade a relay. Opportunity was taken of this short maintenance interval to attach the data acquisition equipment to the SFG, with bandwidth 150–200kHz, connected to the de-energised line in the SMTS. No short circuits were placed on the line and the far end of the PLC communications network in the DDTS was open circuit.

Table 2: PLC channels on line 1 operating during the test (carrier frequency is listed first, i.e. single side-band channels transmit information in lower sideband)

Go TX (SMTS-DDTS) (kHz)	RETURN RX (DDTS-SMTS) (kHz)	Function
84–80	88–84	VFT*
100–96	104–100	data (polling with ping-pong)
120–116	116–112	VFT
136–132	132–128	data
176–172**	172–168	VFT
192–188**	188–184	data

* VFT = voice frequency tones
** inband channels

4.1 Line topology and geography

Lines 1 and 2 are both horizontal, single circuit with two earth wires and have a separation of 110 feet; they cross rivers, distribution circuits (not shown in Fig. 6)

and a large body of water in Lake Eildon. The two transpositions on line 2 are also highlighted at tower 362 (T362) and tower 168 (T168), hereafter these are referred to as transposition 1 (T1) and transposition 2 (T2), respectively. In addition, three other EHV lines travel for varying lengths in parallel with lines 1 and 2.

4.2 Existing PLC channnels

During the service period all the PLC communication channels were switched offline 2 (open-circuit terminations) and diverted to line 1. Table 2 lists the single-sideband (SSB) PLC channels in operation on this line. The channels have bandwidths of 4kHz and occur in pairs, one for the 'go' direction and the other for the return direction. Transmit powers were 1 watt. It is seen that the last two channel pairs lie within the 150–200kHz band of the spread-spectrum line-probing signal. Even though these PLC signals were switched to the adjacent line, there was still a considerable amount of interference from these channels because of the high crosstalk coupling between the two lines. All six channel pairs were therefore present as an interference signal to the received spread spectrum waveform. No attempt was made to filter out the four channel pairs outside of the band of the probing signal. These were also coupled into the antialiasing filter and A/D converter from line 1, further reducing the available dynamic range of the receiver.
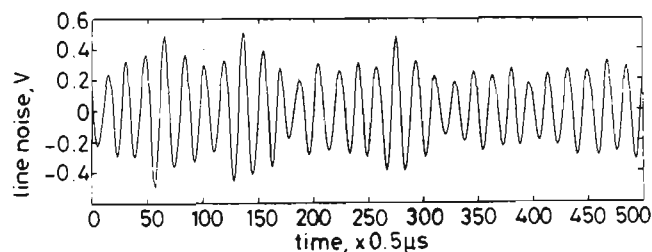

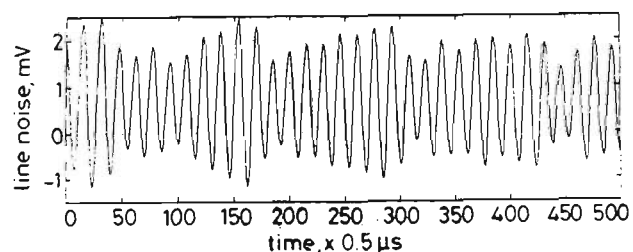**Fig.7** *Line noise (time domain)*
No averaging

Fig.8 *Line noise (time domain)*
4095 averaging

IEE Proc.-Gener. Transm. Distrib.. Vol. 143. No. 5. September 1996

431

4.

SECV line measurements have previously shown that there can be up to 10dB crosstalk between parallel lines sharing the same towers entering a terminal station. This usually prevents frequency reuse [8]. The crosscoupling will be less in this case because the lines do not share the same towers, even so the interference signal produced is still appreciable. Fig. 7 shows the interference and noise on line 2 logged with the transmitter idle, and the upper trace in Fig. 9 is the windowed frequency spectrum clearly showing the six PLC channel pairs operating on line 1 coupling into line 2. The power spectral density was derived from the 5040 data points using Welch's averaged periodogram method [9]. with FFT and Hanning windows of lengths 1024 without overlap. Near-end crosstalk is usually the strongest and comes from the six transmitters located at SMTS. Fig. 8 and the lower plot in Fig. 9 are the equivalent plots with the input waveform averaged $N_A = 4095$ times. Table 3 compares the statistics of the two recorded noise waveforms.
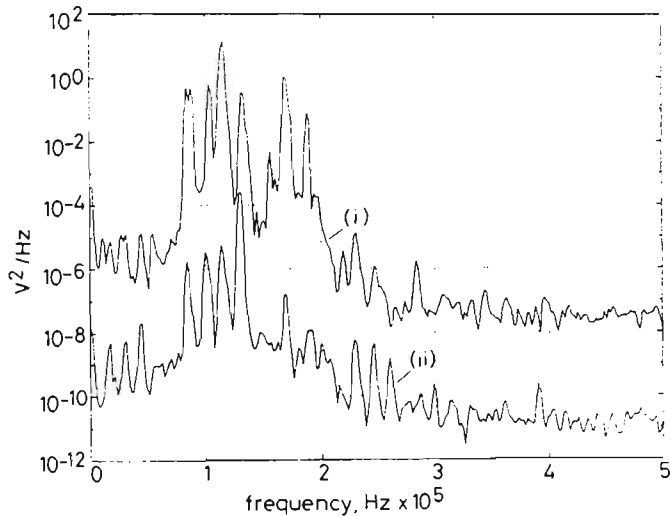
The averaging gain is 255 which is greater than the theoretical $\sqrt{(4095)} = 64$. This is probably due to the non-gaussian nature of the interference. Fig. 10 shows the cross-correlation between the noise and the PN code of length 63 according to eqn. 1 for both the averaged and unaveraged cases. Ripples at the chip rate of 25kHz are evident in the unaveraged case and it is seen that the averaging improves the noise floor by a factor of about 2500. We conclude that signal averaging is a very effective way of reducing noise and interference in this environment.

4.4 Line profiles

The PN code length used was 1023 with two different transmit powers and the average of 4095 received waveforms were recorded by the receiver. Fig. 11 shows the correlation coefficient of Section 3.1 with the maximum transmitter feedthrough peak normalised to unity. The transmit voltage was 2.4V (0.08W) and all the PLC channels of Section 4.2 were operational. Fig. 12 illustrates the correlation coefficient with a higher transmit voltage of 8.7V (1W) and with the major inband PLC channel interference (176–172kHz) disabled. Consequently the signal to noise ratio was improved.

Fig.9 *Windowed spectra of line noise*
(i) no averaging
(ii) 4095 averaging

Fig.11 *Normalised correlation coefficient of received signals with transmitted PN code of length 1023*
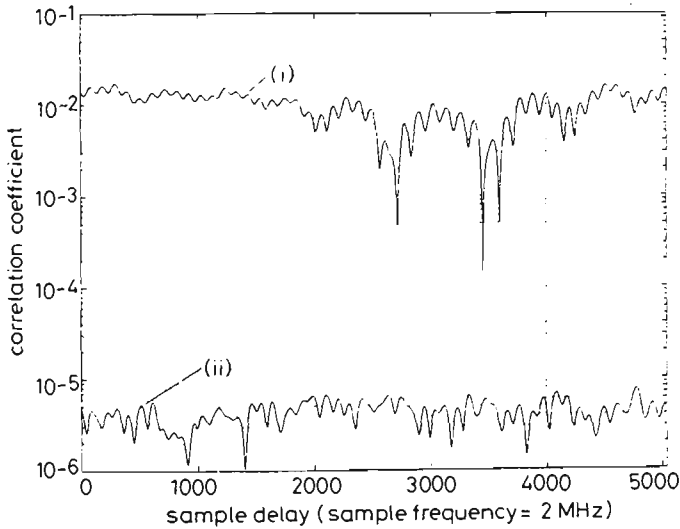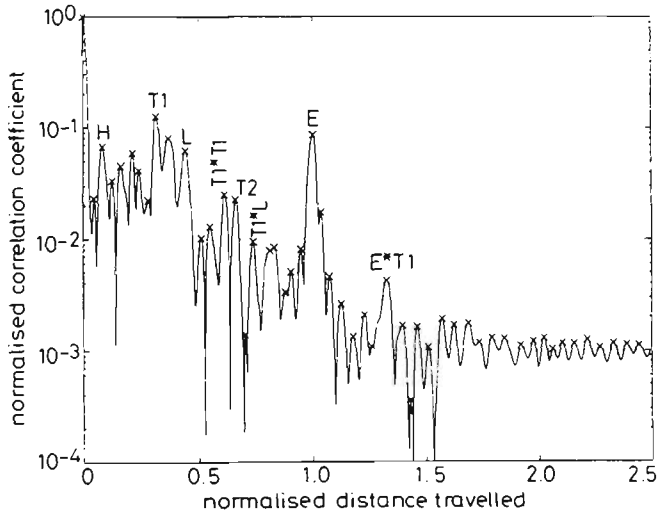Transmitted power = 0.08W, all channels on line 1 operational
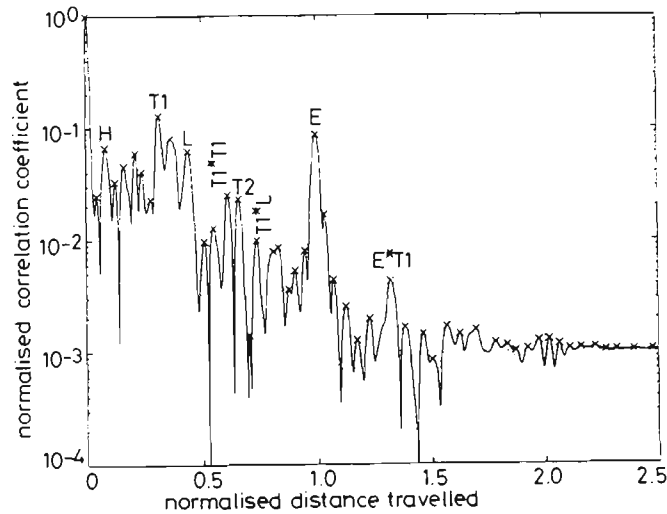
Fig.10 *Correlation coefficient of PN code of length 63 with noise and interference (transmitter idle)*
(i) no averaging
(ii) 4095 averaging

Fig.12 *Normalised correlation coefficient of received signals with transmitted PN code of length 1023*
Transmitted power = 1W, channel 176-172kHz on line 1 disabled

Table 3: Statistics of noise waveform both with and without averaging

	No averaging	Averaged 4095 times
Peak-to-peak voltage	1.25V	4.54mV
RMS voltage	0.241V	0.943mV

Figs. 11 and 12 are virtually identical indicating that the results are not dependent on the signal-to-noise ratio. In both graphs the horizontal axis is scaled to

432

IEE Proc.-Gener. Transm. Distrib., Vol. 143, No. 5, September 1996

give ... . signals making up the correlation peaks. with the length of travel of the primary reflection from the line end normalised to unity. The major correlation peaks are identified in Fig. 13 as reflections from the transpositions T1 and T2, and the line end (E). The time delays to all the peaks were determined by cubic spline interpolation and then converted to distance by interpolation between the known distance of 225.34km to the line end.
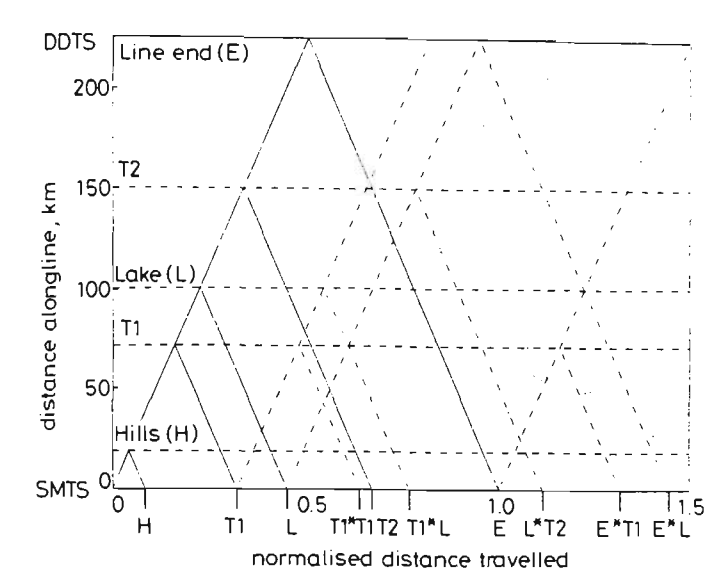

Fig. 13 *Lattice diagram for SMTS-DDTS line*

To interpret the many other peaks in Fig 11 a lattice diagram for line 2 is drawn in Fig. 13. The lattice diagram shows all signal paths with up to three reflections. The main reflections are the transpositions (T1 and T2), the line end (E) and a reflection from the transmission path over Lake Eildon (L). These are shown as solid lines. The major signal paths involving more than one reflection are shown as dashed (- - -) lines. Most of the major correlation peaks can be identified from these four main reflections. The remaining peaks can be attributed to other impedance changes, such as the change in ground constants when the lines pass over a range of wooded hills (H) and other geographical or physical conditions.

Table 4: Estimated and actual distances to line transpositions

	T1	T2
Distance calculated from Fig. 10 (km)	71.21	148.7
Actual distance (km)	71.65	150.3

The lattice diagram shows that a change in line conditions at one point (such as a fault) will produce a number of peaks in the correlation output caused by the various reflection combinations. It is the first peak that determines the distance. Previous work by the authors [1] illustrated this effect using simulations where the first correlation peak caused by a fault had an amplitude comparable to that of a transposition near the line end. The distance to the fault was easily measured. Unfortunately for this test, the line concerned was not out of service long enough to attach a short, but the transpositions can be easily detected indicating that the method would have no trouble in discerning a fault. Table 4 shows the predicted and actual distance to the two transpositions. The accuracy is 0.71% of the line length but would improve for a fault

condition since T1 and T2 form an accurate reference. Further improvements in accuracy would require a higher chip rate R_c and so a larger bandwidth. This would reduce the relative widths of the correlation peaks allowing more detail as well as improved accuracy.

It was found that over the 2 hour period the line was available for measurements the results of Figs. 11 and 12 were highly repeatable. indicating that every peak was caused by a line condition and not by external spurious noise signals. The technique could therefore be used for monitoring small long-term impedance changes in the line by comparing the correlation plot to a previous correlation template. This method could be of benefit in long-term line diagnostics.

The incoming line reflections after the primary reflection from the line end are around 60dB down from the transmitter feedthrough signal which is close to the bandwidth limited MLS code self-rejection ratio of $20\log_{10}(1023) = 60.2$dB [5]. This indicates that considerably more interference could be tolerated which raises the possibility of using spread-spectrum line-monitoring techniques with existing PLC equipment operating on the same line. Alternatively, the amount of averaging can be reduced or eliminated which will give a faster response time.

5 Conclusions

This paper has described the use of direct-sequence spread spectrum waveforms at power-line carrier frequencies for remote line diagnostics. The technique is suitable for both energised and de-energised lines because it uses an active probing signal.

The proposed method is sensitive enough to detect impedance discontinuities owing to faults, transpositions and the line end. In addition large geographical anomalies appear as strong reflection peaks. Using the line end as a distance reference, the distance to the first transposition was measured to within 0.5km and the distance to the second transposition was measured to within 1.6km. If the technique was to be used for fault location, greater accuracy could be obtained because the transpositions as well as the line end could be used as a distance reference. Greater resolution and accuracy could be obtained by using a wider bandwidth spread-spectrum probing signal. In this experiment the bandwidth was limited to 50kHz by a line-separation filter used by the existing PLC equipment. Bandwidths up to 450kHz could be obtained if the line separation filters were bypassed.

This performance was achievable in the face of strong interference from PLC channels operating concurrently on an adjacent parallel line in the same bandwidth as the probing signal. This robustness required the application of interference suppression techniques in this case the use of an averaging capability in the receiver. The use of a much longer code would be equally effective. Long codes increase the data analysis time and averaging requires a longer data acquisition interval.

In the results shown here the processing was done offline on a computer workstation. However, real-time operation is possible with the use of modern DSP components and typical data acquisition and processing times are listed in Table 5. The numbers in Table 5 are for N_p (the number of samples in a code period) = 2^{16} and $f_s = 1.6$MHz. These figures are similar to the con-

IEE Proc.-Gener. Transm. Distrib., Vol. 143. No. 5. September 1996

433

results. Acquisition time is determined by the signal transmission time needed to get the required number of averages ($T_p \times N_A = LN_A/R_c$). Processing time depends on the number of samples in a code period ($N_p = T_p f_s = Lf_s/R_c$), the particular algorithm implemented, and the performance of the DSP processor. From [10] the time required to evaluate the circular correlation of eqns. 2 and 3, using Fast fourier transform (FFT) routines, is

$$T_{circ} = 2k_{ct}N_p \log_2(N_p) + k_m N_p$$

where k_{ct} and k_m are constants depending on the speed of the particular processor being used. k_{ct} is related to the time it takes for a single FFT butterfly operation and k_m depends also on the time required for a complex multiply operation. While this equation assumes that N_p is a power of two, similar processing times are achievable provided that N_p has many factors. The approximate processing times listed in Table 5 are for the Texas Instruments TMS320C30 floating point digital signal processor running at 20 MFLOPS and are based on the radix-2 complex FFT routine listed in [11]. These processing times would be reduced using a split radix or higher radix algorithm, and using a real FFT for the forward transform $H(f_k) = F[r(t_i)]$ of eqn. 2.

Table 5: Data acquisition and processing times on a 20 Mflops TMS320C30 processor, with and without averaging, for $N_p = 2^{16}$ data points and sample frequency $f_s = 1.6$MHz

	4095 averaging	no averaging
data acquisition time	167.73 sec	40.96 msec
data processing time	0.49 sec	0.49 sec
total response time	168.2 sec	0.53 sec

The Table values for the processing and acquisition times are very conservative because of the large over-sampling rate used in the measurements. It should be possible to reduce the sampling frequency closer to the Nyquist limit of 2 × signal bandwidth = 2 × 200 = 400kHz.

The method is flexible in that both low and high-speed operation is possible. The first can tolerate strong interference, while the last requires little interference (i.e. PLC channels switched off) so that the averaging and code length requirements can be reduced.

Separate lines entering a terminal station may be probed simultaneously by using different codes on each line. Provided the crosscorrelation discrimination between the codes is sufficient to compensate for the crosstalk across the lines the method will be applicable to these network grids.

6 Acknowledgments

7 References

1   TAYLOR. V., FAULKNER. M., KALAM. A., and HAYDON. J.: 'Digital simulation of fault location on EHV lines using wideband spread spectrum techniques'. *IEE Proc., Gener. Transm. Distrib.*, 1995, **142**, (1), pp. 73–80
2   SKOLNIK. M.I.: 'Introduction to radar systems' (McGraw-Hill Kogakusha, 1980, 2nd edn.)
3   SKOLNIK. M.I.: 'Theoretical accuracy of radar measurements'. *Trans. IRE*, 1960, **ANE–7**, (4), pp. 123–129
4   STEVENS. D., OTT. G., POMEROY. W., and TUDOR. J.: 'Frequency modulated fault locator for power lines', *IEEE Trans.*, 1972, **PAS–95**, (5), pp. 1760–1768
5   DIXON. R.C.: 'Spread spectrum systems' (Wiley, 1984, 2nd edn.)
6   ROHLING. H., and PLAGGE .W.: 'Mismatched filter design for periodical binary phased signals'. *IEEE Trans.*, 1989, **AES–25**, (6), pp. 890–896
7   RABINER. L.R., and GOLD. B.: 'Theory and application of digital signal processing' (Prentice–Hall, 1975)
8   FAULKNER. M.: 'A new modulation for power protection signalling'. IREECON international electronics convention, Sydney, 1987
9   WELCH. P.D.: 'The use of fast Fourier transform for the estimation of power spectra: a method based on time averaging over short, modified periodograms'. *IEEE Trans.*, 1967, **AU–15**, pp. 70–73
10 STOCKHAM. T.G.: 'High speed convolution and correlation'. Proceedings of 1966 spring joint computer conference (AFIPS), 1966. Vol. 28, pp. 229–233
11 PAPMACHALIS. P. (Ed.): 'Digital signal processing applications with the TMS320 family'. Texas Instruments, 1990, Vol. 3, Chap. 4, Appendix A1

434

IEE Proc.-Gener. Transm. Distrib., Vol. 143, No. 5, September 1996